

https://dspace.org/

Evaluation of flooding induced mining seismicity with a view to characterize safety margins for surface structures under existing and flooded condictions in the Central Rand, Johannesburg

Ali, Sarfraz

2016
http://hdl.handle.net/10539/20642

Downloaded from a DSpace repository. https://dspace.org/

EVALUATION OF FLOODING INDUCED MINING SEISMICITY WITH A VIEW TO CHARACTERIZE SAFETY MARGINS FOR SURFACE STRUCTURES UNDER EXISTING AND FLOODED CONDITIONS IN THE CENTRAL RAND, JOHANNESBURG

Sarfraz Ali

A thesis submitted to the Faculty of Engineering and the Built Environment, University of the Witwatersrand, Johannesburg, in fulfilment of the requirements for the degree of Doctor of Philosophy.

Johannesburg, 2016

DECLARATION

I declare that this thesis is my own, unaided work. Where use has been made of the work of others, it has been duly acknowledged. It is being submitted for the Degree of Doctor of Philosophy in the University of the Witwatersrand, Johannesburg. It has not been submitted before in any form for any degree or examination in any other University.

Signed:



Sarfraz Ali

Student No. 703423

9 February 2016

ABSTRACT

The recent mining-induced seismic history and increased flooding of abandoned mines in the Central Rand, Johannesburg, has established uncertainty as to the magnitudes and intensities of the future seismicity. The Central Business District (CBD) area of Johannesburg is located close to the mined-out reef (abandoned mines) and consists of surface structures of various types, such as masonry, concrete, steel, low-rise and high- rise buildings. In the absence of site-specific mining-induced seismic parameters, there exists an uncertainty in the evaluation of risk to the safety and stability of surface structures from the mining-induced seismicity in future.

The CBD area comprises many geological groups dipping steeply in a southward direction. This complex geological stratum underlain by flooded abandoned mines is likely to trigger multiple seismic source mechanisms, such as slip along a fault, fall of ground, collapse of pillar, and so forth. The orientation of the geological structures and contrast in the material properties have a direct influence on the seismic wave propagation. The available methods to estimate mining-induced seismicity do not take these complexities into account. Advanced numerical modelling techniques, such as 3DEC (3 Dimensional Distinct Element Method) and FLAC (2 Dimensional Finite Difference Method) are used to simulate various source mechanisms for estimation of site-specific ground motions.

Three source mechanisms: impulsive slip, fall of ground and pillar collapse are simulated with a view to generate seismic events in the earthquake magnitude range varying from M_L 2.5 to 5.0 under both dry and flooded conditions. Seismic parameters of the seismic events simulated under flooded conditions are estimated in the form of velocity-time histories which ranged from 2 to 6 mm/sec, duration of the events varied from 1.5 to 2.0 sec and frequency which ranged from 8 to 12 Hz. 3DEC simulations reveal that the effect of flooding in abandoned mines manifests in lowering the peaks of ground motions in all the source mechanisms. In case of impulsive slip along the wet joint, the peak velocity reduces by approximately 30% (from 10.10 mm/sec to 6.50 mm/sec) in the hanging wall. The amount of reduction in peak velocities is non-uniform in

all three source mechanisms and is also different at different points in each geological group of the study area.

Dynamic structural analyses are performed using the estimated seismic parameters in flooded conditions. In view of Uniform Building Codes/ASCE guidelines on drift/horizontal displacement for structures/slopes, it has been found that estimated ground motions are not likely to pose a risk to the safety of structures and stability of soil/rock slopes. Also, the potential to trigger liquefaction of tailings dam slopes and slip of a confined fault is unlikely. Research, however needs to be carried out for estimation of ground motions for seismic events of higher magnitudes for evaluating their adverse effects.

The research reveals that 3DEC is an appropriate tool to evaluate site-specific seismic potential in terms of “time histories” at any point and depth at the candidate site, whereas FLAC is suitable for evaluation of liquefaction potential and stability of slopes. In view of the research conducted, a framework is suggested to estimate the ground motions and evaluate its effects on mining and civic infrastructures. The research has the potential to facilitate seismic micro-zonation, re-mining in Central Rand and development of building standards for South Africa.

DEDICATION

To my loving wife for her faith in me, my brilliant sons for happily sacrificing the time they deserved so much, my loving parents and caring siblings for their moral support.

ACKNOWLEDGEMENTS

Heartfelt acknowledgements are due to the following spectacular individuals for their guidance, support, encouragement and contributions in making my research work successful:

- My supervisor, Prof Nielen Van Der Merwe, (School of Mining Engineering, University of Witwatersrand), for his indispensable and crucial academic guidance throughout the research and prompt reading of the draft chapters and draft thesis.
- Prof F.T. Cawood (Former Head, School of Mining Engineering, University of Witwatersrand), for providing School's support to get much needed training on 3DEC and FLAC codes from the USA.
- Dr Loren Lorig, my mentor at Itasca Consulting Inc., Minneapolis USA, for his academic guidance on use of 3DEC and FLAC.
- Prof C. Musingwini (Head, School of Mining Engineering, University of Witwatersrand), for providing School's support to get much needed training on dynamic module of 3DEC from Portugal.
- Dr Jose Lemos, National Civil Engineering Laboratories, Portugal for his guidance on dynamic module of 3DEC code.
- Council for Geoscience (Michelle Grobler and Denver Birch) for providing data on the CBD area.
- Zafar; my brother in Sydney for his gift of an efficient computer which made my life easy and this research work successful.
- Dr Bekir Genc (School of Mining Engineering, University of Witwatersrand), for his guidance on thesis write-up.
- Lindy, Mona and Sonja (School of Mining Engineering, University of Witwatersrand), for their moral support throughout the stay at School.
- Tariq Feroze and Intikhab Hussain for their help in printing and formatting.

Table of Contents

ABSTRACT ..... **ii**

DEDICATION ..... **iv**

ACKNOWLEDGEMENTS ..... **v**

List of Figures ..... **xiii**

List of Tables ..... **xxiv**

1. INTRODUCTION **1**

1.1. Background 1

1.2. Problem Statement 4

1.3. Scope and Objectives of the Research 5

1.4. Relevance of the Research and Research Questions 5

1.5. Research Conceptual Framework and Methodology 6

1.6. Thesis Structure 7

1.6.1. Chapter 1 – Introduction 7

1.6.2. Chapter 2 - Literature review 7

1.6.3. Chapter 3 – Site characterization 8

1.6.4. Chapter 4 – Methodology 8

1.6.5. Chapter 5 – Evaluation of mining-induced seismicity 8

1.6.6. Chapter 6 – Effects of mining-induced ground motions on surface structures 8

1.6.7. Chapter 7 - Conclusions and recommendations 8

1.7. Significance of the Study 9

1.8. Conclusion 9

2. LITERATURE REVIEW **10**

2.1. Introduction 10

2.2. Natural (Tectonic) Seismicity vis-à-vis Mining-Induced Seismicity 11

2.3. Mining-Induced Seismicity: Evidence and Pattern in the South Africa 12

2.3.1. Seismic scales (magnitude and intensity) in South Africa 15

2.4. Causal Factors and Characteristics of Mining-induced Seismicity 16

2.4.1. Causal factors 16

2.4.2. Characteristics of the mining-induced seismicity highlighted by various researchers 18

2.4.2. Recent large magnitude mining-induced seismic events and their damage to surface structures 22

2.4.3. Salient features of the mining-induced seismicity in the Central Rand, Witwatersrand Basin 26
2.5. Evaluation of Mining-induced Seismicity 27
2.5.1. Propagation of seismic waves through geological media 27
2.5.1 Empirical methods 30
2.5.2. Effect of flooding of the abandoned mine void on the mining-induced seismicity 32
2.6. Considerations and Methods for Evaluation of Hazard to Surface Structures 32
2.6.1. Consideration for evaluation of structural hazard 33
2.6.2. Methods for evaluation of structural hazard 38
2.7. Evaluation of Seismic Risk to Surface Structures 41
2.7.1. SANS 10160-4:2009 42
2.7.2. Unified building codes, Searer et al. (2004) 44
2.7.3. Liquefaction potential of a tailings dam slope 45
2.8. Knowledge Gaps 46
2.9. Conclusion 46
3. METHODOLOGY 47
3.1. Introduction 47
3.2. Conceptual Framework and Methodology 48
3.3. 3DEC Numerical Modelling for Evaluation of Mining Induced Seismicity 49
3.3.1. Site Characterization 50
3.3.2. Numerical simulation considerations 50
3.3.3. Transmission of waves 51
3.3.4. Effect of flooding in 3DEC simulations 52
3.3.5. Simulation scenarios 53
3.3.6. Simulation stages 54
3.3.7. Estimation of ground motions 54
3.4. Evaluation of Effects of the Mining-induced Seismicity on Surface Structures 55
3.4.1. Seismic structural considerations 56
3.4.2. Use of numerical methods for seismic structural analysis 57
3.4.3. Numerical simulation stages for the seismic structural analysis 59
3.5. Assessment of Risk to Surface Structures 59
3.5.1. Masonry and Concrete Buildings 59

3.5.2. Liquefaction Potential of a Tailings Dam Slope and Stability of Rock/Soil Slopes 61
3.6. Conclusion 62
4. SITE CHARACTERIZATION 63
4.1. Introduction 63
4.2. Factors Considered for Site Characterization 64
4.3. Site Topography 65
4.4. Regional and Local (Study Area) Stratigraphy 66
4.4.1. Central Rand group 68
4.4.2. West Rand group 69
4.5. Site Geology 69
4.6. Site Hydrology 71
4.7. Seismological Conditions 82
4.8. Field Stresses 82
4.9. Site Geotechnics; Types and Characteristics of the Foundation Soils and Rocks 84
4.9.1. Northern area 84
4.9.2. Central area 85
4.9.3. Southern area 85
4.9.4. Geotechnical properties of rocks and soils 85
4.10. Geotechnical Characteristics of the Geological Discontinuities (Faults/Joints) 88
4.11. Surface Structures; Types and Characteristics 90
4.12. Idealized Geomechanical Model for Evaluation of Mining Induced Seismicity and Its Effects on Surface Structures 91
4.13. Conclusion 92
5. EVALUATION OF MINING INDUCED SEISMICITY 94
5.1. Introduction 94
5.2. Geomechanical Considerations 94
5.3. Seismological Considerations 94
5.4. Numerical Modelling Considerations 94
5.5. 3DEC Model Parameters 96
5.5.1. 3DEC features 96
5.5.2. 3DEC modelling approach 96
5.5.3. Model size and geometry 96
5.5.4. Initial conditions and in-situ stresses 98

5.6. Constitutive Models 99
5.6.1. Block material constitutive model 99
5.6.2. Rock discontinuity constitutive model 99
5.7. Wave Transmission 100
5.7.1. Mesh size versus wave frequency 100
5.7.2. Model boundary condition and reflection of waves 101
5.7.3. Effect of discontinuities on transmission of waves 102
5.8. Damping Parameters 104
5.9. 3DEC Simulation Stages 105
5.9.1. Partial density scaling to minimize model runtime 105
5.9.2. Stage 1 - model set-up 106
5.9.3. Stage 2 - initialize insitu stresses 106
5.9.4. Stage 3 - initial static equilibrium 107
5.10. 3DEC Simulations for Estimation of Mining Induced Ground Motions 109
5.11. 3DEC Simulation for Impulsive Slip 111
5.11.1. Empirical aspects 111
5.11.2. Conceptual aspects 112
5.11.3. Simulation aspects common to impulsive slip under dry and flooded conditions 113
5.11.4. Simulation for impulsive slip along a dry joint 115
5.11.5. Discussion on ground motions due to impulsive slip along a dry joint 118
5.11.6. Simulation for ground motions due to impulsive slip along a flooded joint 119
5.11.7. Discussion on ground motions estimated due to impulsive slip along a flooded joint 122
5.12. 3DEC Simulations for Fall of Ground 124
5.12.1. Empirical considerations 124
5.12.2. Conceptual considerations 124
5.12.3. 3DEC Simulation aspects common to fall of ground in dry and flooded conditions 125
5.12.4. Simulation for fall of ground in a dry void 128
5.12.5. Discussion on ground motions due to fall of ground in a dry void 131
5.12.6. Simulations for fall of ground in a flooded void 132
5.12.7. Discussion on ground motions due to fall of ground in a flooded void 135
5.12.8. Comments / comparison of ground motions due to fall of ground in a dry and flooded void 136
5.13. Simulation of Seismicity Due to Collapse of Pillar (s) 137

5.13.1. Empirical considerations 137
5.13.2. 3DEC considerations 138
5.13.3. 3DEC simulation aspects common to pillar (s) collapse in dry and flooded void 139
5.13.4. Simulation of simultaneous failure of large number of pillars in dry condition 143
5.13.5. Discussion on ground motions due to simultaneous collapse of a large number of pillars under dry conditions 146
5.13.6. Simulation for failure of large number of pillars in the flooded voids 148
5.13.7. Discussion on ground motions due to the simultaneous failure of large number of pillars under flooded conditions 151
5.14. Summary of Findings of 3DEC Simulations for Ground Motions Common to All Scenarios 153
5.14.1. Applicability of 3DEC for estimating mining induced ground motions 153
5.14.2. Characteristics of the Estimated Ground Motions (Velocity Time Histories) Mining Induced Seismicity 154
5.14.3. Effects of flooding on mining induced seismicity 155
5.15. Ground Motion Recommendations for Evaluation of effects on Surface Structures 157
5.16. Conclusion 158
6. EFFECTS OF MINING INDUCED SEISMICITY ON SURFACE STRUCTURES 159
6.1. Introduction 159
6.2. Seismological Parameters 159
6.2.1. Seismic sources 160
6.2.2. Seismic input parameters 160
6.3. Geomechanical Parameters 162
6.4. Structural Parameters 163
6.5. Dynamic Structural Analysis 163
6.6. Dynamic Analysis of a Two Storey Masonry Building 166
6.6.1. Model size, geometry and properties 166
6.6.2. Initial static equilibrium 168
6.6.3. Dynamic simulations 168
6.6.4. Comments on the response of the two storey masonry building 172
6.7. Dynamic Analysis of a Two Storey Concrete Building 173
6.7.1. Model size, geometry and properties 173
6.7.2. Initial static equilibrium 175

6.7.3. Dynamic simulations 176
6.8. Comments on the dynamic response of two storey concrete building 178
6.9. Dynamic Analysis of a Four Storey Concrete Building 179
6.9.1. Model size, geometry and properties 180
6.9.2. Initial static equilibrium 180
6.9.3. Dynamic simulations 181
6.9.4. Comments on the dynamic response of four storey concrete building 185
6.10. 3D Seismic Analysis of an Eight Storey Concrete Building 185
6.10.1. Model size, geometry and properties 186
6.10.2. Initial static equilibrium 186
6.10.3. Comments on dynamic response of eight storey concrete building 190
6.11. Dynamic Analysis of a Jointed Rock Slope with Building Load at the Crest Using 3DEC 191
6.11.1. Model size, geometry and properties 191
6.11.2. Initial static equilibrium 193
6.12. Dynamic Analysis for Evaluation of Liquefaction Potential in a Tailings Dam Slope Using FLAC 203
6.12.1. Model size, geometry and properties 203
6.12.2. Initial static equilibrium 204
6.12.4. Damped Mohr-Coulomb simulation assuming no liquefaction 208
6.12.5. Finn-Byrne simulation 209
6.13. Dynamic Analysis to Evaluate Stability a Soil Slope using FLAC 211
6.13.3. Factor of safety under static conditions 213
6.13.4. Dynamic loading and boundary conditions 216
6.14. Dynamic Analysis to Evaluate Stability of a Rock Block with a Confined Joint 218
6.14.1. Model size, geometry and properties 218
6.14.2. Initial static equilibrium 220
6.14.3. Dynamic simulations 220
6.15. Conclusion 221
7. CONCLUSIONS AND RECOMMENDATIONS 224
7.1. General 224
7.2. Key Findings of the Research 224
7.3. Research Contribution: Framework for the Evaluation of Mining Induced Seismicity 226
7.4. Research Limitations 227

7.5. Recommendations for the Future Research Work 229
References 232

List of Figures

Figure 1.1 Location of seismic events around abandoned mines in Central Rand, Council for Geoscience (2012).....2
Figure 1.2 Mining areas and developments in the Central Rand, source, van der Merwe (2013).....3
Figure 1.3 Conceptual framework of the study 6
Figure 2.1 Process and components of the literature review.....10
Figure 2.2 Witwatersrand Basin, Randgold (2010) 12
Figure 2.3 Central Rand Gold Reefs and Goldfields, Mphephu (2001) 13
Figure 2.4 Location of seismological stations in the Witwatersrand Basin, Council for Geoscience (2013) 14
Figure 2.5 Study area and location of mining induced earthquakes in the Central Rand, CGS, (2012).....14
Figure 2.6 Sources of induced seismicity; changes in shear stress (Δt), pore pressure (Δp), volume change (Δv) and applied forces (Δn), McGarr et al. (2002) 17
Figure 2.7 Mechanism for mining seismicity, Hasegawa et al., (1989) 18
Figure 2.8 Velocity time history of a mining induced earthquake at Savuka Mine, South Africa, Julia et al. (2009) 19
Figure 2.9 Peak velocity recorded at surface, 2.7 km above the source due to a mining induced earthquake of M4.4, McGarr (2002).....19
Figure 2.10 Peak particle velocities of the seismic events at Tau Tona mine, Milev and Spottiswoode (2005).....20
Figure 2.11 Correlation of peak velocity, magnitude and distance in South Africa mining areas, Potvin and Wesseloo (2010).....20
Figure 2.12 Level of mining induced (rockburst) ground motions, Saebimoghaddam (2010).....21
Figure 2.13 Damage to a multi-storey building during M_L 5.2 seismic event in Welkom area, Durrheim et al. (2006).....23
Figure 2.14 Damage to the Bel-Eaton court building during M_L 5.3 seismic event in Stilfontein area, source: van der Merwe (2013).....24
Figure 2.15 Damage to the masonry building during M_L 5.3 seismic event in Stilfontein area, van der Merwe (2013) 24

Figure 2.16 Damage due to ML 5.3, Orkney seismic event on 5 August 2014. A; pointed masonry building, B; plastered masonry building, Varvaeck (2014) C; ground displacements, D; ceiling, Varvaeck (2014) 25
Figure 2.17 Shake map of 5 August 2014, Orkney seismic event, USGS (2014) 26
Figure 2.18 Considerations and methods for dynamic structural analyses 33
Figure 2.19 Natural period of various structures, Arnold (2013) 34
Figure 2.20 Vulnerable buildings; 6 to 20 Storey during the Mexico City earthquake in 1985, Arnold (2013) 36
Figure 2.21 Typical response spectra, Arnold (2013) 37
Figure 2.22 Response spectra for various damping values, Satratta (1987) .. 38
Figure 2.23 Numerical modelling techniques vis-à-vis type of medium 39
Figure 2.24 Panoramic view of high rise concrete buildings in CBD area, Johannesburg 41
Figure 2.25 Seismic Zones in South Africa, SANS 10160-4:2009 42
Figure 2.26 Normalized design response spectra according to SANS 10160-4:2009 (for ground type, refer o Table 2.3) 43
Figure 2.27 Guideline for the structural systems for dynamic analysis, SANS 10160-4:2009 44
Figure 2.28 Spectral acceleration and the spectral displacement of natural earthquakes, Searer et al. (2004) 45
Figure 3.1 Conceptual framework and methodology 48
Figure 3.2 Process for evaluation of ground motions 50
Figure 3.3 Length scales in rock mass and joint, Itasca (2014) 53
Figure 3.4 Boundary stress to represent effect of flooded voids in 3DEC 53
Figure 3.5 History points shown in black & yellow dots for ground motions 55
Figure 3.6 Methodology for evaluation of effects of mining induced seismicity on surface structures 56
Figure 3.7 Idealized model showing depth of seismic source, geological layers and surface structure 57
Figure 3.8 Spectral acceleration and the spectral displacement of natural earthquakes, after Searer et al. (2004) 60

Figure 3.9 Modulus reduction curve for clayey soil (FLAC default hysteric damping with L1 = -3.156, L2 = 1.904), Itasca (2014).....61
Figure 3.10 Damping ratio curve for clayey soil (FLAC default hysteric damping with L_1 = -3.156, L_2 = 1.904), Itasca (2014) 62
Figure 4.1 Gold bearing conglomerate reefs of the Central Rand Group, Superior Mining (2013) 63
Figure 4.2 Underground mining method (breast stoping) for mining of narrow conglomerate reefs, Viljoen (2009).....64
Figure 4.3 Factors considered for site characterization 65
Figure 4.4 Topography of the study area, after CGS (2013).....66
Figure 4.5 Generalized geological model of the study area (not to scale), after Gold Fields (2011).....67
Figure 4.6 North-south cross-section through the Witwatersrand Basin beneath Johannesburg city (not to scale), after Norman and Whitfield (2006) 67
Figure 4.7 Simplified regional stratigraphy of Witwatersrand, after Guy (2012) 68
Figure 4.8 Geological structures in the Central Rand, Boer and Reimond (2005).....70
Figure 4.9 Geological map of the study area, after CGS (2013).....70
Figure 4.10 Hydrological relief of the Central Rand (Study area shown in red, not to scale), after Winde (2011).....72
Figure 4.11 A north-south oriented idealized model (not to scale) to visualize flooding levels in abandoned mines, after Winde (2011).....73
Figure 4.12 An east-west oriented profile (not to scale) showing Final Mine Water Level indicating a safety margin of 106 m below the Standard Bank building, after Winde (2011) 73
Figure 4.13 Material distributions idealized for research.....91
Figure 4.14 Left; stratigraphy (layering) of material, Right; orientation of joints 92
Figure 5.1 Research matrix for evaluating mining induced seismicity 95
Figure 5.2 Numerical considerations for evaluation of mining induced seismicity 95

Figure 5.3 Model Geometry; left-elevation from the West, Right-material groups (labelling shown in the right figure holds good for the left figure as well) 97
Figure 5.4 Material Groups (left) and Geological Discontinuities (right) (labelling shown in Figure 5.3 (right) holds good for the left figure as well) 97
Figure 5.5 Seismic waveform with one discontinuity (frequency = 5 Hz, amplitude = 9.6 mm) 102
Figure 5.6 Seismic waveform with two discontinuities (frequency = 3.5 Hz, amplitude = 1.65 cm) 103
Figure 5.7 Seismic waveform with three discontinuities (frequency = 0.30 Hz, amplitude = 2.5 cm) 103
Figure 5.8 Partial density scaling / un-damped; left-vertical velocity histories, right-vertical displacement histories 106
Figure 5.9 Insitu stresses initialized in the 3DEC model 107
Figure 5.10 Initial Static Equilibrium; left-Unbalanced Force, Right-Vertical Velocity Histories 107
Figure 5.11 Initial Static Equilibrium; left-Vertical Displacement Histories, Right-Joint Slip (no joint slip observed) 108
Figure 5.12 Initial Static Equilibrium; left-stress in xx-plane, Right-Stress in yy-plane 108
Figure 5.13 Initial Static Equilibrium; left-stress in zz-plane, Right-Joint Shear Displacement 109
Figure 5.14 3DEC simulation scenarios; “Impulsive Slip”, “Fall of Ground”, and “Collapse of Pillar” 110
Figure 5.15 History points (black circles) at the bedrock (100 m below ground surface) 110
Figure 5.16 Model geometry; left – location of the slip area, right - size of the slip area 114
Figure 5.17 Initial static equilibrium; left – plot of unbalanced force, right – plot of vertical displacement histories in Foot Wall 114
Figure 5.18 Initial static equilibrium; left – plot of vertical displacement histories in Hanging Wall, right – plot of vertical displacement histories in Main Reef 115

Figure 5.19 Post excavation equilibrium; left – plot of unbalanced force, right – plot of vertical displacement histories in Foot Wall 115
Figure 5.20 Slip along a dry joint; left – plot of joint shear displacement, right – plot of unbalanced force and velocity vectors 116
Figure 5.21 Slip along a dry joint, plots of velocity time histories on the west edge of model; left – vertical velocity time histories, right – horizontal velocity time histories 116
Figure 5.22 Slip along a dry joint, plots of velocity time histories on centre of the model; left – vertical velocity time histories, right –horizontal velocity time histories 117
Figure 5.23 Slip along a dry joint, plots of velocity time histories on east edge of the model; left – vertical velocity time histories, right – horizontal velocity time histories 117
Figure 5.24 Slip along a dry joint, plots of velocity time histories on the entire model; left – vertical velocity time histories, right –horizontal velocity time histories 118
Figure 5.25 Slip along a flooded joint due to gradual rise in pore pressure; left – plot of joint shear displacement, right – plot of unbalanced force and velocity histories 120
Figure 5.26 Slip along a flooded joint due to gradual rise in pore pressure, plots of velocity time histories on the west edge of model; left – vertical velocity time histories, right –horizontal velocity time histories 120
Figure 5.27 Slip along a flooded joint due to gradual rise in pore pressure, plots of velocity time histories on the centre of the model; left – vertical velocity time histories, right –horizontal velocity time histories 121
Figure 5.28 Slip along a flooded joint due to gradual rise in pore pressure, plots of velocity time histories on the east edge of the model; left – vertical velocity time histories, right –horizontal velocity time histories 121
Figure 5.29 Slip along a flooded joint due to gradual rise in pore pressure, plots of velocity time histories on the entire model; left – vertical velocity time histories, right –horizontal velocity time histories 122
Figure 5.30 Static equilibrium; left-plot of unbalanced force, right-plot of vertical displacement histories in Hanging Wall..... 126

Figure 5.31 Static equilibrium; left-plot of vertical displacement histories in Main Reef, right-plot of vertical displacement histories in Foot Wall 126
Figure 5.32 Excavation; left-location of Main Reef and Fall of Ground, Right-close-up of Excavation and Fall of Ground 127
Figure 5.33 Post excavation equilibrium; left-plot of unbalanced force, right-plot of displacement histories in Hanging Wall 127
Figure 5.34 Post excavation equilibrium; left-plot of vertical displacement histories in Main Reef, right-plot of vertical displacement histories in Foot Wall 128
Figure 5.35 Ground motions due to fall of ground on the west edge of the model; Left-vertical velocity time histories, Right-horizontal velocity time histories 129
Figure 5.36 Ground motions due to fall of ground at the centre of the model; Left-vertical velocity time histories, Right-horizontal velocity time histories 129
Figure 5.37 Ground motions due to fall of ground at the east of the model; Left-vertical velocity time histories, Right-horizontal velocity time histories 130
Figure 5.38 Ground motions due to fall of ground at the entire model; Left-vertical velocity time histories, Right-horizontal velocity time histories 130
Figure 5.39 Ground motions due to fall of ground at the west edge of the model; Left-vertical velocity time histories, Right-horizontal velocity time histories 133
Figure 5.40 Ground motions due to fall of ground at the centre of the model; Left-vertical velocity time histories, Right-horizontal velocity time histories 133
Figure 5.41 Ground motions due to fall of ground at the east of the model; Left-vertical velocity time histories, Right-horizontal velocity time histories 134
Figure 5.42 Ground motions due to fall of ground at the entire model; Left-vertical velocity time histories, Right-horizontal velocity time histories 134

Figure 5.43 Model geometry (left) and Main Reef (right), hanging wall is removed to show location of excavations and pillars.....140
Figure 5.44 Location and layout of mining pillars (shown in grey colour) and excavations (shown in pink colours).....140
Figure 5.45 Initial static equilibrium condition of the model; plot of unbalanced force on left and vertical displacement histories at the centre points on the right.....141
Figure 5.46 Initial static equilibrium condition of the model; left; plot of vertical displacement histories on eastern points, right; vertical displacement histories at the western points on the model.....141
Figure 5.47 Initial static equilibrium condition of the model; left; plot of velocity vectors, right; displacement vectors 142
Figure 5.48 Excavations shown in white colour in the left figure, plot of unbalanced force on right 142
Figure 5.49 Plot of displacement vectors on left, vertical displacement histories at the centre points on the model shown on right.....143
Figure 5.50 Plot of vertical displacement histories of point located on the eastern points is shown in the figure on left and western points on the right.....143
Figure 5.51 Plot on left shows excavated pillar, plot on right shows the model is critically damped.....144
Figure 5.52 Left; vertical velocity histories, Right; horizontal velocity histories at the centre of each geological group.....145
Figure 5.53 Left; vertical velocity histories, Right; horizontal velocity histories at the western edge of each geological group 145
Figure 5.54 Left; vertical velocity histories, Right; horizontal velocity histories at the eastern edge of each geological group 146
Figure 5.55 Left; all vertical velocity histories, Right; all horizontal velocity histories 146
Figure 5.56 Left; one pillar excavated, Right; creation of six regions for setting boundary stress to represent effect of water filled voids.....149
Figure 5.57 Left; vertical velocity histories, Right; horizontal velocity histories at the centre of each geological group.....149

Figure 5.58 Left; vertical velocity histories, Right; horizontal velocity histories at the western edge of each geological group 150
Figure 5.59 Left; vertical velocity histories, Right; horizontal velocity histories at the eastern edge of each geological group 150
Figure 5.60 Left; all vertical velocity histories, Right; all horizontal velocity histories 151
Figure 5.61 Plots of horizontal velocity histories under dry and flooded conditions in all the three scenarios; left-Impulsive Slip, centre-Fall of Ground, right-Pillar Collapse 156
Figure 5.62 Ground motion recommendations for seismic structure analysis 157
Figure 6.1 Considerations for evaluation of the effects of the mining induced seismicity on surface structures in CBD Area 159
Figure 6.2 Ground motions in terms of horizontal velocity time histories in dry and flooded condition 161
Figure 6.3 Ground motions estimated at Hanging Wall, Main Reef and Foot Wall.....162
Figure 6.4 Ground motion (horizontal velocity time history) selected for dynamic structural analysis.....162
Figure 6.5 Dynamic application at the bedrock.....165
Figure 6.6 Model Geometry; left-foundation ground (quartzite rock), right-geometry and layout of two storey masonry building 167
Figure 6.7 Model Geometry; left-concrete elements (foundation, windows, doors, roofs), right-geometry of brick walls of 1st and 2nd stories 168
Figure 6.8 Initial equilibrium; left-plot of vertical velocity, right-plots vertical displacements.....168
Figure 6.9 Horizontal displacement at T =0.5 sec.....169
Figure 6.10 Horizontal displacement at T =1.0 sec.....170
Figure 6.11 Horizontal displacement at T =1.5 sec.....171
Figure 6.12 Horizontal displacement at T =2.0 sec.....172
Figure 6.13 Model size and geometry of two storey concrete building.....174
Figure 6.14 Plot of unbalanced force (left) and vertical velocity histories (right) 175

Figure 6.15 Plot of vertical displacement histories (left) and contour of horizontal displacement (right) 175
Figure 6.16 Horizontal displacement at T =0.5 sec 176
Figure 6.17 Horizontal displacement at T =1.0 sec 177
Figure 6.18 Horizontal displacement at T =1.50 sec 178
Figure 6.19 Horizontal displacement at T =2.0 sec 179
Figure 6.20 Model size and geometry of four storey concrete building 180
Figure 6.21 Plot of unbalanced force (left) and vertical velocity histories (right) 181
Figure 6.22 Plot of vertical displacement histories (left) and contour of horizontal displacement (right) 181
Figure 6.23 Horizontal displacement at T=0.5 sec 183
Figure 6.24 Horizontal displacement at T=1.0 sec 183
Figure 6.25 Horizontal displacement at T=1.5 sec 184
Figure 6.26 Horizontal displacement at T=2.0 sec 185
Figure 6.27 Model size and geometry of eight storey concrete building 186
Figure 6.28 Plot of unbalanced force (left) and vertical velocity histories (right) 187
Figure 6.29 Plot of vertical displacement histories (left) and contour of horizontal displacement (right) 187
Figure 6.30 Horizontal displacement at T=0.5 sec 188
Figure 6.31 Horizontal displacement at T=1.0 sec 189
Figure 6.32 Horizontal displacement at T=1.5 sec 190
Figure 6.33 Horizontal displacement at T =2.0 sec 190
Figure 6.34 Quartzite slope geometry 192
Figure 6.35 Joint sets in the slope 192
Figure 6.36 Plot of unbalanced force 193
Figure 6.37 Plot of vertical displacement history of a point (shown in yellow cross) at the crest 194
Figure 6.38 Displacement contours and vectors at 0.5 sec duration 195
Figure 6.39 Velocity contours and vectors at 0.5 sec duration 195
Figure 6.40 Joint shear slip magnitude at 0.5 sec duration 196
Figure 6.41 Displacement contours and vectors at 1.0 sec duration 197
Figure 6.42 Velocity contours and vectors at 1.0 sec duration 197

Figure 6.43 Joint shear slip magnitude at 1.0 sec duration 198
Figure 6.44 Displacement contours and vectors at 1.5 sec duration 199
Figure 6.45 Displacement contours and vectors at 1.5 sec duration 199
Figure 6.46 Joint shear slip magnitude at 1.5 sec duration 200
Figure 6.47 Displacement contours and vectors at 2.0 sec duration 201
Figure 6.48 Velocity contours and vectors at 2.0 sec duration 202
Figure 6.49 Joint shear slip magnitude at 2.0 sec duration 202
Figure 6.50 Geological profile of the tailings dam slope.....203
Figure 6.51 Geometry of the model.....204
Figure 6.52 Plot of unbalanced force showing the model reached equilibrium 205
Figure 6.53 Plot of pore-pressure contours showing equilibrium (steady state condition) 206
Figure 6.54 Plot of contours of vertical stress showing equilibrium (gradual distribution).....206
Figure 6.55 Input ground motion (velocity time history).....207
Figure 6.56 Maximum shear strain contours during un-damped and elastic material.....208
Figure 6.57 Maximum shear strain contours; damped Mohr Coulomb simulation 209
Figure 6.58 Maximum shear strain contours; damped Finn-Byrne model ..210
Figure 6.59 Pore-pressure contours; gradual gradients show no signs of plastic deformation/liquefaction 210
Figure 6.60 Slope geometry 211
Figure 6.61 Plot of unbalanced force; initial static equilibrium 212
Figure 6.62 Plot of shear strain contours showing elastic strain range.....213
Figure 6.63 Plot of unbalanced force 214
Figure 6.64 Plot of x-displacement histories 214
Figure 6.65 Plot of shear strain contours.....215
Figure 6.66 Plot of plasticity indicator and factor of safety 215
Figure 6.67 Plot of x-displacement contours 216
Figure 6.68 Plot of y-displacement contours 217
Figure 6.69 Plot of plasticity indicators.....217
Figure 6.70 Geometry of the rock block 219

Figure 6.71 Location and orientation of the joints.....219
Figure 6.72 Joint shear displacement at the end of static simulation.....220
Figure 6.73 Joint shear displacement at the end of the dynamic simulation 221
Figure 7.1 Framework for evaluation of mining induced seismicity 228
Figure 7.2 Proposed framework for evaluation of mining induced seismicity 231

List of Tables

Table 2.1 Peak velocity and magnitude data from California earthquakes, Boore (1980).....21
Table 2.2 Illustration of the period and frequency of various surface structures 34
Table 2.3 Values of the parameters describing the design spectra, SANS 10160-4:2009 43
Table 4.1 Geomechanical Parameters estimated for evaluation of mining induced seismicity.....87
Table 5.1 Mesh size vis-à-vis frequency of waves that can transmit through geological blocks 101
Table 5.2 Magnitude of seismic event vis-à-vis area of slip for a constant magnitude of slip.....112
Table 5.3 Ground motions at various history points due to Impulsive Slip along a dry joint (Figure 5.3 and Figure 5.15) 118
Table 5.4 Ground motions due to Impulsive Slip along a flooded joint 122
Table 5.5 Ground motions due to fall of ground in a dry void.....131
Table 5.6 Ground motions due to fall of ground in a flooded void.....135
Table 5.7 Ground motions due to collapse of mining voids under dry conditions 147
Table 5.8 Ground motions due to collapse of mining voids under water filled void conditions.....151
Table 5.9 Seismic parameters for dynamic structural analysis 157
Table 6.1 Seismic parameters for dynamic structural analysis 160
Table 6.2 Material Properties of two storey masonry building 167
Table 6.3 Joint properties of two storey masonry building 167
Table 6.4 Displacement record of two storey masonry building 173
Table 6.5 Material Properties of two storey concrete building 174
Table 6.6 Material Properties of two storey concrete building 174
Table 6.7 Displacement record of two storey concrete building 179
Table 6.8 Displacement record of four storey concrete building 185

Table 6.9 Displacement record of eight storey concrete building 191

Table 6.10 Material properties of quartzite slope 193

Table 6.11 Comparison of displacement, velocity and joint shear displacement 201

Table 6.12 Tailings dam slope properties.....204

Table 6.13 Soil slope properties 212

Table 6.14 Material and joint properties of a rock block with confined joint 218

Table 6.15 Drift (horizontal displacements of structures) 221

1. INTRODUCTION

1.1. Background

Seismic events triggered by tectonic plate boundary conditions are well known to practicing mining and civil engineers from the risk and remedial viewpoints. However, knowledge of mining-induced seismic events (earthquakes) vis-à-vis potential hazards is still evolving and is currently being studied by researchers. Mining-induced seismic events were first reported in the Witwatersrand Basin in 1908, Wong (1993). Mining in the Witwatersrand Basin commenced almost 120 years ago in 1886 and is still continuing in some parts of the Basin at depths as great as 4000 m, Handley (2014). The mining-induced seismic events are reported in both abandoned and active mining areas in the Basin.

In the Central Rand, the mines started closing in the 1950s and the last operational mine closed in 2008, City of Johannesburg, (2011). The closure of the mines with a history of more than 100 years of mining left extremely large volumes of voids underground. According to Durrheim et al. (2006), a large gold mine alone in its lifetime mines a volume of approximately 55 million cubic metres. This fact highlights the volume of excavations underground of all the closed mines ready to be flooded. According to Viljoen (2009), Crown Mines Limited alone has left underground excavations of over 1600 km with the surface footprint of 42 square km. The surface footprint of all the closed mines roughly equals $1/7^{th}$ of the area of Johannesburg. As per Goldbach (2009), many of the gold mines will flood when closed due to the gradual rising of groundwater. Subsequent to the closure of operational mines, the dewatering process (no longer required) also ceased which resulted in the flooding of abandoned mines, later known as “Acid Mine Drainage” (AMD). Besides environmental hazards, the flooding of abandoned mines has also given rise to mining-induced seismic events.

According to the Council for Geoscience (2013), seismic events of magnitudes between M_L 0.2 to M_L 3.4 were located from April 2010 to October 2012 in areas around abandoned mines, Figure 1.1. These seismic events are oriented along north-west and north-east striking zones. Seismic events of M_L 2.5 and more were mostly located around East Rand Proprietary Mines (ERPM) that is, on the

right side of Figure 1.1. The magnitude and hazard of the seismic events depends mainly on the type of source mechanism and its depth. Their effects are generally confined to the immediate vicinity of the seismic sources. According to Kijko and Cichowicz (2006), serious damage due to mining-induced seismicity is restricted to within 10 km of the epicentre.

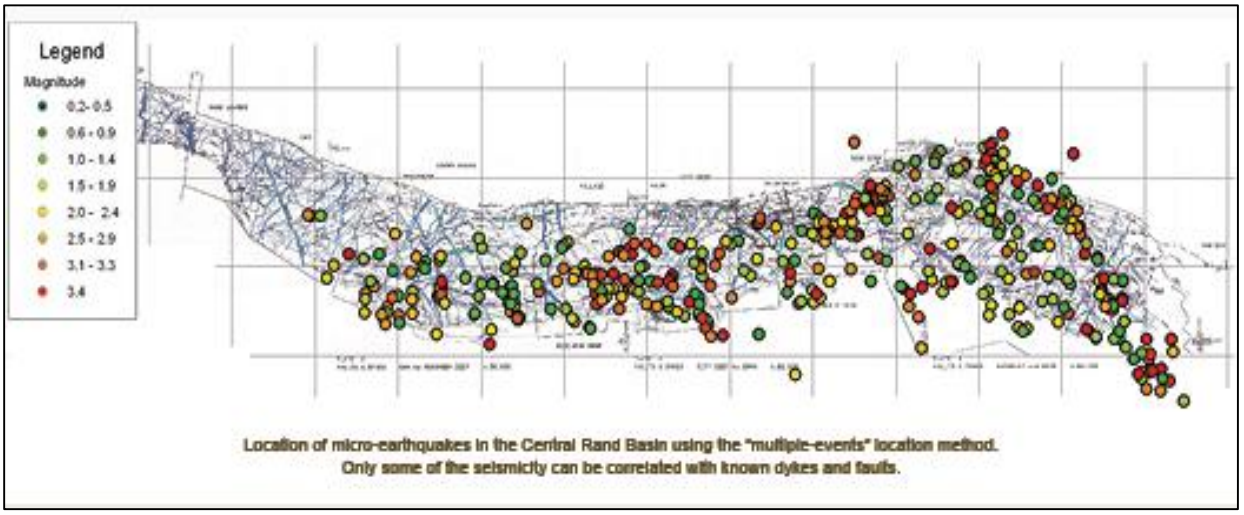


Figure 1.1 Location of seismic events around abandoned mines in Central Rand, Council for Geoscience (2012)

Damage to surface structures and underground mining infrastructures have been attributed to mining-induced events in South Africa. As per Fernandez and Guzman (1977), a mining-related seismic event of M_L 5.2 struck the Welkom District on 8 December 1976 which resulted in the collapse of a large apartment building. On 5 August 2014, the most recent and largest mining-induced seismic event of M_L 5.3 struck Orkney, Klerksdorp District and resulted in the loss of one life, injured 38 people and damaged many buildings, Council for Geoscience (2014). These recent events have necessitated the need to investigate the potential risk from future mining seismicity. To highlight the importance of the problem, the affected areas around abandoned mines in the Central Rand are shown in Figure 1.2.

To evaluate damaging effects, it is necessary to understand the causal factors and possible magnitude of the mining-induced seismicity. The main causal factors of mining-induced earthquakes include shear failure of the rock mass around excavations, failure of pillar(s), rock burst and slip along the geological discontinuities, Spottiswoode, et al. (1971). Empirical methods are available to

approximate the seismic magnitude and ground motions vis-à-vis source mechanisms. Aki and Richards (1980) proposed a relationship between the area of slip along the discontinuity, amount of slip and rock-mass shear modulus to estimate the seismic moment. From the estimated seismic moment, it is possible to approximate the seismic magnitude using a correlation suggested by Hanks and Kanamori (1979). Methods are also available to estimate seismic magnitudes generated due to pillar collapse and fall of ground.

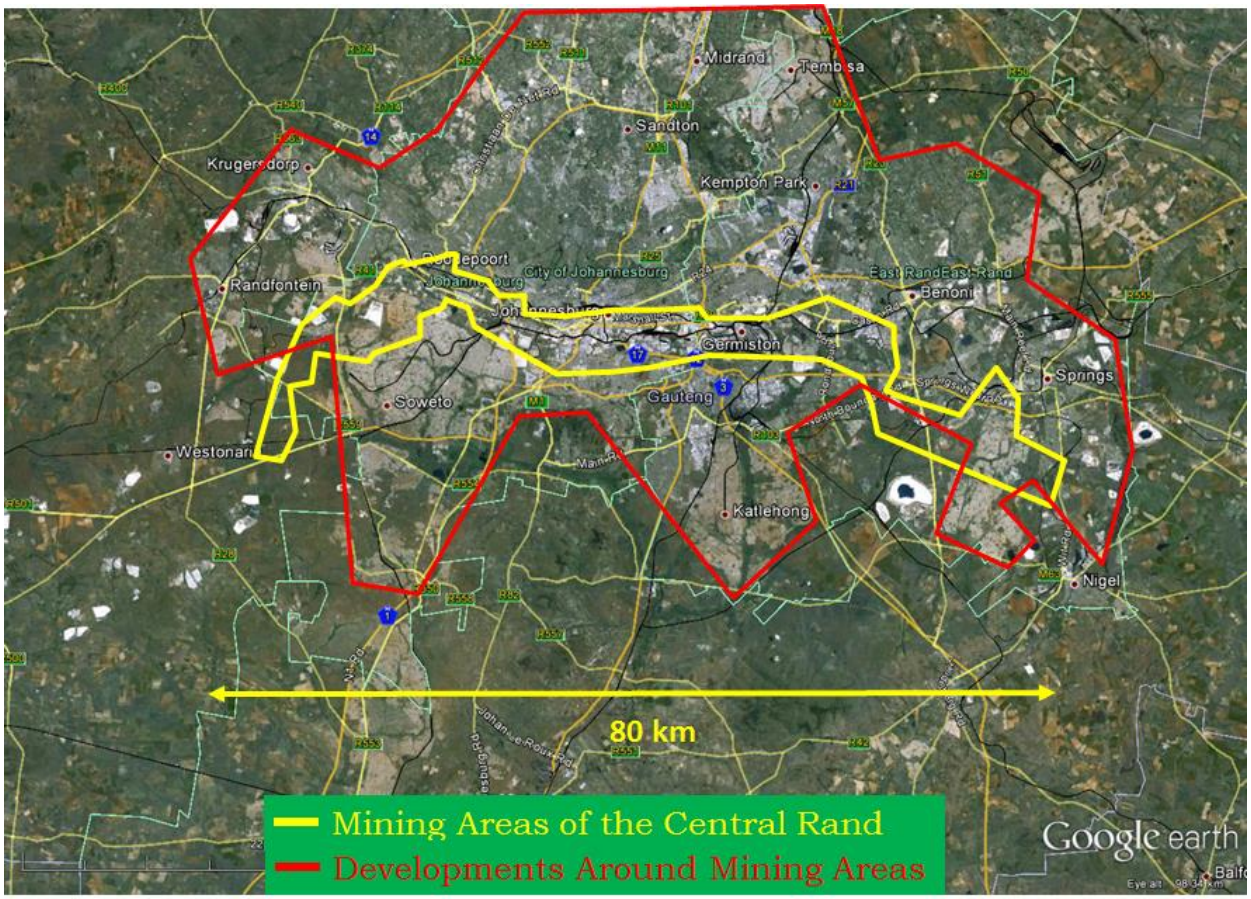


Figure 1.2 Mining areas and developments in the Central Rand, source: van der Merwe, (2013)

For a more reliable evaluation of the damaging effects, information more than just the seismic magnitude, such as ground motion histories, is essential. Therefore, for estimation of ground motions, rigorous methods are needed which would consider all aspects of complex geo-mechanics of the study area. Structural dynamic analysis requires ground motions to be estimated at the bedrock for foundation rock/soil interaction with the structure. Estimation of

site-specific ground motion is, therefore, needed for meaningful structure-foundation (rock/soil) interaction analysis.

Recent studies carried out at the University of Witwatersrand and elsewhere have suggested considerable amounts of mineable gold in the defunct Central Rand Gold Mines, Viljoen (2009). A mining company, "Central Rand Gold" is planning re-mining operations in an area spread over 40 km, Viljoen (2009). The revival of re-mining in the Central Rand in conjunction with flooding of abandoned mines is likely to increase seismicity. Future mining seismicity in close vicinity of built-up areas, therefore, needed to be investigated.

1.2. Problem Statement

As a consequence of mine closures in the Central Rand, both rate and quantum of the flooding are on the rise in the abandoned mines. The recent seismic history suggested that increased flooding had a greater potential to accelerate the triggering of the seismic source mechanisms (slip along geological discontinuities, shear failure of the rock mass, etc.). In view of the limited capability of existing techniques, uncertainty exists in estimating the seismic ground motions due to future mining-induced seismic events. The damaging effects of uncertain seismic events on the surface structures are, therefore, unknown.

Because of the existing uncertainties, there was a need to conduct research to estimate site-specific mining-induced ground motions duly considering the effects of flooding. Advanced numerical techniques, such as 3DEC and FLAC, were used to study complex geomechanical problems involving flooding and discontinuities. 3DEC is an explicit three-dimensional distinct element method for discontinuum media and FLAC is an explicit two-dimensional finite difference method for continuum media. 3DEC was used to estimate ground motions and evaluate stability of jointed rock masses to evaluate mining-induced ground motions and evaluate the effects of the estimated ground motions on masonry and concrete structures founded on rock. FLAC was used to evaluate effects of estimated ground motions on a tailing dam slope and a soil slope.

1.3. Scope and Objectives of the Research

The scope of the research was to evaluate the mining-induced seismicity duly considering the effects of flooding and its effects on surface structures. The objectives of the study included the following:

- To develop a geomechanical model of the study area encompassing geological, hydrological and stratigraphical aspects for numerical simulations.
- To evaluate site-specific ground motions due to various source mechanisms in dry and flooded conditions.
- To analyse the effect of estimated ground motions on the surface structures (soil/rock-foundation-structure interaction).
- To evaluate risk to the surface structures due to larger existing/estimated seismic parameters in flooded conditions.
- To develop a framework for the investigation of the mining-induced seismicity (ground motions) for future use/further research.

1.4. Relevance of the Research and Research Questions

The research demonstrated the capability of advanced numerical modelling techniques to study complex geomechanical problems. It enabled the evaluation of mining-induced seismicity and its effects on surface structures. Based on the research, a framework highlighting the requisite parameters, chronology and numerical tools was suggested to investigate the potential of mining-induced ground motions in the future (applicable to the entire Witwatersrand Basin). The thesis sought to answer following questions:

- How mining-induced seismicity differs from tectonic seismicity in terms of magnitude, wave propagation and intensity of ground motions?
- What is the effect of flooding of abandoned mines on ground motions?
- How effective are the available procedures for evaluating the ground motions?
- What is the efficacy of numerical codes, such as 3DEC and FLAC, for the evaluation of mining- induced seismicity?
- What risks are posed to the surface structures due to mining-induced seismicity because of flooding of abandoned mines?
- What is an appropriate framework to evaluate mining-induced seismicity and its effects on the surface structures?

1.5. Research Conceptual Framework and Methodology

The research involved the multi-disciplinary fields of engineering including mining, geological, seismological, geotechnical and structural engineering. A conceptual framework of the study is shown in Figure 1.3. The two main parts of the research encompassed the estimation of mining-induced ground motions and the evaluation of its effects on the surface structures. The methodology included the following:

- A comprehensive literature review related to the scope and objectives of the research.

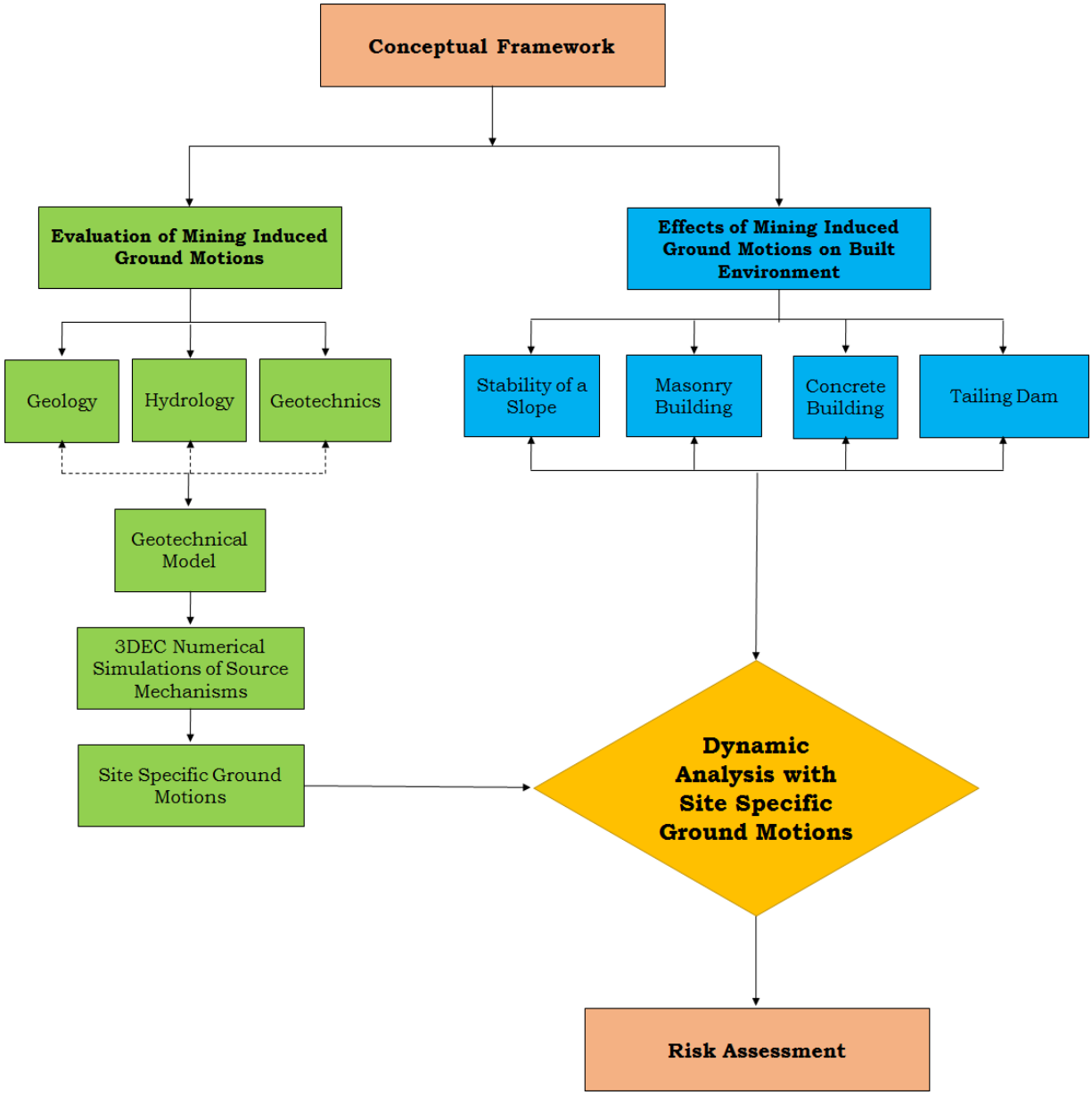


Figure 1.3 Conceptual framework of the study

- The topographical and geological data for development of the geomechanical model was obtained from the office of the Council for Geoscience, Pretoria.
- Material and joint properties required for simulation of ground motions and structural analysis were presumed in light of parameters available in the literature. Initially geotechnical investigation was planned in the study area but could not be executed due to non-availability of sufficient funds.
- Keeping in mind geological and geotechnical aspects as well as the complexity of geomechanical nature of the study area, both continuum (FLAC) and dis-continuum (3DEC) codes were used.
- 3DEC was used for the estimation of ground motions and rock-foundation-structure-analysis.
- FLAC was used for the evaluation of liquefaction potential of a tailings dam slopes and for the stability of a soil slope.
- Surface structures considered for the seismic analysis were as follows:
  - 2-storey masonry and concrete building (high frequency; 6 to 10 Hz).
  - 2-story concrete building (high frequency; 6 to 10 Hz).
  - 4-storey concrete building (medium frequency; 2 to 5 Hz).
  - 8-storey concrete building (low frequency; 0.1 to 1 Hz).
  - Jointed rock slope with building load at its crest (top).
  - Tailings dam slope and a soil slope.
  - Slip potential on a confined joint.
  - Risk to structures was assessed in terms of horizontal displacement (drift).

1.6. Thesis Structure

1.6.1. Chapter 1 – Introduction

Chapter one covers the background and introduction to the problem. It also describes the problem statement, the scope of the research, objectives of the research, research questions, conceptual framework, methodology and organization of the thesis. The significance of the study is also briefly discussed in the chapter.

1.6.2. Chapter 2 - Literature review

Chapter two reviews mining-induced seismicity in South Africa, its causal factors and characteristics, recent large magnitude seismic events, methods

available for the evaluation of mining-induced seismicity and its effects on surface structures. The effect of flooding of abandoned mines and propagation of seismic waves is also highlighted. The chapter identifies the knowledge gaps for the research.

1.6.3. Chapter 3 – Site characterization

This chapter discusses geological, hydrological, seismological and geotechnical aspects of the study area. The chapter suggests a geomechanical model for further research.

1.6.4. Chapter 4 – Methodology

Chapter four explains the methodology adopted for each component of the study and outlines the process for all the parameters involved in the study.

1.6.5. Chapter 5 – Evaluation of mining-induced seismicity

This chapter explains simulations of various source mechanisms under dry and flooded conditions. The chapter includes procedure/stages of the 3DEC simulations for mining-induced ground motions. The chapter provides a summary of ground motions due to various mechanisms and suggests ground motion in terms of velocity time history for an evaluation of its effects on surface structures.

1.6.6. Chapter 6 – Effects of mining-induced ground motions on surface structures

Chapter six evaluates the effects of the ground motions estimated in Chapter 5 on the surface structures. Details of the analysis of masonry building, concrete framed building, tailings dam and stability of a jointed rock slope are given. The chapter also identifies the possible risk.

1.6.7. Chapter 7 - Conclusions and recommendations

This chapter highlights the findings of the study and conclusions drawn. The chapter includes a recommended framework to investigate the possible mining-induced seismicity (ground motions) in future in order to evaluate the safety of surface structures.

1.7. Significance of the Study

This research would contribute to enhancing the understanding of the mining-induced seismicity among the academia and the practicing engineers. It would be beneficial for the evaluation of the safety and stability of existing surface structures as well as future construction in close vicinity of the mining areas. The study would also help refine the national building standards to enhance the safety of the lives of the public and of property.

1.8. Conclusion

The existing and potential mining-induced seismicity in the abandoned mining areas was discussed here. The implications of the seismic ground motions on the surface structures are highlighted. The need for the study is also highlighted with possible research questions to be answered. Methodology is explained to achieve the objectives of the study.

The next chapter covers a review of the mining-induced seismicity in the Central Rand and the damages experienced by the surface structures due to mining seismicity. The chapter also includes discussions and the identification of gaps regarding methods available to evaluate mining-induced seismicity with respect to seismic magnitude and intensity of ground vibrations.

2. LITERATURE REVIEW

2.1. Introduction

According to Ortlepp (2005), mining is the most dangerous pursuit of mankind. Mining-induced seismicity has been observed in many countries including South Africa. Mining-induced seismic events were first observed in Witwatersrand Basin in 1908, Wong (1993). They continue to occur in the Central Rand and elsewhere. The purpose of this chapter is to review the history of mining-induced seismicity in the Witwatersrand Basin and methods available for evaluation of mining seismicity. The review process is illustrated in Figure 2.1.

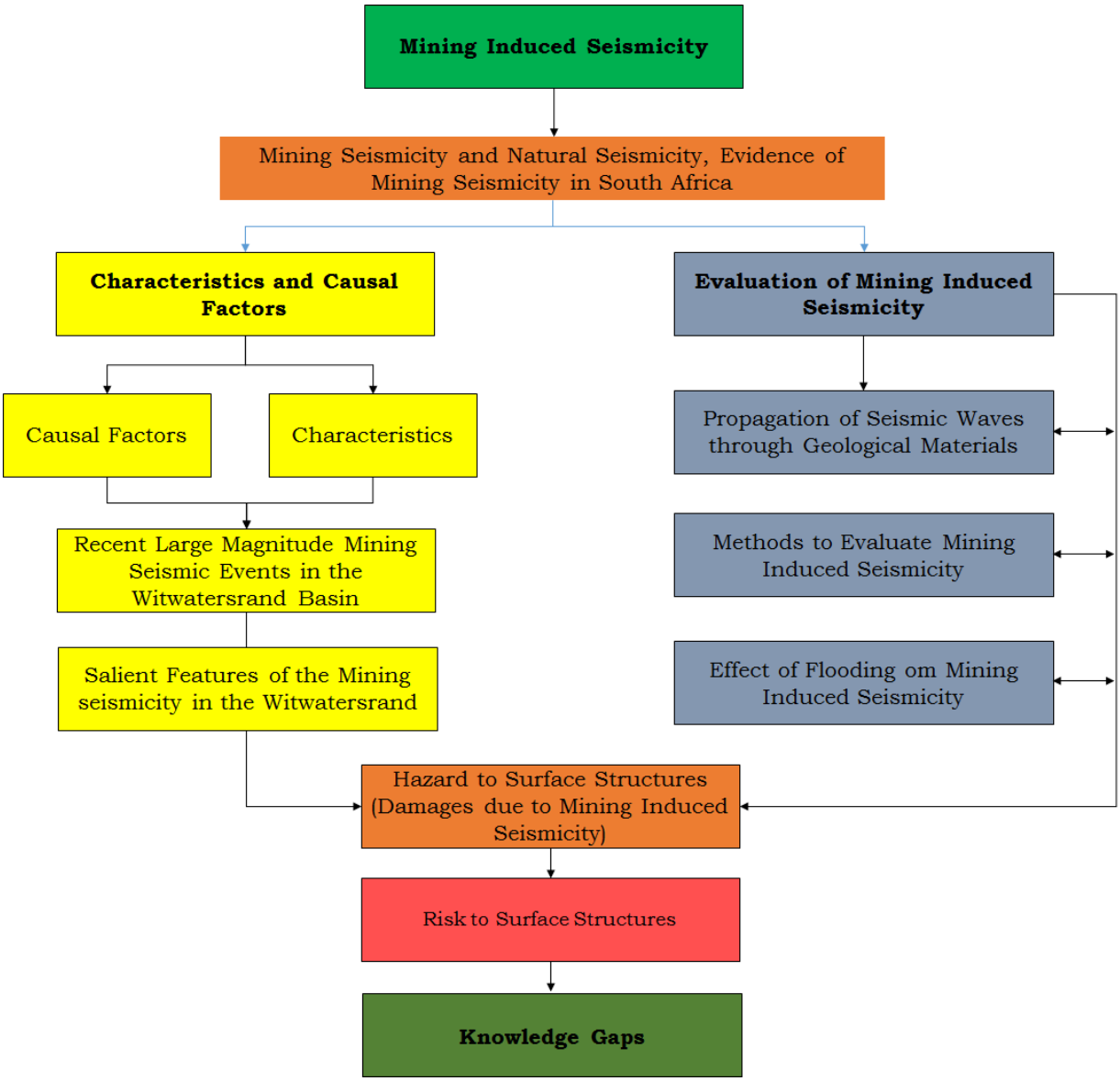


Figure 2.1 Process and components of the literature review

2.2. Natural (Tectonic) Seismicity vis-à-vis Mining-Induced Seismicity

Natural earthquakes are attributed to the conditions where stress at a certain point within the earth's crust surpasses the strength of the rocks. A causal factor of the stress increase is the motion of tectonic plates constantly taking place within the earth's crust. According to Gibson and Sandiford (2013), moderate to large natural earthquakes always occur on pre-existing faults. The rupture causes the generation of seismic waves that dissipate around 1-10% of the total elastic energy, whereas the rest of the energy is consumed in creating new fractures and heating of the surrounding rocks. The magnitude of a natural (tectonic) earthquake and its damaging potential depends on the local geology and the quality of building construction.

Gibson and Sandiford (2013) highlighted the following aspects of natural earthquakes:

- The magnitudes of natural earthquakes range from -0.30 to 9.5. The largest known earthquake recorded was in Chile in 1960.
- Natural earthquakes of magnitude smaller than 3 are felt/heard but rarely cause structural damage.
- The attenuation of ground motion depends on the distance from the source and the soil/rock properties of the candidate site. Unconsolidated hot or young rocks attenuate seismic motion more rapidly with distance than hard, cold or old rocks. This increase is because of the greater energy loss per cycle due to the non-elastic behavior of the materials.
- The variation in attenuation is most significant for high frequency motion. Therefore, most scales are based on displacement which emphasize low frequency motion (natural earthquakes are mostly low frequency earthquakes).

Earthquakes triggered by human activities, such as filling of reservoirs, mining and hydraulic fracturing, are classified as "induced" earthquakes. Large-scale mining activity both at surface and underground can trigger earthquakes. Underground mining manifests in change of stress distribution as a result of blasting and excavations which trigger induced earthquakes of various magnitudes. According to Gibson and Sandiford (2013), earthquakes of a

magnitude as high as 2 are not uncommon due to mining. Large mines can trigger earthquakes as high as magnitude 4 and a maximum magnitude of 5.5 has been observed in mining-related earthquakes.

The induced earthquakes are caused either by a change in stress (mostly vertical stress such as loading due to reservoir pounding or un-loading in an open mine) or a decrease in the shear strength along the faults/joints. According to Gibson and Sandiford (2013), since it is not easy to change horizontal stress, most induced earthquakes are due to increase in pore pressure, that is, a decrease in shear strength along the weak faults.

2.3. Mining-Induced Seismicity: Evidence and Pattern in South Africa

The Witwatersrand Basin is a NE-SW trending basin spread over an area of 450 x 300 km with a 7 km thick sedimentary system, Ryder and Jager (2002), Figure 2.2. The basin owes its importance to the fact that it holds the world's largest gold reserves, estimated to be 70,000 tonnes in 30 different reefs, Ryder and Jager (2002). The gold-mining history in South Africa dates back to 1886, Handley (2014). Gold mining continues today in some parts of the Basin.

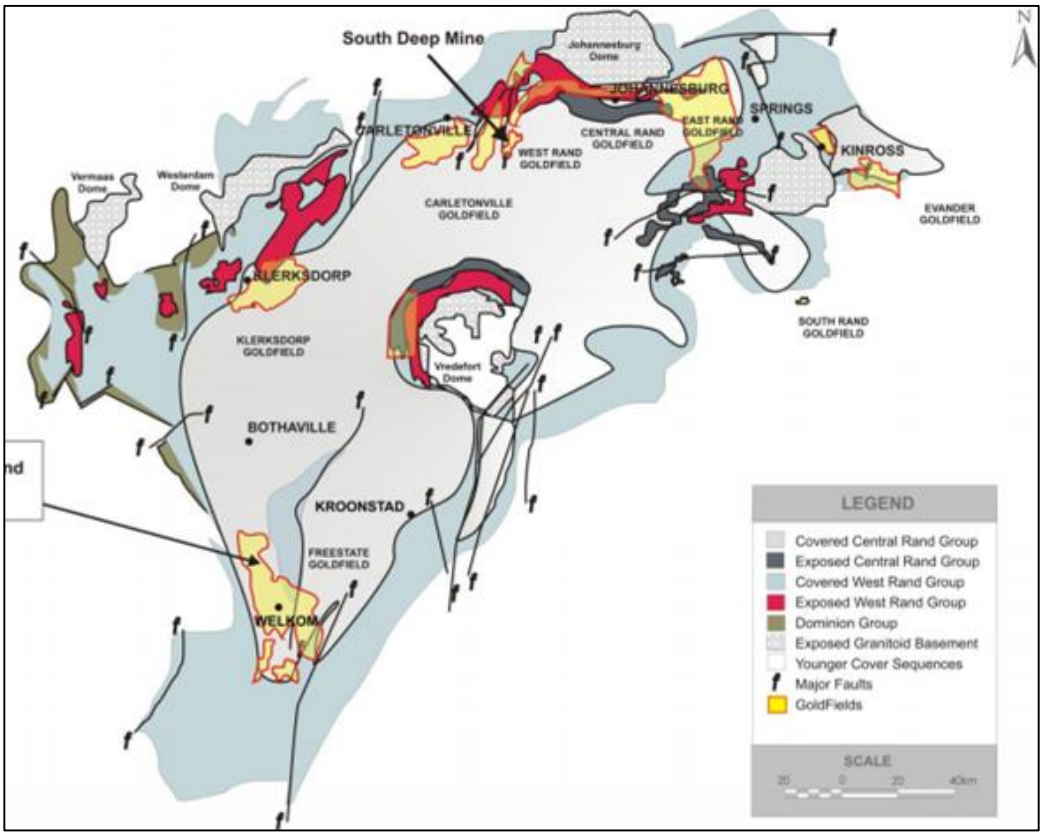


Figure 2.2 Witwatersrand Basin, Randgold (2010)

Some of the major gold-bearing reefs are located immediately south of the CBD, Johannesburg, Hill et al. (1981) and Mphephu (2001), as shown in Figure 2.3. The Main Reef dips steeply at 30°-70°, Bird Reef dips at 31°-37°, whereas Kimberley Reef dips at 31°. At present, mining depths are as deep as 4000 m in an extensional but inactive tectonic setting and extend around 6.2 kilometres down the dip along the Main Reef Leader, McGarr et al. (2002). Mining excavations in the steeply dipping/sub-horizontal gold-bearing reefs induce substantial stress changes in the brittle rocks abutting the stopes thereby manifesting in high levels of seismicity, McGarr, et al., (2002).

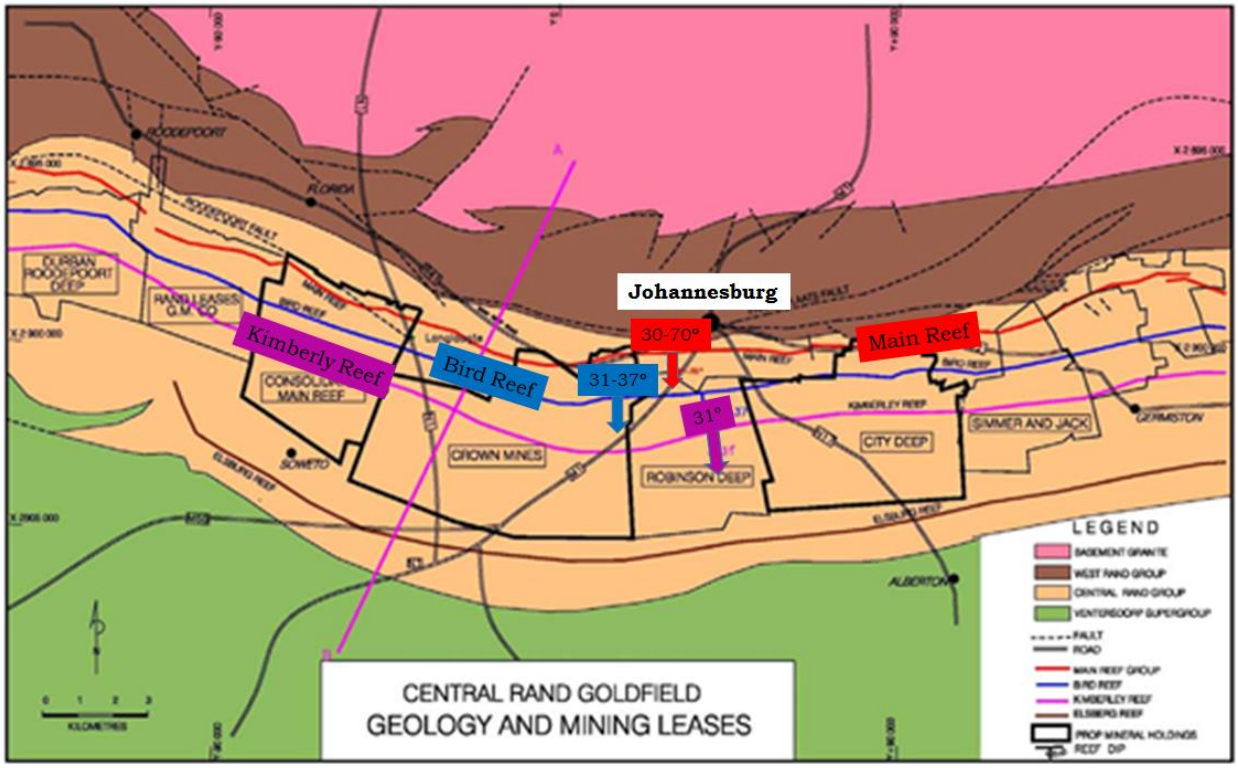


Figure 2.3 Central Rand Gold Reefs and Goldfields, Mphephu (2001)

Mining-induced seismicity in the Witwatersrand Basin has a long history. According to McDonald (1982), the study of "anthropogenic seismicity" commenced in 1894 at a time when earthquakes were first felt in Johannesburg. By 1908, the seismicity in Johannesburg was attributed to mining activity in the Witwatersrand Basin, Cook et al. (1966) and Wong (1993). According to Viljoen (2009), mining-induced seismicity has been quite common around abandoned mines ever since the mines started closing. In view of the enhanced seismicity around abandoned mines, the Council for Geoscience (CGS) started monitoring

seismicity through a network of twelve seismological stations in the Witwatersrand Basin, Figure 2.4. The purpose of the monitoring was to locate epicentres and record source parameters. According to Council for Geoscience (2013), the monitoring network revealed a pattern of seismicity which clusters along faults and dykes around abandoned mines, Figure 2.4. The study area is marked/highlighted in Figures 2.4 and 2.5.



Figure 2.4 Location of seismological stations in the Witwatersrand Basin, Council for Geoscience (2013)

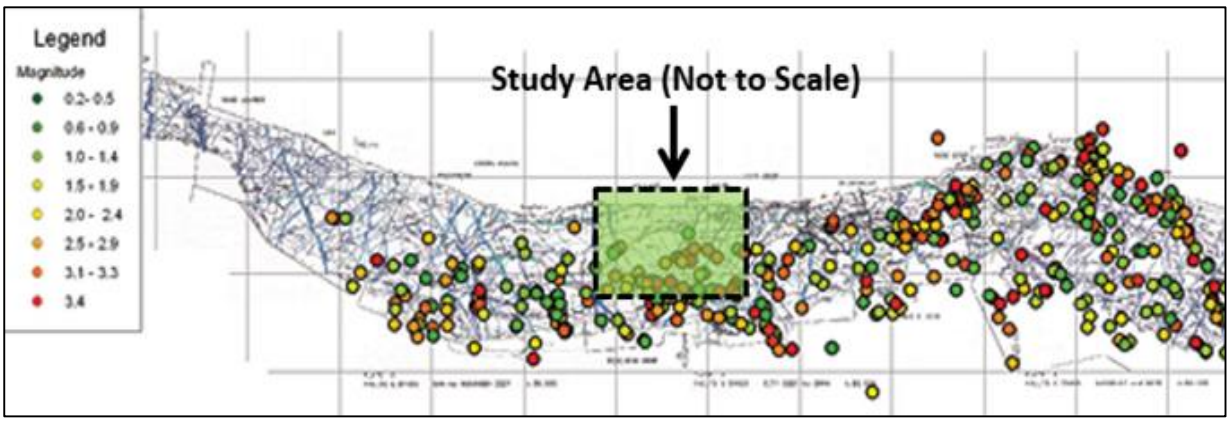


Figure 2.5 Study area and location of mining induced earthquakes in the Central Rand, CGS, (2012)

2.3.1. Seismic scales (magnitude and intensity) in South Africa

Several different scales are used to measure earthquake magnitudes depending on P, S or Surface wave and motion of frequencies. The most common scales are the energy of seismogram (M_e), the maximum displacement of a particular phase (m_B), Richter's local magnitude (M_L), etc. In South Africa, various scales are used to describe the size of the seismic event. According to Gibowicz and Kijko (1994), the local magnitude scale is pervasive and widely used in South Africa. In this study, the local magnitude is used to describe the magnitudes of the seismic events. Salient points regarding earthquake scales highlighted by Gibson and Sandiford (2013) are given as follows:

- Richter scale "M_L" is suitable for small scale earthquakes up to M_L=5.0 within 600 km of seismometer.
- Moment magnitude "M_W" is based on low frequency spectral displacement and is best from M_W 6 to M_W 9.
- Energy magnitude "M_e" is based on high frequency motion.
- Although, originally, all earthquake scales were defined to be consistent with original "M_L" scale, their consistency is restricted to a limited zone.

The seismic scales are correlated to each other and the desired scale can be calculated according to the purpose or preference. According to Hanks and Kanamori (1979), moment magnitude, seismic moment and seismic energy are related according to the Equations 2.1 through 2.3.

$$M_w = \frac{2}{3} log_{10} M_0 - 10.7, \qquad \text{Equation 2.1}$$

$$M_e = \frac{2}{3} log_{10} E_s - 2.9, \qquad \text{Equation 2.2}$$

$$E_s = M_0 \text{ X } 10^{-4.8}, \qquad \text{Equation 2.3}$$

Where,

M_w = moment magnitude (dimensionless number),

M_0 = seismic moment (N-m),

E_s= seismic energy (N-m).

2.4. Causal Factors and Characteristics of Mining-induced Seismicity

2.4.1. Causal factors

McGarr et al. (2002)

According to McGarr, et al. (2002), mining activities are likely to cause changes in the stress state, pore pressure, volume and the applied forces (loads) in the mining areas. In cases where induced stress change equals the ambient shear stress acting on a fault, slip is triggered resulting in a seismic event, McGarr, et al. (2002). McGarr, et al., (1989) attributed earthquakes of magnitude as high as 5.2 in Klerksdorp District to the pre-existing faults and dykes. Besides mining, the induced seismicity is also attributed to quarrying, fluid injection, fluid extraction and reservoir impoundment, as shown in Figure 2.6.

Spottiswoode et al. (1975), Brummer and Rorke (1990), **Dor et al. (2001)**

Many researchers, such as Spottiswoode et al. (1975), Dor et al. (2001), Brummer and Rorke (1990), associate large rock bursts as one of the causal factors of mining-induced seismicity, with pre-existing geological features, such as faults and dykes. Spottiswoode et al. (1975), also attribute many large seismic events in mining areas to shear failure on existing faults or other weak geological structures. Dor. et al., (2001) investigated the Welkom Mine earthquakes and indicated that earthquakes larger than magnitude 4.0 induce into displacements along geological faults.

Hasegawa et al., (1989)

Hasegawa et al. (1989) proposed six different mechanisms for the mining-induced seismicity as shown in Figure 2.7 and include cavity collapse (fall of ground), pillar burst and tensional failure of the cap-rock.

Kijko and Cichowicz (2006)

As per Kijko and Cichowicz (2006), earthquakes in the mining areas are a result of a sudden release of energy within a confined region that undergoes deformations. As a result of these deformations, elastic strain energy is stored till the time stress levels reach the rock strength. Thereafter, the rock mass undergoes failure, fracture and /or faulting occurs and energy is released in the form of heat, the crushing of rock and the generation of seismic waves. As

described by various researchers, the causal and triggering factors of mining-induced seismicity are numerous with varying potential of seismic magnitude and risk. In short, mining-induced seismicity is attributed to the following aspects:

- Failure of the rock mass on pre-existing geological features such as faults, dykes and joints, which results in medium- to large-size events often far away from the mine workings.
- Failure of intact rock mass in the form of shear fractures resulting in large events close to workings.

Failure of brittle rock mass or localized rock bursting often called strain-bursting or face-bursting, resulting in small events close to mine workings.

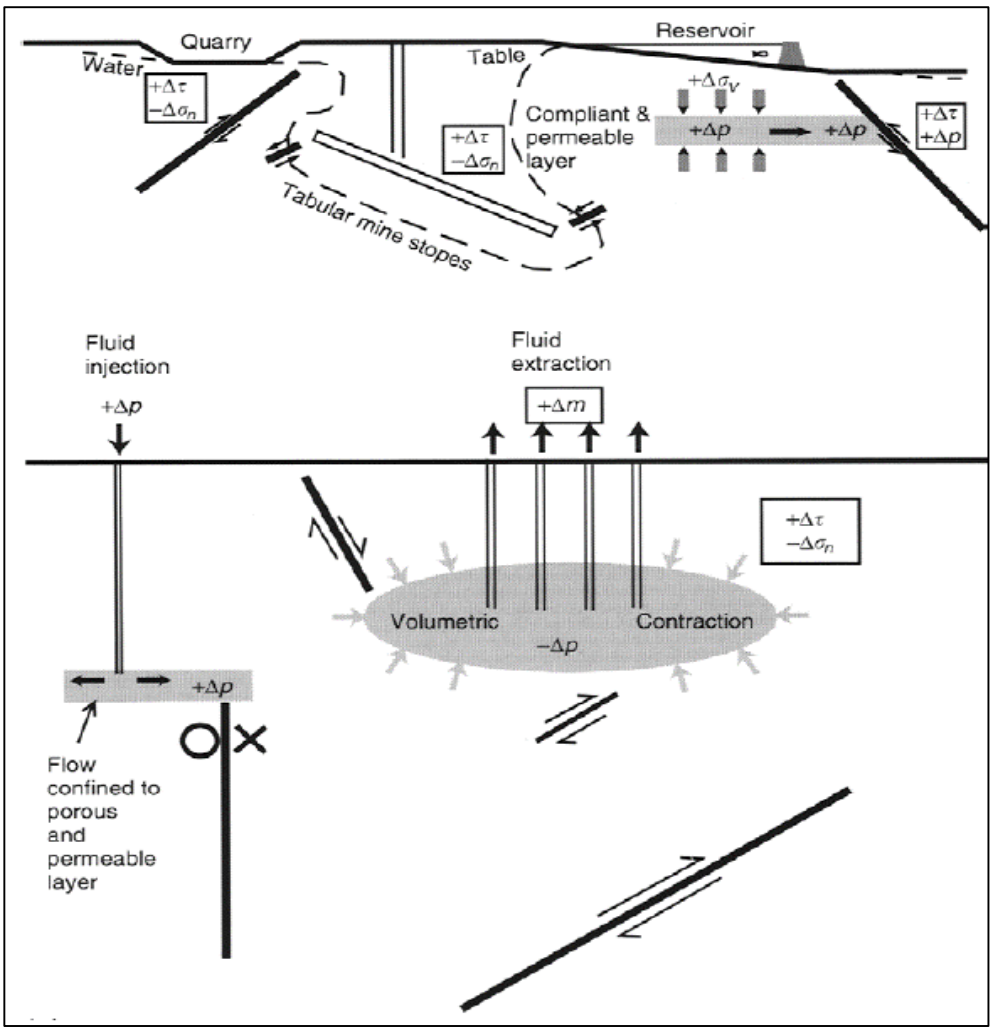


Figure 2.6 Sources of induced seismicity; changes in shear stress (Δt), pore pressure (Δp), volume change (Δv) and applied forces (Δn), McGarr et al. (2002)

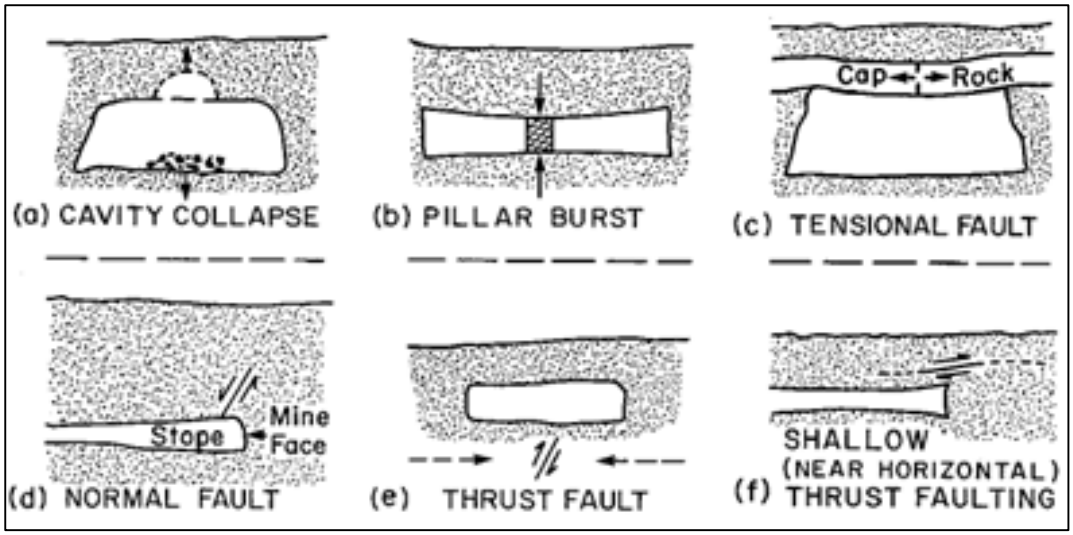


Figure 2.7 Mechanism for mining seismicity, Hasegawa et al., (1989)

2.4.2. Characteristics of the mining-induced seismicity highlighted by various researchers

Mining-induced seismic events are characterized with very high frequency, very short duration, rapid attenuation, and shallow focal depths. According to Bennitt, (1995), rock burst-induced seismic events behave as "explosion like" events, with very short duration/time period, and with low excitation of long-period waves (Rayleigh waves).

A recorded velocity time history at Savuka Mine, South Africa, of an underground seismic event is shown in Figure 2.8. Its peak velocity record at surface is shown in Figure 2.9. These records indicate a very short duration (less than a second) of the mining-induced seismic events. On the basis of the peak velocity, the United States Geological Survey shake map of the Orkney earthquake shows that the event belongs to the "strong" category of earthquakes (Intensity VI) with peak velocity of 6.5 cm/sec, USGS 2014).

A predominant component of peak particle velocities of the seismic events at Tau Tona Mine is shown in Figure 2.10, Milev and Spottiswoode (2005). According to this figure, around 1000 seismic events are characterized with peak particle velocities ranging from 0.1 to 1000 mm/sec. Although there is no mention of the source mechanism of these seismic events, it is considered that these events comprise all kinds of source mechanisms.

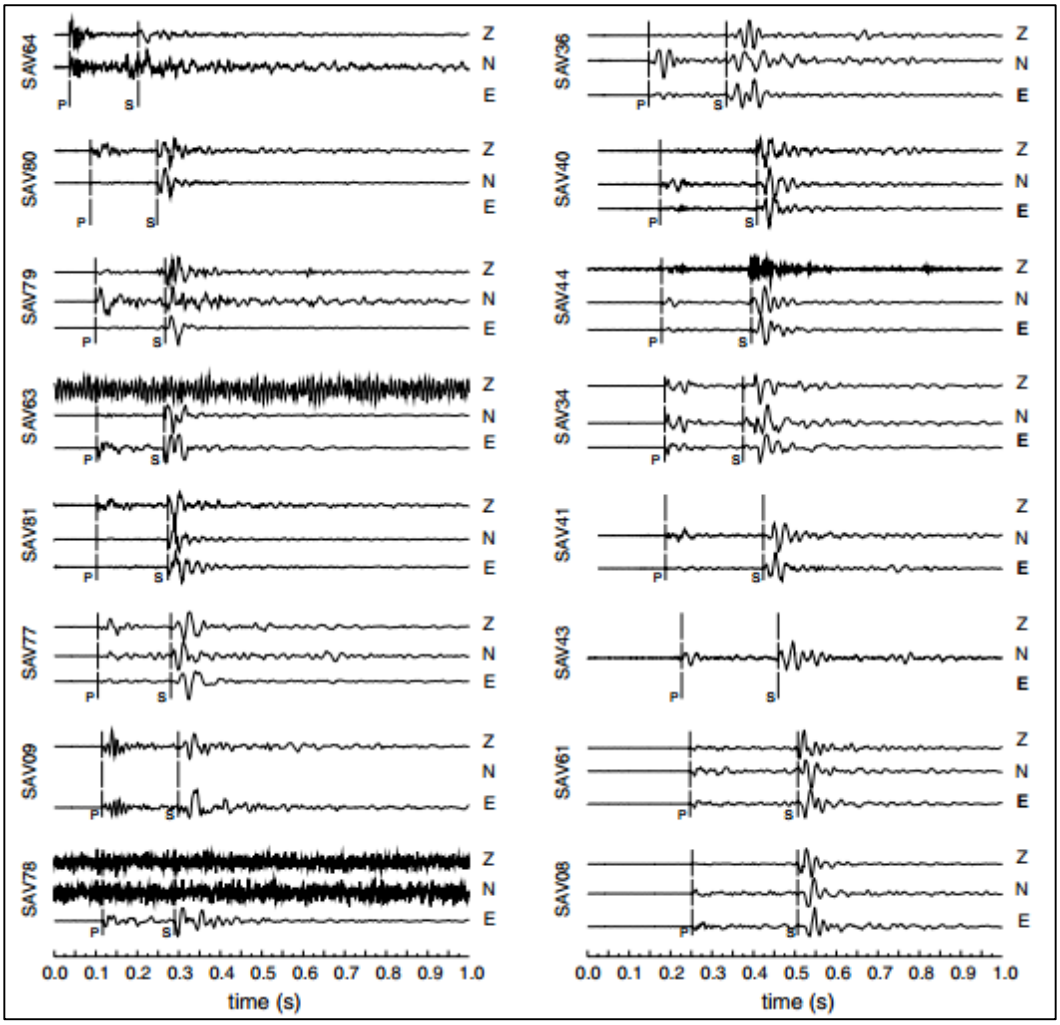


Figure 2.8 Velocity time history of a mining induced earthquake at Savuka Mine, South Africa, Julia et al. (2009)

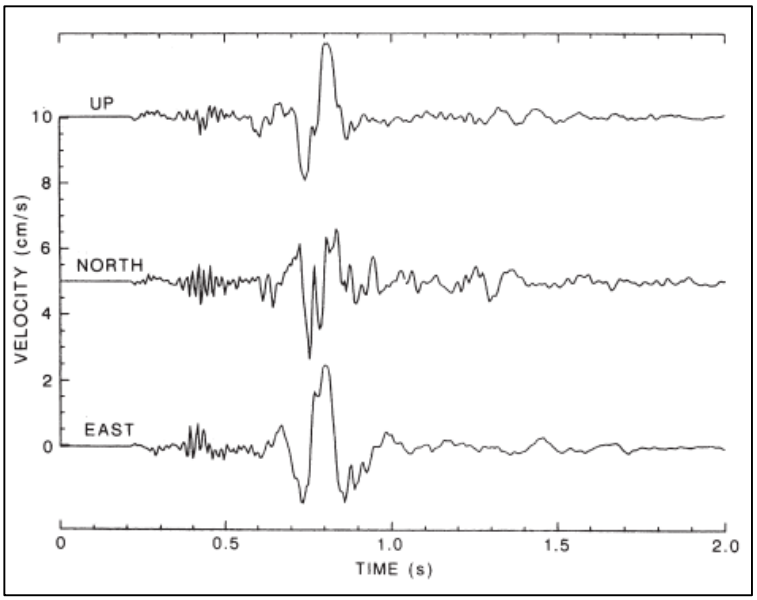


Figure 2.9 Peak velocity recorded at surface, 2.7 km above the source due to a mining induced earthquake of M4.4, McGarr (2002)

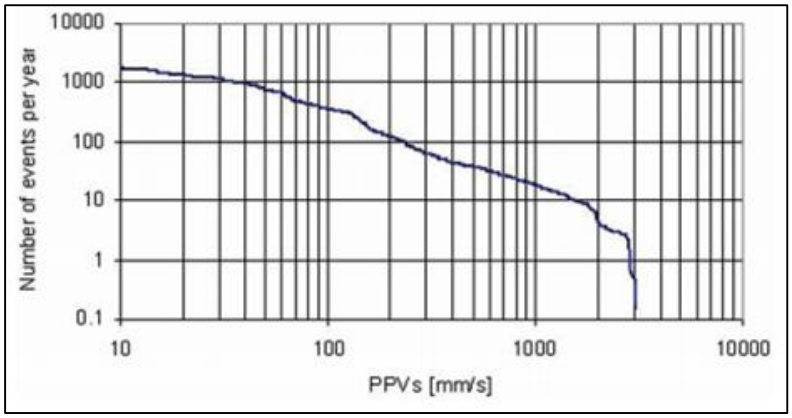


Figure 2.10 Peak particle velocities of the seismic events at Tau Tona mine, Milev and Spottiswoode (2005)

Correlation of peak velocity, magnitude and distance, proposed by Potvin and Wesseloo, (2010), for South African mining areas, shown in Figure 2.11, suggests a peak velocity of around 6 mm/sec for a seismic event of M_L 3.5 at a distance of 1000 m. A similar relationship suggested by Saebimoghaddam, (2010) regarding Canadian mining areas is shown in Figure 2.12. According to Zembaty (2003), ground motions of rock burst-induced seismicity in copper mines in Western Poland, in terms of acceleration and velocity varied from 0.05-0.15 g and 3-10 cm/sec respectively. For comparison with natural earthquakes, peak velocity and magnitude data of earthquakes (tectonic) in California, USA, proposed by Boore (1980) is given in Table 4.1.

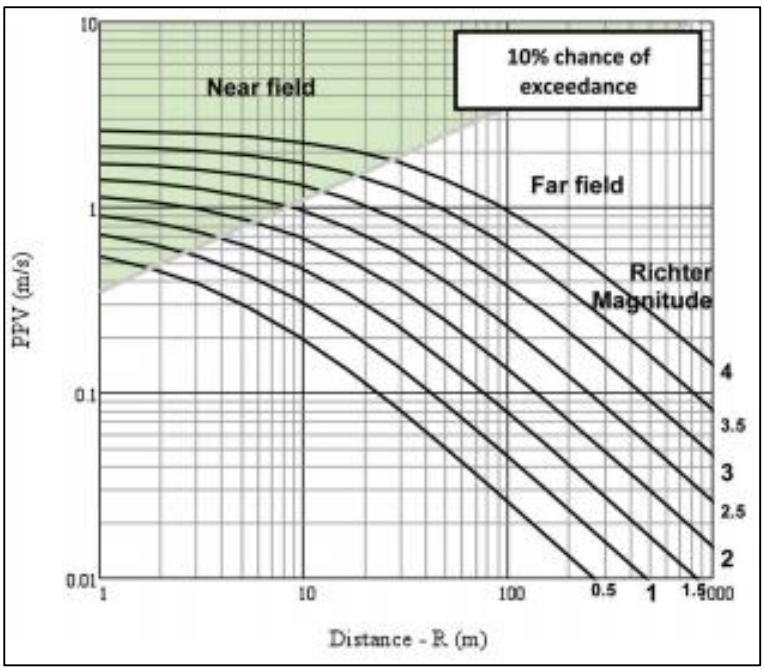


Figure 2.11 Correlation of peak velocity, magnitude and distance in South Africa mining areas, Potvin and Wesseloo (2010)

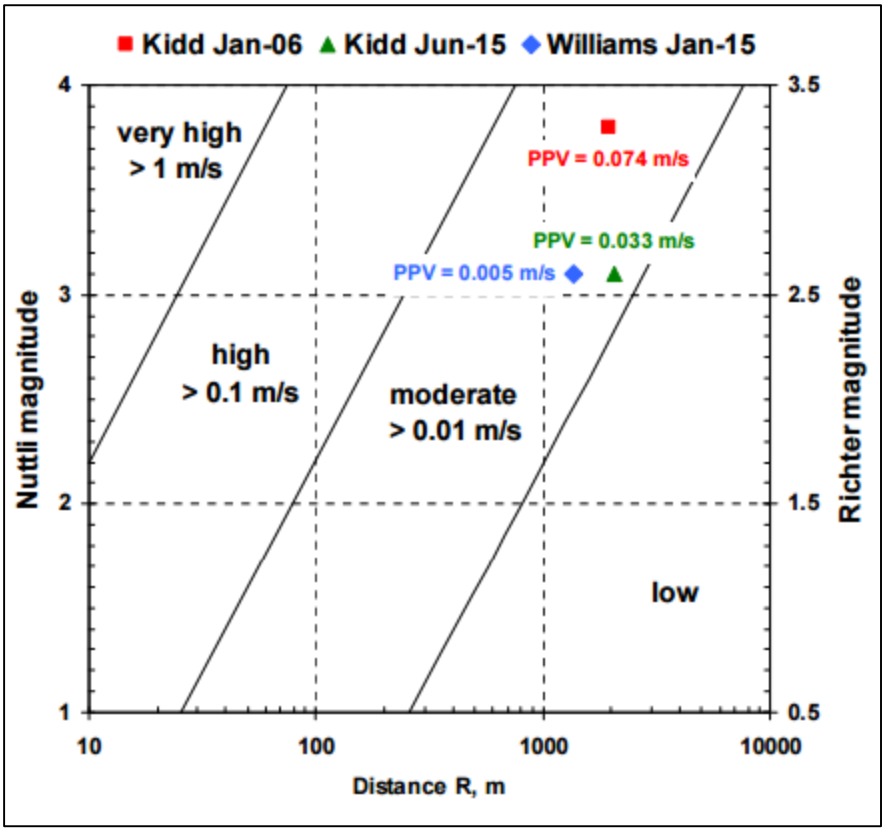


Figure 2.12 Level of mining induced (rockburst) ground motions, Saebimoghaddam (2010)

Table 2.1 Peak velocity and magnitude data from California earthquakes, Boore (1980)

Event	M_L	Station/Distance[2] (km)	Peak Velocity (cm/sec)
Imperial Valley, 1979	6.5	(interpolated)/10	45[1]
Imperial Valley, 1940	6.4	El Centro/6	37
San Fernando, 1971	6.4	Pacoima Dam/3	110
Long Beach, 1933	6.3	Public Utilities Bldg./∿15	30
Oroville, 1975	5.7	Oroville Dam/8	5.0
Parkfield, 1966	5.5	Cholame-Shandon #2/7	78
Lytle Creek, 1970	5.4	Wrightwood/15	9.6
Oroville, 1975	4.7	CDMG #5/12	7.7
Oroville, 1975	4.0	CDMG #5/11	2.1
Bear Valley, 1973	3.9	PNM/13	1.2
Oroville, 1975	3.6	CDMG #5/12	1.0

The emphasis of the review of characteristics of mining-induced seismicity (ground motions) was to understand the general trend in peak velocities and duration observed in South Africa and elsewhere (on the basis of peak velocity

vis-à-vis magnitude). During the course of research, the source mechanisms were triggered, such that the estimated ground motions were approximately close to those observed in the Witwatersrand Basin. Keeping in mind the discussion on peak velocity and magnitude data, salient points are listed as follows:

- From Figure 2.11, it is revealed that the seismic events of magnitudes M_L 2, M_L 3, and M_L 4 (Richter Magnitude) at a distance of 500 m from the source produce peak velocities of 1.5 cm/sec, 5 cm/sec and 15 cm/sec respectively.
- From Figure 2.12, peak velocities of seismic events of magnitude M_L 2.5 to M_L 3.5, at a distance of 1100 m from the source, vary from 5 mm/sec to 7.4 cm/sec.
- According to Table 2.1, peak velocities of natural earthquakes of magnitude M_L 3.6 to M_L 4.7 vary from 1 cm/sec to 7.7 cm/sec.
- Although, peak velocities of the natural and the mining-induced seismic events appear to have similar trends, their dynamics are very different.
- The natural earthquakes are a consequence of the release of very large amounts of seismic energy compared to the mining-induced earthquakes. Also, the natural earthquakes are recorded at relatively greater distances than the mining-induced earthquakes. The two are described only with a view to highlight the pattern of peak velocities vis-à-vis magnitudes.

2.4.2. Recent large magnitude mining-induced seismic events and their damage to surface structures

Welkom district

On 8 December 1976, a seismic event of M_L 5.2, struck the Welkom district which resulted in the collapse of a large multi-storey block of flats in the centre of the town, Fernandez and Guzman (1977), Figure 2.13. Fortunately, there was no loss of life in the event. Other buildings in the near vicinity also suffered extensive damages. Brick masonry buildings suffered from diagonal shear cracks.



Figure 2.13 Damage to a multi-storey building during M_L 5.2 seismic event in Welkom area, Durrheim et al. (2006)

Klerksdorp district

According to Fernandez and Van der Heever, (1984), a seismic event of M_L 5.2 occurred on 7 April 1977 in Klerksdorp district. The event resulted in appreciable damage to surface structures in all the surrounding towns located within 6 km from the epicentre. The most common types of damage to structures included broken windows, corner cracks varying in length from 50 cm to 3 m and cracks in brick walls as long as 1.5 m and 5 mm wide.

The seismic event also rendered the access tunnels in the Vaal Reefs gold mine inaccessible, whereas ground falls were reported over an area of 7 km^2 around the epicentre. The seismic event was characterized with the horizontal acceleration of 0.5 g at an epicentral distance of 2.5 km and dominant energy in the frequency range of 10-15 Hz. According to Bejaichund and Hattingh (2009), a seismic event of M_L 4.9 occurred on 6 September 2004 in the Stilfontein area in the Klerksdorp district. The tremors were noticed in high-rise buildings in Pretoria (200 km away from the epicentre) and in the Potchefstroom area, some 50 km away. No serious damage was reported in the event.

A seismic event of M_L 5.3 occurred in the Stilfontein area on 9 March 2005. According to Goldbach (2009), the event killed two miners and caused damage

to several buildings. According to Saunders, et al., (2007), buildings in the Stilfontein CBD area suffered extensive damage. Some flats in Bel-Eaton building, Figure 2.14, were declared unsafe for public residence, whereas some other masonry buildings, Figure 2.15, also suffered damage including broken windows, cracks in the walls, etc. The diagonal pattern of cracks in walls is the typical pattern observed due to cyclic loading. The pattern varies according to the layout of the building, size and spacing of doors, windows, presence or absence of lintels, quality of construction, etc.



Figure 2.14 Damage to the Bel-Eaton court building during M_L 5.3 seismic event in Stilfontein area, source: van der Merwe, (2013)



Figure 2.15 Damage to the masonry building during M_L 5.3 seismic event in Stilfontein area, source: van der Merwe, (2013)

Orkney district

The most recent and largest mining-induced seismic event of M_L 5.3, struck Orkney, on 5 August 2014. It was the largest mine-related earthquake. The earthquake caused one fatality, injured 38 people and damaged 400 homes, Vervaeck (2014). Damage to some of the buildings due to this seismic event is shown in Figure 2.17.



Figure 2.16 Damage due to ML 5.3, Orkney seismic event on 5 August 2014. A; pointed masonry building, B; plastered masonry building, Varvaeck (2014) C; ground displacements, D; ceiling, Varvaeck (2014)

The event resulted in substantial damage to underground facilities, whereas damage to the surface structures was relatively low. Shake map of 5 August 2014, Orkney seismic event is shown in Figure 2.17, USGS (2014). According to the shake map, the event belonged to intensity VI with acceleration of 0.8 g and velocity of 6.5 cm/sec at the epicenter.

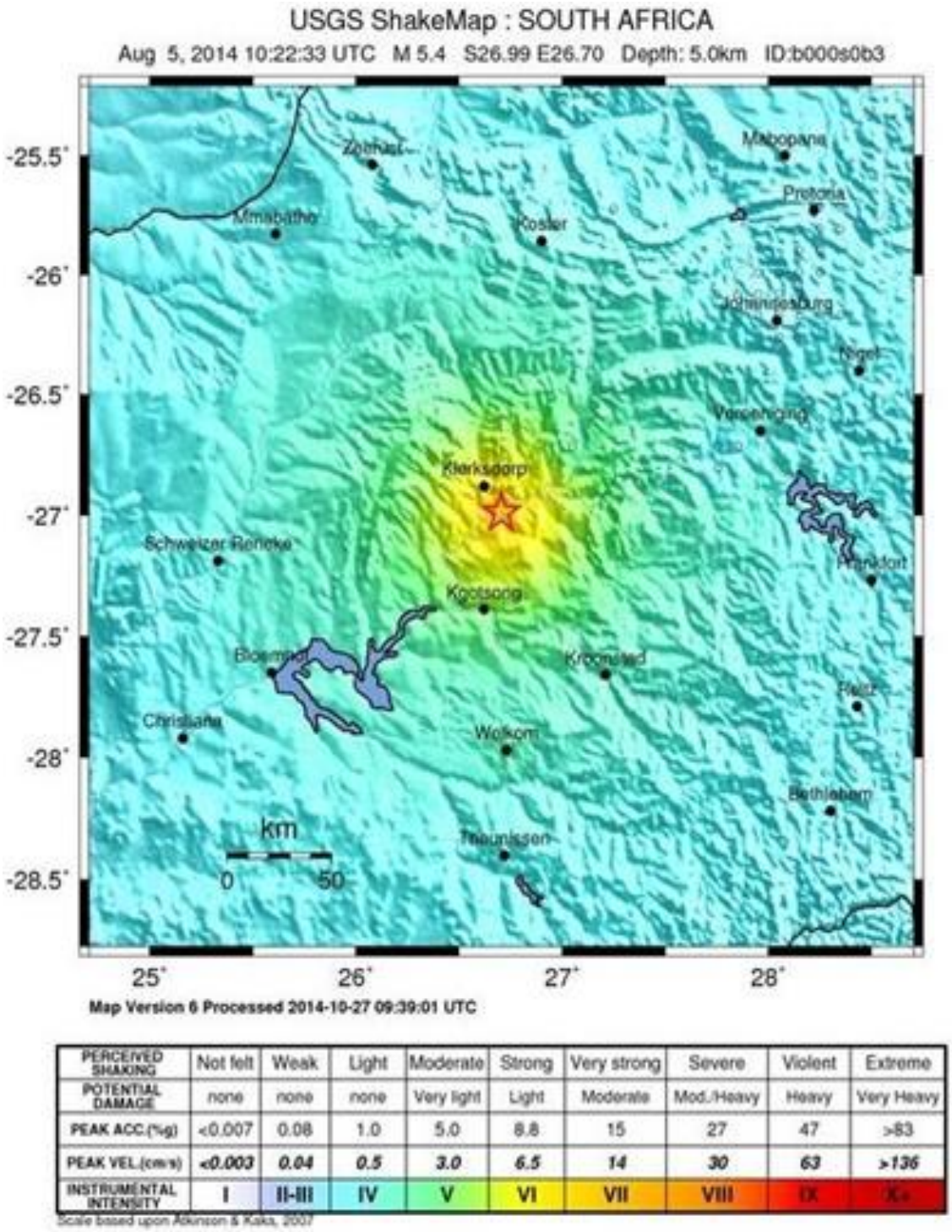


Figure 2.17 Shake map of 5 August 2014, Orkney seismic event, USGS (2014)

2.4.3. Salient features of the mining-induced seismicity in the Central Rand, Witwatersrand Basin

Salient characteristics of the mining-induced seismic events in the Central Rand, Witwatersrand are compared to the shake map of the recent event at Orkney. The salient points are summarized as follows:

- The seismic events of M_L 1 to M_L 4 (existing seismic history) corresponding with Modified Mercalli Intensity of I to IV are described as “feeble” to “moderate”.
- According to Figure 2.17, the peak velocity of this range of seismic events range from 0.03 mm/sec to 5 mm/sec. This range of seismicity in not likely to cause any structural damage.
- Seismic events of M_L 4.7 to M_L 5.3 corresponding with Modified Mercalli Intensity of IV to VI are described as “moderate” to “strong”.
- According to Figure 2.17, peak velocities of seismic events of intensity IV, V, and VI are 0.50 cm/sec, 3.0 cm/sec and 6.50 cm/sec respectively.
- The damage potential of seismic events of intensity IV, V, and VI vary from “none”, to “very light” to “light” respectively.
- Dominant energy of the ground motions is observed to be in the frequency range of 10-15 Hz.
- Durations of the seismic events vary from a few seconds to as much as 10 seconds.

Trollope, et al. (2014) highlighted the following salient aspects related to seismic magnitudes in South African mining areas:

- Mining-induced seismic events are generally shallower than 4000m with magnitude (M_L) < 5.5.
- A seismic event with M_L = 2 is barely perceptible at the ground surface. However, it can cause serious damage to mine workings located close to the seismic source.
- The risk of damage and injury is most pronounced within a 1 km radius of the seismic source.

2.5. Evaluation of Mining-induced Seismicity

2.5.1. Propagation of seismic waves through geological media

Material stiffness properties

Propagation of elastic waves in an elastic anisotropic heterogeneous model is influenced by the stiffness properties of the stratigraphic units and orientation of geological discontinuities. The geological structures cause plurality of seismic

waves due to various velocities of propagating waves across discontinuities because of multiple refraction and reflection processes. According to Ryder and Jager (2002), the most important consequence of the plurality of waves of different velocities at the interface(s) is the distortion of the source waveform. This distortion results in scattering/variable wave attenuation patterns across the media and poses considerable practical difficulties in recording the ground motions.

Geometrical, hydrological and infill material properties

The propagation of seismic waves (body waves; P-waves and S-waves) in abandoned mines is affected by the geomechanical properties of gouge material (if present along joints), geometrical aspects (size, layout, orientation, etc.) and hydrological aspects (dry, partially filled, completely filled, etc.) of the mining voids. In rocks, the body waves (P-waves and S-waves) propagate in a slightly different manner; P-waves propagate through the rock mineral and the pores, whereas S-waves travel through the rock mineral only (not through pores).

According to Eitzenberger (2012), P-wave velocity in highly porous saturated rocks is lower than in less porous rocks, whereas the S-wave velocity is nearly insensitive to water saturation as it travels through the mineral structure only. Water saturation, however, does influence the shear strength of the rock mass and joints which directly affects the triggering of the seismic source.

Stiffness properties of the discontinuities

According to Eitzenberger (2012), joint (discontinuity) properties influencing the propagation of waves are joint shear stiffness, joint normal stiffness, number and spacing of the discontinuities. The amplitudes of transmitted and reflected waves depend on the angle of incidence of a seismic wave and geometrical properties of the discontinuity as well as constitutive model considered for the rock mass and discontinuity. In the case of upper rock mass (roof/overburden) with properties different than the host rock mass, this condition normally amplifies the peak particle velocity especially in the horizontal direction at the ground surface, Eitzenberger (2012).

Wave frequency and wavelength

Frequency and wavelength is another important parameter affecting the wave propagation through the rock mass. A high frequency wave (short wavelength) has the most part of the wave reflected whereas in the case of low frequency wave (long wavelength), the most part of the wave energy is transmitted, Pyrak-Notle, et al. (1990B). At the welded interface of geological materials (high shear strength and stiffness properties), wave frequency has no effect on amplitude of reflected and refracted waves, Eitzenberger (2012). In this research, the joints are considered welded therefore, it is considered that the propagation of seismic waves is not affected by the frequency content. However, jointing is important in relation to presence/absence of water in joints/mining voids.

Effect of free surface (ground surface)

A free surface induces wave reflections. Therefore, the waveform (ground motion) recorded at ground surface is inappropriate for direct use in the dynamic analysis for the surface structures. The ground motions specified for a particular site, such as those required for seismic design of structures, are the outcrop motions which must be de-convoluted to the depth of bedrock before using for the structural analysis.

Attenuation of seismic waves

Attenuation refers to the changes in seismic wave amplitudes and, as described earlier, it is influenced by the geometrical spreading, reflection, scattering, geological discontinuities, material stiffness and intrinsic damping. According to Toksoz et al. (1979), the attenuation of seismic waves (P and S waves) in rocks strongly depends on the physical state, that is, dry or flooded/saturated conditions. With changes in the physical conditions of the rocks, variation in attenuation is more pronounced than the seismic wave velocities.

Attenuation of seismic waves in rocks is measured in the laboratory using techniques such as pulse transmission, spectral ratio, etc. The measurements have shown that fluid saturation (flooded/saturated conditions) increases attenuation, whereas increasing pressure (rocks at depth) decreases attenuation, Gardner, et al. (1964). According to Ryder and Jager (2002), in far field conditions (where distance from source is much larger than the size of the

source), site effects that attenuate more rapidly with distance become less important.

2.5.1 Empirical methods

The causal factors of mining-induced seismicity have already been discussed. The focus of this research included seismicity due to three sources: slip, falls of ground and pillar collapse. The procedures/methods to evaluate seismicity from these sources are discussed as follows:

Joint/fault slip (seismic moment-magnitude correlation)

In order to simulate a mining-induced seismic event due to impulsive slip, guidelines were taken from Aki and Richards (1980) and Hanks and Kanamori, (1979) for seismic moment energy/earthquake magnitude and magnitude/area of slip respectively. The seismic moment was evaluated based on the relationship proposed by Aki and Richards (1980) using parameters of the area of slip, the magnitude of slip, and rock mass shear modulus, given by Equation 2.4.

$$M_\circ = G u_s A, \qquad \text{Equation 2.4}$$

Where, G is the rock mass shear modulus, u_s is average slip and A is the slip area. The seismic moment $M_\circ$ is measured in N-m.

The Richter magnitude of the seismic event generated by the slip is estimated using relationship proposed by Hanks and Kanamori, (1979), Equation 2.5 which is suitable for $3 \leq M_L \leq 7.5$.

$$M = \frac{2}{3} log\, M_\circ - 10.7, \qquad \text{Equation 2.5}$$

Where, M is the Richter magnitude of the seismic event and $M_\circ$ is the seismic moment in dyne-cm (1 N-m = 10000000 Dyne-cm).

This method does not take into account the shear strength properties of the rock mass, geological structures and effects of flooding (pore pressures) which is so important for evaluation of seismicity in the Witwatersrand Basin.

Pillar collapse (pillar strain - seismic energy)

To approximate the simultaneous failure of large number of pillars vis-à-vis the magnitude of seismicity, an effort was made to use correlations proposed by Sjoberg, et al., (2011) and Hanks and Kanamori, (1979), Equation 2.6 and Equation 2.7 respectively. Equation 2.6 correlates strain energy with stresses and volume of a pillar (considering linear-elastic material) and Equation 2.7 correlates earthquake magnitude with the seismic moment.

$$E_{s-tot} = \int \sigma\epsilon \, dV = \int \frac{\sigma^2}{E} dV, \qquad \text{Equation 2.6}$$

Where E_{s-tot} is the total strain energy, σ is the stress (major principal stress used), ϵ is the strain, E is the Young's modulus of rock, V is the volume.

$$M = \frac{2}{3} \, log \, M_{\circ} - 10.7 = M = \frac{2}{3} \log E_{s-tot} - 10.7, \qquad \text{Equation 2.7}$$

According to Sjoberg, et al., (2011), seismic magnitude due to pillar collapse can be estimated using Equation 2.7 (in lieu of better, site-calibrated, alternatives). Since this equation assumes that all the strain energy is converted into seismic energy, the estimated magnitude belongs to the upper limit of a possible earthquake magnitude. This method takes into account neither the shear strength properties of the rock mass and geological structures nor the effects of flooding (pore pressures).

Fall of ground

According to Riemer and Durrheim (2012), a fall of ground (hanging wall) of 2500 tons took place in Robinson Deep Mine during August 1908 but apparently not the slightest shock was observed at the surface. It is observed that empirical correlations for seismicity due to falls of ground have not received due attention. This factor might be attributable to either absence/minimal seismicity observed in Witwatersrand Basin or insufficient volume of rock fall needed to cause significant seismicity.

2.5.2. Effect of flooding of the abandoned mine void on the mining-induced seismicity

The strength of geological discontinuities is characterized by the cohesion of the infill materials and frictional resistance of the asperities. It is evident that discontinuities developed during the course of mining or developed later as a consequence of stress re-distributions are devoid of clamping forces (unlike natural discontinuities). These are extremely sensitive to the changes in local (and regional) stresses and pore pressures generated due to flooding which might trigger a slip with the potential of inducing seismicity. Flooding of abandoned mines has the following effects:

- Geological (natural/tectonic) discontinuities:
  - In the case of presence of cohesive material, swell pressures are generated,
  - In case of granular material, friction is reduced,
  - Clamping forces on discontinuities are reduced.
- Mining-induced discontinuities:
  - Are lubricated i.e., friction is reduced similar to that of geological discontinuities,
  - Degradation/weathering of mine fills/supports with the potential of subsidence.
  - In the case of a larger collapse of raises, gullies, ore passes, etc., seismicity is generated,
  - Potential to trigger slip along the interface of foot wall and hanging wall.
- Potential of generation of high pore pressures at all types of discontinuities which may overcome the clamping forces and generate seismicity,
- In certain cases, the pore pressures created can be so high that they create new fractures even in the intact rocks through a process called “hydro-fracturing”.

2.6. Considerations and Methods for Evaluation of Hazard to Surface Structures

Dynamic structural analysis is required to evaluate the effects of seismicity on surface structures. In view of the damaging effects of the mining-related earthquakes in the Witwatersrand Basin, site-specific dynamic structural

analysis is required. Figure 2.18 explains the considerations and methods for this analysis.

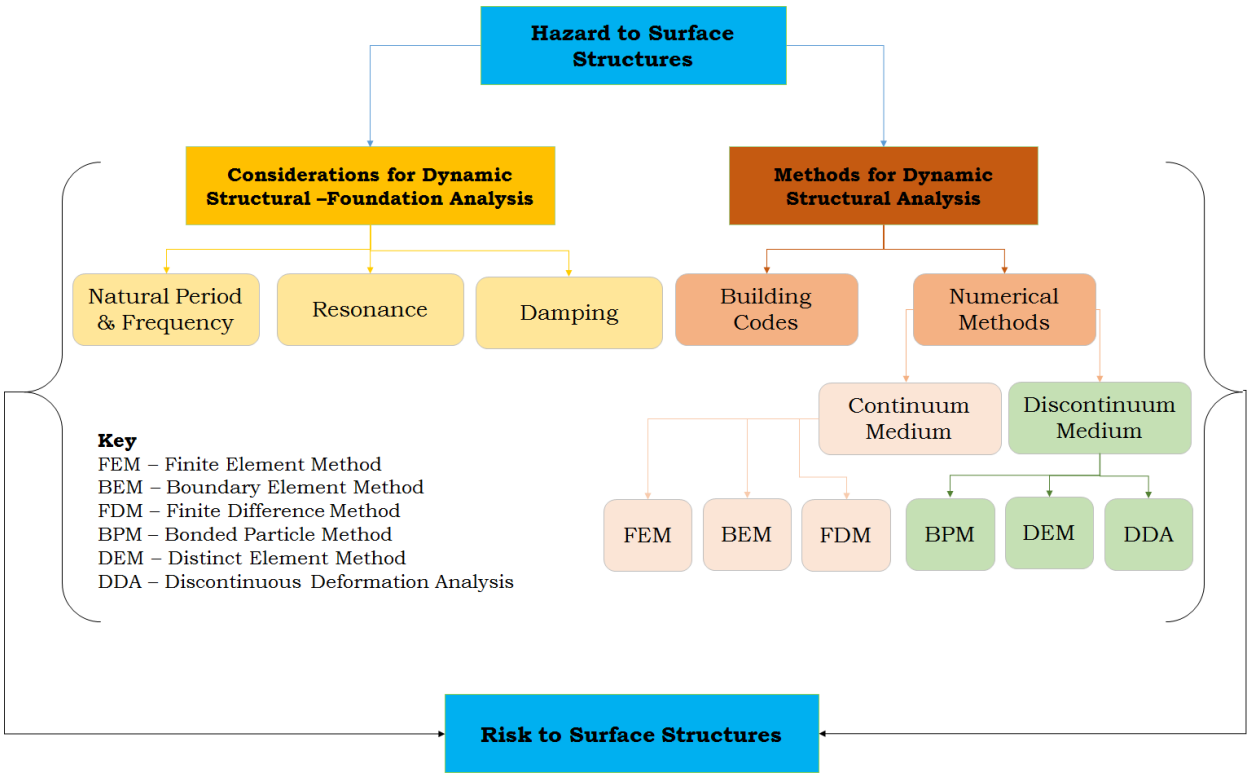


Figure 2.18 Considerations and methods for dynamic structural analyses

2.6.1. Consideration for evaluation of structural hazard

Structural fundamental period and frequency

Period (time required to complete one cycle) or frequency (number of cycles in one second) is an important characteristic of seismic ground motions and determines the seismic behaviour of the surface structures. Every surface structure has a specific fundamental period and frequency at which it has a tendency to move back and forth at an application of even a small horizontal push, Christopher (2013).The natural periods of various buildings suggested by Christopher (2013), Figure 2.19.

Natural periods depend on the structural characteristics, such as type (masonry, concrete, steel, etc.), geometry (height, width, and length), construction material (concrete, bricks, and steel, composite) and type of foundation ground. Sites with hard rocks have short periods and sites with soft soils have relatively long periods (up to 2 seconds), Christopher (2013). Generally

the natural period of a building increases with the increase in building height. As a rule of thumb, the fundamental period of a building equals the number of storeys divided by 10, Christopher (2013). The sixty storey CitiCorp Building in New York has a measured natural time period of 7 seconds, Christopher (2013). A large suspension bridge has a natural period around 6 seconds and natural frequency around 0.17 Hz, Christopher (2013). The natural time period of a particular building is not a hard and fast number as it varies during the seismic loading vis-à-vis the extent of damage the building undergoes during an earthquake. Table 2.2 gives the comparison of the period and frequency of the structures vis-à-vis selected ground motion.

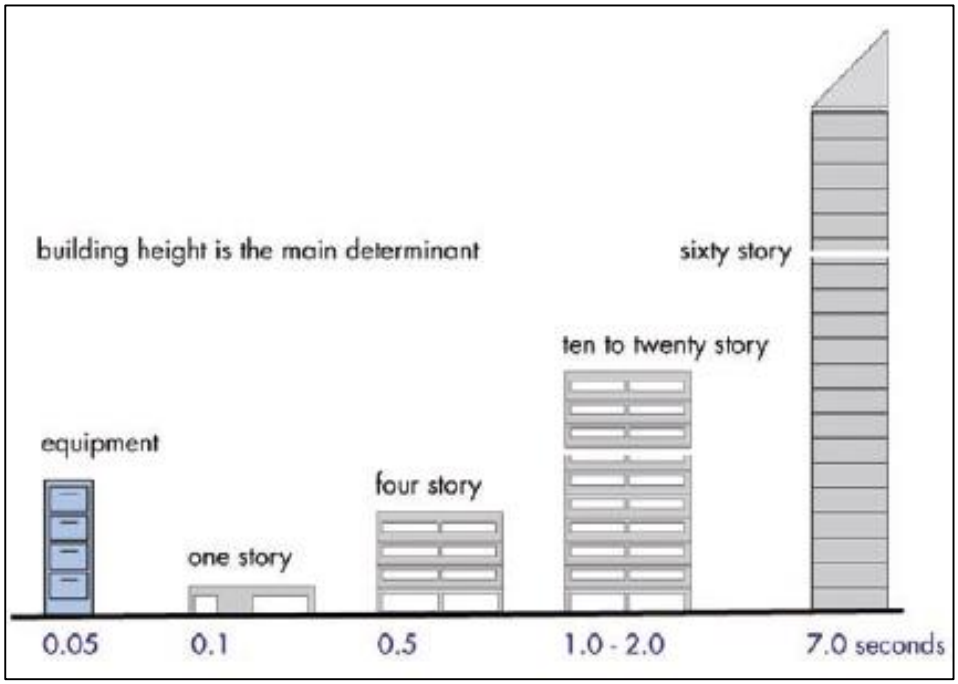


Figure 2.19 Natural period of various structures, Christopher (2013)

Table 2.2 Illustration of the period and frequency of various surface structures

Number of Storeys	Period (sec)	Frequency (Hz)
1	0.14	7
2	0.2	5
4	0.5	2
8	0.8	1.25
10 to 20	1 to 2	1 to .5
60	7	0.14
Period (sec) and frequency (Hz) of selected ground motion	0.08 to 0.10	7 to 12

Structural resonance

The resonance of a structure is a phenomenon wherein the structure undergoes large oscillations at a much smaller push. All surface structures having natural periods close to the periods of foundation ground (soil/rock) are likely to undergo resonance and experience acceleration high as 1g whereas the ground below may be vibrating at an acceleration of only 0.2 g, Christopher (2013). There is also a possibility that the time period of a structure undergoing progressive damage may coincide with the time period of the seismic event and the resonance effect (foundation ground/structure system) may cause excessive damage. This is the main reason for buildings to experience heavy damages at or close to their respective natural frequencies. Christopher (2013) also highlighted following:

- Acceleration of structures under resonance might increase as much as four times.
- The foundation ground (soil/rock) has a natural period of 0.4 to 2 seconds and depends on site-specific geological, hydrological and geotechnical conditions.
- During an earthquake in Mexico City in 1985, all buildings with 6 to 20 storeys suffered heavy losses compared to the other buildings since the natural time period of buildings in this range resonated with the time period of the earthquake.
- The ground motions of the 1989 Mexico earthquake manifested in ground motions (vibration) with a long period of 2 seconds (and for a duration of 90 seconds) of the soft ground located 250 km away from the focal point. The coincidence of natural period/frequencies of the buildings with that of the foundation soil resulted in the resonance effect, Figure 2.20. This resonance amplifies the acceleration of buildings compared to the underlying foundation soils resulting in great damages.

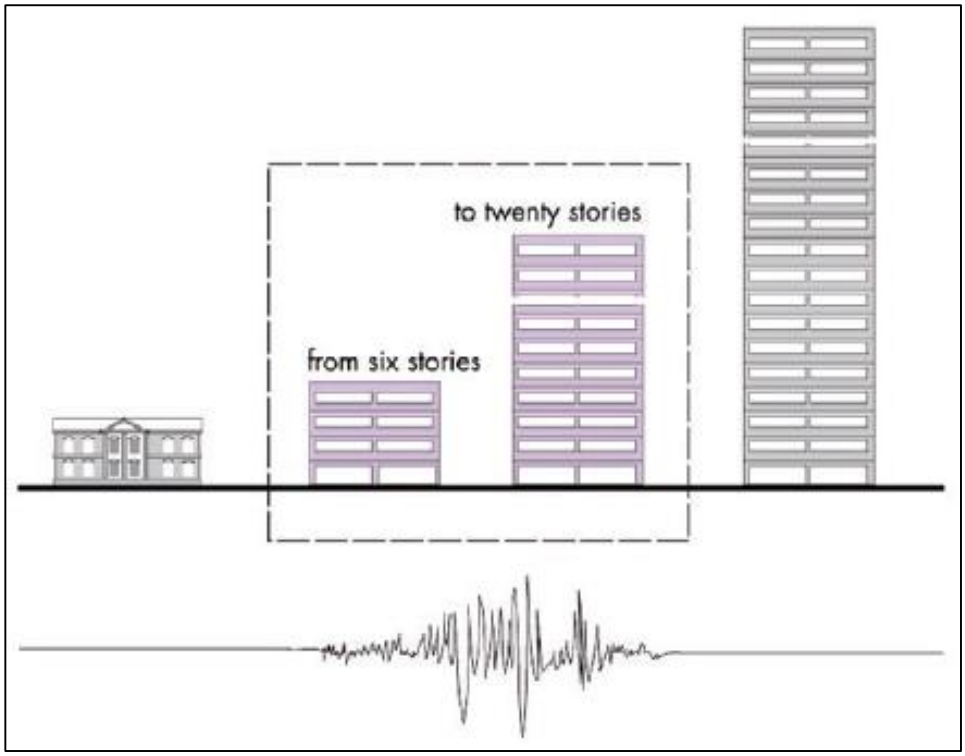


Figure 2.20 Vulnerable buildings; 6 to 20 Storey during the Mexico City earthquake in 1985, Christopher (2013)

Keeping in mind their natural period/frequency, a particular building is likely to behave differently when subjected to different earthquakes. Therefore, it is important that the ground motions of an earthquake are expressed as ground motion time histories, also called site-response spectra. A site-specific response spectrum consists of plots of acceleration, velocity and displacement with respect to the time period of the event at a particular site, Figure 2.21. It is evident from Figure 2.21 that the maximum acceleration of the plotted earthquake occurs at about 0.3 seconds. All buildings having a natural time period close to 0.3 seconds are likely to experience resonance and suffer more severe damages.

The response spectrum of a site helps identify the response of the built structures as described below:

- For tall buildings with longer periods, acceleration and velocity decrease, whereas displacement increases with period of ground motion.
- For 1 to 2 storey buildings with short periods, acceleration and velocity increase, whereas displacement decreases with period of ground motion.

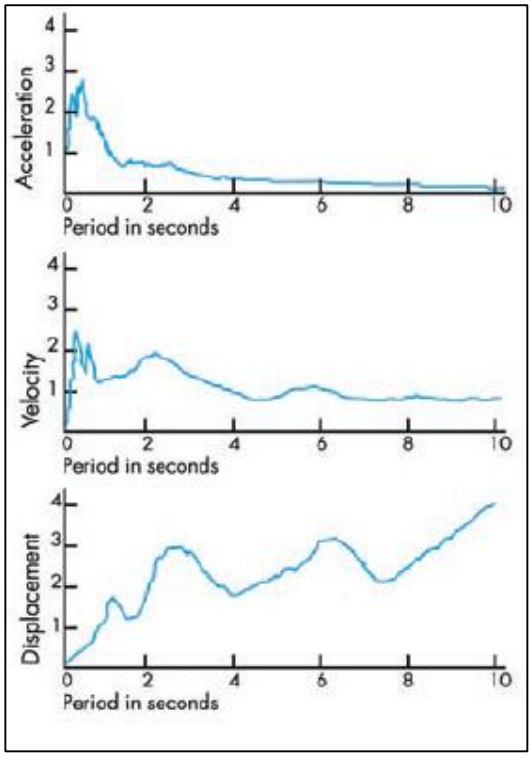


Figure 2.21 Typical response spectra, Christopher (2013)

Structural and foundation rock/soil damping

Earthquake-induced vibrations undergo decay due to energy losses in the form of internal friction, heat, and absorbed energy. Damping is a term used to describe the decay of earthquake vibrations in the structures. Nature and the type of structures affect damping behaviour. For example, heavy masonry and concrete structures exhibit more damping compared to the light structures.

Damping is measured according to a theoretical value called “critical damping”. The critical damping is the lowest amount of damping required to bring a particular structure to its original position (once the vibrations are discontinued). For geological materials, the critical damping varies from 2 to 5 % whereas for most surface structures, it varies from 2 to 10%, Biggs (1964). Higher values belong to softer geological materials and heavier structures, whereas lower values of damping pertain to rocks and light steel structures. The engineering significance of damping is described below and shown in Figure 2.22, Satratta (1987):

- With the increase in damping, the acceleration curves become flatter (decreases) and vice versa.

- At a damping value of 0%, the acceleration is 3.2 g. For damping values of 2%, 5%, and 10%, the acceleration values are 1.2 g, 1.0 g and 0.65 g respectively.
- For typical seismic structural analysis, damping value should be used with care according to the seismic provisions of the respective area. A conservative preliminary analysis may begin with low damping.

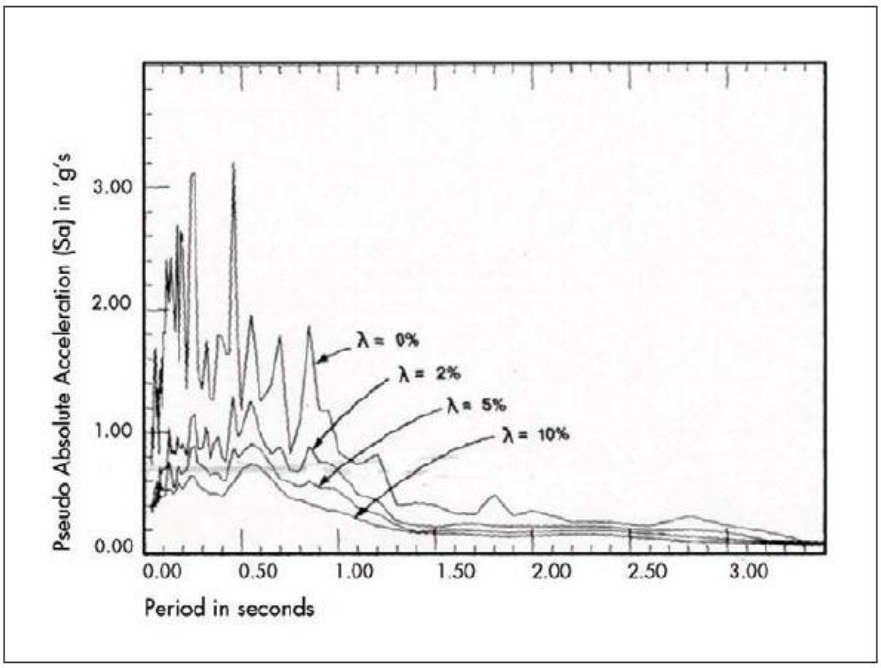


Figure 2.22 Response spectra for various damping values, Satratta (1987)

2.6.2. Methods for evaluation of structural hazard

Dynamic structural analysis can be performed using two methods, equivalent static/pseudo-static and dynamic analysis. Since mining-induced seismic events are characterized differently than natural earthquakes because of their short duration, high frequency and rapid attenuation, dynamic structural analysis was performed using numerical techniques.

Numerical dynamic analysis

Geo-materials comprising a jointed rock mass, soil cover and geological discontinuities exhibit highly non-linear behaviour. The reasons are attributed to geological history, inherent mechanical properties, groundwater and loading conditions. In this situation, numerical techniques are viable tools to analyse the structural behaviour under dynamic loading conditions. However, all

numerical techniques require certain assumptions to be made, Bobet (2010). The analysis and interpretation thus rest with the professional judgement of the analyser. Some of the assumptions usually made for numerical analysis are given as follows:

- Constitutive behaviour; elastic, plastic, etc.,
- Geological coherence; homogeneous, heterogeneous, isotropic, anisotropic, etc.,
- Time-dependent behaviour,
- Loading conditions; static and dynamic, and so forth.

Various numerical modelling techniques, shown in Figure 2.23, are available to analyse a particular medium. For a continuum medium, the common numerical techniques include Finite Element Method (FEM), Boundary Element Method (BEM), Finite Difference Method (FDM), and FEM-BEM Hybrid Method, Bobet (2010). For a dis-continuum medium, common numerical modelling techniques are the Distinct Element Method (DEM), Discontinuous Deformation Analysis (DDA) and Bonded Particle Method (BPM), Bobet (2010).

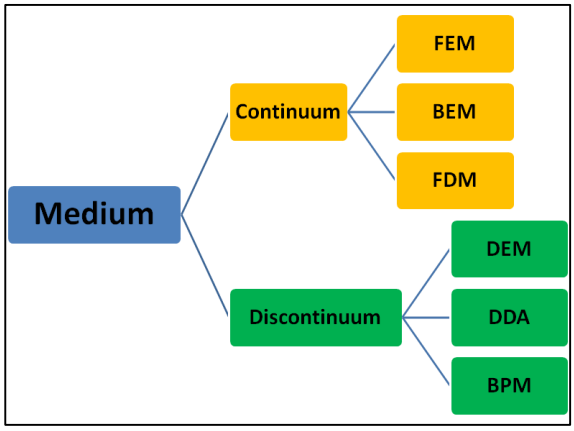


Figure 2.23 Numerical modelling techniques vis-à-vis type of medium

- **Finite element method (FEM)**

In this method, the model is divided into a finite number of elastic zones; material properties and boundary conditions are applied. According to Singh (2012), FEM uses an implicit function scheme which solves and saves information of all the elements simultaneously. For large and complex problems, this method makes the computational time extremely large and requires a very

efficient computer (speed and memory), Singh (2012). The method also requires a regular mesh which makes its utility for a problem with multiple joints and varying orientations more difficult.

- **Boundary element method (BEM)**

  In this method, only the boundary of the model is discretized (meshed) and the interior of the model is ignored which makes the computational time relatively smaller than FEM. The accuracy of the model results within the inner region is relatively less, Singh (2012). The model is more suited for general deformation analysis of underground excavations, tunnels, etc.

- **Finite difference method (FDM)**

  From discretization and mode set up view, the method is similar to FEM. However, it uses an explicit function scheme, Itasca (2014). The method uses full equations of motion and discretized elements which requires less memory on the computer. This enables modelling of much bigger problems with finer mesh size in less computational time when compared to FEM, Singh (2012). This method also requires a regular mesh and cannot model many discontinuities. It is suitable for continuum media (soils-like materials). FLAC and FLAC3D, developed by Itasca Consulting Inc., are among the FDM codes.

- **Distinct element method (DEM)**

  This method is based on dis-continuum mechanics (rocks), Xie and Zhao (2009). The model is treated as an assemblage of blocks (rigid or deformable) which require specifying the constitutive models both for the blocks and contacts. During the process of computation, the contacts are continuously identified and contact information updated, Itasca (2014). This code is well suited for analysis of dis-continuum geo-materials. UDEC and 3DEC developed by Itasca Consulting Inc., are DEM codes.

- **Discontinuous deformation analysis**

  This is a dis-continuum code developed to estimate stress, strain, sliding and opening of rock blocks, Shi and Goodman (1988). The method uses implicit functions and, therefore, requires larger computational time when compared to DEM.

- **Bonded particle method**

  As per Kazerani and Zhao (2010), this method belong to discontinuum media and has extensively been used for modelling brittle material failures. In this technique, the material is modelled as an assemblage of particles connected by contacts and requires calibration of the micro-parameters of the particles which make sits usage relatively difficult.

2.7. Evaluation of Seismic Risk to Surface Structures

The study area comprises buildings of all types; masonry, concrete, steel, low-rise and high rise, and so forth. A panoramic view of the high-rise buildings in the Johannesburg CBD area is shown in Figure 2.24. Structural risk is usually assessed according to the building codes of the respective area. The South Africa building code, SANS 10160-4:2009 specifies the guidelines to evaluate risk to the surface structures due to mining and natural seismicity. Guidelines provided by the Uniform Building Codes and Searer and Freeman (2004) are described which compare the spectral distance vis-à-vis acceleration of natural earthquakes.



Figure 2.24 Panoramic view of high rise concrete buildings in CBD area, Johannesburg, source van der Merwe, (2013)

2.7.1. SANS 10160-4:2009

South African National Standard SANS 10160-4:2009 provides the basis for the design and analysis of structures against seismic actions. This building code is still in the draft stage. South Africa is divided in two zones, Figure 2.25. Zone 1 includes areas where natural seismicity is perceived, whereas Zone 2 covers areas with potential of both mining-induced and natural seismicity. The code provides guidelines in the form of "Normalized Design Response Spectra for 5% damping", Figure 2.26 and values for relevant parameters [period (S), limits of constant spectral acceleration (T_B and T_C), beginning of constant displacement range (T_D), and ground type], shown in Table 2.3.

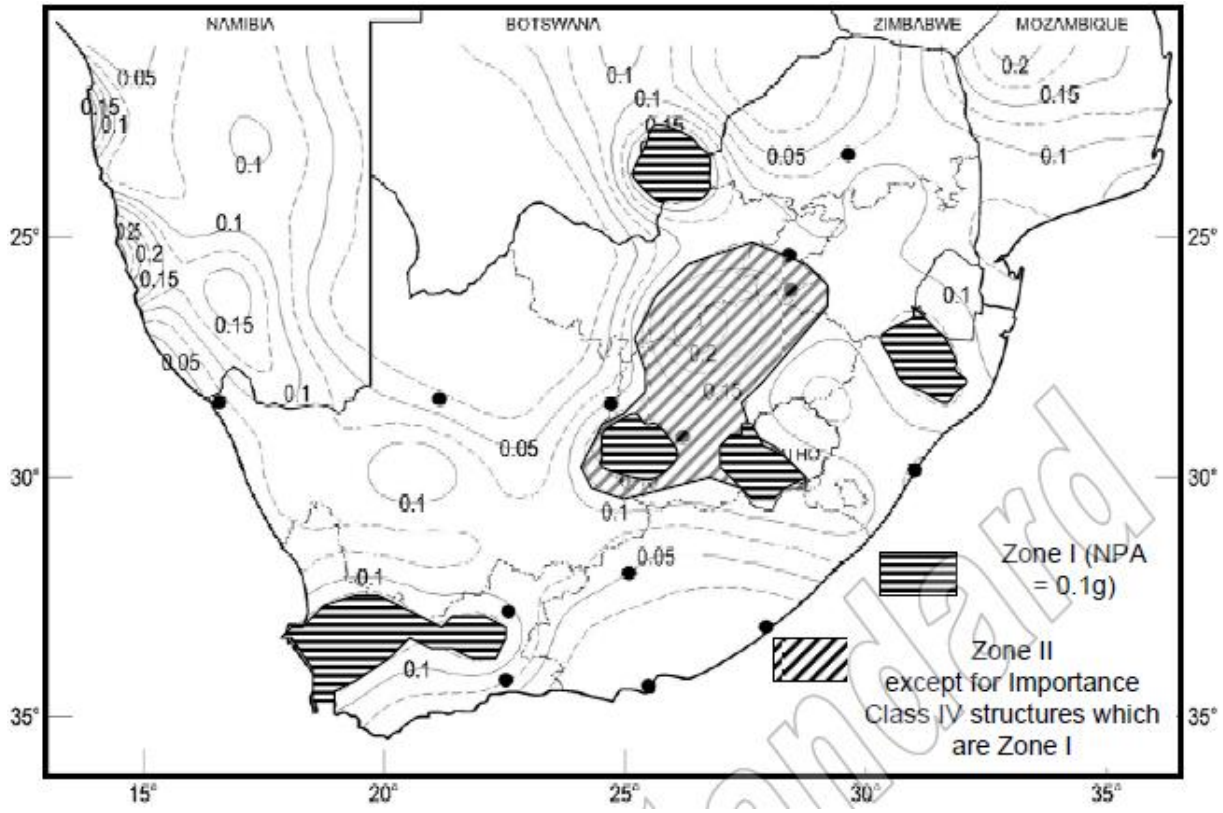


Figure 2.25 Seismic Zones in South Africa, SANS 10160-4:2009

The building code provides guidelines for a simplified pseudo-static analysis which does not take into account spectral distribution of the dynamic loading (acceleration, velocity or displacement), foundation-structure-interaction, material anisotropy, etc. Numerical techniques allow modelling of many such aspects. Since the numerical approach was adopted for dynamic structural analysis in this research, further details on the building code were not covered.

Table 2.3 Values of the parameters describing the design spectra, SANS 10160-4:2009

1	2	3	4	5
Ground Type	Parameters			
	S	T_B	T_C	T_D
1	1.0	0.15	0.40	2.0
2	1.20	0.15	0.50	2.0
3	1.15	0.20	0.60	2.0
4	1.35	0.20	0.80	2.0

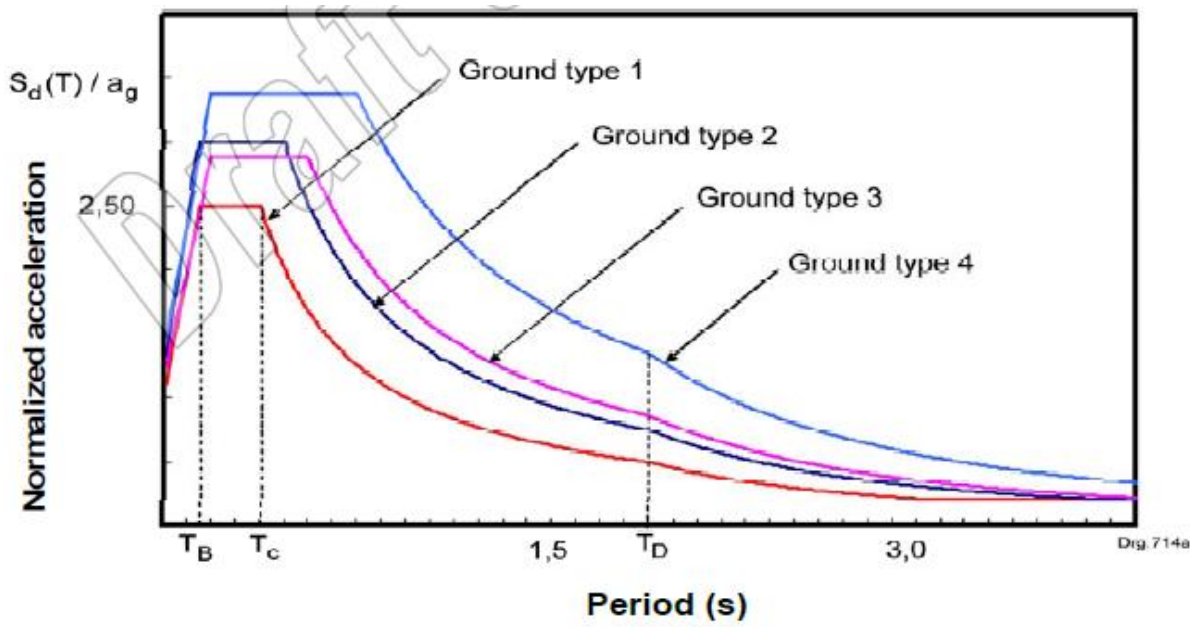


Figure 2.26 Normalized design response spectra according to SANS 10160-4:2009 (for ground type, refer o Table 2.3)

SANS 10160-4:2009 specifies the drift or horizontal displacement of the structures subjected to the dynamic loading. Structural guidelines for the dynamic analysis are given in Figure 2.27. This displacement should include the translational and torsional deflection effects. The code also provides guidelines for calculation of the inelastic displacement should this be required. It is inferred that this drift/displacement is, therefore, the spectral displacement (absolute magnitude) at the end of the dynamic loading. The storey drift limitations laid down by SANS 10160-4:2009 state; the storey drift ($d_{ri - j}$) between two stories "1" and "j" (with j = i + 1) shall be limited as:

$$d_{ri-j} \leq 0.025\ h_s \quad \text{if } T < 0.7s, \qquad \text{Equation 2.8}$$

$$d_{ri-j} \leq 0.020\ h_s \quad \text{if } T > 0.7s, \qquad \text{Equation 2.9}$$

Where,

$d_{ri-j} = d_{si+1} - d_{si}$

h_s = storey height in metres,

T = fundamental period of vibration ($T = C_T \times h_t^{3/4}$),

C_T = 0.075 for reinforced concrete buildings, 0.05 for all other buildings.

h_t = height of building in metres from foundation or from top of a rigid basement in metres.

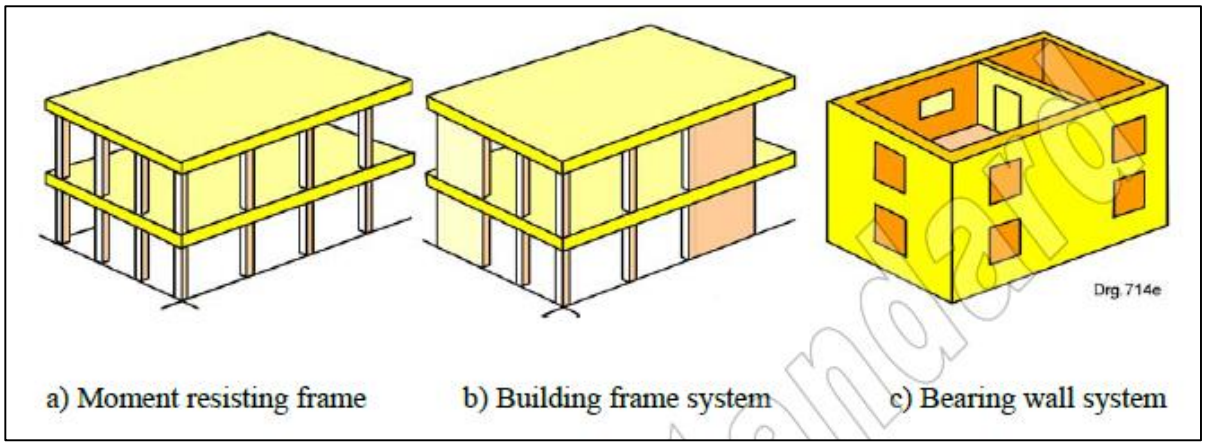


Figure 2.27 Guideline for the structural systems for dynamic analysis, SANS 10160-4:2009

2.7.2. Unified building codes, Searer et al. (2004)

Searer, et al. (2004), compared the spectral displacement (drift time history) of the five natural earthquakes vis-à-vis spectral acceleration, as shown in Figure 2.28. In this figure, black and brown lines indicate the UBC (Uniform Building Code, 1977) design spectrum of spectral displacement (drift time history,) whereas plots in purple, pink, red, green, and blue show the spectral displacement (drift time histories) of various earthquakes as mentioned in the Figure 2.28. In this study, seismic events of magnitude M_L 3 to 4 with likely acceleration of 0.4 g to 0.6 g were simulated and the structural response was compared with the response given in Figure 2.28, for time period of 0.5 to 1.0 seconds.

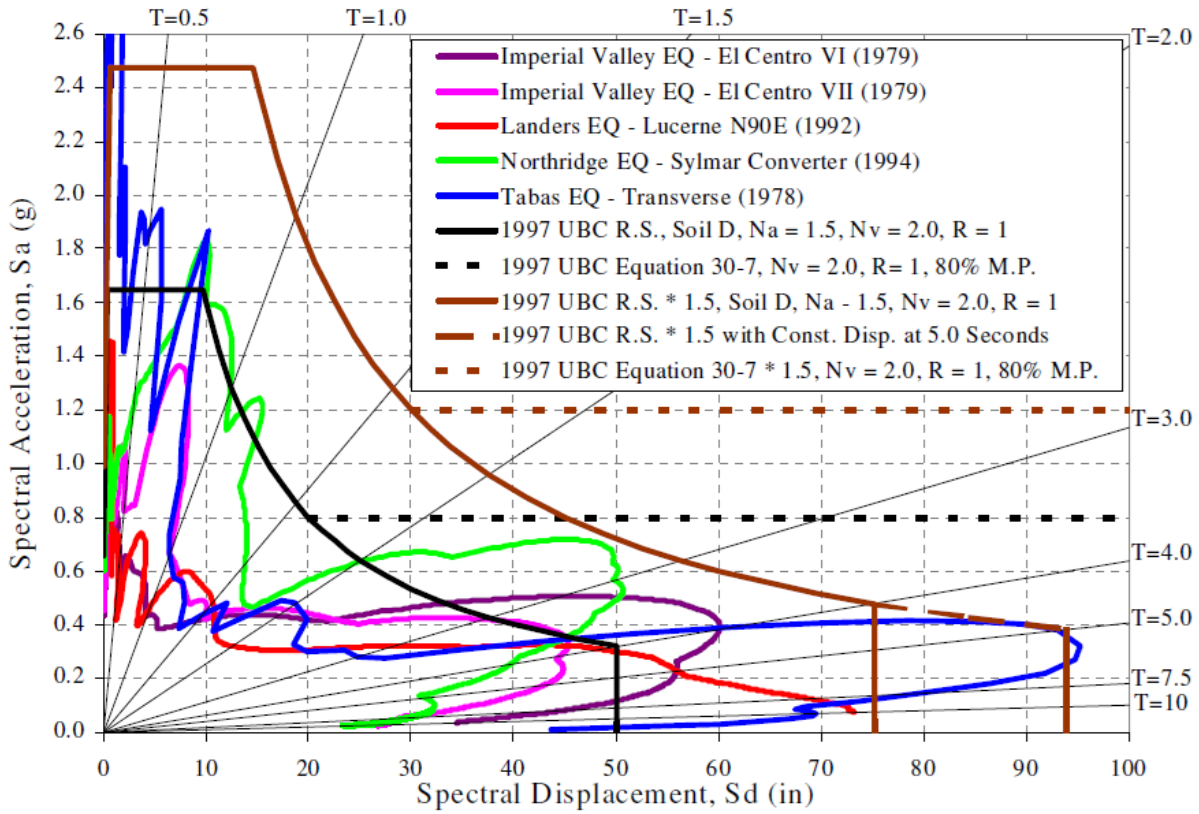


Figure 2.28 Spectral acceleration and the spectral displacement of natural earthquakes, Searer and Freeman (2004)

2.7.3. Liquefaction potential of a tailings dam slope

Seismicity produces cyclic loading which causes saturated soils to undergo pore pressure changes (increase) which, in turn, results in decrease in effective stress, Itasca (2014). The decreased effective stress can lead to soil liquefaction. Therefore, the liquefaction potential in a saturated slope was evaluated using an "effective-stress analysis" approach.

According to Itasca (2014), effective stress analyses are well suited to the coupled mechanical-fluid flow problems involving liquefaction potential. The drained soil properties are suitable for effective stress analysis. The dynamic characteristics of the soils (mechanical and stiffness properties) are governed by the modulus reduction factor (G/G_{max}) and damping ratio (λ) curves, Itasca (2014). Analysis of a tailings dam slope should consider appropriate modulus reduction and damping ratio curves for the type of soil being analysed. Further detail of liquefaction analysis is covered in the methodology chapter.

2.8. Knowledge Gaps

Based on the review of the existing site conditions, recent mining-induced seismicity, techniques available to estimate the potential of seismicity in future and effects on surface structures, the following gaps were identified:

- Empirical methods available for evaluation of mining induced seismicity were general in nature and did not take into account the existing (and future) site conditions with mining voids partially/fully flooded.
- Site-specific ground motions, in terms of acceleration or velocity time histories (required for the seismic analysis of critical structures), were not available in the Central Rand. Existing empirical methods and building codes did not allow for the estimation of the ground motion in terms of time histories.
- Existing methods did not provide information on the ground motion variation with respect to distance from the seismic source.
- The structural capacity (or seismic deficiency) of the structures constructed before the seismic provision were uncertain which could best be evaluated using ground motion in terms of time histories.
- Effect of flooding on the mining-induced seismicity (propagation of seismic waves) was not known.

2.9. Conclusion

This chapter reviewed the mining seismicity in the Witwatersrand Basin and its effects on the surface structures. Empirical methods for estimating the mining-induced seismicity were discussed with respect to the variables. These were taken into account and others were not considered. The chapter also included a brief description of the numerical techniques which were more rigorous and took into account relevant parameters for the evaluation of mining-induced seismicity and its effects on surface structures.

The next chapter explains the methodology adopted for the study. It covers the research matrix of the study and details of the numerical techniques used for the evaluation of mining-induced seismicity and its effects on surface structures.

3. METHODOLOGY

3.1. Introduction

The literature review of the subject revealed complexity in dealing with existing site conditions, mining-induced seismicity and its effects on the surface structures. The study area comprised geological groups dipping steeply in the southward direction. The boundaries (geological discontinuities) between these geological groups marked the contrast in stiffness properties of each geological group. The interface between the upper soil and underlying weathered/highly weathered rock had an influence on the wave propagation.

The literature review also highlighted that flooding of the abandoned mines is resulting in gradual deterioration of the stability of abandoned mines. The challenges posed by the complexity of the understudy research are listed as following:

- The nature of the research problem was 3D in view of the layout of the study area, material distribution, orientation of joints, etc.
- The study area required geomechanical site characterization with a view to developing a representative geomechanical model in order to facilitate numerical modelling/analysis.
- Triggering of the sources and 3D wave propagation across the study area.
- Propagation of seismic waves across multiple geological discontinuities (material boundaries/joints) with varying orientation.
- Inclusion of the effect of flooding in abandoned mining voids and wet joints vis-à-vis transmission of seismic waves.
- Estimation of amplitude and time histories of the seismic waveform (ground motions) at different points in the study area.
- Evaluation of the effect of ground motions on the surface structures taking into account the interaction of foundation rock/soil-foundation-structure.
- Criteria for assessing the adverse effects of mining seismicity on surface structures.

3.2. Conceptual Framework and Methodology

The overall conceptual framework adopted to address the research challenges is shown in Figure 3.1. Among other approaches discussed in the Literature Review were advanced numerical codes.

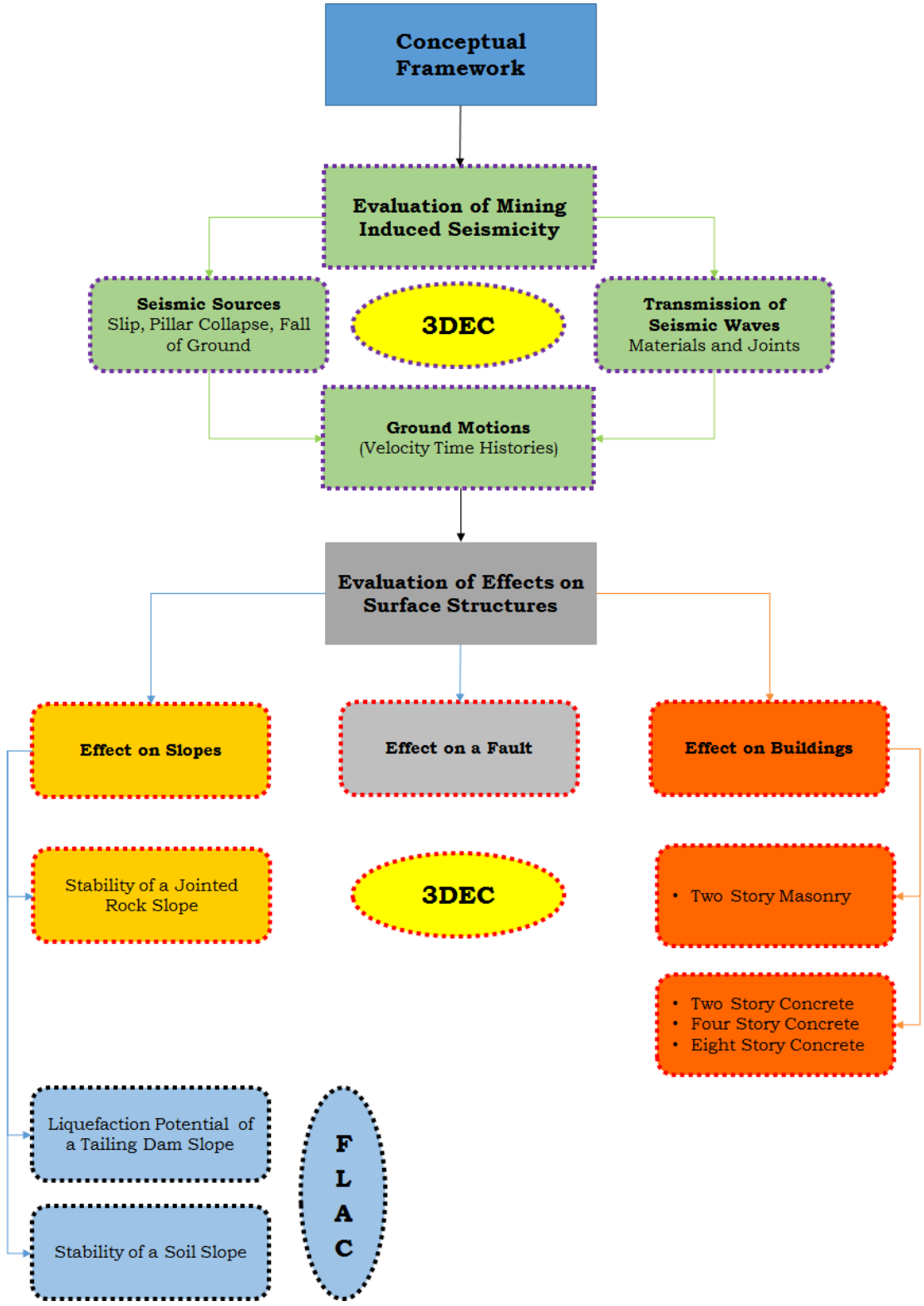


Figure 3.1 Conceptual framework and methodology

3DEC and FLAC codes were used for the research in view of the following aspects:

- Highly non-linear behaviour due to the presence of jointed rock mass, geological discontinuities, ground water, and so forth.
- Various constitutive behaviour models (elastic, plastic, etc.) of the materials and discontinuities.
- Various loading conditions (static, dynamic), construction stages and ground water conditions.
- The codes were ideally suited for the large deformations of blocks and displacement of joints.
- The codes simulated the transmission of seismic waves through the complex geological medium (intact, jointed, partially or fully flooded, pillars, etc.).
- The codes were explicit and allowed estimation of ground motions in real time in terms of displacements, velocity or acceleration time histories.
- The codes provided highly interactive manipulation of screen images for the interpretation of results.

3.3. 3DEC Numerical Modelling for Evaluation of Mining Induced Seismicity

The process for evaluating mining-induced seismicity using 3DEC is illustrated in Figure 3.2. 3DEC was best suited for modelling dis-continuum media with many intersecting discontinuities in 3D that exhibited highly nonlinear behaviour. Details of the following components are explained:

- Site characterization,
- 3DEC simulation considerations,
- Transmission of waves,
- Seismic simulation scenarios and Simulation stages,
- Estimation of ground motions.

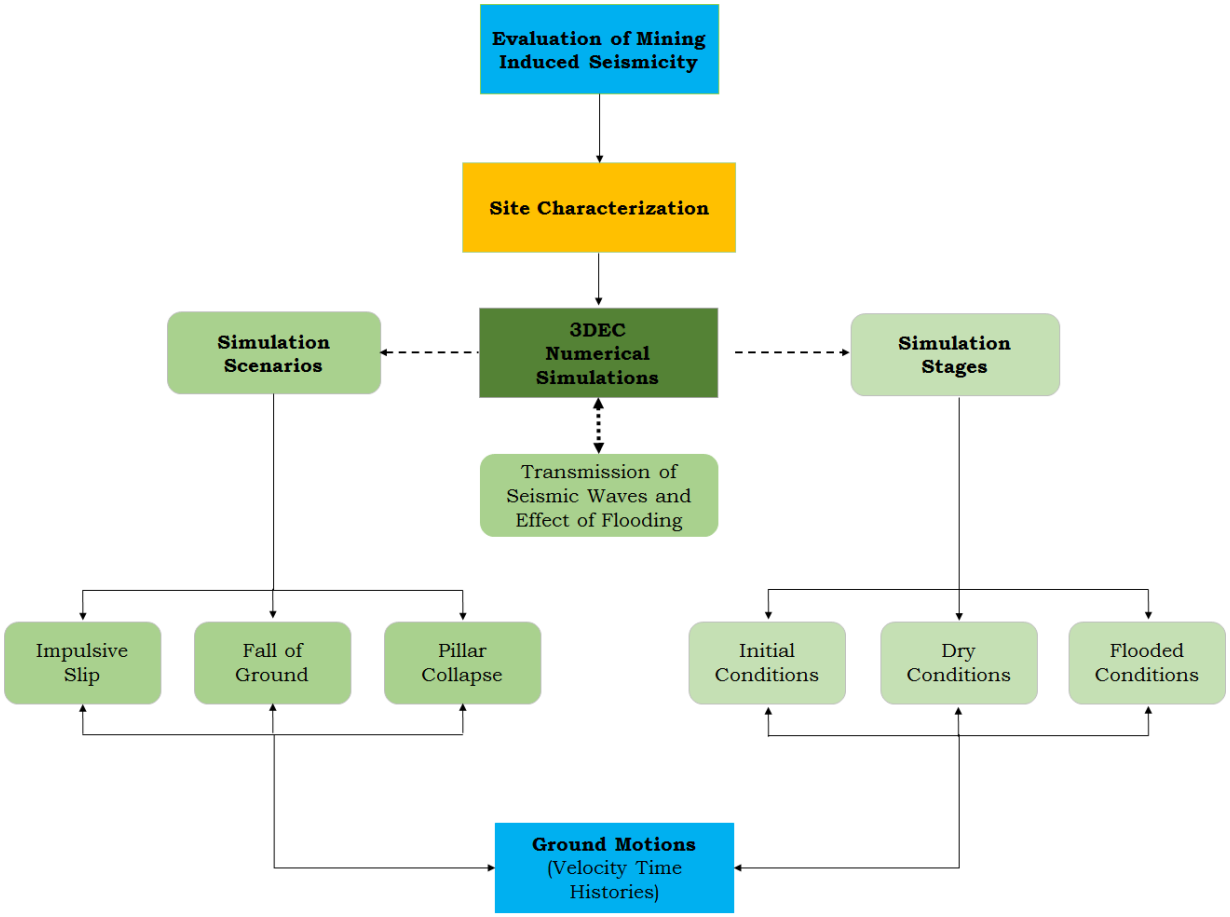


Figure 3.2 Process for evaluation of ground motions

3.3.1. Site Characterization

3DEC numerical modelling requires knowledge of material geometry, material properties, joint properties, *in situ* stress state, and so forth. Site characterization was performed (Chapter 4) to develop a representative (idealized) geomechanical model with all the relevant data needed for the evaluation of mining-induced seismicity.

3.3.2. Numerical simulation considerations

3DEC is a distinct element method that allows simulation for the interaction of blocks, joints, fluid, voids, and so forth, in both static and dynamic modes. The study used 3DEC version 5.0. The simulations considered the following aspects:

- A discontinuous medium was modelled as an assemblage of polyhedral blocks (rigid/deformable),
- Discontinuities were treated as boundary conditions between the blocks,

- Motion along discontinuities was governed by linear and non-linear force-displacement relations for movements in both normal and shear directions,
- Steady state fluid flow in joints (complete flooding of mining voids) was considered for simulation of flooded mining voids.

3.3.3. Transmission of waves

In the event of a seismic event, the seismic waves radiating to the ground surface are reflected and refracted due to the fractured rock mass, mining voids and joints. Among other parameters, the stiffness of the joints has a substantial influence on the propagation of waves through a jointed rock mass, 3DEC Manual (2013). According to Myer, et al. (1990), the joint stiffness in dry fractures has a strong influence on the attenuation of high frequency seismic waves which changes the travel time of waves. In order to perform adequate seismic analysis of the candidate site, the influence of joint stiffness had to be considered with great care. Efforts were made to avoid numerical distortion of the wave propagation during numerical analysis by using appropriate joint stiffness.

Itasca (2013), highlights that the numerical accuracy of the wave transmission is also affected by the frequency content of the input wave and the wave speed. To accurately represent the wave transmission through a model, Kuhlemeyer and Lysmer (1973) suggest a relationship, given as Equation 3.1, between the spatial element size of the model and wavelength of the highest frequency component of the seismic wave. For a reliable dynamic analysis of the jointed and fractured rock mass, the numerical method had to adhere to the Kuhlemeyer and Lysmer criterion given by Equation 3.1.

$$\Delta l \leq \frac{1}{8} \times \gamma, \qquad \text{Equation 3.1}$$

Where Δl = length of the spatial element, $\gamma =$ wavelength of waves propagating through the medium (associated with the highest frequency component of peak velocities and joint spacing/block size). This guideline was vitally important and was complied with during simulations for estimating the ground motions. The study incorporated the Kuhlemeyer and Lysmer criterion of wave transmission.

3.3.4. Effect of flooding in 3DEC simulations

According to Itasca (2014), fluid flow in 3DEC is considered only along the fractures/joints and flow in rock mass is ignored. The joints are considered to separate the impermeable blocks. Itasca (2014) highlights the salient features related to the fluid flow in 3DEC as follows:

- The deformability of the joint is much larger that the intact rock.
- The area of contact between joints is much smaller than the area of the overlap.
- The shear strength of the rock mass in the plane of the joint is much smaller than the shear strength of the intact rock mass.
- The joints are the discontinuities in the rock mass and resistance to the shear deformation (shear strength) depends on the area of the contact between the joints.
- The cross-sectional area of the joint is much larger than the cross-sectional area of the pores in the intact rock mass. Therefore, fluid flow rates are much larger than the flow through pores in the intact rock mass.
- The matrix porosity of the rock mass is much larger than the porosity due to joints. Therefore, fluid flow through rocks is controlled by joints, whereas most of the fluid is stored in the intact rock mass.

The length scale of joint roughness ($l_{roughness}$) is much smaller than the length scales of the joint (l_{joint}) and structure ($l_{structure}$), Figure 3.3. In an engineering analysis of the scale of a rock block or engineering structure, consideration of the joint roughness made the modelling process extremely inefficient. Therefore, details of the joint roughness were ignored, Itasca (2014).

For large scale models, the joints were considered as 2D discontinuities and characterized with constitutive properties (joint normal and shear strength, joint friction, joint dilation and hydraulic aperture) on the macro scale, Itasca (2014). The numerical modelling of the study took advantage of the 3DEC code to consider the effect of flooding in two ways; pore pressure in the joints and pressure in the mining voids. In addition to the joint properties described earlier, appropriate pore pressure was also specified, whereas the effect of water in the voids was specified in the form of boundary stress as illustrated in Figure 3.4.

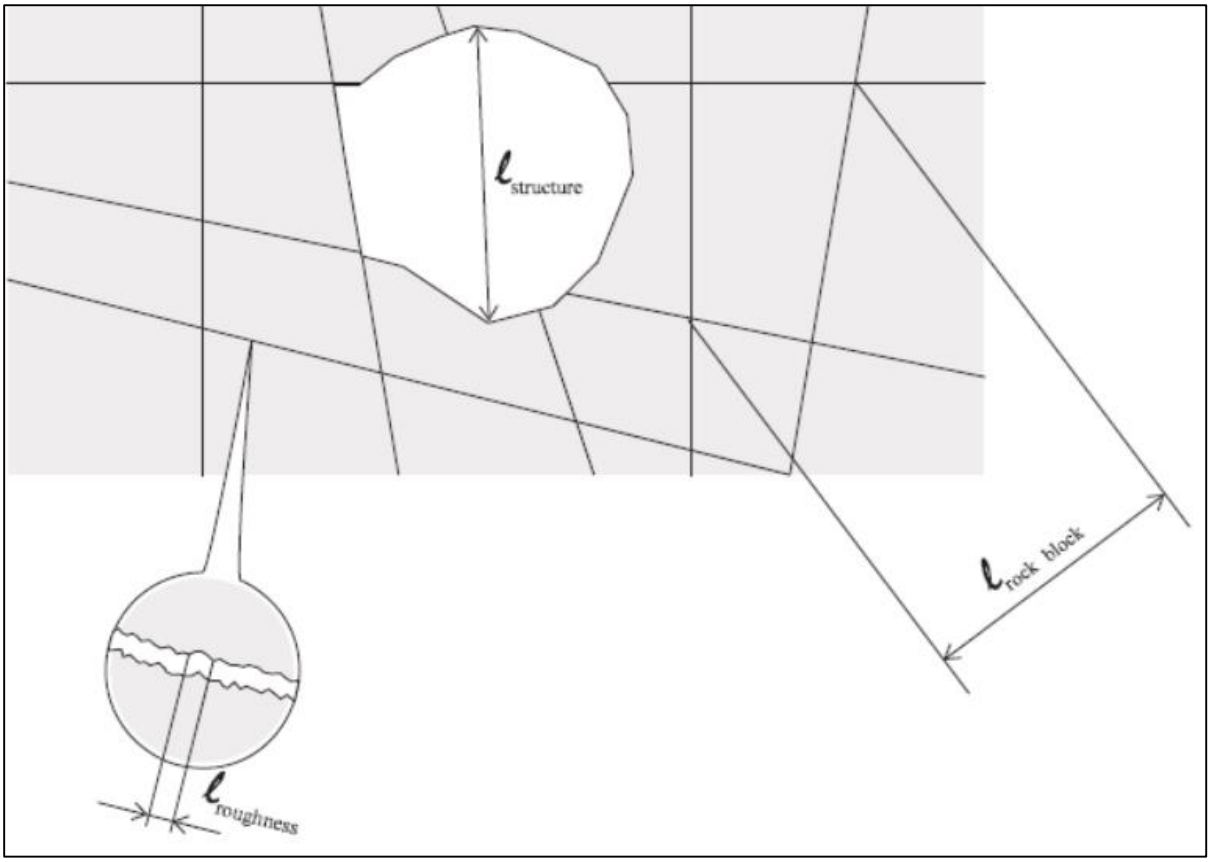


Figure 3.3 Length scales in rock mass and joint, Itasca (2014)

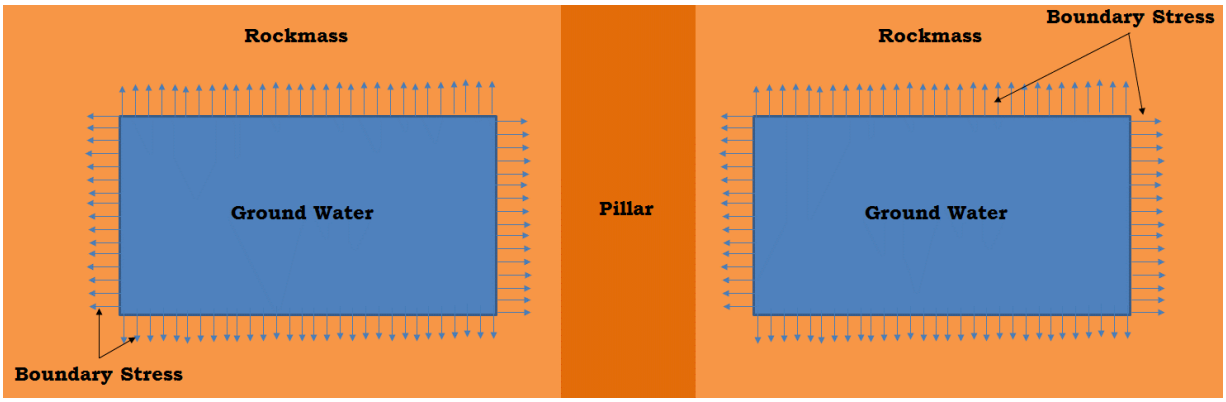


Figure 3.4 Boundary stress to represent effect of flooded voids in 3DEC

3.3.5. Simulation scenarios

Of the six source mechanisms described in the Literature Review (Chapter 2), three source mechanisms: "Impulsive Slip", "Fall of Ground", and "Pillar Collapse", were considered for simulations. These sources were simulated with a view to generate seismic events similar to those witnessed in the Central Rand. In the case of Impulsive Slip, the amount of slip and area of slip was selected so as to generate ground motions comparable to seismic magnitudes of M_L 3 to 4.

Similarly, scenarios of Fall of Ground and Pillar Collapse were also simulated to generate ground motions comparable to seismic magnitudes of M_L 3 to 4. Further details on the simulations of the considered scenarios are covered in the next chapter. Simulations were made both under dry and flooded conditions of the mining voids.

3.3.6. Simulation stages

In all civil and mining projects, there is an *in situ* stress state in the ground, before any construction or excavation is made. In 3DEC simulations, the creation of initial conditions representative of the *in situ* stress state was the first step. For the initial conditions of the study area, field stresses were used from Birch and Handley (2014), as discussed in Chapter 2. In the next stage, simulations were made considering dry conditions in all the scenarios. In the last stage, the effect of flooding was incorporated in the simulations. In the case of Impulsive Slip, the effect of flooding was simulated in the form of pore pressure in the joints. For the scenarios of Fall of Ground and Pillar Collapse, the effect of flooding was simulated in the form of boundary stress as illustrated in Figure 3.4.

3.3.7. Estimation of ground motions

The power of 3DEC was used in the estimation of ground motions in the form of "Velocity of Time Histories" at all the geological groups. The ground motions were recorded at a depth of 100 m below the ground surface; the interface of intact rock and upper strata comprising weathered rock and a soil layer, Figure 3.5 (idealized model).

The recording of ground motions at this depth also eliminated the need for "deconvolution"; a process required for using the ground motions as an input to the structural analysis. The peak velocity (amplitude) of the estimated ground motions under flooded conditions was compared with the peak velocity (of seismic events observed) inferred from the Shake Map for Orkney earthquake (Figure 2.17) for dynamic structural analysis.

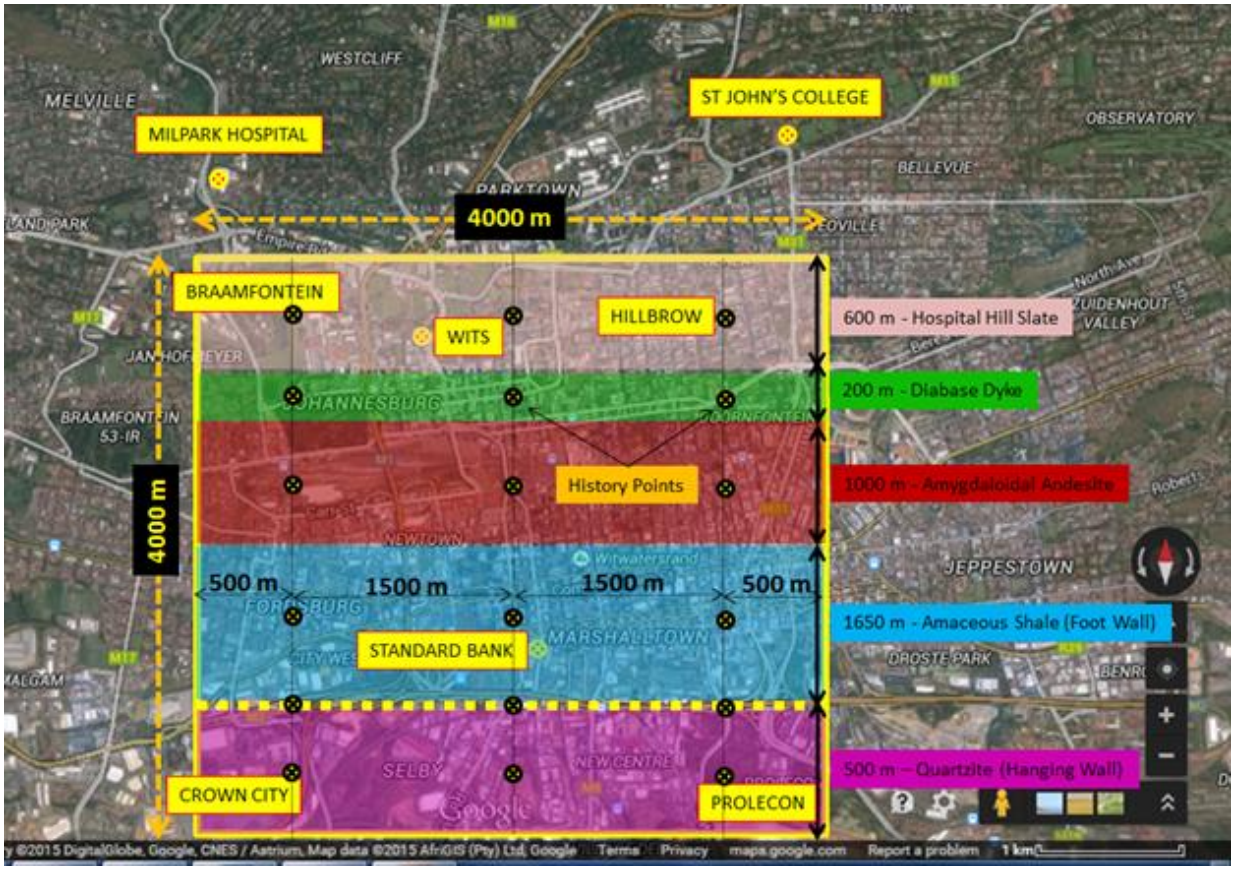


Figure 3.5 History points shown in black & yellow dots for ground motions

3.4. Evaluation of Effects of the Mining-induced Seismicity on Surface Structures

For the evaluation of the seismic effects on surface structures, the seismic source parameters and the seismic wave characteristics were essential considerations. The source parameters include mechanisms, such as normal-dip-slip, distance to the source mechanism, depth to the source, whereas seismic wave considerations included magnitude, duration, frequency, time histories of velocity, acceleration, and displacement.

The methodology adopted for the evaluation of effects of the mining-induced seismicity on surface structures is explained in Figure 3.6. Structural characteristics, such as geometry, mechanical and stiffness properties, were obtained from the literature (details are included in Chapter 5: Effects of mining-induced seismicity on surface structures).

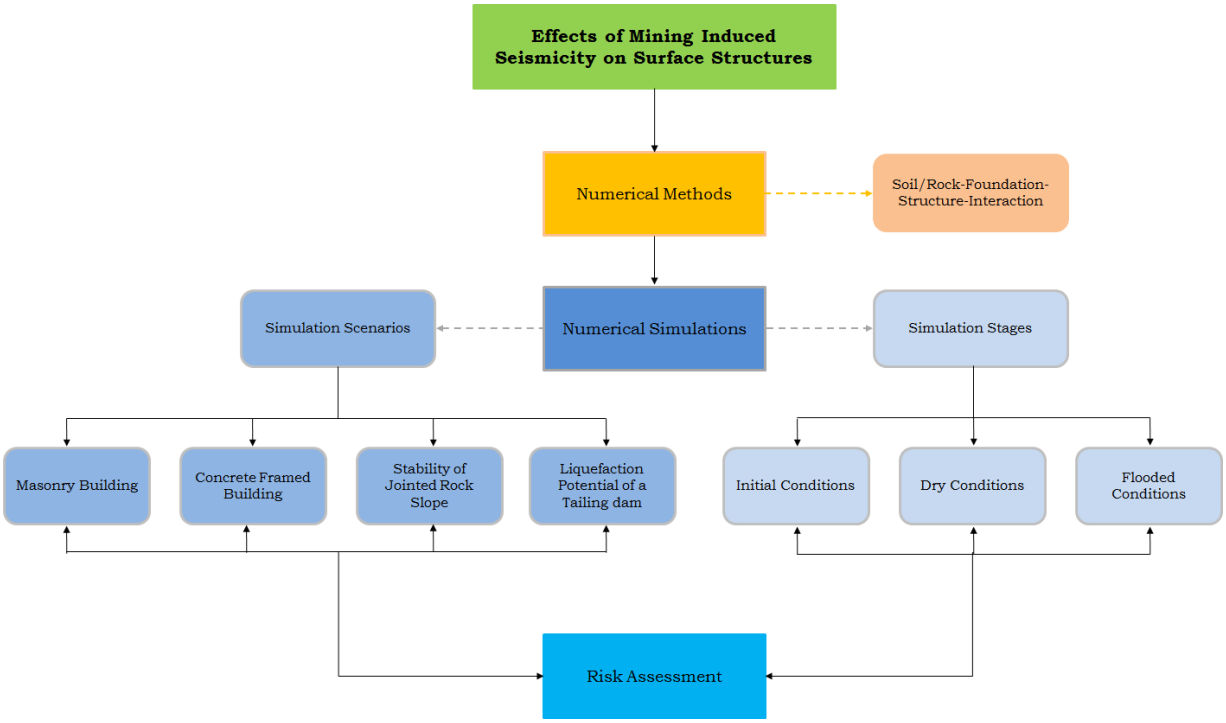


Figure 3.6 Methodology for evaluation of effects of mining induced seismicity on surface structures

3.4.1. Seismic structural considerations

Structural characteristics, such as height, geometry, type (masonry, concrete, steel, etc.), construction quality and seismic design provisions were essential considerations for the seismic structural analysis. Structures built with good quality of construction and according to the seismic provisions suffer less damage compared to poor quality structures without seismic provisions. The resonance effect, another characteristic of the structures, could also had a severe damaging effect on structures that is when seismic wave oscillations travelling in the foundation soil coincide with the natural frequency of the structures. The resonance effect explained the fact that every structure behaved differently to the same seismic event and underwent different degrees of damage since every structure had a different natural frequency.

Generally, low-rise buildings were more affected by the high-frequency waves (short duration), whereas high-rise buildings were more affected by the low-frequency (long duration) seismic waves, Christopher (2013). The candidate structures in the study area were varied in type (low-rise, high-rise, masonry, concrete, etc.) and quality: most of these structures were constructed many

years ago when no seismic provisions were required or available. Also, many structures in the area of study were old and their structural capacity was likely to be uncertain. It was, therefore, imperative to perform seismic structural analysis using seismic input in the form of time histories of acceleration, velocity or displacement.

3.4.2. Use of numerical methods for seismic structural analysis

Numerical methods including Finite Element and Distinct Element were available for the seismic structural which took into account the soil/rock-foundation-structure-interaction of the representative (idealized) model as illustrated in Figure 3.7. Generally, the finite element codes available apply the seismic input at the foundation of the structure in terms of time history or push.

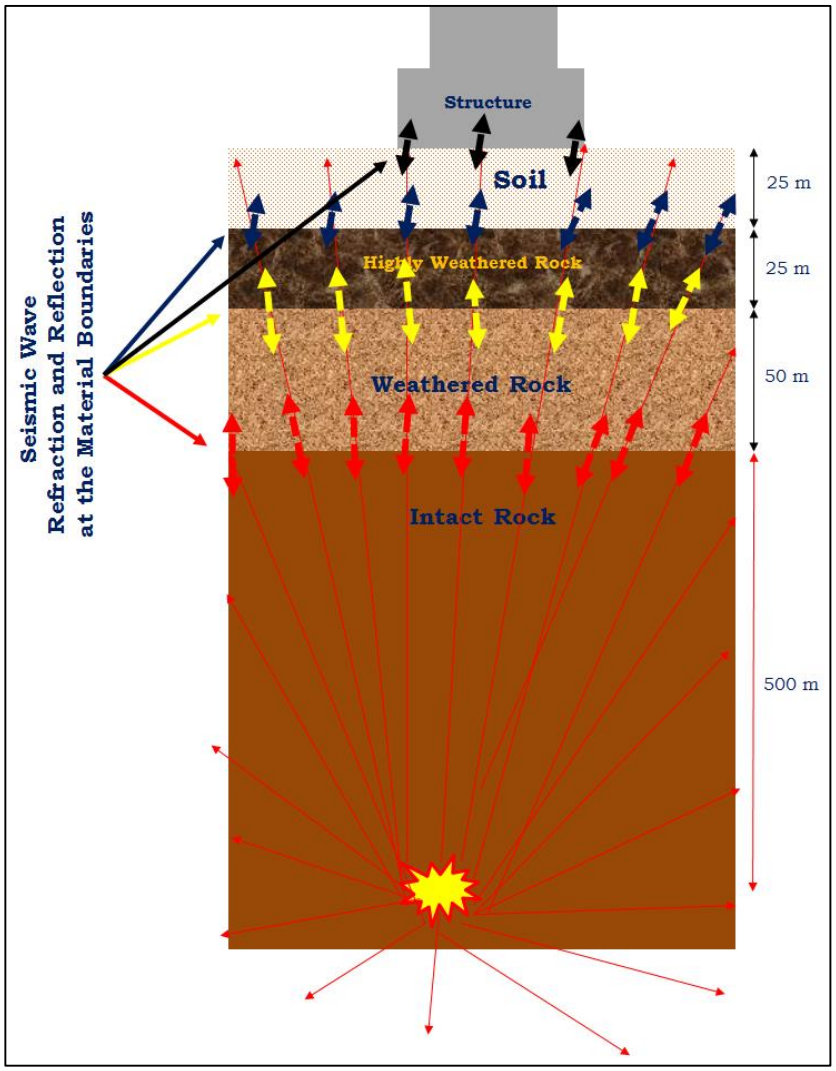


Figure 3.7 Idealized model showing depth of seismic source, geological layers and surface structure

The discrete element method, such as 3DEC and finite difference method such as FLAC, had the feature that allowed the application of seismic input below the foundation soils and simulated the transmission of seismic waves from the source to the structure. Furthermore, 3DEC and FLAC took into account the phenomenon of refraction and reflection of the seismic waves induced due to the presence of discontinuities in the path of wave propagation, as explained in Figure 3.7. From the stratigraphic viewpoint, two possibilities were considered for the seismic structural analysis: foundation layer consisting of either soil or highly fractured rock (outcrop, slope, etc.).

3DEC was used for the analysis of structures founded on rocks, whereas FLAC was used for the analysis of structures founded on soil and a tailing dam slope. The reason for using FLAC for foundation soils was the stiffness contrast between the materials that is the bedrock, the soil and the candidate structure. Analysis of a model with high stiffness contrast took a very long time with 3DEC. Also 3DEC is a dis-continuum code and less efficient for the analysis of continuum mediums for which FLAC was ideally suited.

According to Itasca (2014), FLAC is a general-purpose code that can simulate a full range of nonlinear static and dynamic mechanical problems, with coupled fluid flow, heat flow and structural interaction. It is suited to modelling continuous materials containing, perhaps, a few discontinuities that exhibit nonlinear behaviour. It can represent any geometry and the boundary conditions are quite general. Salient features of the FLAC code are given as follows:

- FLAC simulates the behavior of nonlinear continua (with embedded interfaces) by the generalized finite difference method (arbitrary element shapes), also known as the finite volume method.
- FLAC solves the dynamic equations of motion in the time domain and follows any constitutive relation in large or small strain mode.
- Every feature of FLAC is accessible from a powerful Graphical User Interface.
- The code has many built-in block and joint constitutive models that are representative of the geologic or similar materials. It also has a user-defined constitutive model option.

- The structural element module helps to models cables, beams, and liners to study the rock-structure-interaction.
- The code allows modelling of transient and steady state fluid flow in joints.
- The code provides highly interactive manipulation of screen images for the interpretation of results.
- The code solves the full dynamic equations of motion even for quasi-static problems.
- The code is explicit and allows for the estimation of ground motions in real time in terms of displacements, velocity or acceleration time histories.

3.4.3. Numerical simulation stages for the seismic structural analysis

FLAC simulation stages are similar to the 3DEC simulation stages, that is, it also considers the *in situ* stress state in the ground before any construction or excavation is made. In FLAC simulations, the creation of initial conditions representative of the *in situ* stress state was the first step. For the initial conditions of the study area, field stresses were used from Birch and Handley (2014), as discussed in Chapter 2. In the second stage, simulations were made for the seismic structural analysis. FLAC was used for the analysis of a tailings dam slope and evaluation of the stability of a soil slope.

3.5. Assessment of Risk to Surface Structures

3.5.1. Masonry and Concrete Buildings

The seismic structural analysis was implemented in order to estimate the drift capacity (horizontal displacement) of surface structures. In civil engineering terminology, design drift is the maximum spectral displacement a building can sustain without affecting its structural integrity and function. As such, building standards in South Africa as contained in SANS 10160-4:2009 (draft stage) do not specify provisions of structural drift limits (spectral displacement vis-à-vis earthquake acceleration) therefore, guidelines were taken from Searer and Freeman (2004).

Searer and Freeman (2004), compared the spectral displacement (drift time history) of the five natural earthquakes namely spectral acceleration, as shown in Figure 3.8. In this figure, black and brown lines indicate the UBC (Uniform Building Code, 1977) design spectrum of spectral displacement (drift time

history), whereas plots in purple, pink, red, green, and blue show the spectral displacement (drift time histories) of various earthquakes as mentioned in the figure.

In this study, seismic events of magnitude M_L 3 to 4 with likely acceleration of 0.4 g to 0.6 g were simulated and the structural response was compared with the response given in Figure 3.8, for time period of 0.5 to 1.0 seconds.

The buildings considered for the seismic analysis were characterized with a time period of 0.10 to 1.0 seconds with their natural frequency in the range of 10 to 0.1 Hz. In view of the seismic parameters and the structural aspects of the study, the average spectral displacement (drift) from Figure 3.8 was considered as 127 mm (5 inches) for the hazard/risk assessment (drift demand vs capacity).

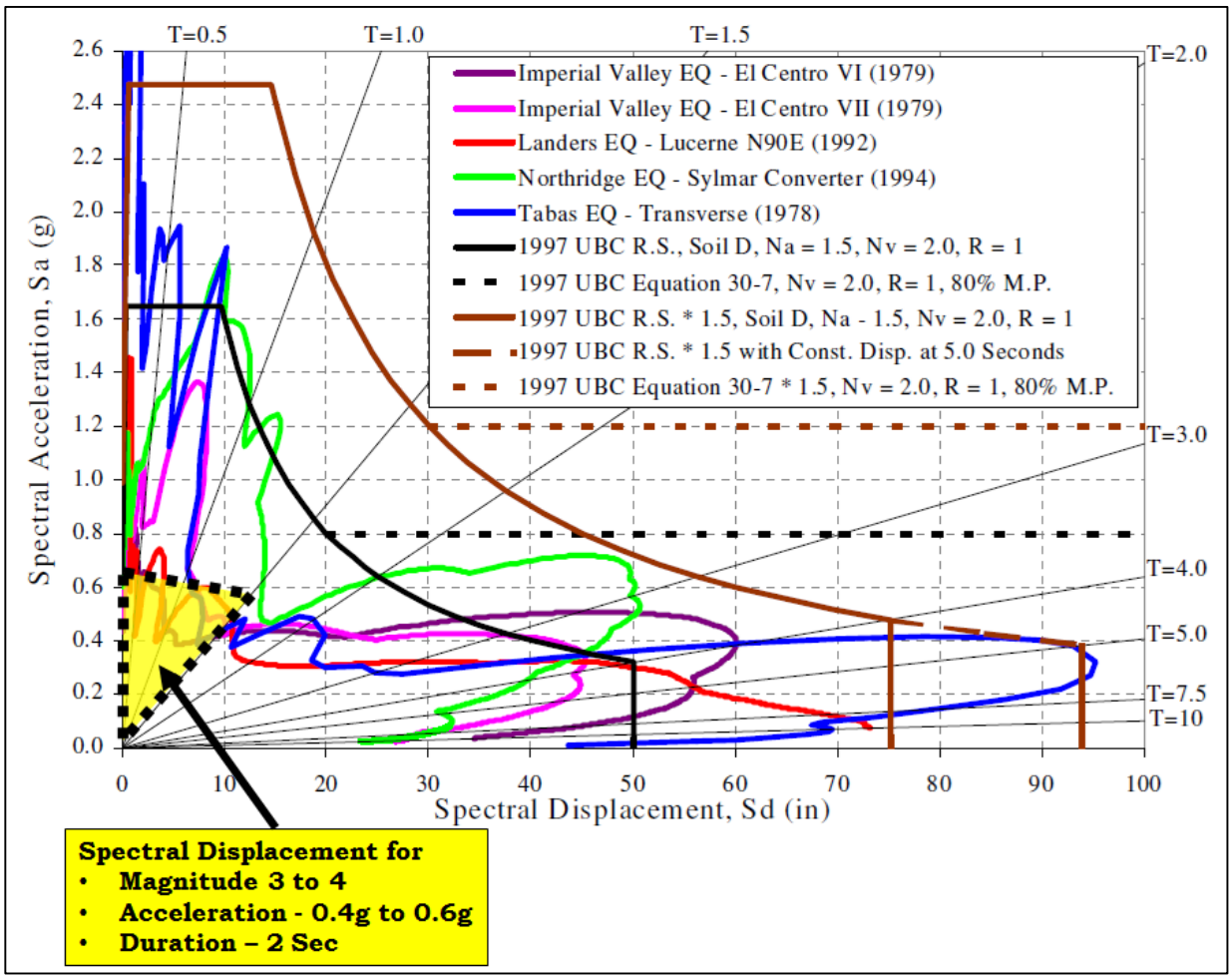


Figure 3.8 Spectral acceleration and the spectral displacement of natural earthquakes, after Searer and Freeman (2004)

3.5.2. Liquefaction Potential of a Tailings Dam Slope and Stability of Rock/Soil Slopes

Liquefaction potential was analysed using the Finn-Byrne liquefaction model provided in FLAC, Itasca (2014), which required an estimation of parameters C_1 and C_2 from the normalized standard penetration test (SPT) values (further details of C_1 and C_2 parameters are available in Itasca (2014) and are not covered in this chapter). A normalized SPT value of 10 was assumed for the upper two layers of the tailings dam slope which corresponded to C_1 = 0.4904 and C_2 = 0.8156.

Liquefaction analysis requires appropriate modulus reduction and damping ratio curves. The soil properties considered for the tailing dam slope were those of liquefiable soils (similar to the ones considered in the FLAC Manual) therefore modulus reduction and damping curves were adopted from Itasca (2014), as shown in Figures 3.9 and 3.10. Stability of rock and soil slopes against the seismic loading was assessed according to the guidelines provided by ASCE (American Society of Civil Engineers) which are described in Chapter 6 along with the respective slope analyses.

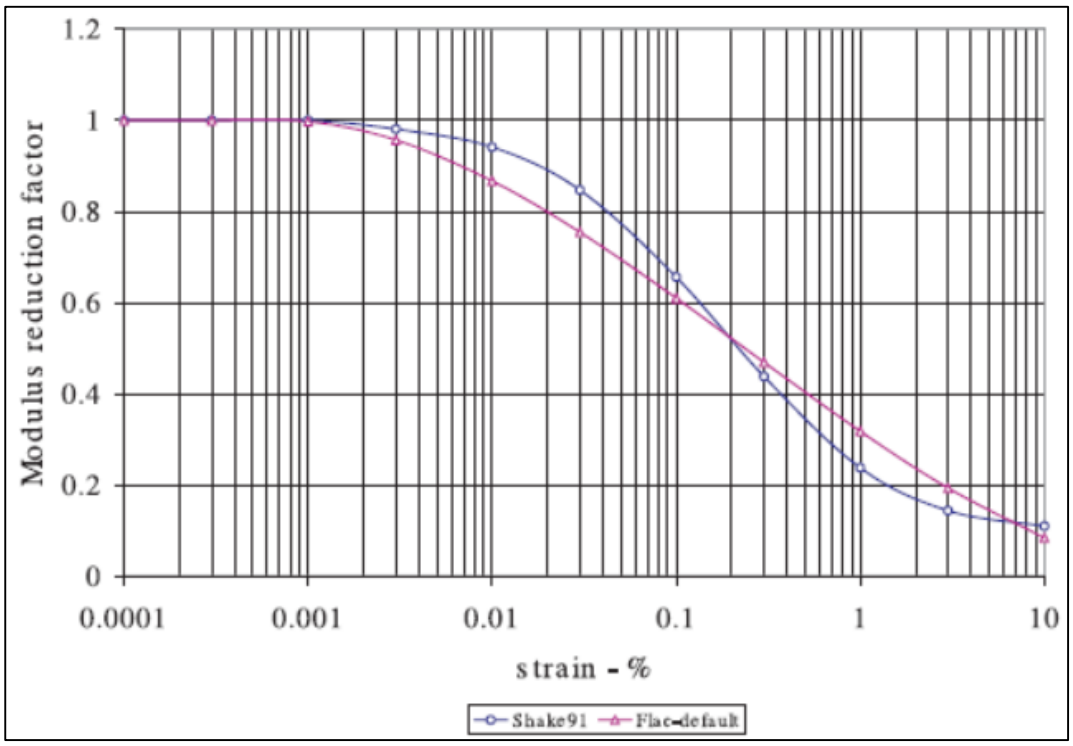


Figure 3.9 Modulus reduction curve for clayey soil (FLAC default hysteric damping with L1 = -3.156, L2 = 1.904), Itasca (2014)

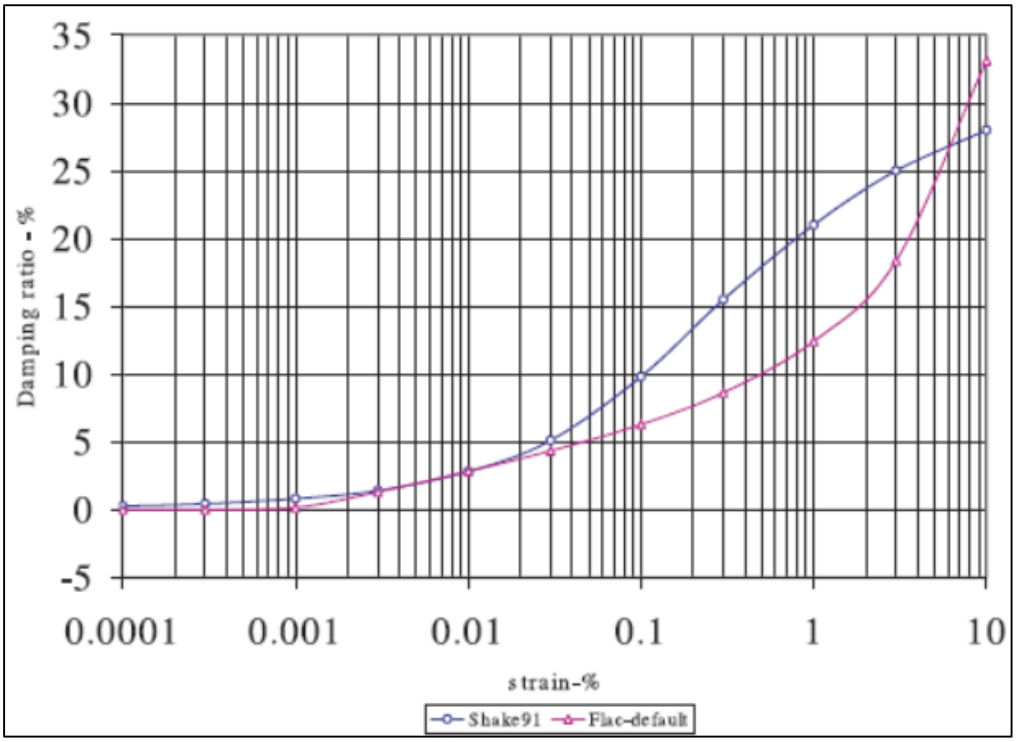


Figure 3.10 Damping ratio curve for clayey soil (FLAC default hysteric damping with L_1 = -3.156, L_2 = 1.904), Itasca (2014)

3.6. Conclusion

The chapter described the conceptual framework of the study as a whole and of the two main components, Mining-induced Seismicity and Effects on Surface Structures. Details on the methodology adopted for each component of the study were also discussed.

The next chapter. Site Characterization, covers the geomechanical aspects of the study area and provides a geomechanical model for numerical modelling for simulation of the ground motions in terms of velocity time histories at various points in the study area.

4. SITE CHARACTERIZATION

4.1. Introduction

The Central Business District (CBD) area of Johannesburg is located close to the mined out reefs and consists of surface structures of various types such as masonry, concrete, low-rise and high rise building, and so forth. The gold deposits in the Central Rand existed mainly in the form of conglomerate reefs with varying orientation along the dip and strike. The list of gold-bearing reefs in the Central Rand includes Main Reef, Main Reef Leader, South Reef, Bird Reef, and Kimberly Reef, and so forth as shown in Figure 4.1. Gold mining in the Central Rand continued over an extended period of time, and active mining practically ceased in 1977, Viljoen (2009).

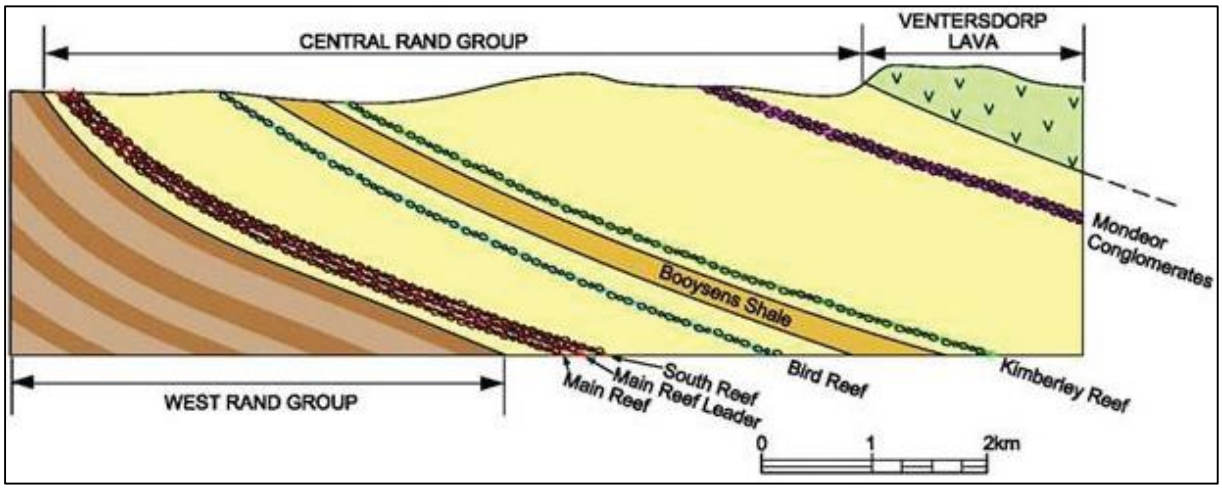


Figure 4.1 Gold bearing conglomerate reefs of the Central Rand Group, Superior Mining (2013)

In view of the layout of the gold reefs, mining methods employed in the Central Rand included open pit and underground mining methods. The underground mining mainly comprised breast stoping wherein the development was kept in the footwall, Raise cuts were made between the ends and from these raises, gullies were cut at angles of 45 degrees, Viljoen (2009) as shown in Figure 4.2.

The footprint of the abandoned mines is an extremely large area along both the dip and strike in the Central Rand and elsewhere in the Basin. According to Viljoen (2009), among various other Central Rand Mines, Crown Mines Limited alone has left over 1600 km of underground excavations within the surface

footprint of 42 square km. The overall area of the mine leases in the Central Rand is approximately six times that of the Crown Mines Limited.

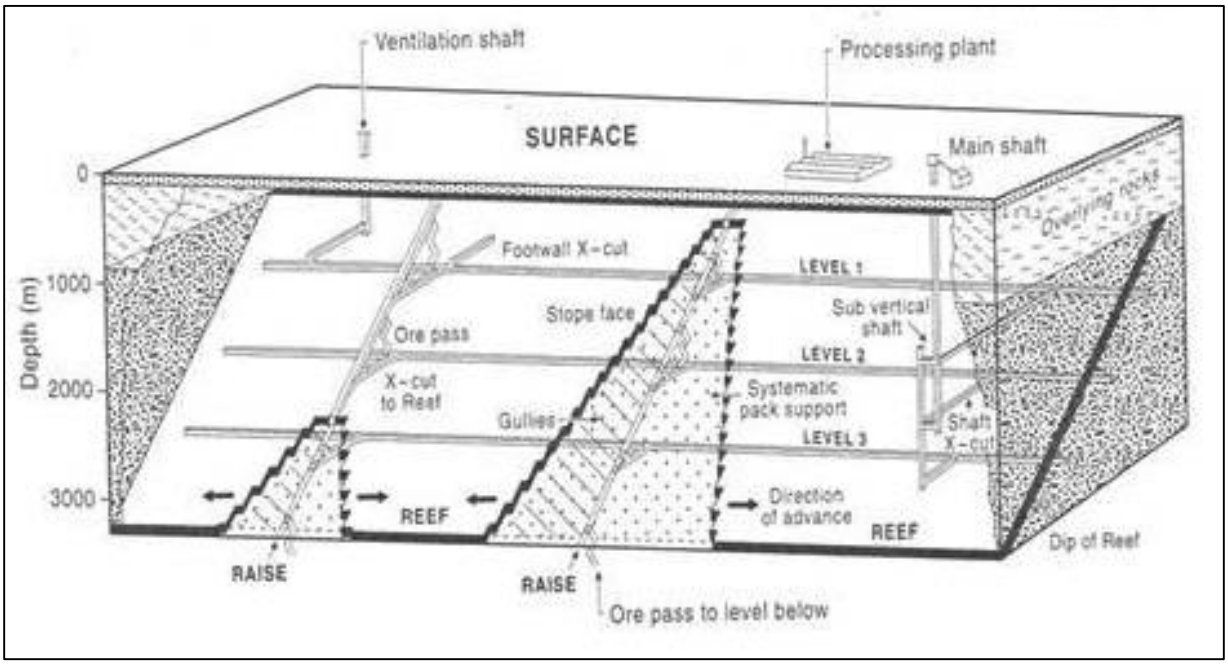


Figure 4.2 Underground mining method (breast stoping) for mining of narrow conglomerate reefs, Viljoen (2009)

According to the approximate extrapolation of the footprint of the Crown Mines Limited over the entire Central Rand, the approximate footprint of all the mines approximates to 252 km^2 almost $1/7^{th}$ of the area of Johannesburg (1645 km^2). In the post-mine closure scenario, these mining methods had an inherent tendency to trigger slip/fall of ground/pillar collapse due to the failure of support systems as result of sustained weathering (more so in flooded conditions) and also because of the stress relief fracturing.

4.2. Factors Considered for Site Characterization

Evaluation of mining-induced seismicity and its effects on the surface structures involved a study of the site response to dynamic loading. The site response to dynamic loading depended on the geological, geotechnical, hydrological and seismological conditions; identification/investigation of these conditions which was termed as site characterization. The purpose of this chapter is to characterize site conditions of the study area as shown in Figure 4.3. The data on all factors was gathered from the Council for Geoscience and the literature.

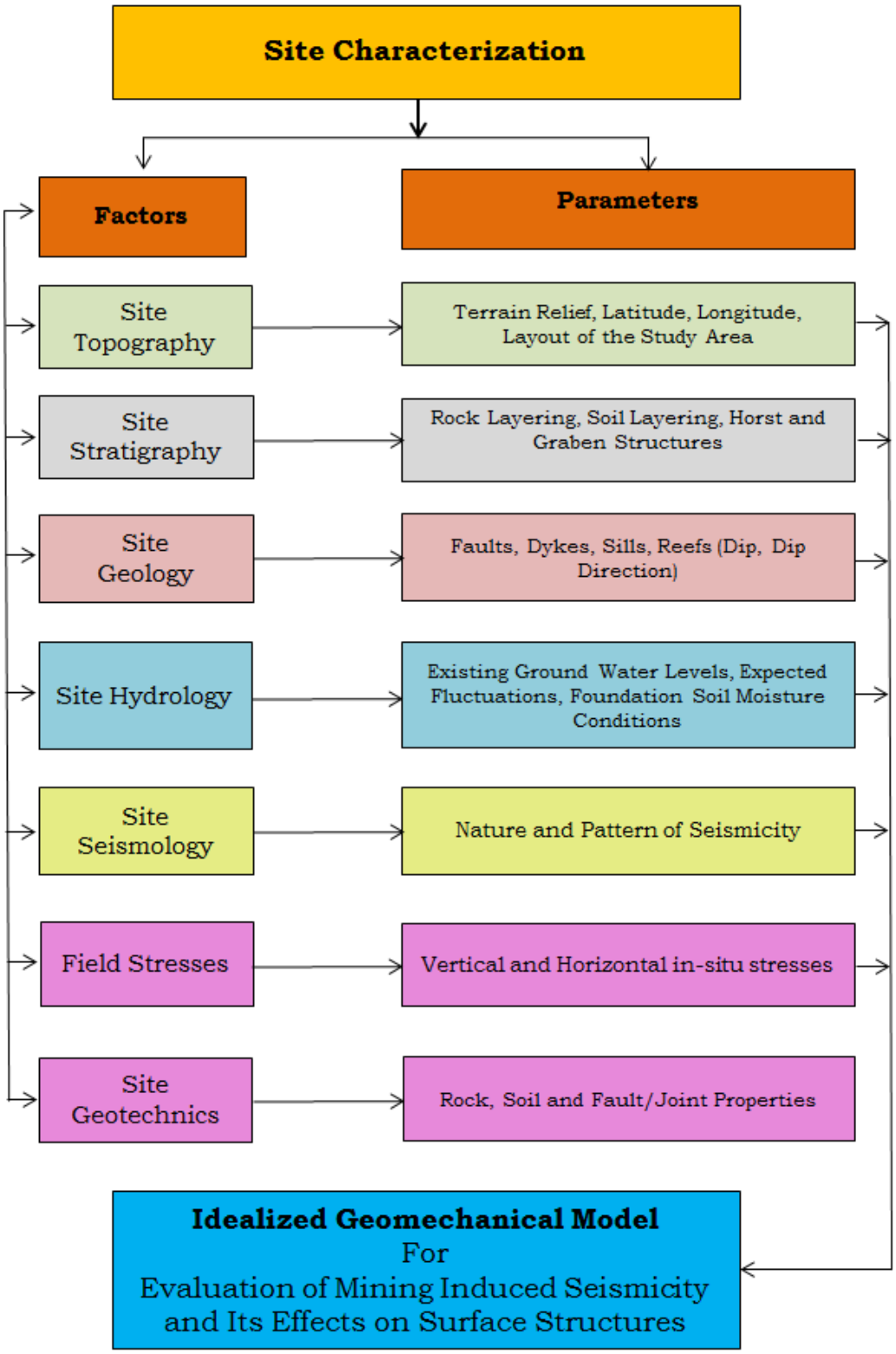


Figure 4.3 Factors considered for site characterization

4.3. Site Topography

The study measures of 4000 m x 4000 m and is part of the Central Business District (CBD), Johannesburg, shown in yellow in Figure 4.4. The topographic

map of the study area was obtained from the office of The Council for Geoscience, Pretoria. Most of the study area was located on the north side of the M2 highway. The elevation of the area varied from 1594 m (Main Reef, Fordsburg, etc.) to 1838 m (Hillbrow, Wits University, etc.). General relief of the study area dips towards the south.

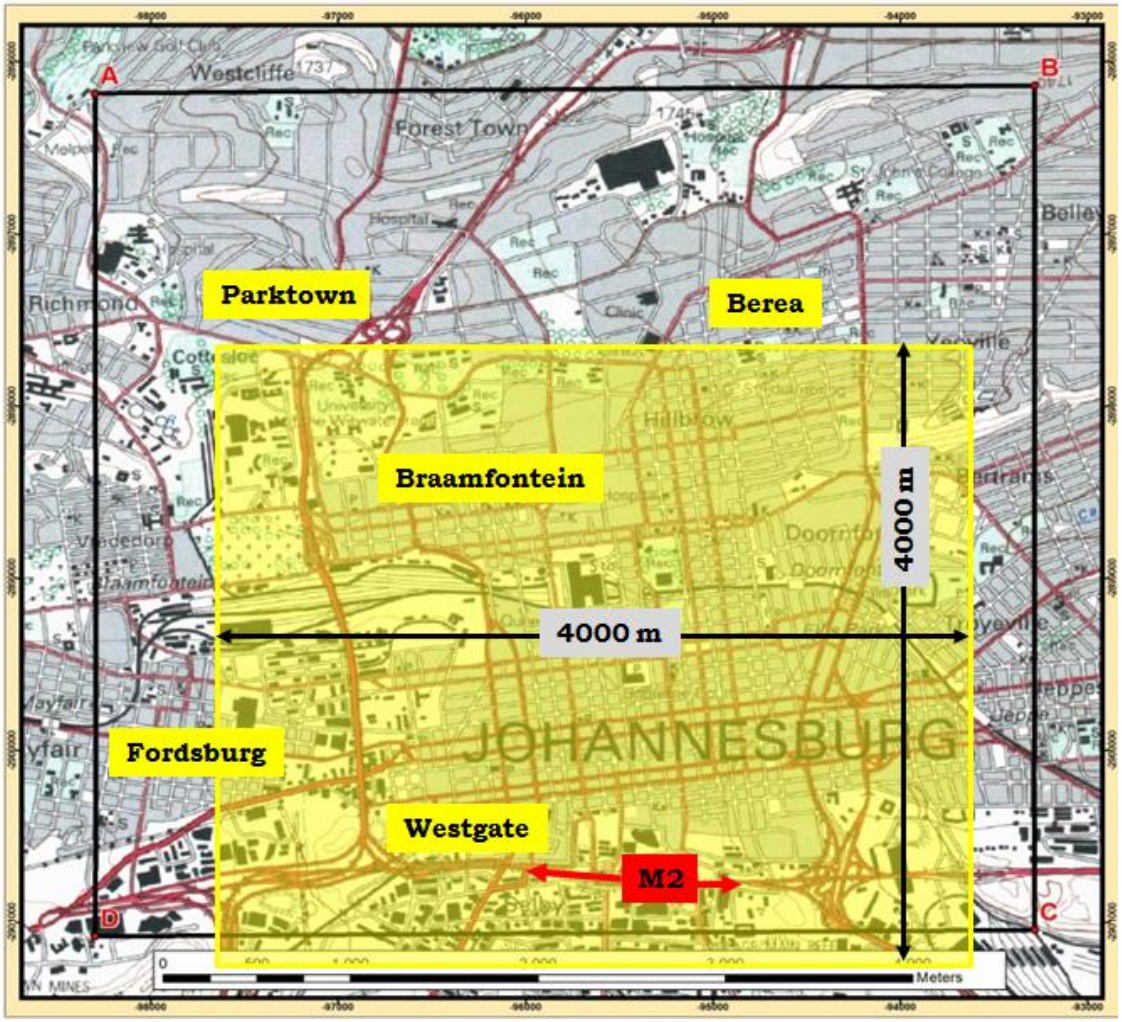


Figure 4.4 Topography of the study area, after Council for Geoscience (2013)

4.4. Regional and Local (Study Area) Stratigraphy

Simplified regional stratigraphy of the Witwatersrand Super Group is illustrated in Figure 4.5 and Figure 4.6, whereas the stratigraphic profile is shown in Figure 4.7. The study area belongs to the Johannesburg subgroup of Central Rand Group and Jeppestown, Government and Hospital Hill subgroups of Western Rand Group, shown in Figure 4.7 (marked with red and green). All stratigraphic units are dipping southward.

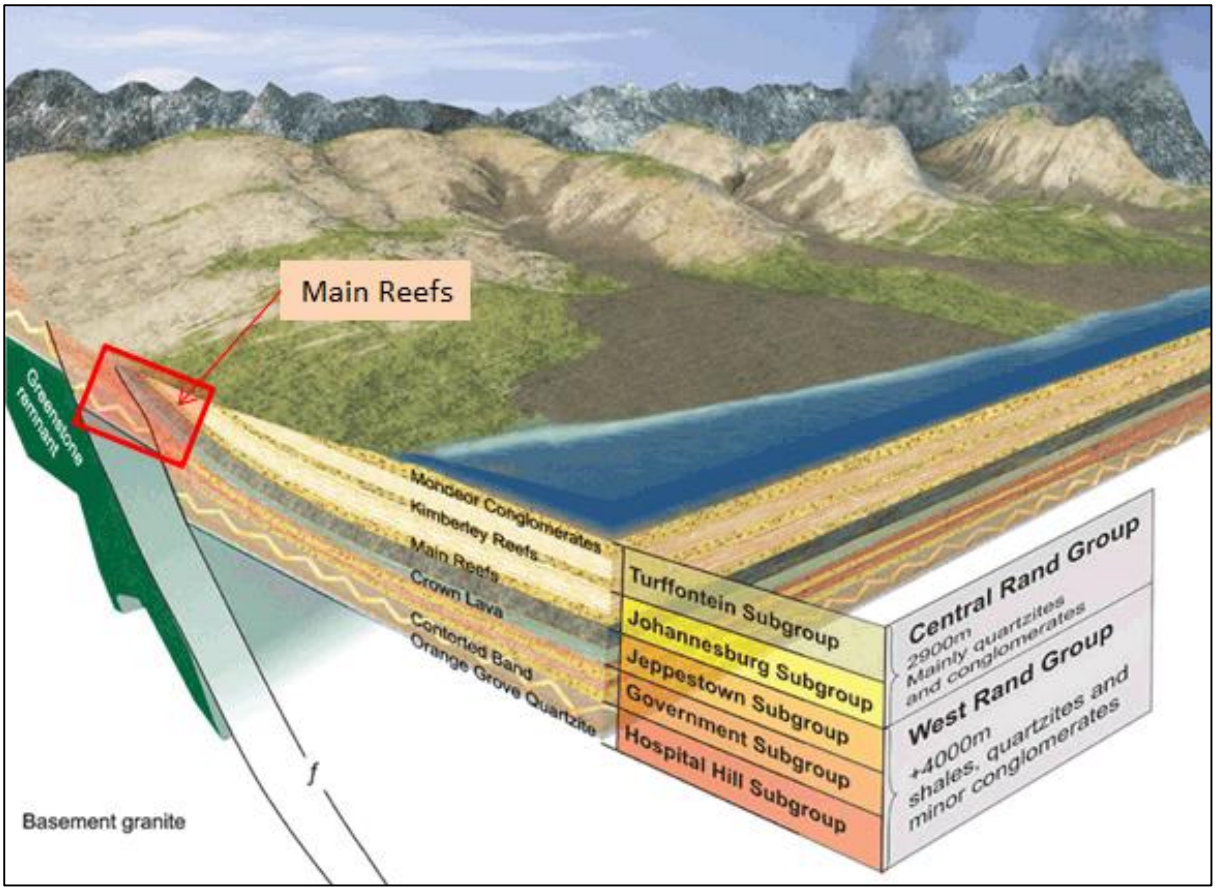


Figure 4.5 Generalized geological model of the study area (not to scale), after Gold Fields (2013)

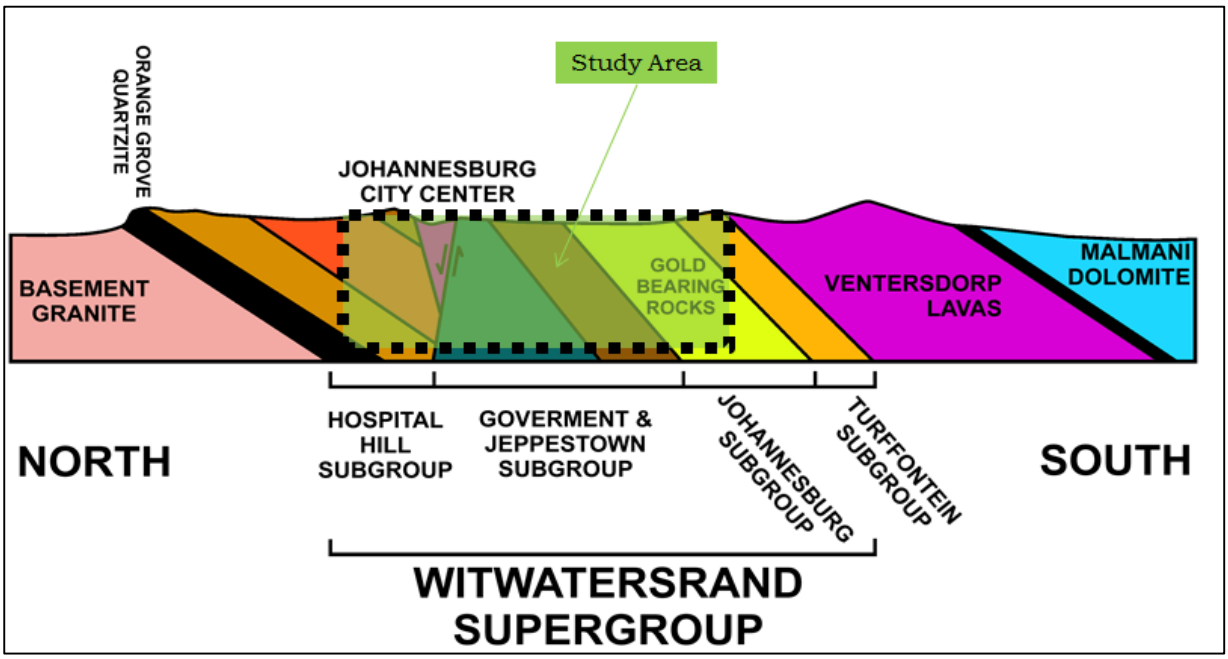


Figure 4.6 North-south cross-section through the Witwatersrand Basin beneath Johannesburg city (not to scale), after Norman and Whitfield (2006)

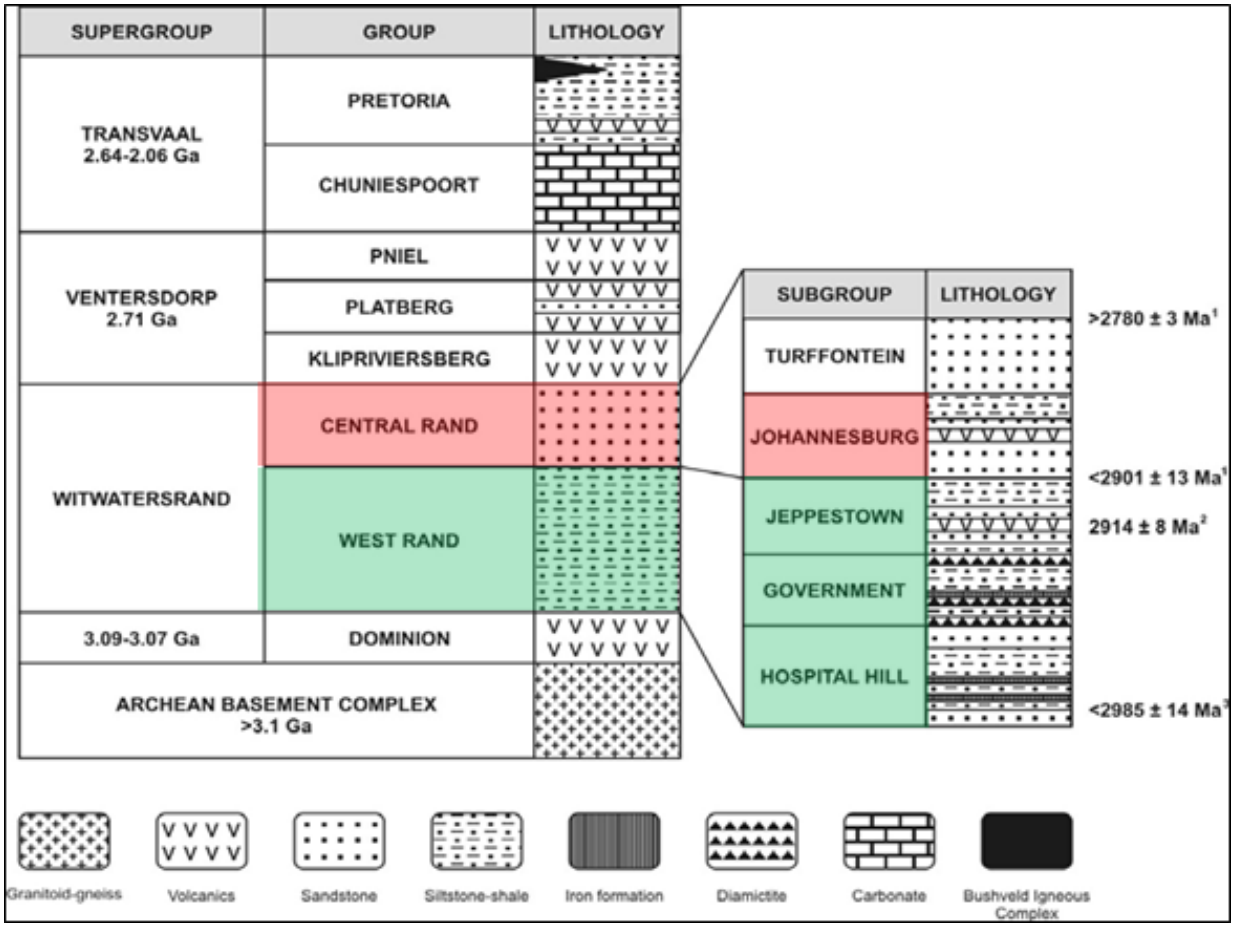


Figure 4.7 Simplified regional stratigraphy of Witwatersrand, after Dankert and Hein (2010)

4.4.1. Central Rand group

This group is the central part of the Basin and does not conform to the layout of the West Rand Group. It is 2880 m thick and subdivided into two groups, namely the Johannesburg Subgroup and the Turffontein Subgroup, Porter Geoconsultancy (2011). The base of the Johannesburg Subgroup is a conglomerate overlying quartzite of the Maraisburg Formation. The two units are locally truncated and overlain by the wide-spread deposition of conglomerates called the Main Formation. It contains the economically important reefs; Main Reef, Carbon Leader Reef and Main Leader Reef in both the Central and West Rand. The Main Formation is overlain by the Randfontein Formation which consists of conglomerate and quartzite. Along the northern margin of the Basin, the South Reef of the Central Rand comprises its base. The Johannesburg Subgroup is overlain by the Turffontein Subgroup. The study area involved only the Main Reef and Quartzite of the Johannesburg Subgroup.

4.4.2. West Rand group

Overlying the Dominion Groups, the West Rand Group is 5150 m thick having angular unconformity, Porter Geoconsultancy (2014). It is subdivided in three groups; the Jeppestown Subgroup, the Government Subgroup and the Hospital Hill Subgroup. The Jeppestown Subgroup is 1200 m thick underlying the Main Formation of the Central Rand Group. It consists of inter-bedded conglomerate, quartzite and shales and andesitic volcanic rock. Two sub-economic reefs are recognized in this subgroup. The Government Subgroup underlying the Jeppestown Subgroup and has more diverse lithology. It comprises inter-bedded conglomerate, shale, and iron formations. The base of this subgroup is a major regional unconformity of diamictite. Three sub-economic reefs are recognized in this subgroup. The Hospital Hill Subgroup is 2500 m thick having lithology composed of shallow marine deposits of diverse nature such as conglomerate, shales, siltstone, and banded ironstone and does not have any economic reefs. The study included rocks from the Jeppestown subgroup, Government subgroup and Hospital Hill subgroup.

4.5. Site Geology

The study area was located at the northern edge of Witwatersrand Basin as highlighted in the red circle in Figure 4.6. The Witwatersrand is an extensional arcuate basin just south of the area where two faults run very close (almost parallel) to each other. The study area was bounded by the Robinson Deep Syncline on the West and City Deep Anticline on the East. The other major geological features of the central Rand Group included the Reitfontein Fault Zone, the Roodepoort Fault and many anticlines and synclines, Figure 4.8. The presence of these geological structures had a potential to influence the propagation of seismic waves (reflection and refractions manifesting into complex waveforms). Geologically, the Central Rand consists of horst and graben structures of sandstone and conglomerate layers with varying geology, Figure 4.9. The graben comprises Amygdaloidal Andesite (Ventersdorp Lava). The southern horst (located generally south of the Main Reef) consists of quartzite, whereas the northern horst (located generally north of the Main Reef) is a mix of quartzite, slates and Archean granite rocks. Theses rocks are of siliciclastic

nature; mostly consolidated under the fluvial depositional environment, Porter GeoConsultancy (2007).

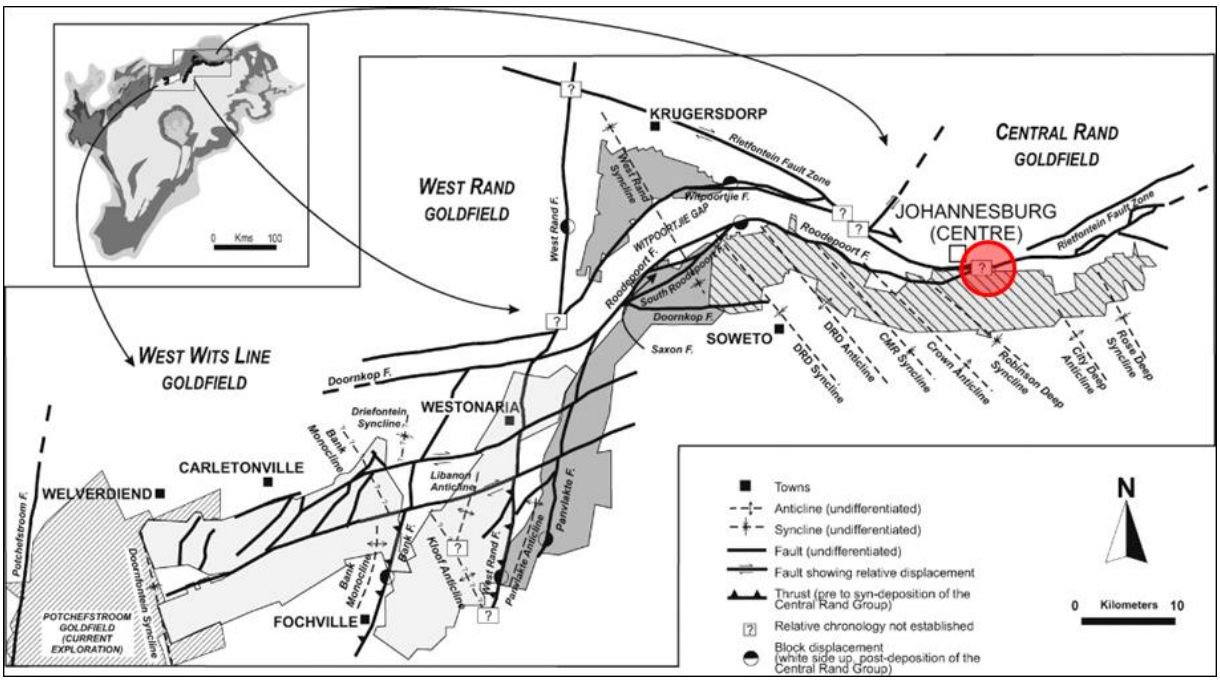


Figure 4.8 Geological structures in the Central Rand, Dankert and Hein (2010)

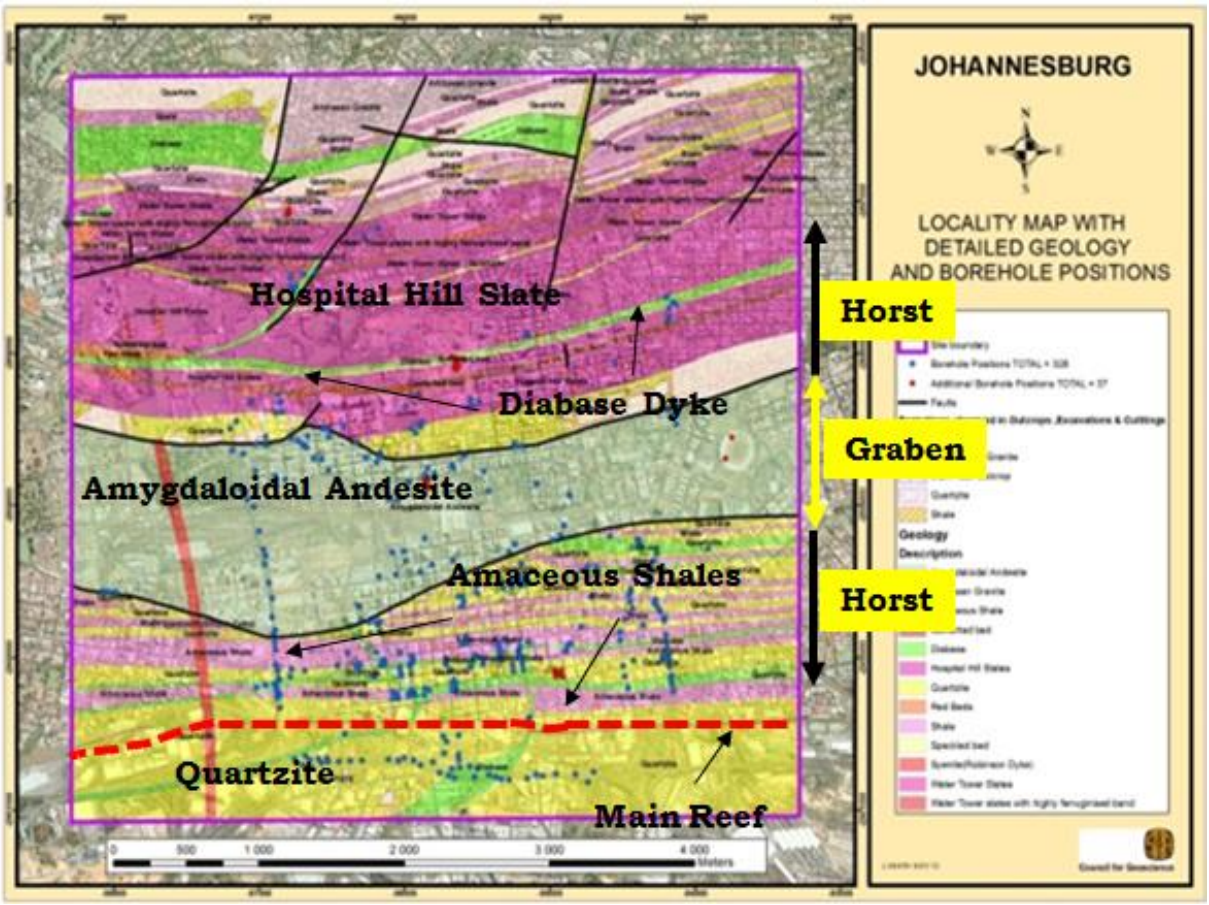


Figure 4.9 Geological map of study area, after Council for Geoscience (2013)

The presence of shallow marine quartz in the Booysens formation in the Central Rand suggests few transgressive events in the depositional arena, Bailey et al. (1990), Beukes and Nelson (1995). The geological profile of the study area comprising geological materials of various nature greatly affects the ground behaviour during seismic events and, consequently, the response of the surface structures. The stiffness contrast between graben and horst materials affects the wave propagation and had to be considered while performing dynamic studies.

4.6. Site Hydrology

During the period of active mining, the excavations were dewatered, supported with timber and selectively backfilled for short- to long-term stability. With the closure of the mines, the dewatering process in the mines was discontinued (no longer needed) which later on, resulted in the flooding of the abandoned mines. The phenomenon was first noticed in 2002 at a mine shaft in Mogale City (Randfontein area of West Rand), Acid Mine Drainage Report (2010).

According to McCarthy (2011), water in the Central Rand Basin rose at the rate of 12 m per month until 2011. The general groundwater relief dips southward of Johannesburg with existing ground water level of 400 m in the Central Rand whereas the water table is very shallow (close the ground surface) in the West Rand areas. The report also highlighted that a similar situation was developing in Central Rand (Johannesburg Area) and East Rand (Springs-Nigel Area).

According to Birch and Handley (2012), the groundwater in the Central Rand during 2013 remained at a depth of 400 m. The hydrological relief of the study area is generally towards the south as shown in Figure 4.10. According to Winde (2011), the final mine water level in the abandoned mines in the Central Rand would remain 100 m below the ground surface as illustrated in Figures 4.11 and 4.12 (General location of the study area is shown in red block (not to scale)). The factors considered by Winde (2011) included elevation of potential outflow points, hydraulic and charging properties in mining voids, final decant volume and local ground water flow inversions.

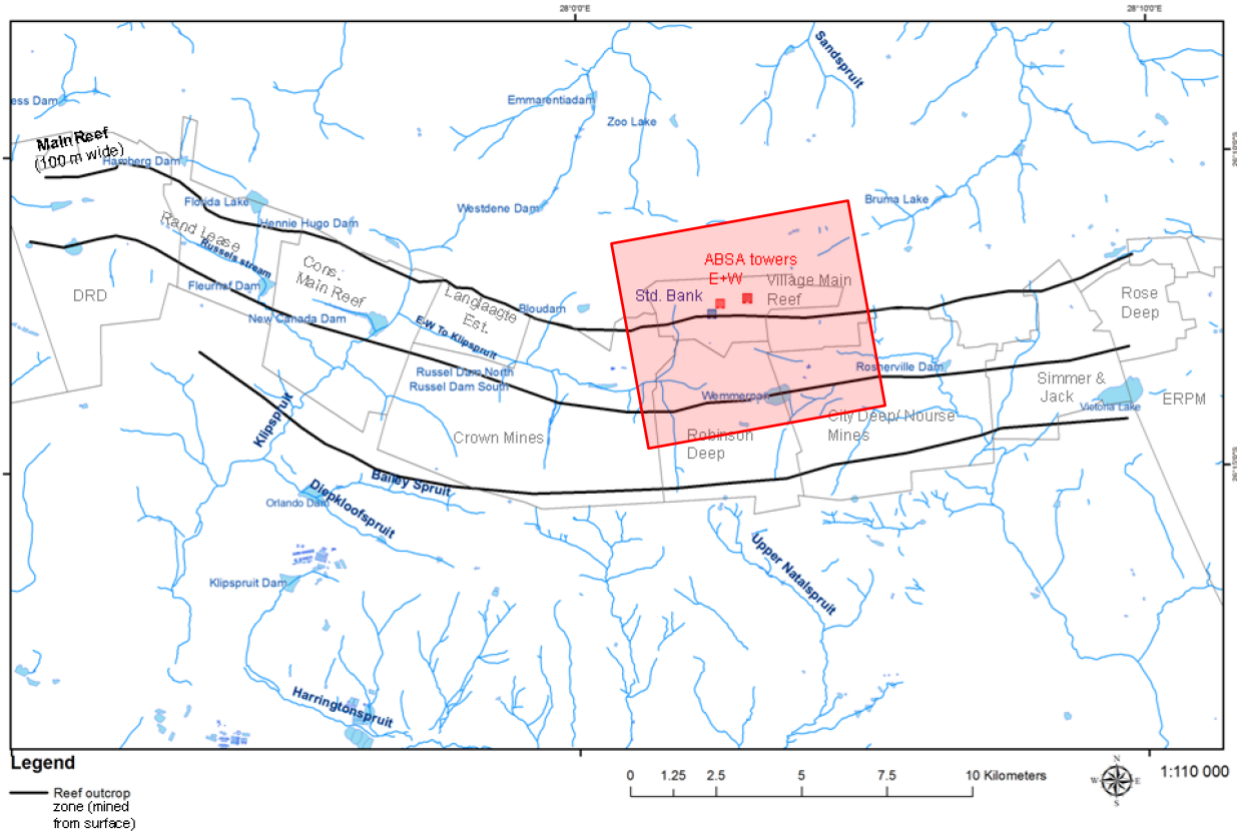


Figure 4.10 Hydrological relief of the Central Rand (Study area shown in red, not to scale), after Winde (2011)

Keeping in mind the mining methods, layouts and steep dip angles, the phenomenon of flooding is likely to adversely affect the support systems, weathering of rock mass, strength of rock mass and strength of discontinuities (geological and mining induced). The fact was duly recognized in the light of the report by Council for Geoscience (2012) which stated that increased seismicity had been observed around abandoned mines in the period spanning from April 2010 to October 2012. An end to the dewatering of the abandoned mines in the Central Rand adversely affected the long-term stability of abandoned mine excavations and stability of geological discontinuities. The flooding of abandoned mines had the potential to manifest in increased seismicity with adverse effects on surface structures, surface subsidence in close vicinity of the abandoned mines and Acid Mine Drainage (AMD).

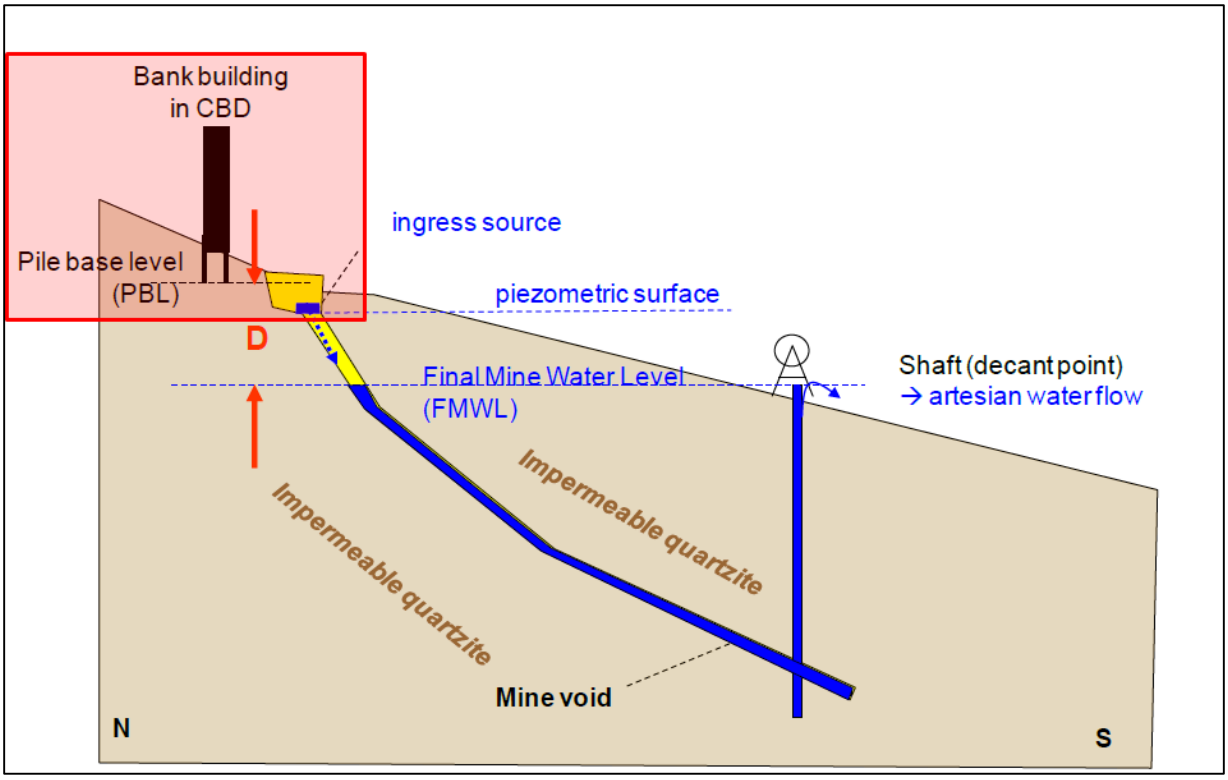


Figure 4.11 A north-south oriented idealized model (not to scale) to visualize flooding levels in abandoned mines, after Winde (2011)

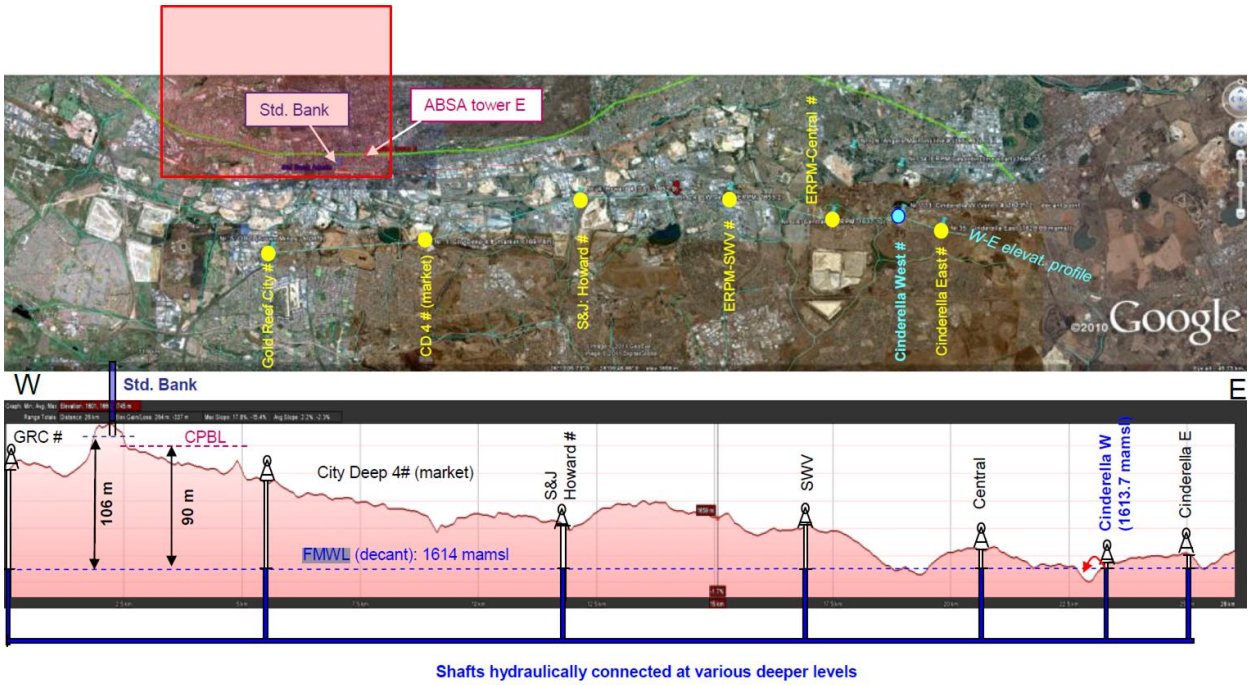


Figure 4.12 An east-west oriented profile (not to scale) showing Final Mine Water Level indicating a safety margin of 106 m below the Standard Bank building, after Winde (2011)

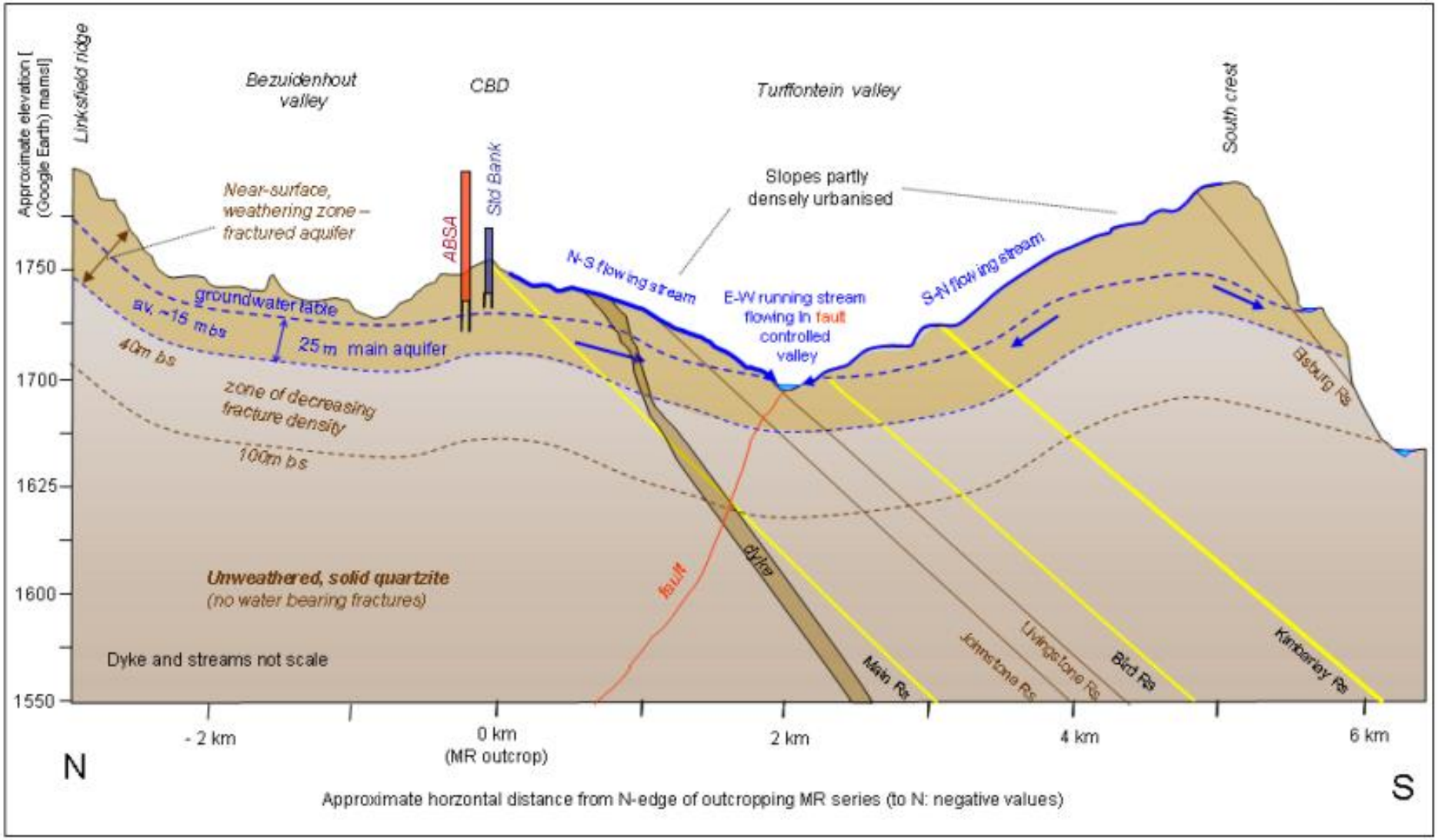


Figure 4.13 Post mining geological and geohydrological conditions in the central part of the Central Rand, Winde (2011)

Salient aspects of the existing geo-hydrological conditions are highlighted in Figure 4.13 and listed as follows:

- The upper strata from the existing ground surface to a depth of 100 m is fractured and has the potential to host ground water.
- Below a depth of 100 m, the rocks are unweathered and do not have water-bearing fractures.
- The main aquifer is generally 25 m thick and is located at a depth of 15 m from the ground surface.

In abandoned mines below a depth of 100 m, ground water exists only in the mined-out reef (excavations and fractures). Both hanging walls and foot walls are solid and do not contain ground water.

- For the purposes of research, the effects of ground water on mining induced seismicity were considered as follows:
  - For the simulation of Impulsive Slip, pore pressure was incorporated along the joint slip area.
  - For the simulation of Fall of Ground, the voids were considered as completely flooded.
  - For the simulation of Collapse of Pillar, voids (either side of the pillar) were considered as completely filled with water.

4.7. Seismological Conditions

Details of the seismological conditions were discussed in Chapter 2.

4.8. Field Stresses

The Witwatersrand Basin, like all other areas, possesses certain inherent in situ tectonic stresses. These field stresses, during and after mining (at varying depth horizons, layouts, time span, etc.), change and are termed as “mining-induced stresses”. The resultant stress redistribution in both vertical and horizontal extents around mining excavations and pre-existing geological structures had a potential to trigger mining-induced seismicity.

According to Wong (1993), in a tectonic compressive stress regime, a decrease in lithostatic stress (minimum principal stress) or an increase in the maximum horizontal stress could lead to failure, resulting in a mining-induced seismic event.

The study carried out by Spottiswoode, et al. (1993), on the focal mechanisms for various earthquakes in East Rand Proprietary Mines, enabled the authors to distinguish between tectonic and mining-induced earthquakes and also the risk of insitu stresses on mining seismicity. According to the theoretical stress model proposed by McGarr (1971), maximum principal stress *(in situ* stress) in a stope is oriented nearly vertical in both footwall and hanging wall, 10 m ahead of the mining face (highly stressed zone).

However, Spottiswoode, et al. (1971) found considerable variations in the minimum principal stress. Although the McGarr (1971) model of maximum vertical stress agrees with a condition typical to tectonic earthquakes, the observations of Spottiswoode et al. (1971) suggest seismicity due to changes in the *in situ* stresses due to mining.

According to McGarr, et al. (2002), the changes in stresses as small as 0.01 MPa may trigger seismic events. According to Byerlee (1978), the strength of the upper pervasively faulted crust depends on the sliding friction across the faults in the crust. In the post-mine closure scenario, factors such as flooding of the abandoned mines, weathering of the rock mass and deterioration of the support systems are continually evolving new sets of field stresses in the entire Basin. The effect of the new stresses is detrimental to the strength of the upper stratum with the possibility of mining-induced seismicity.

The estimate of these total stresses (virgin stresses and mining-induced stresses) is essential for any regional and site-specific seismic analysis. Birch and Handley (2012) in their report on “Investigating Rock Mass Stability after Mine Flooding in the Central Rand Basin” carried out a comparative analysis using four crustal stress models (Lithostatic Stress Model, Rigid Confinement Model, Denudation Model and Simple Tabular Model) and proposed a stress model for

Rock Mass Stability Analysis in the Central Rand. The authors used the Southern African Stress Database as a guide during their analysis.

This study used the stress model proposed by Birch and Handley (2012). Salient features of this stress model are as follows:

- For depths shallower than 500 m, $\sigma_v = \sigma_h$
  Where, σ_v = vertical stress
  σ_h = horizontal stress
- For depths greater than 500 m:
  - Vertical stress $\sigma_v = 0.027z$ MPa, where z is depth below surface (metres),
  - Horizontal stress, $\sigma_h = 0.72\sigma_v \cong 0.02z$
  - At the ground surface (z = 0), σ_v = 0 and σ_h = - 3.5 MPa.

4.9. Site Geotechnics; Types and Characteristics of the Foundation Soils and Rocks

Site geo-technics encompass all aspects related to soil and rock mechanics, such as physical, mechanical and stiffness properties. Site geo-technics affect the type and magnitude of the seismicity, which triggers the source and propagation of seismic waves. Also, the ground behaviour and soil/rock-structure-interaction depends on the site geo-technics. For site-specific evaluation of the mining-induced seismicity and its effects on surface structures, the study area was divided into geotechnical domains (with similar geotechnical characteristics) as follows:

- Northern area (foot wall) comprising quartzite rocks.
- Central area (Main Reef) composed of conglomerates.
- Southern area (hanging wall) comprising shales, andesite, slates and quartzite rocks.

4.9.1. Northern area

Soils in this area are classified as Clayey Silty Sands, Silty Sands, and Sandy Clays with the presence of fine quartz gravel. The origin of these soils was traced to transported soils and weathering of granitic rocks. The upper soil layer and the lower residual soils were separated by “Pebble Marker” layer, de Beers

(1965). Soils derived from Diabase dyke are Silty Clays to Clayey Silts and are present up to a depth of around 20 meters at dyke locations, de Beers (1965).

4.9.2. Central area

The soils in this area are mainly Silty Clays derived from Ventersdorp Lavas. These soils are present to a depth exceeding 45 meters and also overlain by transported soils, de Beers (1965).

4.9.3. Southern area

The soils in this area are silty clays and silty sands. The origin of these soils was traced to transported soils and weathering of parent rocks.

4.9.4. Geotechnical properties of rocks and soils

During seismic rates of loading (in the order of 1000 mm/m/sec, the strength of the rock was expected to increase by 20-30 %. Resultant dynamic moduli tended to increase around 35 %, Ryder and Jager (2002). Therefore, keeping in mind the dynamic nature of research analyses using 3DEC and FLAC codes, dynamic geotechnical properties (dynamic bulk and shear modulus) were estimated.

Estimated rock mass properties for evaluation of mining-induced seismicity using 3DEC code are given in Table 4.1. Young's modulus values of rocks (intact) were reduced for rock mass using the Equation proposed by Hoek and Diederichs (2005), given below:

$$E_{rm} = E_i \left[\frac{1 - \frac{D}{2}}{1 + e^{\frac{(60 + 15D - GSI)}{11}}} \right] \qquad \text{Equation 4.1}$$

Where,

E_{rm} = Young's modulus for rockmass,

E_i = Young's modulus for intact rock,

D = damage factor, GSI is geological strength index.

A GSI of 75 and damage factor of 0 was assumed for all rock materials while calculating the rock-mass modulus- E_{rm}.

Rock characteristics (Young's Modulus, and Poisson's Ratio) used in the research analysis were obtained using Hooke's Law (equations for stress/strain by Lama and Vutukuri (1978)).

The equations for dynamic moduli, p-wave and s-wave wave velocities are given as:

$$G_d = \rho\, C_s{}^2, \qquad \text{Equation 4.2}$$

Where G_d is dynamic shear modulus (GPa), ρ is rock density (kg/m^3), and C_s is s-wave speed in m/sec.

$$E_d = 2\, G_d\, (1 + v_d), \qquad \text{Equation 4.3}$$

Where E_d is dynamic Young's modulus (GPa) is, G_d is dynamic shear modulus (GPa), and v_d is dynamic Poisson ratio.

$$v_d = \frac{1-2\left[\frac{V_s}{V_p}\right]^2}{2\left[1-\left(\frac{V_s}{V_p}\right)^2\right]}, \qquad \text{Equation 4.4}$$

Where v_d is dynamic Poisson ratio, V_s is s-wave speed (m/sec), V_p is p-wave speed (m/sec).

$$C_p = \left[\left\{\frac{K+\frac{4}{3}G}{\rho}\right\}\right]^{\frac{1}{2}}, \qquad \text{Equation 4.5}$$

Where C_p is p-wave velocity, K is bulk modulus, G is shear modulus, and ρ is the rock density.

$$C_s = \left[\frac{G}{\rho}\right]^{\frac{1}{2}}, \qquad \text{Equation 4.6}$$

Where C_s is s-wave velocity, G is shear modulus, and ρ is rock density.

Table 4.1 Geomechanical Parameters estimated for evaluation of mining induced seismicity

Rock Type	Density kg/m^3	Static Constants		Rock Mass	Static Constants		Dynamic Constants		P-wave m/sec	S-wave m/sec
		E (GPa)	*V*	E_{rm} (GPa)	Bulk Modulus K (GPa)	Shear Modulus G (GPa)	Bulk Modulus K (GPa)	Shear Modulus G (GPa)		
Quartzite	3000	70	0.19	57	31	24	34	26	4570	2829
Conglomerate Main Reef	2800	90	0.15	73	35	32	37	34	5260	3378
Amaceous Shale	2400	65	0.23	53	33	22	38	25	5060	2998
Amygdaloidal Andesite	2900	80	0.21	65	38	27	42	30	5032	3051
Diabase Dyke	3000	100	0.20	82	45	34	50	38	5495	3367
Hospital Hill Slate	2780	90	0.28	73	56	29	71	37	5810	3213
Water Tower Slate	2700	80	0.30	65	54	25	73	34	5704	3050
Archean Granite	2950	70	0.17	57	29	24	31	26	4560	2877
Soil	2000	1.0	0.30	-	0.50	0.30	0.50	0.30	-	273

4.10. Geotechnical Characteristics of the Geological Discontinuities (Faults/Joints)

Nine geological material groups were considered in the analysis. The boundaries between these blocks were considered as geological discontinuities. These discontinuities posed spatial heterogeneity in the initial stress state for numerical modelling different than the *in situ* stresses at the site. This was attributed to the stress path history followed by the candidate site during its geological history which was difficult to represent in any numerical model. However, for a small-scale model, it was possible to represent the stress state more accurately to mimic the geological history and mining operations. For a large-scale model, such as the one used in this research, the representative stresses were initialized using a stress model proposed by Birch and Handley (2012).

Like all rock masses, the research area contained geological discontinuities (faults, bedding planes, dykes, sills, joints, shear zones) as well as the mining-induced discontinuities in and around the mining voids. These discontinuities affect the rock-mass behaviour. In areas of low stresses (shallow depths and around stress-relieved mining voids), the behaviour of the rock mass was controlled by the pre-existing planes of weakness. Also, geological discontinuities played an important role in propagation of seismic waves. According to Perino (2013), an elastic wave undergoes attenuation upon incidence at a discontinuity (fault, joint, etc.); part of the energy is transmitted and part of it is reflected.

The boundary between soil/weathered rock and bedrock was provided with the relatively high-strength and stiffness properties (compared to typical soil stiffness properties) to avoid plastic failure and reflection of seismic waves. By doing so, this interface did not act as a joint between the material groups. Except for the geological discontinuities between the geological material groups, no other joint sets were considered in the analysis. The soil/weathered rock interface with bedrock was deemed horizontal, whereas all geological entities were considered dipping south. According to Hill et al. (1981), the gold reefs dip at varying angles from 30 to 85 along the 70 km strike in the Central Rand,

Witwatersrand Basin. However, for the purpose of this research, Main Reef dip of 45^0 is considered.

The 3DEC numerical code required five parameters to capture the behaviour of a discontinuity in the "coulomb slip model", namely: joint shear stiffness (jk_s), joint normal stiffness (jk_n), joint cohesion (c), joint friction (Ø) and joint dilation (Ψ). In any rock mass with discontinuities, parameters: jk_n, jk_s, and Ψ are nonlinear and change with changes in the operating normal stress and deformations. Values of these parameters have to be chosen with care, Ryder and Jager (2002).

The model had multiple and parallel discontinuities. According to Zhao, et al. (2006), seismic waves with wave lengths not much larger than the spacing of multiple parallel discontinuities undergo multiple reflections at successive discontinuities. These multiple reflected waves reach a particular point in the area of interest at different times. The waveform recorded at a given point is thus the sum of all these reflected waves. This analysis aimed at recording ground motions at bedrock (presumed) due to the compound effect of the given conditions of model geometry, rock-mass properties, multiple discontinuities and discontinuity properties, under dry and wet conditions for fall of ground, collapse of mining voids, and impulsive slip. The effect of an individual discontinuity and inter-discontinuity spacing was not included in the analysis.

Properties for discontinuities were selected to represent their expected physical response. All joints other than those along the main reef were considered welded to avoid displacement along these joints during the analysis. Joints along the main reef (pre-existing and mining induced) away from locations of fall of ground, mine collapse and impulsive slip were also considered welded. A representative set of joint properties used for this research is given below (Birch and Handley (2012) used these values for modelling contacts between dyke and host rock).

- Joint normal stiffness 2e10 N/m
- Joint shear stiffness 2e10 N/m
- Joint cohesion 10e6 Pa

- Joint tension 1e6 Pa
- Joint friction 40^{o}

4.11. Surface Structures; Types and Characteristics

Consequent to the extensive gold-mining history spread over a span of more than a century, the Basin attracted a tremendous amount of industrialization and population around the mining areas. At present, there exists a large variety of civic infrastructure such as low- and high-rise buildings, bridges, and roads close to and directly above the abandoned mines. These abandoned mines are now vulnerable to flooding and faced with the potential of enhanced mining seismicity as already observed by the Council for Geoscience. In the recent past, damage to the surface structures has been reported due to mining-induced seismic events.

The existing structures were built with a variety of foundation types. Important and high-rise building such as the Standard Bank building are built on deep foundations (pile), Stacy et al. (1983), whereas ordinary and low-rise buildings are built on Shallow Foundation (strip, raft, mat, etc.). The type of foundation plays an important role in the structural response to seismic events and was, therefore, an important factor in the evaluation of soil/rock-structure-interaction. The following structural information was required for seismic structural analysis:

- Nature and type of buildings on the basis of natural frequency (low; 0.1 to 1.0 Hz, medium; 2.0 to 5.0 Hz, high; 6.0 to 10.0 Hz),
- Type of foundations; strip, raft, piles, and so forth,
- The depth of foundation.
- Type of foundation soil (s) and its characteristics.
- The known performance of structures in previous seismic events, settlement/cracks, and so forth.
- Ground behaviour; subsidence, and so forth.
- Building Code provisions for seismicity.

4.12. Idealized Geomechanical Model for Evaluation of Mining Induced Seismicity and Its Effects on Surface Structures

Keeping in mind the various aspects of the site characterization discussed in this chapter and for reasons of simplicity, the study area was idealized into six material groups. The material groups were based on the geological map of Council for Geoscience, shown in Figure 4.9. Salient features of the idealized model were:

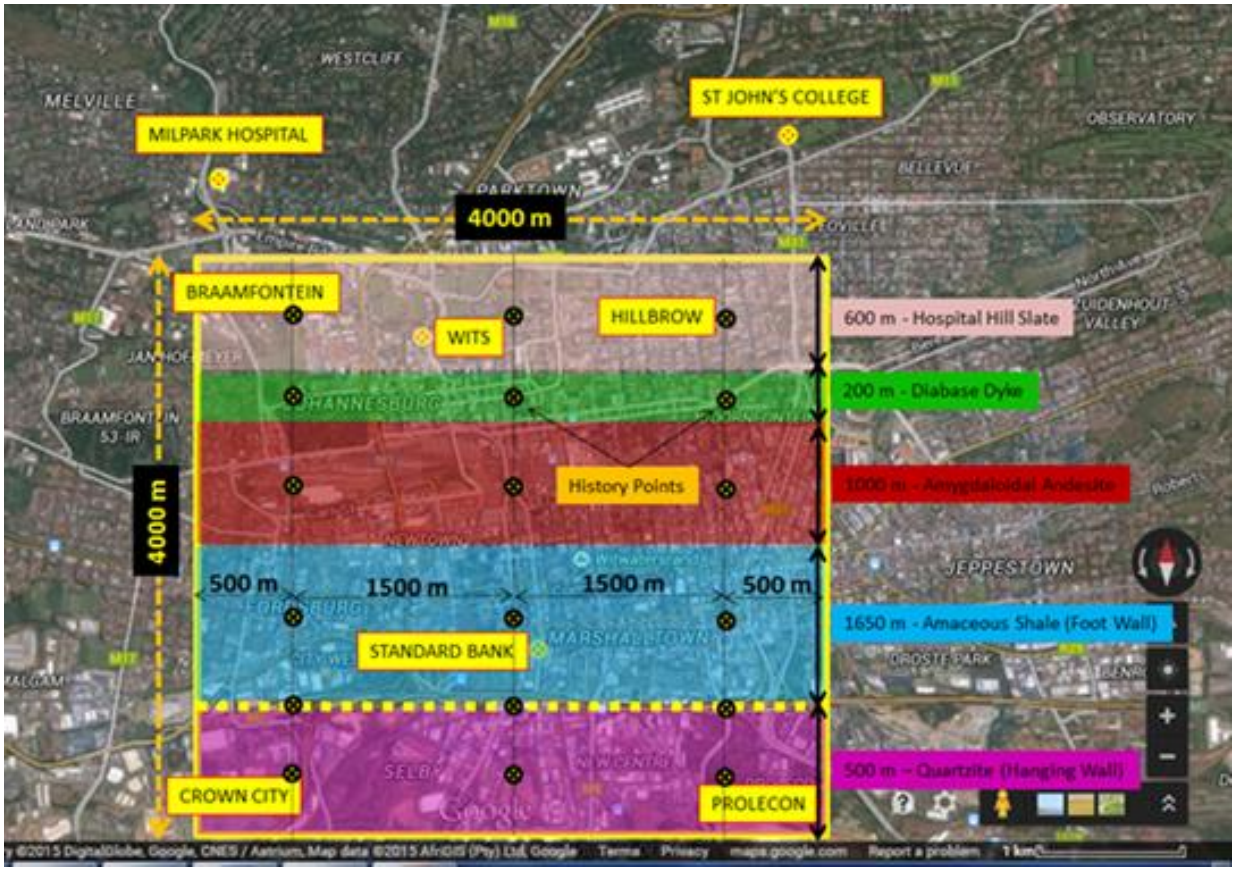


Figure 4.13 Material distributions idealized for research, after Council for Geoscience (2012)

- Geologically the material was divided into groups as shown in Figure 4.13.
- Stratigraphy (layering pattern) of the materials was considered as shown in Figure 4.14,
- The bedrock was considered at a depth of 100 m below the ground surface.
- The ground motions were recorded at the bedrock, that is, 100 m below the ground surface. This consideration was made to avoid stiffness contrast between intact rock and soil as it increased the numerical/computational

run-time. For the evaluation of mining-induced seismicity and its effects on surface structures, this aspect was considered where necessary.

- Orientation of the Main Reef and other material interfaces were considered dipping at steep angles,
- All material interfaces were considered as joints. During numerical modelling, these joints were provided with properties similar to joints/faults. These joints affected the wave propagation but no slip was allowed along these joints.
- For the evaluation of mining-induced seismicity under flooded conditions, the ground water level was assumed at the ground surface.

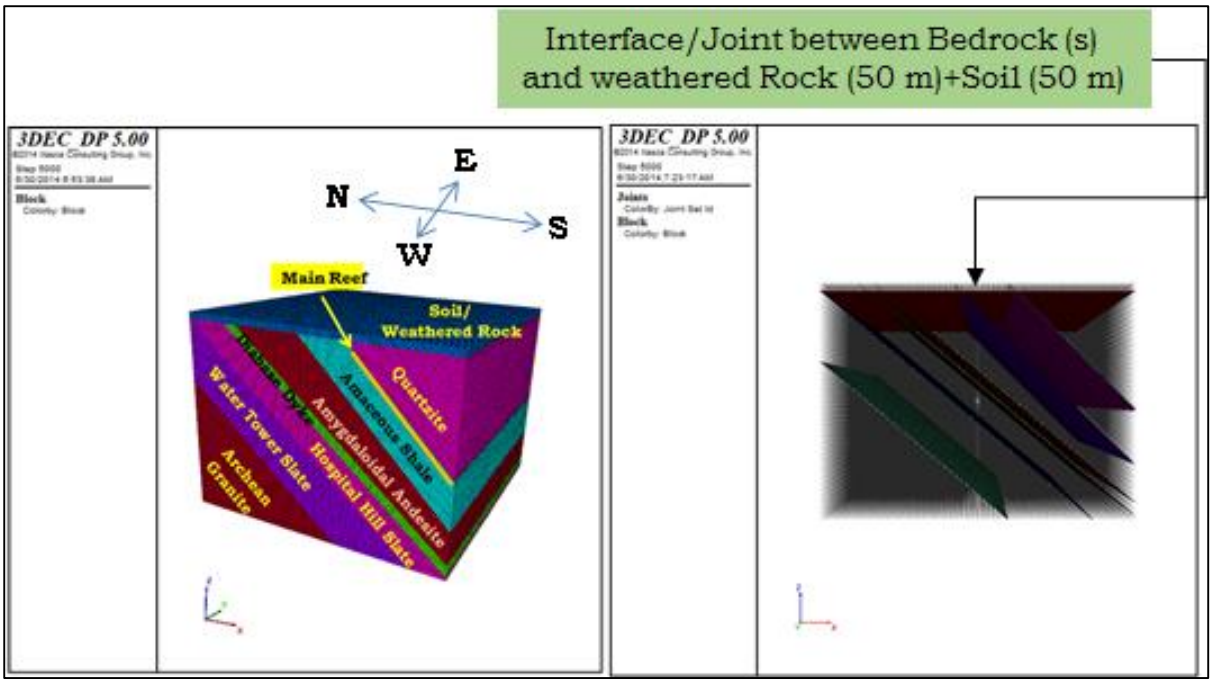


Figure 4.14 Left; stratigraphy (layering) of material, Right; orientation of joints

4.13. Conclusion

The chapter described the complexity involved in the geological, geotechnical, hydrological and seismological conditions of the study area. Since, in numerical-based evaluations, it was not possible to include all the details. Simplifications would be required with regard to geometry of study area, orientation of geological structures, material properties, and so forth, during mining simulations for seismicity and dynamic analysis of surface structures.

In next chapter, mining-induced evaluations are made using 3DEC under dry and flooded conditions of the study area. Three possible sources/scenarios namely slip along a fault, pillar collapse and fall of ground were studied. The models were numerically configured to allow propagation of seismic waves (taking into account the effect of joints between materials) from source to the points of interest. The seismicity was evaluated in terms of velocity time histories.

5. EVALUATION OF MINING INDUCED SEISMICITY

5.1. Introduction

Mining induced seismic events, unlike tectonic earthquakes, generate ground motions with relatively higher frequency and shorter duration. These ground motions are influenced by the seismic source (fall, collapse, slip, etc.), seismic wave propagation path (from source to site) and geomechanical characteristics of the candidate site. In this chapter, ground motions are estimated in the Central Business District (CBD) area using the 3DEC numerical code. The evaluation of ground motions includes many geomechanical and numerical considerations as shown in Figure 5.1.

5.2. Geomechanical Considerations

The relevant geomechanical parameters are very important for the evaluation of mining induced seismicity. Since geomechanical parameters are sensitive to the changing site conditions, their estimation needs to be representative of the conditions considered in this research. Geomechanical considerations have been discussed in Chapter 4: Site Characterization. The geomechanical model proposed in Chapter 4 was used for the numerical simulation.

5.3. Seismological Considerations

Seismological considerations have been discussed in Chapter 4. For evaluation of mining induced seismicity, three types of source mechanisms were simulated; slip, fall of ground and pillar collapse such that the seismic events had magnitudes around M_L 3 to 4.

5.4. Numerical Modelling Considerations

According to Board (1994), numerical methods are useful techniques to study mining induced seismicity triggered due to shear failure along geological discontinuities. As an investigative tool, these techniques allow incorporation of variability in pre-mining and mining induced stresses and orientation of geological structures. 3DEC was used to evaluate mining induced seismicity: the process is shown in Figure 5.2.

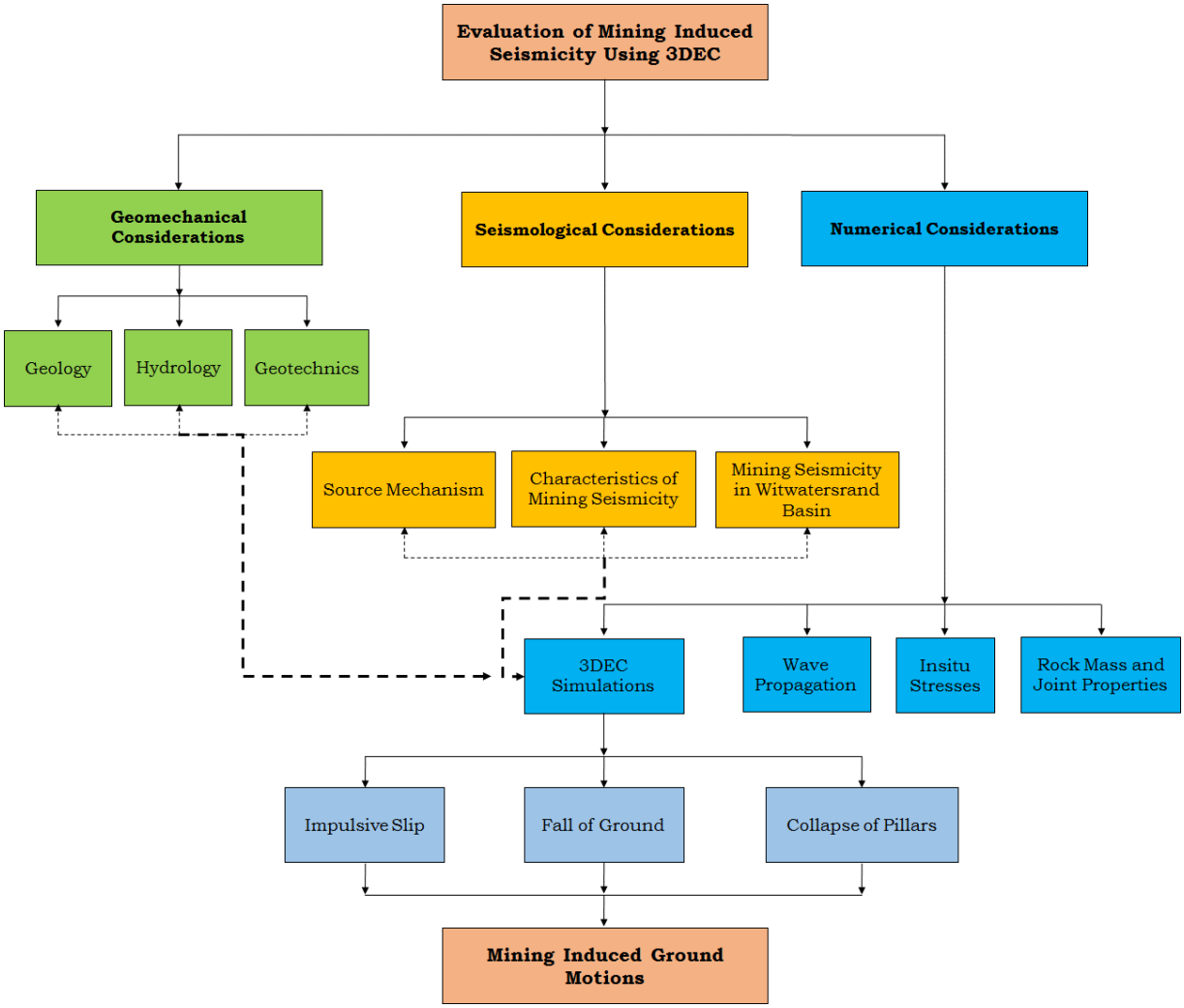


Figure 5.1 Research matrix for evaluating mining induced seismicity

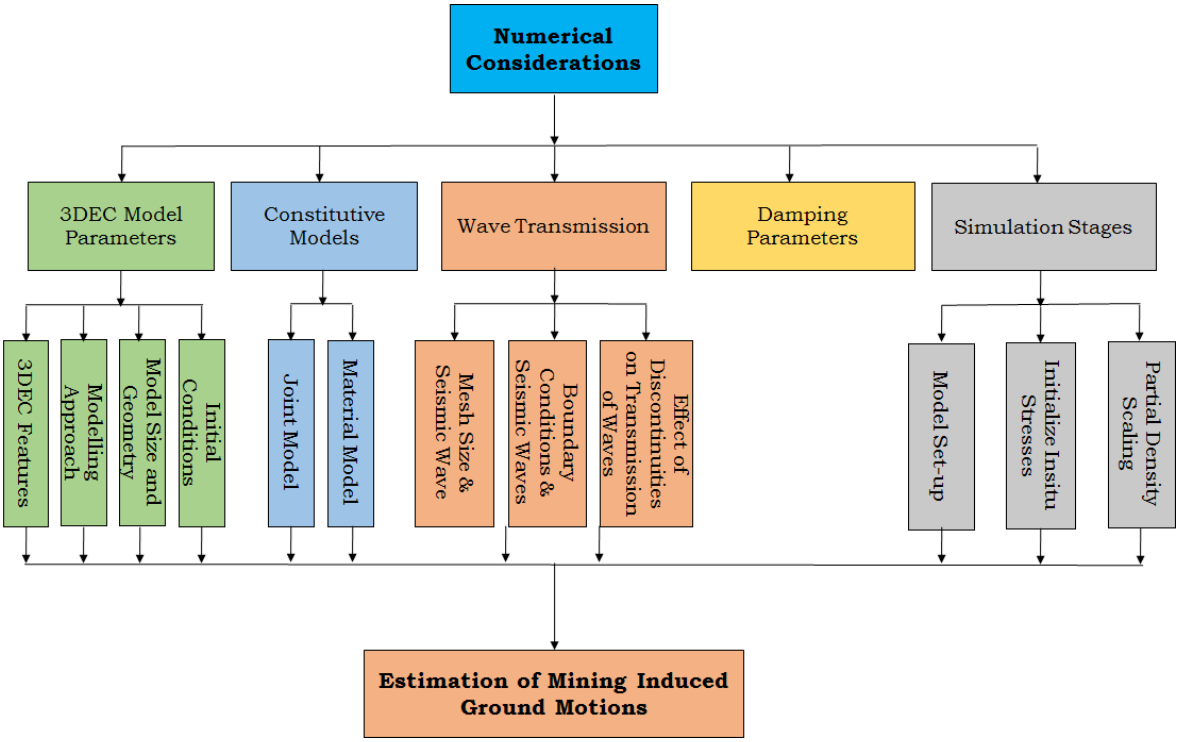


Figure 5.2 Numerical considerations for evaluation of mining seismicity

Distinct element codes are suitable for a model with large geometrical variations such as number and orientation of discontinuities, vis-à-vis candidate source/triggering mechanism (fall of ground, collapse of mining voids, impulsive slip). These codes are used to study seismic wave transmission from the area of shear failure (source) to bedrock (within the rock mass); considered at a depth of 100 m from ground surface (a linear interface of soil and weathered rock with intact rock).

5.5. 3DEC Model Parameters

5.5.1. 3DEC features

3DEC is suitable to perform dynamic analysis and study wave propagation phenomenon in the given model under the given set of properties of materials and geological discontinuities. For a more realistic dynamic analysis, Itasca (2014) requires using appropriate parameters of boundary conditions, damping and mesh size. Salient features of 3DEC code have been covered in Chapter 3 (Methodology).

5.5.2. 3DEC modelling approach

Numerical simulation of mining induced seismicity performed in this study was one of the largest model size ever analysed in 3DEC. Since it is also not possible to include all the details of the problem at hand, an idealized geomechanical model was used. In view of the limited data, limited computational power of the personal computer (available for research) and constraints of numerical complexity, the following simplified approach was adopted:

- The idealized geomechanical model developed in Chapter 4: Site Characterization, was used to study the effects of a given set of material and discontinuity properties.
- Geotechnical properties were considered the same in all simulations.

5.5.3. Model size and geometry

The study area is composed of intercalated geological formations of quartzite, shales, conglomerates, slates, etc. The 3DEC model derived from the geomechnaical model is shown in Figure 5.3 and Figure 5.4.

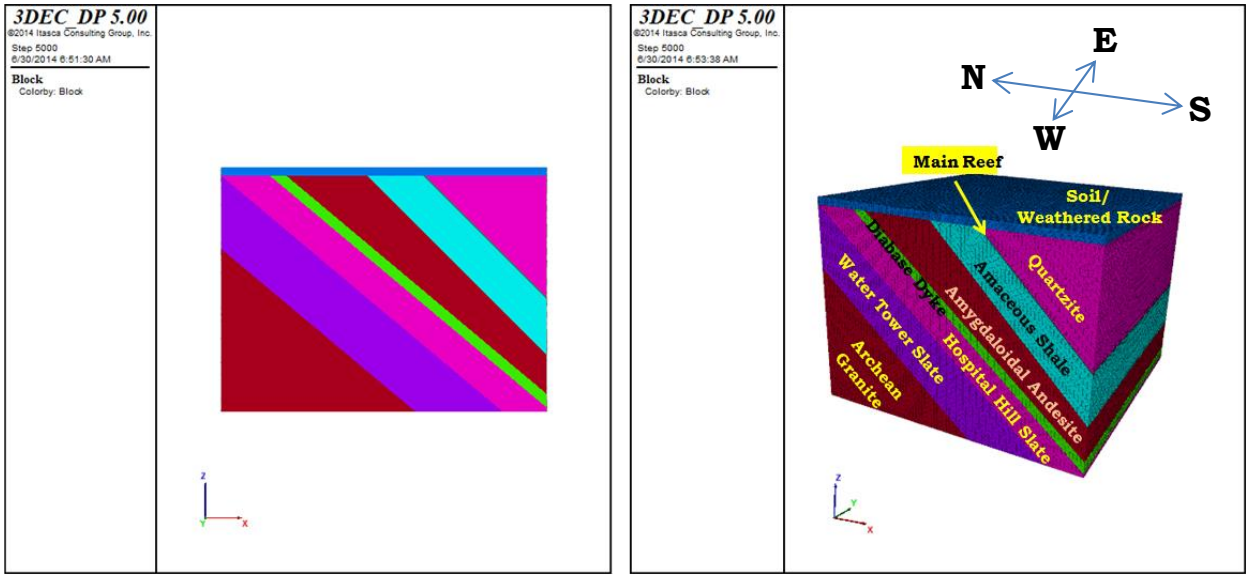


Figure 5.3 Model Geometry; left-elevation from the West, Right-material groups (labelling shown in the right figure holds good for the left figure as well)

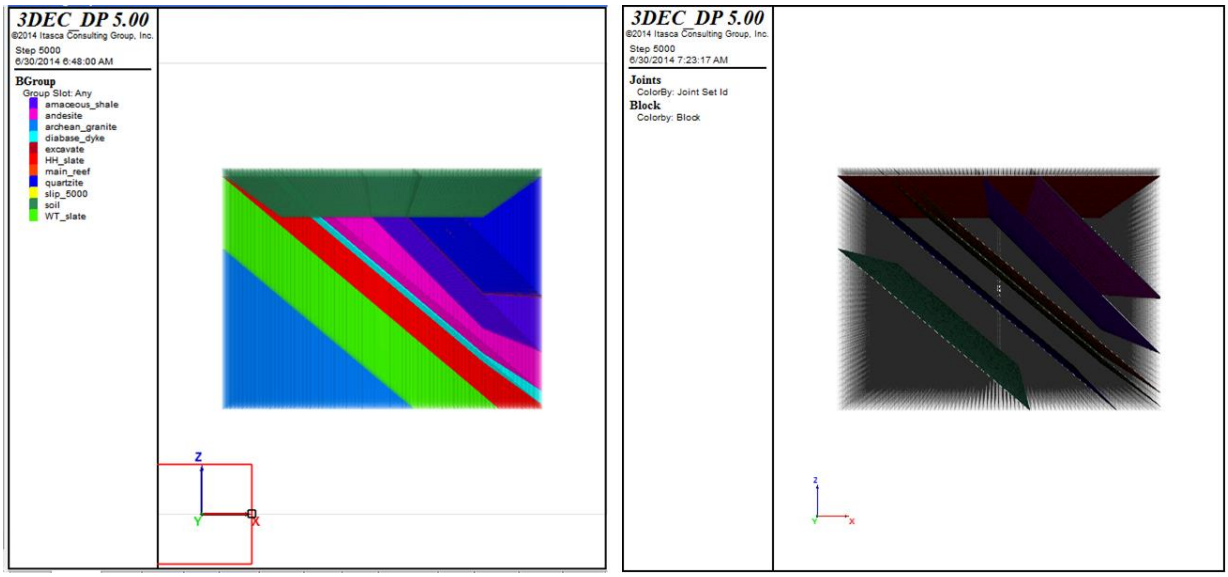


Figure 5.4 Material Groups (left) and Geological Discontinuities (right) (labelling shown in Figure 5.3 (right) holds good for the left figure as well)

Salient features of the model size and geometry are given as:

- Stratigraphic/geological details are inferred from the generalized model shown in Figure 4.3, provided by Council for Geoscience (CGS) office, Pretoria.
- Orientation of geological discontinuities varies from 30°-45° (dipping southward). The Main Reef dip of 45° is considered for the research.
- All discontinuities are planar in nature.

- Size of the model is 4000 m along X-direction (East-West), 4000 m along Y-direction (North-South) and 3000 m along Z-direction (below ground surface).
- According to Ryder and Jager (2002), the thickness of gold bearing reefs varies from a meter contact between HW and FW to 10 m thickness and 30 m as an assemblage of quartzite and conglomerates. However, in view of the maximum size of the spatial element of 50 m considered for this research, thickness of Main Reef is considered 50 m in the model. Both sides of the reef were modelled as discontinuities.
- The model is built with nine material groups/blocks and eight joints.
- Each material group is discretized into tetrahedral zones (meshed).
- It is the desire of every modeller to include the maximum possible details in the model. Itasca (2014), has listed three main reasons against this approach:
  - It is not possible to have all the desired data to model jointed rock mass in every detail.
  - The computing requirements (computer's processing, graphics and memory capacity, etc.) for a very detailed model quickly exceed the capacity which are typically available for the projects (and to the researchers).
  - Most importantly, controlled engineering understanding of model results becomes less effective as more details are added.

5.5.4. Initial conditions and in-situ stresses

Initial conditions in the 3DEC model are set to represent the pre-mining stress conditions in the model by initializing the in-situ stresses derived from the stress model adopted from Birch and Handley (2012).

- Depth (z) of the model is 3000 m.
- Vertical stress, σ_v = 0.027 x Z MPa
  = 0.027 x 3000
  = -81 MPa at depth of 3000 m
- Vertical stress has a gradient of 27 kPa/m.
- Horizontal stress, σ_h = $0.72\sigma_v$
  = 0.020 x Z
  = 0.020 x 3000

= -60 MPa at depth of 3000 m

- Horizontal stress has a gradient of 18.83 kPa/m.
- At ground surface σ_v = 0, σ_h = -3.5 MPa.

5.6. Constitutive Models

5.6.1. Block material constitutive model

In 3DEC, geological materials were assigned a "constitutive model" to represent their physical behaviour under the given conditions, Itasca (2014). Also, according to Itasca (2014), the elastic model is appropriate for elastic materials exhibiting well-defined elastic anisotropy whereas the Mohr-Coulomb plasticity model is suitable for materials which yield once subjected to shear loading. The yield stress depends on major and minor principal stress only and intermediate stress has no effect on yield, Itasca (2014). The constitutive material model selected for use in 3DEC depends on the intended application. To study the propagation of seismic waves in the model with a number of planar discontinuities, the elastic anisotropic model was used in view of the following considerations:

- The research area is composed of strong and massive rocks and for modelling purposes considered to have planar discontinuities dipping at various angles.
- The loading (slip, fall and collapse) was assumed not to surpass the respective material strengths at the model scale.
- Slip was considered to be the predominant failure mechanism and failure of the intact material is not intended.

5.6.2. Rock discontinuity constitutive model

As of block material models, joint models are specified to represent the physical behaviour of the rock discontinuities, Itasca (2014). 3DEC has two built in joint material models; the joint area contact Coulomb slip model and the continuously yielding model. The continuously yielding model is more complex and is suitable for continuously weakening behaviour as a function of accumulated plastic shear displacement, Itasca (2014).

The joint area contact model is appropriate for closely packed material blocks with area contact, Itasca (2014). Joint area contact i.e. Coulomb slip model was

used for the evaluation of mining induced seismicity. The intact rock blocks were considered to behave fully elastically with constant stiffness properties (Young's Modulus and Poisson's Ratio). According to Itasca (2014), salient features of the joint area contact model are:

- Provides a linear representation of joint stiffness and yield limit.
- Is based upon elastic (stiffness, frictional, cohesive, tensile strength) properties and dilation characteristics common to rock joints.
- Simulates displacement-weakening of the joint due to loss of cohesive and tensile strength at the onset of tensile or shear failure.

5.7. Wave Transmission

5.7.1. Mesh size versus wave frequency

Numerical accuracy of wave transmission in 3DEC depends on the input frequency content and wave speed characteristics of the model. The Kuhlemeyer and Lysmer (1973) restrictions on the size of the grid/spatial element /joint spacing/block size have been explained in Chapter 2 (Literature Review).

According to Perino (2013), for a mesh size "$\Delta l > \frac{1}{8}\gamma$", the error in the accuracy of wave propagation in the discretized model increases exponentially and for $\Delta l = \frac{1}{\pi}\gamma$, the wave travelling across the discretized model undergoes attenuation which grows exponentially. Keeping in view various considerations discussed earlier, a mesh element size of 50 m is considered for all the scenarios. This mesh size allows propagation of shear-waves with a maximum frequency of 7 Hz and p-waves with a maximum frequency of 11.40 Hz. Table 5.1 shows estimates of frequencies of all the geological blocks vis-à-vis mesh size (50 m).

The natural frequency of oscillation of the model estimated from Equation 4.8, Itasca (2014), is approximately 1.0 cycles/second.

$$Frequency = \frac{1}{2\pi}\left(\frac{ka}{m}\right)^{1/2}, \qquad \text{Equation 5.1}$$

Where a is joint area (54000 m^2), k is joint stiffness (2e^{10} N/m), m is mass of upper block (39.86e^{12} kg)

Table 5.1 Mesh size vis-à-vis frequency of waves that can transmit through geological blocks

Material	Frequency		Frequency		Comments
	P-Wave (m/Sec)	Frequency (Hz)	S-Wave (m/Sec)	Frequency (Hz)	
Quartzite (HW)	4570	11.40	2829	7.07	Assume Δl = 50 m γ = 8 x 50 = 400 m $f = C_p/\gamma$ $f = C_s/\gamma$
Main Reef (MR)	5260	13.15	3378	8.45	
Amaceous Shale (FW)	5060	12.65	2998	7.50	
Amygdaloidal Andesite (AA)	5032	12.58	3051	7.63	
Diabase Dyke (DD)	5495	13.74	3367	8.52	
Hospital Hill Slate (HH)	5810	14.53	3213	8.03	
Water Tower Slate	5704	14.26	3050	7.63	
Archean Granite	4560	11.40	2877	7.19	

5.7.2. Model boundary condition and reflection of waves

During dynamic analysis, the outward propagating waves are reflected back into the model at the boundaries. To prevent reflection of these waves, dynamic analysis in 3DEC allows use of non-reflecting/absorbing boundaries called viscous boundaries, developed by Lysmer and Kuhlemeyer (1969). The concept considers attaching independent dashpots to the boundaries in normal and shear directions which provide tractions given by following equations:

$$t_n = -\rho\, C_p\, V_n, \qquad \text{Equation 5.2}$$

$$t_s = -\rho\, C_s\, V_s, \qquad \text{Equation 5.3}$$

Where V_n and V_s are normal and shear components of the velocity at the boundary, ρ is the mass density, C_p and C_s are primary and shear wave velocities respectively.

In 3DEC, the tractions are applied at every time step similar to the boundary loads. This scheme is suitable for both deformable and rigid blocks. According

to Itasca (2014), viscous forces are calculated from the velocities lagging by half the time step, however, no reduction of the time step is required while using this scheme. It is emphasized that time restrictions posed by joint stiffness and small zone size is duly considered for the dynamic analysis. In 3DEC, in the case where velocity boundaries are used for the static conditions, non-reflecting boundaries can be used without any numerical changes to the model.

5.7.3. Effect of discontinuities on transmission of waves

As discussed earlier in the geotechnical consideration, discontinuities in rock mass affect the transmission of seismic waves. To visualize the effect of an increasing number of discontinuities in 3DEC, a model is run with one, two and three planar discontinuities (parallel). The model is built, mesh generated with edge length of 50 m, insitu stresses initialized and boundary conditions are set as discussed earlier in this Chapter.

No damping and partial density scaling is used as it was desired to simply observe the effect of increasing numbers of discontinuities on the waveform, shown in Figures 5.5 through 5.7. It is observed that the frequency of the waves decreased approximately from 5 Hz to 0.3 Hz whereas the amplitude of displacement increased from 9.6 mm to 2.5 cm.

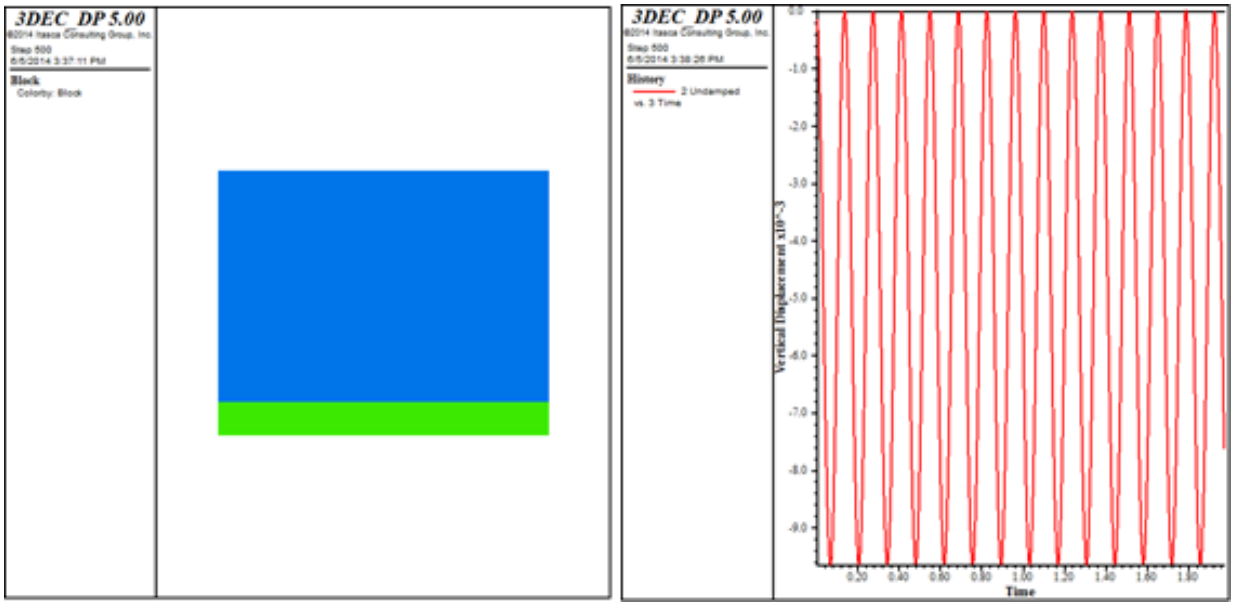


Figure 5.5 Seismic waveform with one discontinuity (frequency = 5 Hz, amplitude = 9.6 mm)

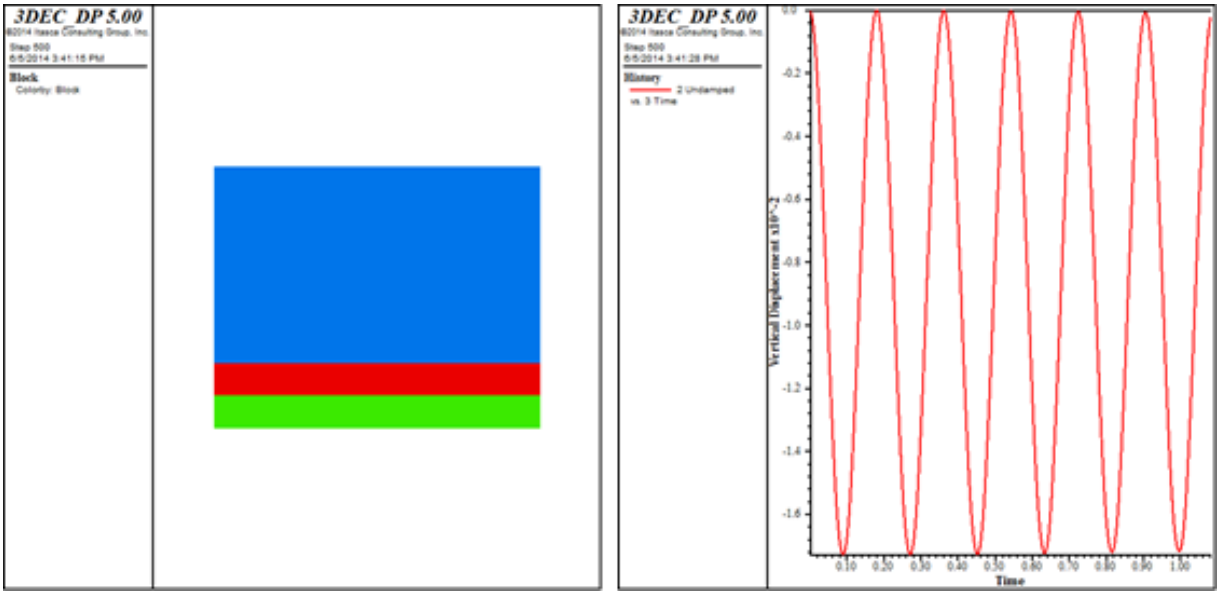


Figure 5.6 Seismic waveform with two discontinuities (frequency = 3.5 Hz, amplitude = 1.65 cm)

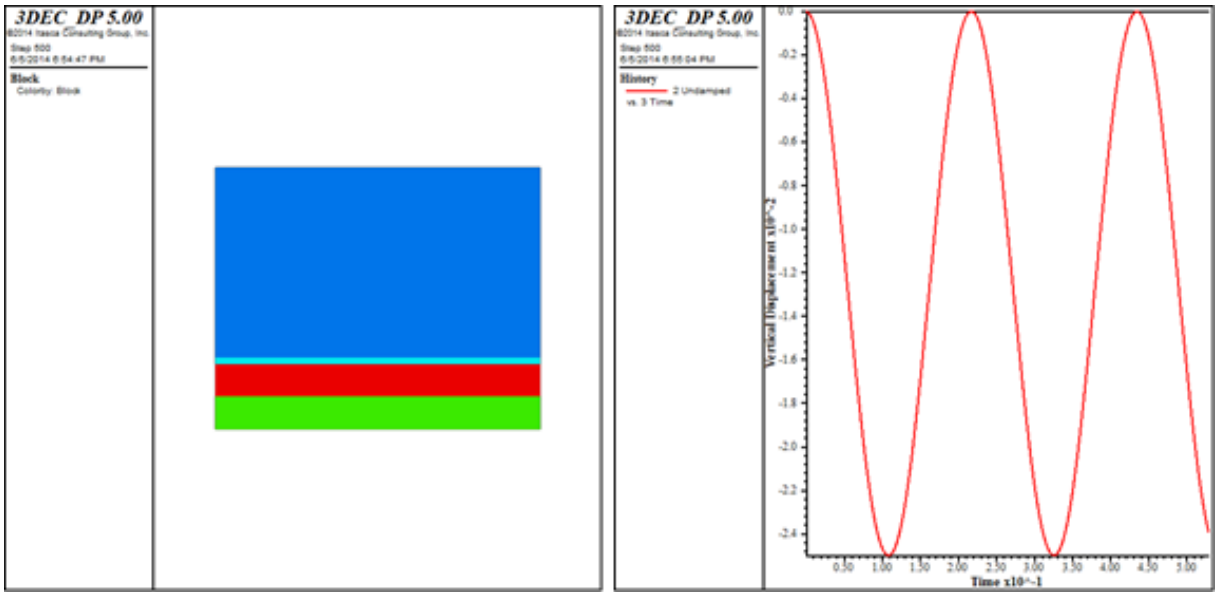


Figure 5.7 Seismic waveform with three discontinuities (frequency = 0.30 Hz, amplitude = 2.5 cm)

The simulations with the increasing number of discontinuities revealed that the waveforms in the idealized geomechanical model would be complex due to multiple/steeply dipping discontinuities which is the expected behaviour. Also, the frequency would be relatively lower with higher velocity amplitude i.e., the damaging potential would be higher.

5.8. Damping Parameters

All natural dynamic systems possess certain damping of the vibrational energy which causes the system to reach static equilibrium within a particular timeframe which depends on the damping characteristics of the system, Itasca (2014). The damping characteristics depend on geomechanical properties and are different for different materials. Damping is attributed to the loss of energy due to slippage along the faults/joints of the blocks (rockmass), internal friction loss in the intact material (rockmass), or resistance caused by the surrounding air or fluids within or surrounding the structure, Itasca (2014).

3DEC uses two types of mechanical damping; mass proportional damping and stiffness proportional damping, separately or in combination. Combination of both forms of damping is termed as Rayleigh damping, Bathe and Wilson (1976). Mass proportional damping applies a force which is proportional to absolute velocity and mass but in the direction opposite to the velocity. This damping is dominant at lower angular frequencies.

Stiffness proportional damping applies a force which is proportional to the incremental stiffness matrix multiplied by the relative velocities or strain rates to contacts or stresses in the zones. This is dominant at higher angular frequencies. Biggs (1964) suggested a damping of 2-5% for geological materials and 2-10% for structural systems. The analysis was performed using 2% damping. Regarding damping, Itasca (2014) also highlights following:

- In 3DEC, Rayleigh damping is specified with two parameters; fundamental frequency of the system and fraction of the critical damping ratio.
- In a seismic analysis involving large movement of blocks, mass damping is inappropriate since the block motion might be artificially restricted such as free flow or fall of blocks under gravity, and explosive/impulsive loading of blocks.
- Stiffness proportional damping is more appropriate in such situations. Damping is doubled whenever only one of the 'mass' or 'stiffness' proportional damping is used.

- The correct level of damping and appropriate boundary conditions is essential for any seismic analysis.

5.9. 3DEC Simulation Stages

For a numerical simulation to be reliable and accurate, it must take into account the physical processes the system has experienced in its history as best as possible. The stages in the numerical simulation process are described briefly.

5.9.1. Partial density scaling to minimize model runtime

A model with complex geometry and discontinuities can often result in very small block zones during the process of meshing. These small zones require very small time steps for the numerical stability of the explicit algorithm which makes the dynamic analysis very time consuming, Itasca (2014).

3DEC uses the "density scaling" technique to improve the calculation efficiency in quasi-static and dynamic analysis by introducing a small density scaling for very small zones in such a way that system inertia is negligible. In dynamic analysis, this is called "partial density scaling". In 3DEC;

- The user has the option to control the scaling suitable to the model.
- To start with, the code calculates the initial time step, thereafter, the user can specify the time step using the command "MSCALE part dt" and the code applies density scaling to achieve the desired time step "dt".
- The user can cycle to determine the number of grid point masses scaled and the additional mass added to the system.
- The effect of this scaling is shown in Figure 5.8; Left 20100 steps were needed without any density scaling to simulate what was possible with only 10000 steps with partial scaling.
- The wave pattern is similar while the efficiency is much higher due to this small mass scaling. All analyses were performed using "MSCALE part dt" of $4e^{-4}$.

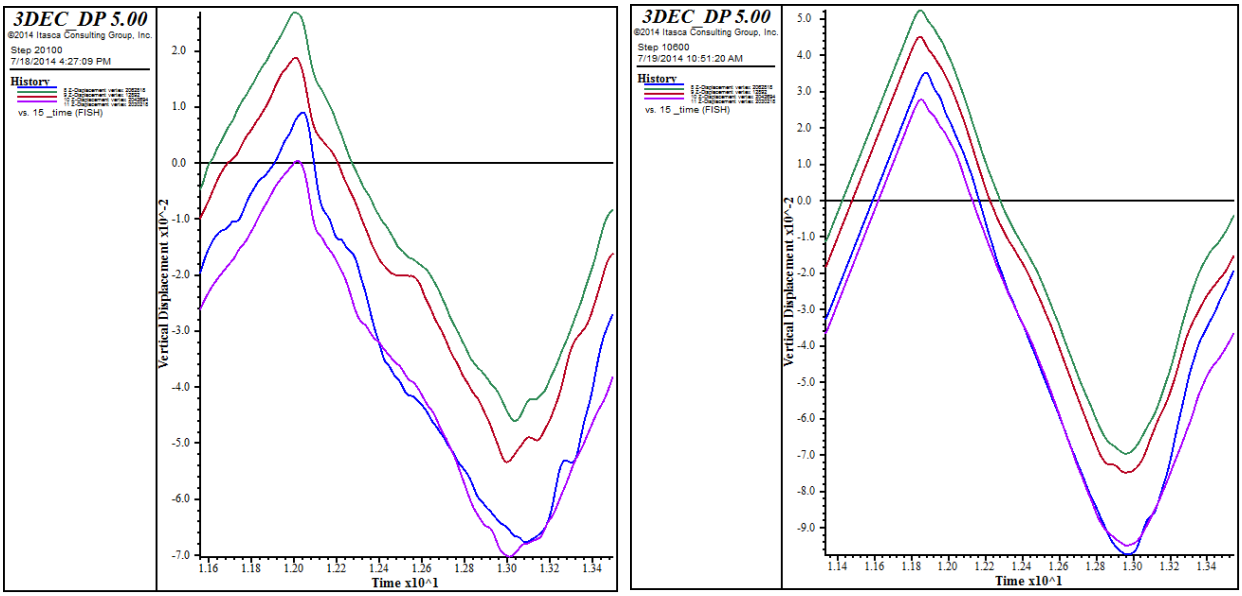


Figure 5.8 Partial density scaling / un-damped; left-vertical velocity histories, right-vertical displacement histories

5.9.2. Stage 1 - model set-up

The basic model geometry was similar in all three cases; impulsive slip, fall of ground and mine collapse. The material groups/blocks were separated by planar discontinuities extending in a southward direction (XZ-plane). All blocks were meshed/internally discretized in tetrahedral zones of element length equal to 50 m. This was the maximum mesh length which could be adequately handled by the Core i7 computer available for the research with respect to time and memory.

Non-reflecting boundaries were used at the bottom and sides whereas a free boundary at the top was considered along with soil a layer of 100 m thickness. Displacements were restrained at the bottom and sides by using “fixed” and “roller” boundaries respectively.

5.9.3. Stage 2 - initialize insitu stresses

Figure 5.9 shows in-situ stresses installed in the model in xx and zz extents, estimated in geotechnical consideration. Although distinctive variation in the overall insitu stresses was observed, however due to the relatively coarser mesh of 50 m, some overlapping in the stress gradient was observed in the model.

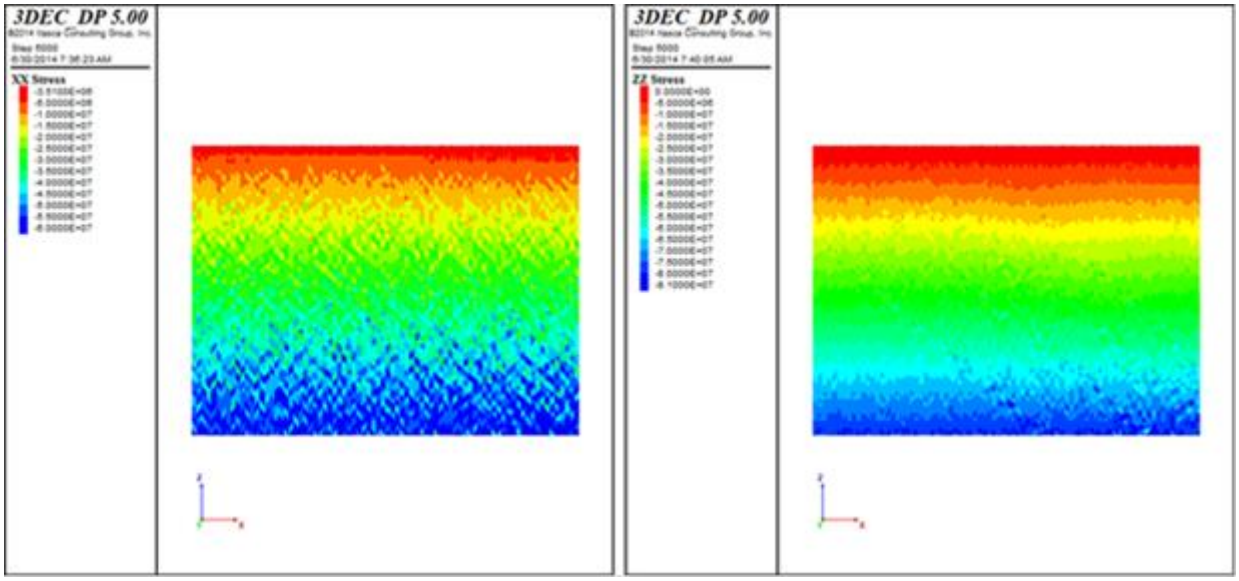


Figure 5.9 Insitu stresses initialized in the 3DEC model

5.9.4. Stage 3 - initial static equilibrium

After having established initial conditions of in-situ stress, the model was run to initial static equilibrium in 5000 steps. Figure 5.10 (left) indicates that the unbalanced force approaches equilibrium. Vertical velocity history shown in Figure 5.10 (right) and vertical displacement shown in Figure 5.11 (left) approach zero velocity and displacement respectively. At the initial equilibrium state, stresses in xx, yy, and zz planes were also similar to the initialized in-situ stresses as shown in Figure 5.9.

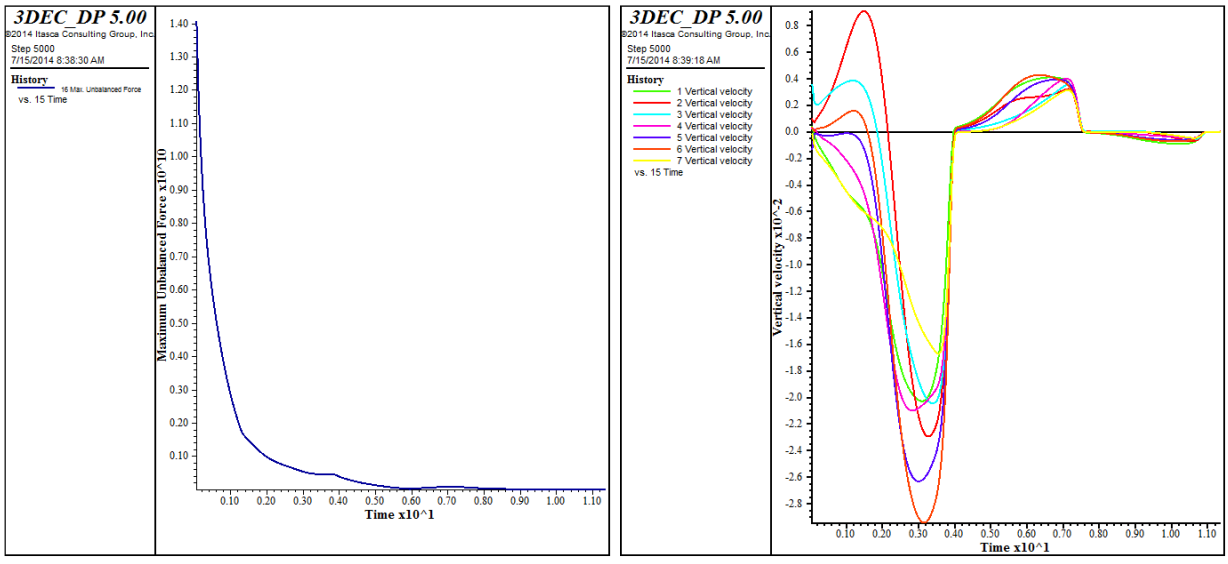


Figure 5.10 Initial Static Equilibrium; left-Unbalanced Force, Right-Vertical Velocity Histories

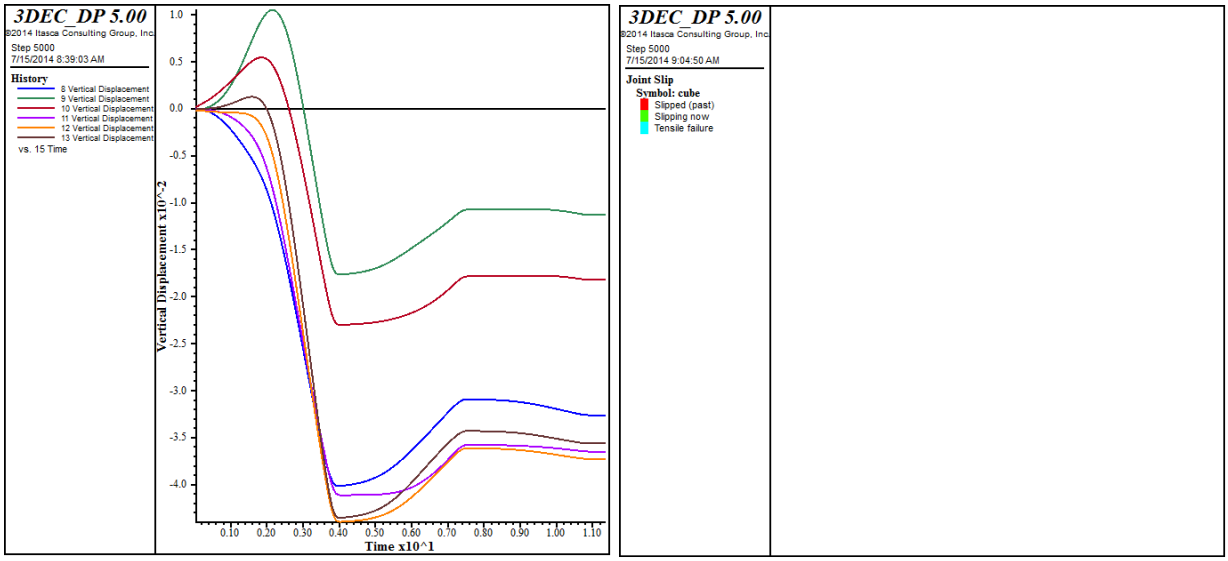


Figure 5.11 Initial Static Equilibrium; left-Vertical Displacement Histories, Right-Joint Slip (no joint slip observed)

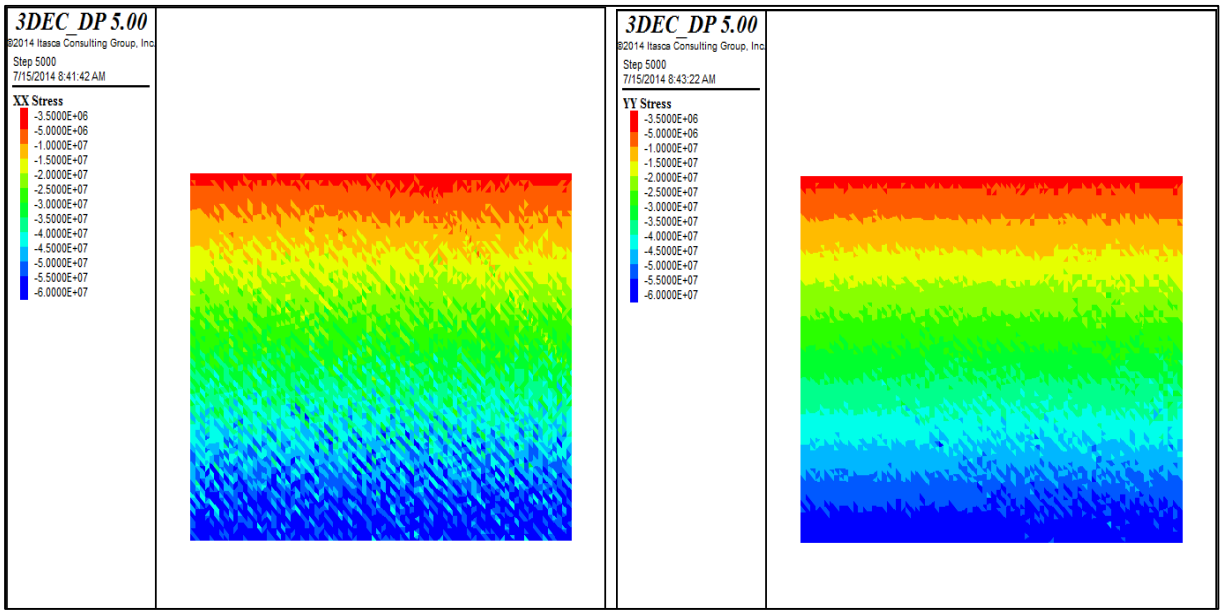


Figure 5.12 Initial Static Equilibrium; left-stress in xx-plane, Right-Stress in yy-plane

Figure 5.13 (right) also shows that maximum joint shear displacement after initial static equilibrium was on the order of 0.0004 m. Such a small confined displacement was considered acceptable as far as initial static equilibrium was concerned, Itasca (2014). With these initial conditions set in the model, the stage was set to perform further simulation i.e., excavation. The model was again brought to equilibrium after excavation; at this stage stress re-distribution

around the excavation was observed which is considered to be the situation in reality. Since the size and pattern of excavation was different for slip, fall and pillar collapse: this stage is discussed under respective simulations.

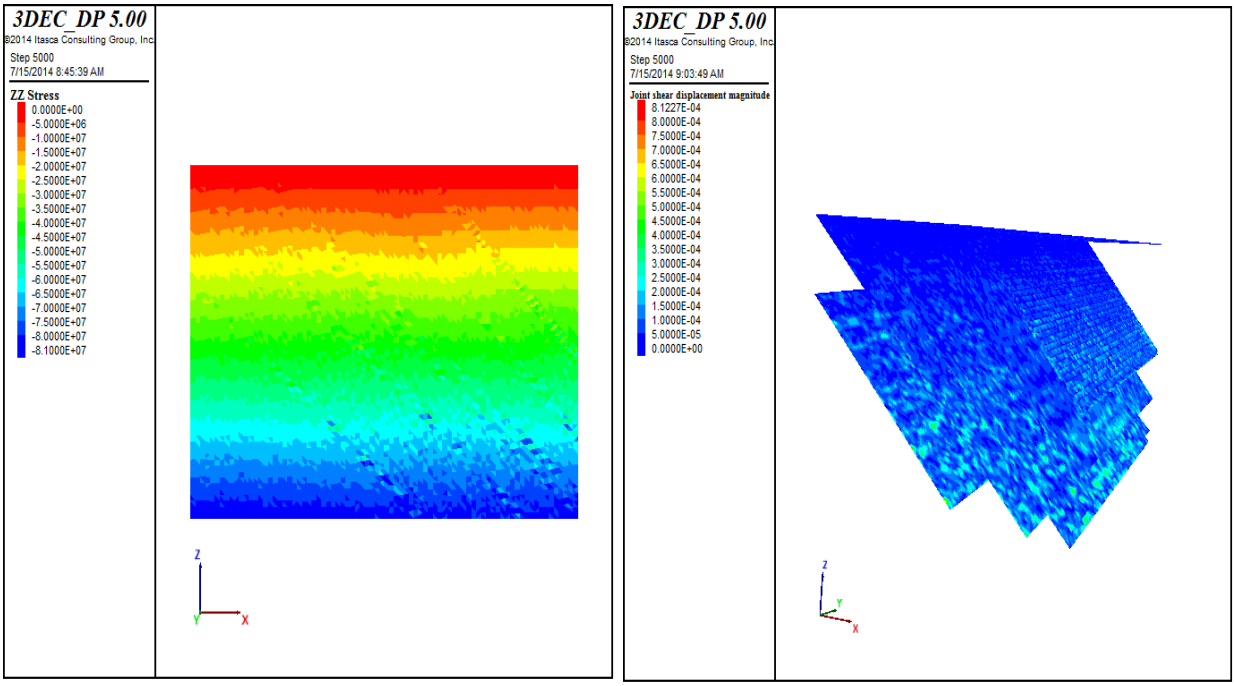


Figure 5.13 Initial Static Equilibrium; left-stress in *zz*-plane, Right-Joint Shear Displacement

5.10. 3DEC Simulations for Estimation of Mining Induced Ground Motions

Durrheim et al. (2006), attribute causal factors of occurrence of large destructive rockbursts (one of the result of mining induced seismicity) to the existence of peculiar structural geology in the Witwatersrand Basin. The most prominent geological features are the faults, dykes and sills that traverse the entire gold bearing strata. In the process of mining, re-distribution of stresses at micro and macro level takes place in rocks, around voids, pre-existing faults and recent shear zones. The ever increasing flood level in the abandoned mines is yet another triggering factor which needs to be studied. The scenarios considered for numerical simulation are described in Figure 5.14. Simulations for each scenario were made both for dry and flooded conditions and ground motions were recorded at three points (black circles) in each geological group at a depth 100 m below ground surface (interface of intact rock and weathered rock/soil),

Figure 5.15. This also eliminated the need for deconvolution of ground motions for dynamic structural analysis.

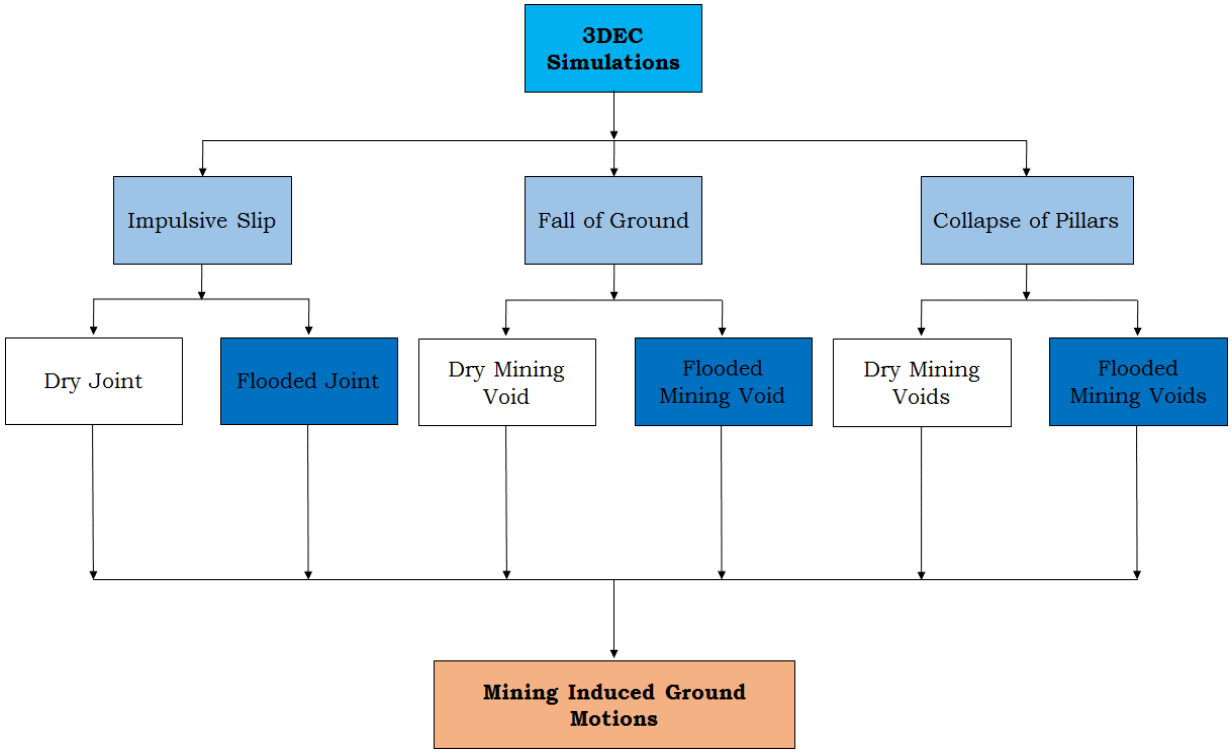


Figure 5.14 3DEC simulation scenarios; “Impulsive Slip”, “Fall of Ground”, and “Collapse of Pillar”

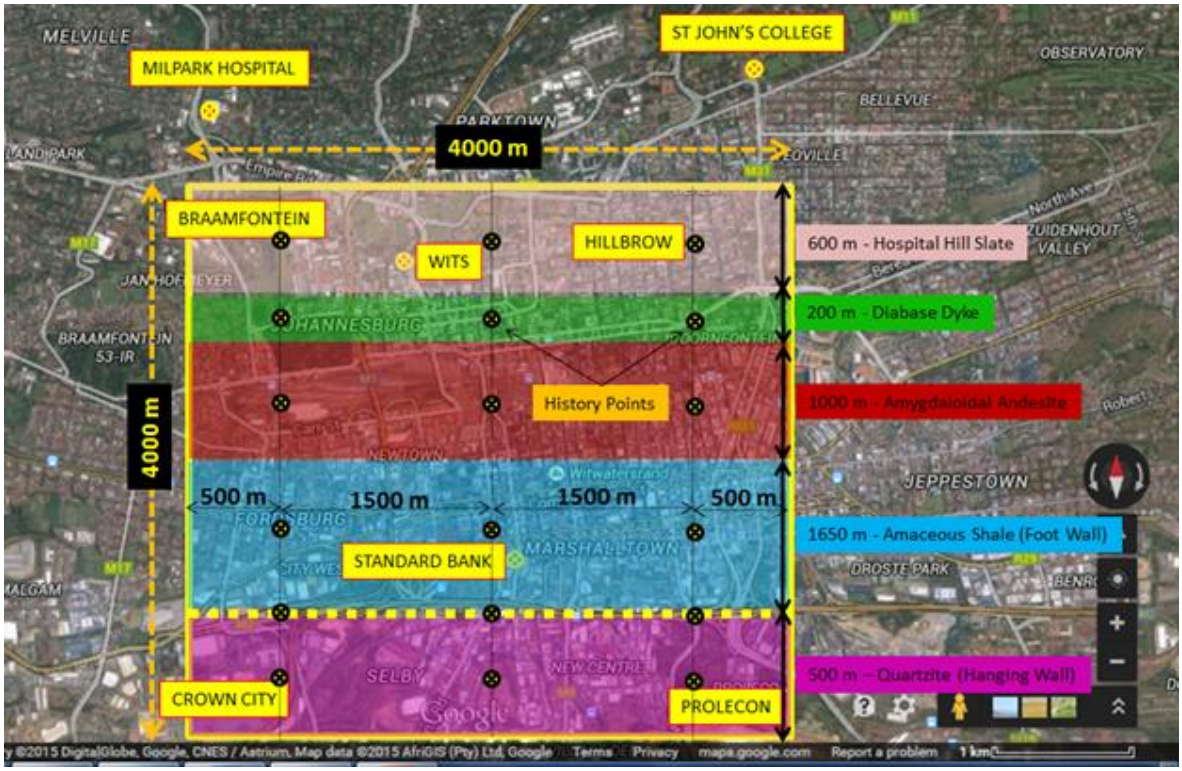


Figure 5.15 History points (black circles) at the bedrock (100 m below ground surface)

5.11. 3DEC Simulation for Impulsive Slip

An impulsive confined planar slip was generated in a linearly elastic, anisotropic, heterogeneous medium along contacts between *Foot Wall, Main Reef, and Hanging Wall*. The type and intensity of seismicity evaluated in this scenario are relevant to the model geometry, material, properties, joint properties and the in-situ stresses used in the model. This simulation is discussed under the following headings:

- Empirical parameters.
- Conceptual considerations.
- Numerical simulation considerations.
- Simulation for estimation of ground motions due to impulsive slip along a dry joint.
- Discussion on ground motions estimated due to impulsive slip along a dry joint.
- Simulation for estimation of ground motions due to impulsive slip along a wet joint – pore pressure generates instantaneously.
- Discussion on ground motions estimated due to impulsive slip along a wet joint – pore pressure generated instantaneously.
- Simulation for estimation of ground motions due to impulsive slip along a wet joint – pore pressure generates gradually.
- Discussion on ground motions estimated due to impulsive slip along a wet joint - pore pressure generates gradually.

5.11.1. Empirical aspects

In order to simulate a mining induced seismic event due to impulsive slip, guidelines were taken from Aki and Richards (1980) and Hanks and Kanamori, (1979) for seismic moment energy/earthquake magnitude vis-à-vis magnitude and area of slip. The seismic moment is evaluated using a relationship proposed by Aki and Richards (1980), Equation 2.5, [($M_\circ = G u_s A$, using parameters of the area of slip (A), magnitude of the slip (u_s), and rock mass shear modulus (G)].

The Richter magnitude of the seismic event generated by the slip is estimated using the correlation proposed by Hanks and Kanamori, (1979) i.e., Equation

2.5 ($M = \frac{2}{3} log\ M_\circ - 10.7$, where, M is the Richter magnitude of the seismic event, $M_\circ$ is the seismic moment in dyne-cm (1 N-m = 10000000 Dyne-cm). In real conditions of abandoned mines, the possibilities for variation in area and magnitude of slip are enormous and difficult to quantify. With a view to present a general idea of the seismic magnitude generated due to a certain slip and area of slip is shown in Table 5.2 (using Equation 5.4 and 5.5).

Table 5.2 Magnitude of seismic event vis-à-vis area of slip for a constant magnitude of slip

Richter Magnitude (M)	Seismic Moment (M_o) N-m	Seismic Moment (M_o) Dyne-cm	Magnitude of Slip (m)	Area of Slip (m^2)
1.4	$1.41x10^{11}$	$1.41x10^{11}$	2.90	-
2.0	$1.122x10^{12}$	$1.122x10^{19}$	2.90	15.47
3.0	$3.548x10^{13}$	$3.548x10^{20}$	2.90	489.37
4.0	$1.122x10^{15}$	$1.122x10^{22}$	2.90	15475
4.24	$2.61x10^{15}$	$2.61x10^{22}$	2.90	36000
5.0	$3.548x10^{16}$	$3.548x10^{23}$	2.90	48.93×10^4
6.0	$1.122x10^{18}$	$1.122x10^{25}$	2.90	15.47×10^6

5.11.2. Conceptual aspects

- Impulsive planar slip is generated in a linearly elastic, anisotropic, heterogeneous medium.
- In view of the geometry of the model, the slip is normal dip-slip shear displacement.
- An attempt is made to create an impulsive slip similar to that in a mining environment, i.e., excavation is created below the area where slip is intended.
- Joint properties of the slip block are then reduced to zero to induce impulsive slip. In this scenario, the area of slip is pre-selected, however, the amount of slip is dependent on the geometrical aspects of the surrounding rock mass.
- The ends of the discontinuities are prevented from slipping by using roller boundaries on the sides, a fixed boundary at the base of the model and setting high frictional properties of the joints.
- All contacts are assumed welded and smooth (at this large scale).
- According to Ryder and Jager (2002), planar discontinuity slips at a relatively lower shear stress and with larger shear displacement than the non-planar

discontinuities. Ground motions estimated in this analysis due to impulsive slip are therefore conservative.

- Mining induced seismic events have high frequency which undergoes rapid attenuation; most of the power is contained in the low frequency components. The model is discretized with spatial element size of 50 m. This mesh size allows propagation of waves with maximum frequency up to 8 Hz for shear and 12 for primary waves.
- Ground motions (velocity histories at the bedrock) are assumed "Far- field", since, $r \gg Ls$ where r is distance from the source and Ls is the size of the source (radius). According to Ryder and Jager (2002), far-field implies that distances are sufficiently great such that the site effects that attenuate more rapidly with distance become unimportant.
- To estimate ground motions at the bed rock, the weight of overburden (soil, weathered rock, and surface infrastructure) is considered in the form of a 100m thick layer with stiffness properties relevant to soil/weathered/weak rocks.
- As stated by Ryder and Jager (2002), thin argillaceous clay layers, inherent to Witwatersrand basin, cause weaknesses parallel to the stoping horizons. These contribute significantly to strata control problems. They are likely to affect seismic behaviour as well however these are not included in the model in view of their small thickness and the modelling simplicity. It is therefore inferred that the measured ground motions are the higher bound values.

5.11.3. Simulation aspects common to impulsive slip under dry and flooded conditions

- An impulsive slip (normal Dip-Slip) along the Main Reef between Quartzite - Hanging Wall (HW) and Amaceous Shale - Foot Wall (FW) was generated to simulate a seismic event as shown in Figure 5.16.
- Along the HW, the slip was between Main Reef (conglomerate) and Quartzite whereas along the FW, the slip was between the Main Reef and Amaceous Shale.
- Plots of initial equilibrium and post-excavation equilibrium are shown in Figures 5.17 through 5.19.

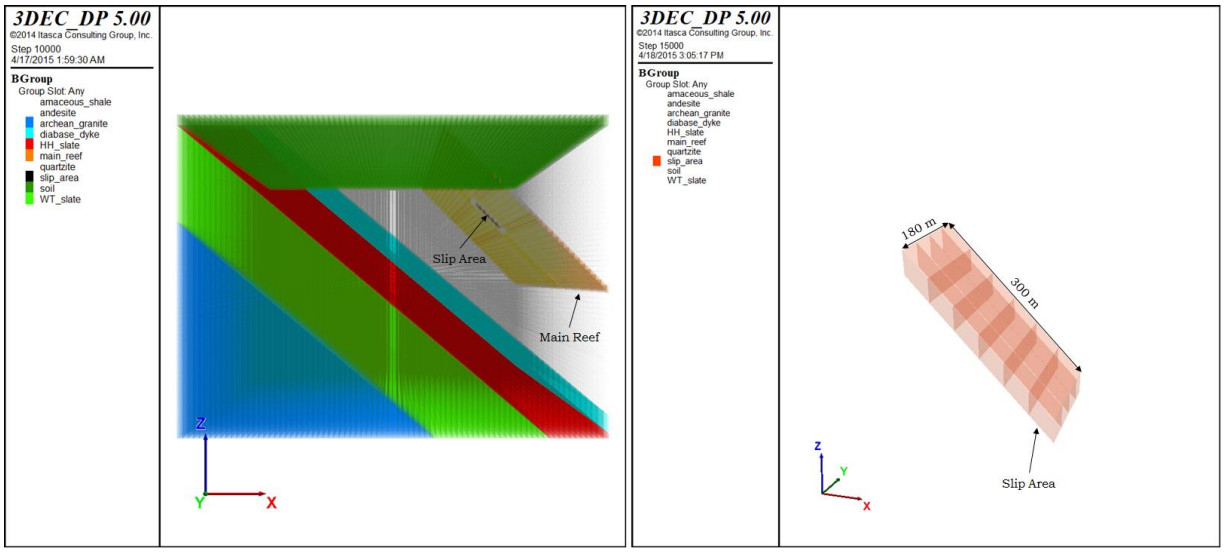


Figure 5.16 Model geometry; left – location of the slip area, right - size of the slip area

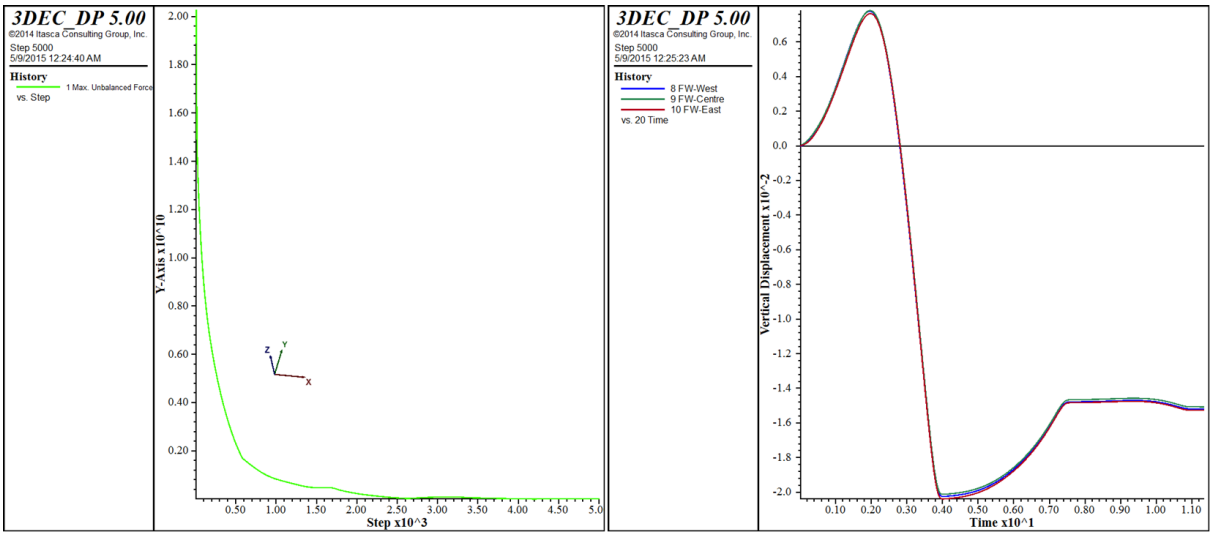


Figure 5.17 Initial static equilibrium; left – plot of unbalanced force, right – plot of vertical displacement histories in Foot Wall

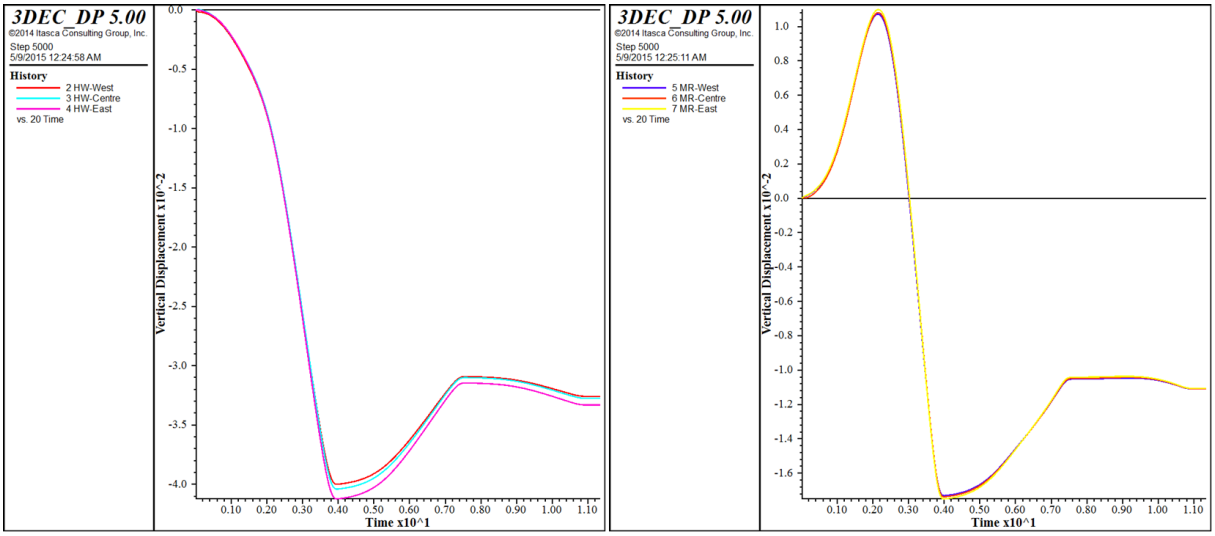


Figure 5.18 Initial static equilibrium; left – plot of vertical displacement histories in Hanging Wall, right – plot of vertical displacement histories in Main Reef

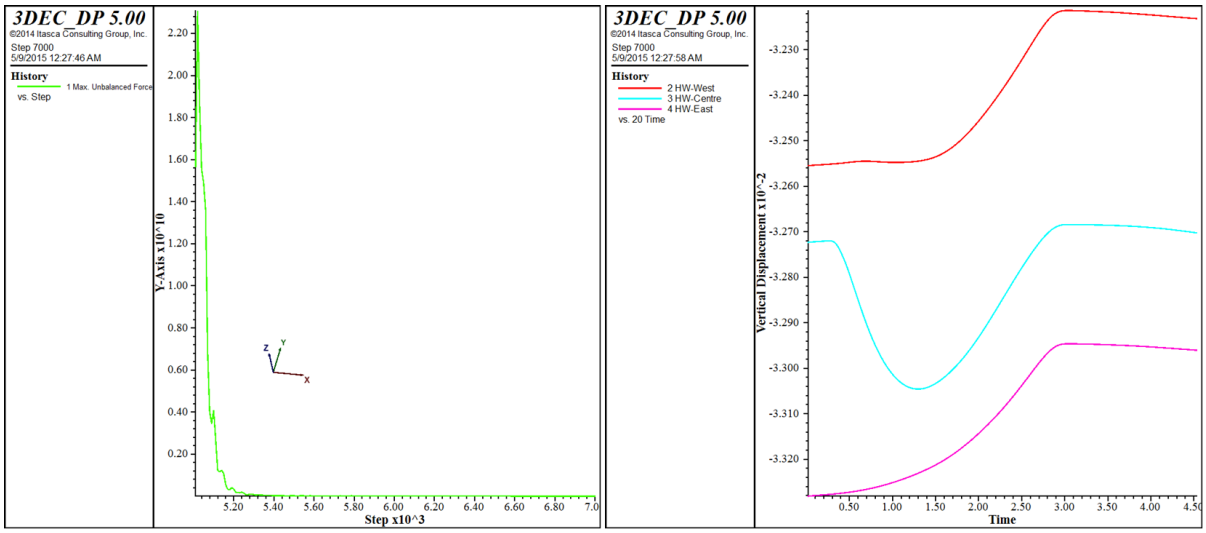


Figure 5.19 Post excavation equilibrium; left – plot of unbalanced force, right – plot of vertical displacement histories in Foot Wall

5.11.4. Simulation for impulsive slip along a dry joint

Results of the simulation for impulsive slip in dry conditions are shown in Figures 5.20 through 5.24.

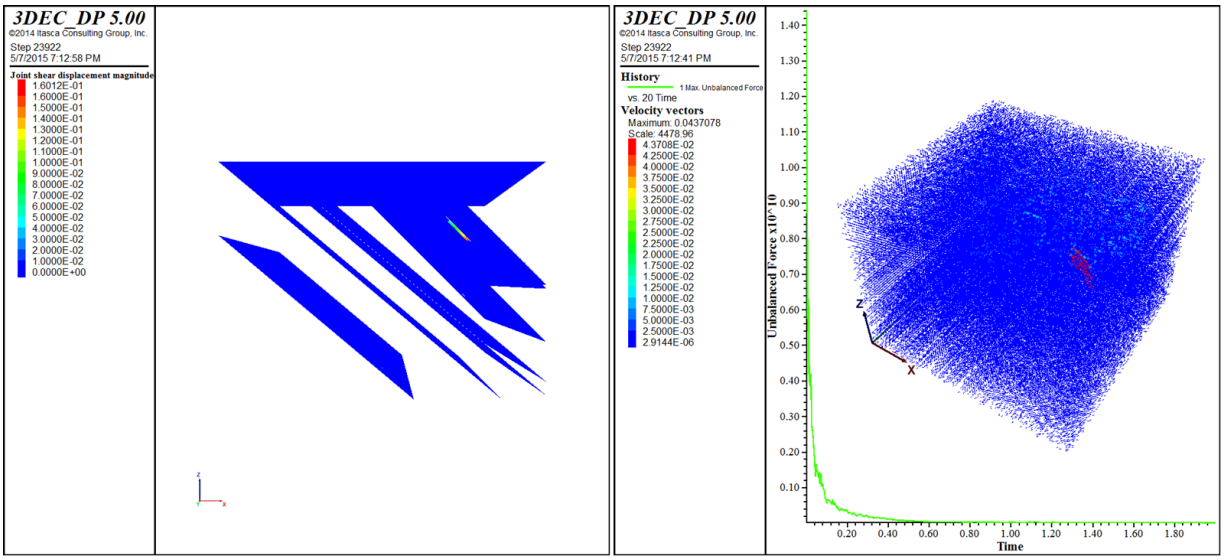


Figure 5.20 Slip along a dry joint; left – plot of joint shear displacement, right – plot of unbalanced force and velocity vectors

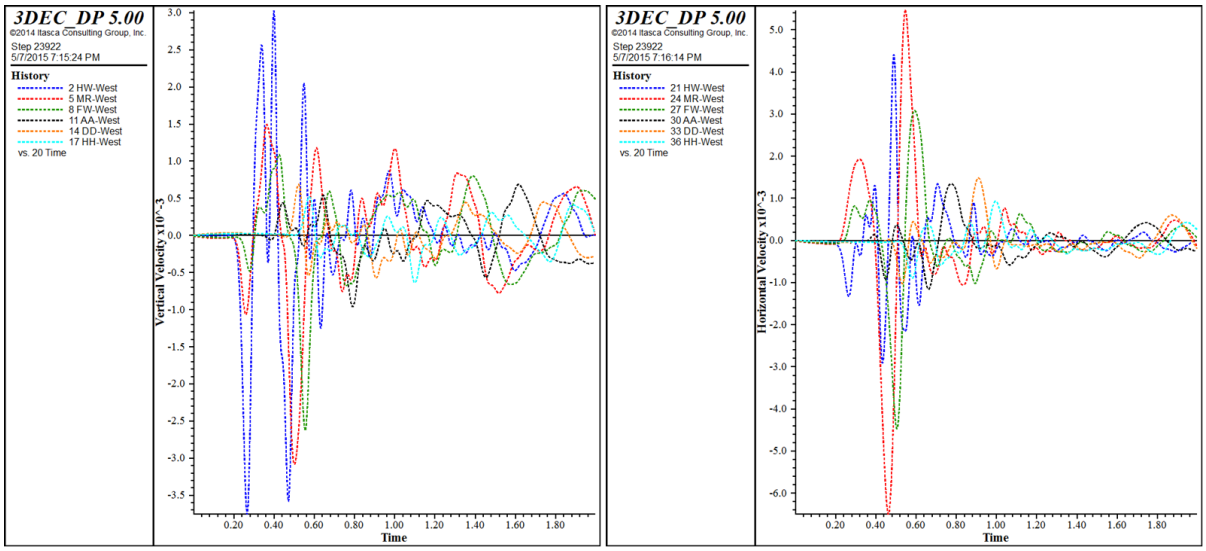


Figure 5.21 Slip along a dry joint, plots of velocity time histories on the west edge of model; left – vertical velocity time histories, right –horizontal velocity time histories

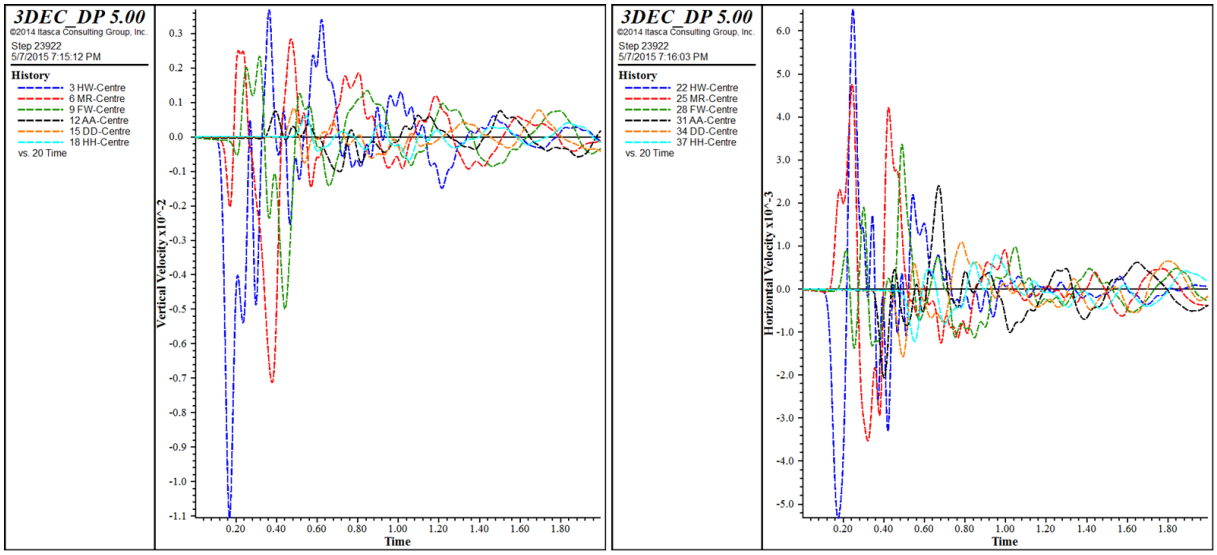


Figure 5.22 Slip along a dry joint, plots of velocity time histories on centre of the model; left – vertical velocity time histories, right –horizontal velocity time histories

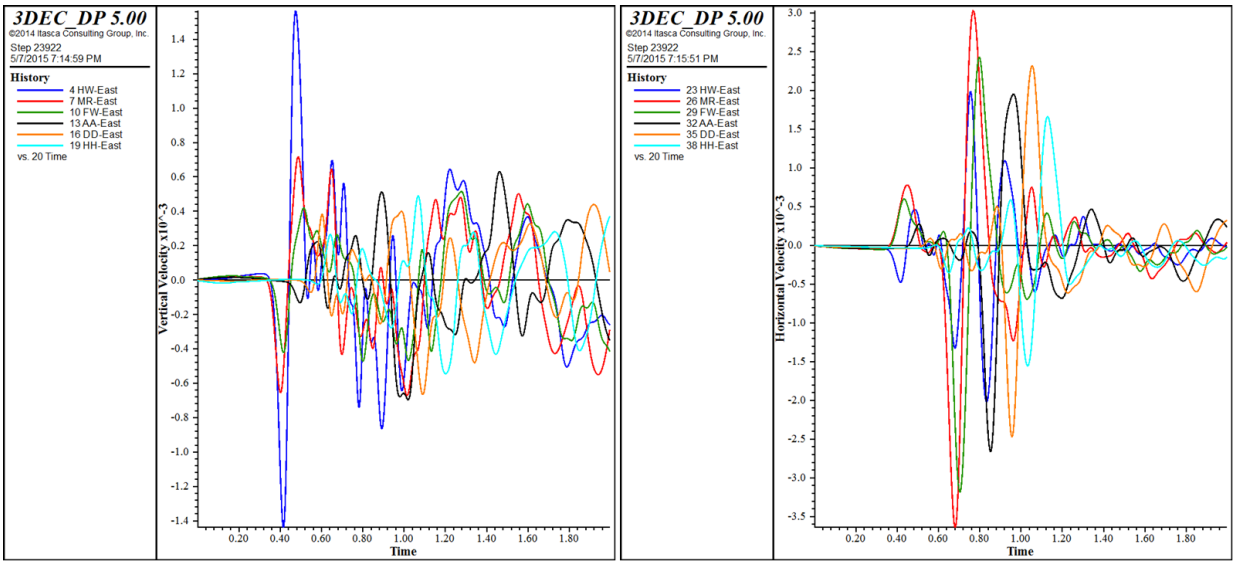


Figure 5.23 Slip along a dry joint, plots of velocity time histories on east edge of the model; left – vertical velocity time histories, right –horizontal velocity time histories

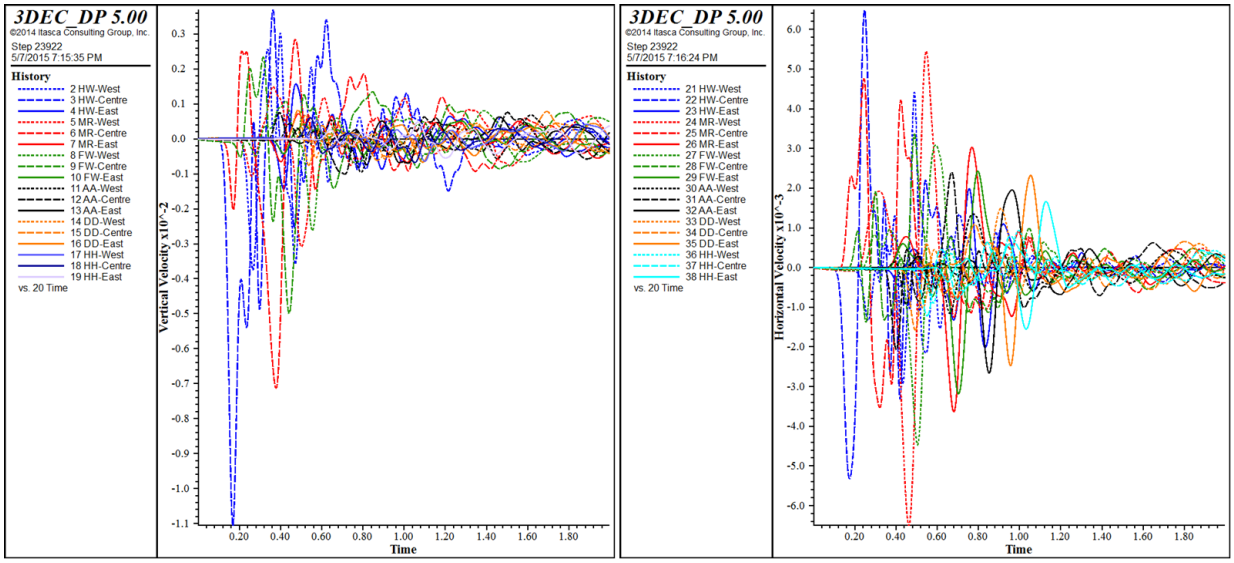


Figure 5.24 Slip along a dry joint, plots of velocity time histories on the entire model; left – vertical velocity time histories, right –horizontal velocity time histories

5.11.5. Discussion on ground motions due to impulsive slip along a dry joint

The maximum velocity amplitudes of the ground motions generated due to the impulsive slip are given in Table 5.3.

Table 5.3 Ground motions at various history points due to Impulsive Slip along a dry joint (Figure 5.3 and Figure 5.15)

Location	East		Centre		West	
	Vertical cm/sec	Horizontal cm/sec	Vertical cm/sec	Horizontal cm/sec	Vertical cm/sec	Horizontal cm/sec
HW	0.158	0.21	1.10	0.64	0.38	0.46
MR	0.07	0.36	0.72	0.49	0.32	0.54
FW	0.04	0.34	0.50	0.36	0.26	0.44
AA	0.07	0.28	0.09	0.024	0.10	0.16
DD	0.06	0.25	0.08	0.014	0.06	0.16
HH	0.056	0.16	0.05	0.010	0.05	0.09
HW-Hanging Wall (Quartzite), MR-Main Reef (Conglomerate), FW-Foot Wall (Amaceous Shale), AA-Amygdaloidal Andesite, DD-Diabase Dyke, HH-Hospital Hill Slates						

Salient points of the results are listed as following:

- The vertical velocity at the centre of the Main Reef are in the range cm/sec; at all other points in the model, velocity histories are in the range of mm/sec.
- Within the Main Reef, the vertical velocity histories are greater than the respective horizontal velocity histories whereas the opposite is the case in all other geological groups. It suggests that in an event of impulsive slip, the vertical velocity is more pronounced in the geological group in which the slip takes place.
- Ground motions (both vertical and horizontal) at the centre of each geological group are larger than the points west and east of the model.
- Horizontal ground motions in the Hanging Wall exhibit with a downward (southward) trend whereas ground motions in Main Reef and Foot Wall initiate with an upward (northward) trend. It suggests that a seismic event due to Impulsive Slip in a dry condition results in Normal-Dip-Slip phenomenon.
- The amplitude above the area of slip is greatest in the HW, followed by MR and FW. It becomes consistent away from the area of slip, at HH; these are almost consistent at the centre and edges of geological block.
- Variation in the ground motion at the centre and edges is more pronounced in HW, MR and FW. This variation is significantly less in other geological units. It shows the effect of geometry and distance has an influence on the ground motions.
- From Figure 5.24, it is assessed that the duration of the seismic event due to impulsive slip along dry joints is around 2.5 seconds.

5.11.6. Simulation for ground motions due to impulsive slip along a flooded joint

Results of the simulation for impulsive slip in flooded conditions are shown in Figures 5.25 through 5.29.

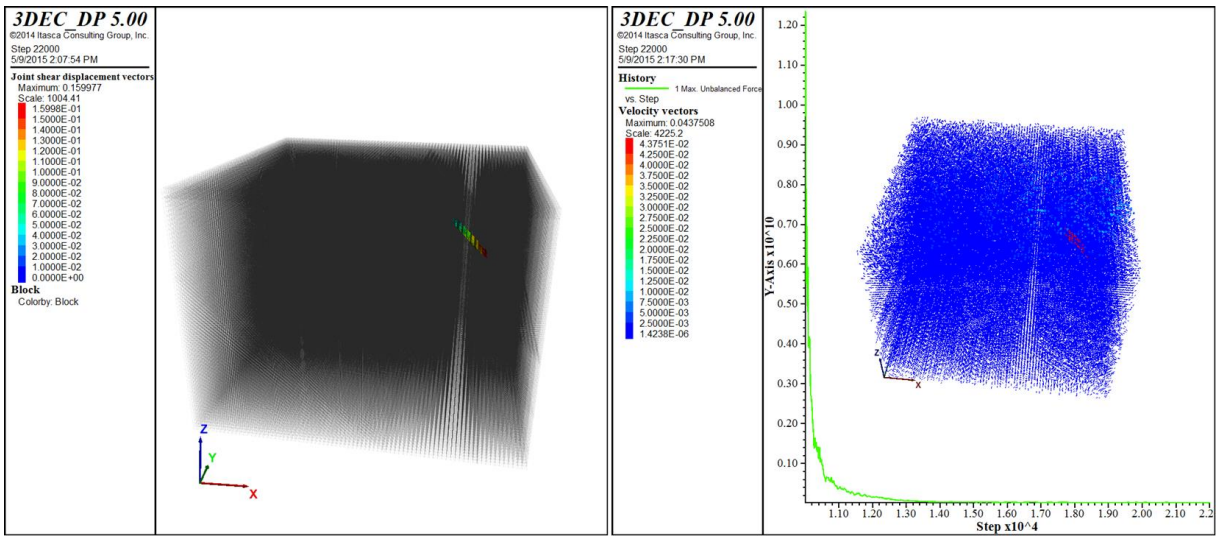


Figure 5.25 Slip along a flooded joint due to gradual rise in pore pressure; left – plot of joint shear displacement, right – plot of unbalanced force and velocity histories

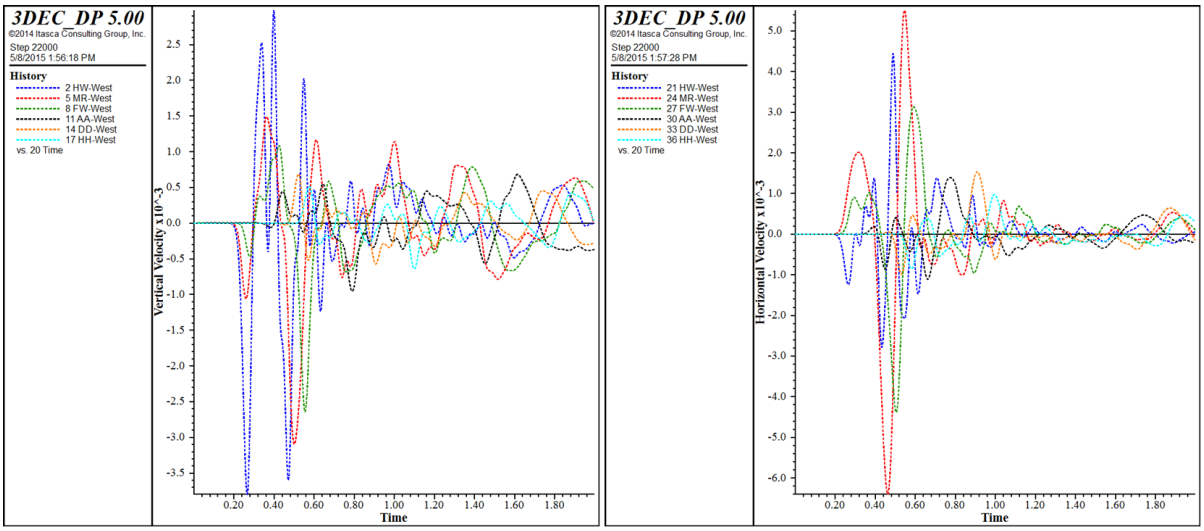


Figure 5.26 Slip along a flooded joint due to gradual rise in pore pressure, plots of velocity time histories on the west edge of model; left – vertical velocity time histories, right –horizontal velocity time histories

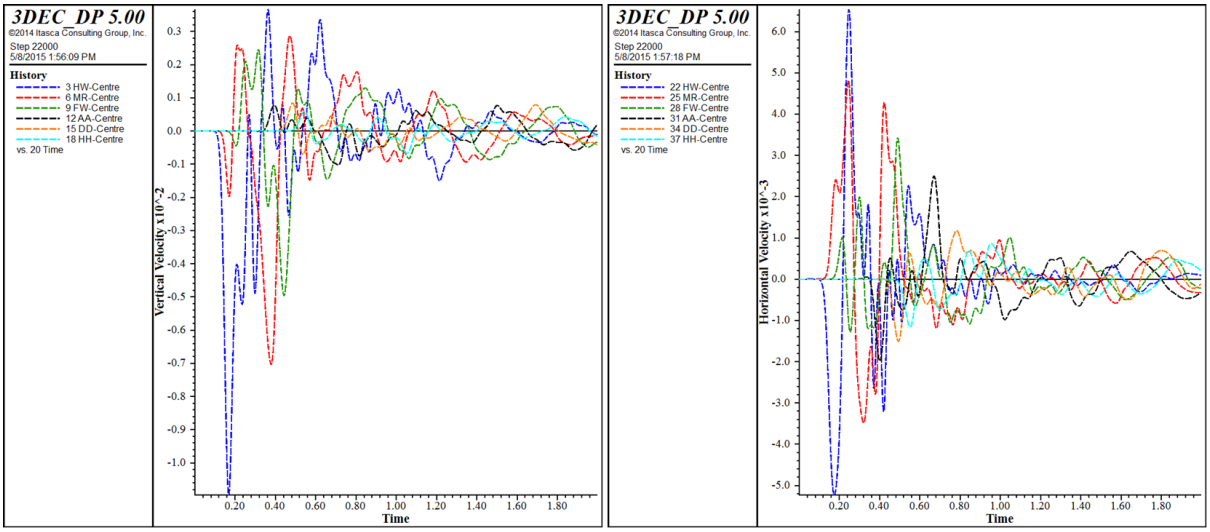


Figure 5.27 Slip along a flooded joint due to gradual rise in pore pressure, plots of velocity time histories on the centre of the model; left – vertical velocity time histories, right –horizontal velocity time histories

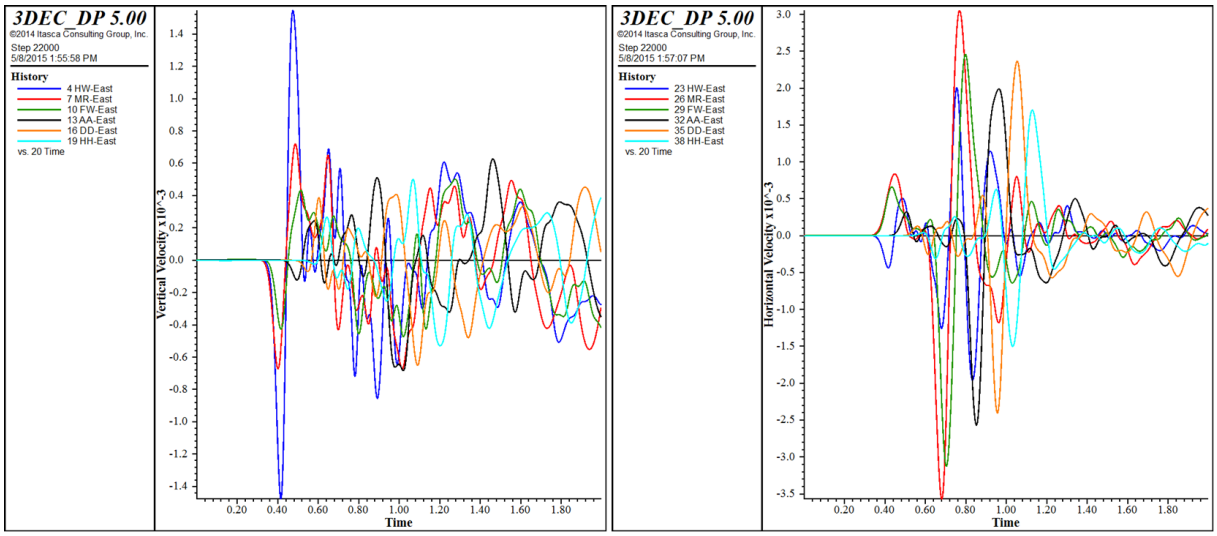


Figure 5.28 Slip along a flooded joint due to gradual rise in pore pressure, plots of velocity time histories on the east edge of the model; left – vertical velocity time histories, right –horizontal velocity time histories

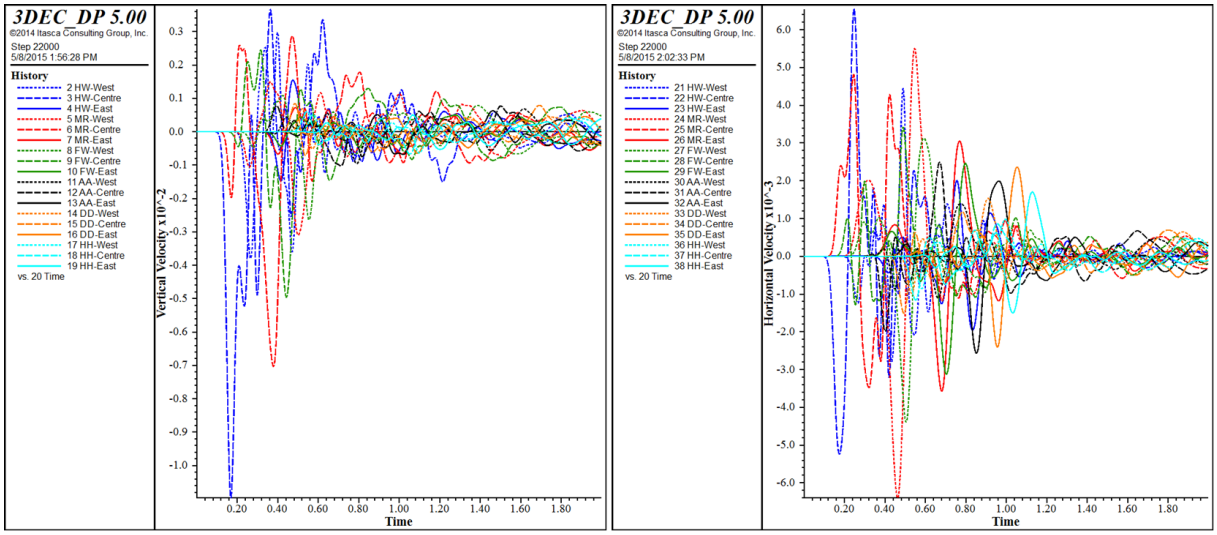


Figure 5.29 Slip along a flooded joint due to gradual rise in pore pressure, plots of velocity time histories on the entire model; left – vertical velocity time histories, right –horizontal velocity time histories

5.11.7. Discussion on ground motions estimated due to impulsive slip along a flooded joint

The maximum velocity amplitudes of the ground motions generated due to impulsive slip are given in Table 5.4.

Table 5.4 Ground motions due to Impulsive Slip along a flooded joint

Location	East		Centre		West	
	Vertical cm/sec	Horizontal cm/sec	Vertical cm/sec	Horizontal cm/sec	Vertical cm/sec	Horizontal cm/sec
HW	0.16	0.21	1.09	0.66	0.38	0.46
MR	0.07	0.36	0.70	0.48	0.32	0.64
FW	0.06	0.32	0.50	0.34	0.27	0.48
AA	0.07	0.26	0.11	0.20	0.10	0.14
DD	0.06	0.25	0.09	0.16	0.06	0.16
HH	0.06	0.15	0.08	0.10	0.05	0.10
HW-Hanging Wall (Quartzite), MR-Main Reef (Conglomerate), FW-Foot Wall (Amaceous Shale), AA-Amygdaloidal Andesite, DD-Diabase Dyke, HH-Hospital Hill Slates						

Salient points of the results are listed below:

- Ground motions (both vertical and horizontal) due to impulsive slip along dry and wet joints are similar, Table 5.3 and Table 5.4. It suggests that flooding has little effect on the intensity of ground motions. However, it is considered that flooding is likely to trigger the slip which otherwise may not slip or slip at a later stage.
- The vertical velocities at the centre of Main Reef are in the range cm/sec; at all other points in the model, velocity histories are in the range of mm/sec.
- Within the Main Reef, the vertical velocity histories are greater than respective horizontal velocity histories whereas it is opposite in all other geological groups. It suggests that in an event of impulsive slip, vertical velocity is more pronounced in the geological group in which the slip takes place.
- Ground motions (both vertical and horizontal) at the centre of each geological group are larger than the points at west and east of the model.
- Horizontal ground motions in the Hanging Wall exhibit with a downward (southward) trend whereas ground motions in Main Reef and Foot Wall initiate with an upward (northward) trend. It suggests that seismic event due to Impulsive Slip results in a Normal-Dip-Slip mechanism.
- The amplitude above the area of slip is greatest in the HW, followed by MR and FW. It becomes consistent away from the area of slip, at HH; these are almost consistent at the centre and edges of the geological block.
- Variation in the ground motion at the centre and edges is more pronounced in HW, MR and FW. This variation is significantly less in other geological units. It shows the effect of geometry and distance has an influence on the ground motions.
- The variation in horizontal velocities at the centre of AA, DD and HH is relatively larger as shown in Table 5.4. This is due to the fact that attenuation is more rapid at a larger distances from the source.
- The duration of the seismic event due to impulsive slip along flooded joints is around 2 seconds.
- The amplitude varies in all the geological units whereas duration remains almost constant.

5.12. 3DEC Simulations for Fall of Ground

According to Hasegawa et al. (1989), fall of ground and cavity collapse is one of the source mechanisms responsible for mining induced seismicity. The simulation of seismicity due to fall of ground is covered under following headings:

- Empirical Considerations.
- Conceptual considerations.
- 3DEC Numerical modelling sequence; initial static equilibrium.
- Simulation for estimation of ground motions due to fall of ground in a dry void.
- Discussion on ground motions estimated due to fall of ground in a dry void.
- Simulation for estimation of ground motions due to fall of ground in a flooded void.
- Discussion on ground motions estimated due to fall of ground in a flooded void.

5.12.1. Empirical considerations

According to Riemer and Durrheim (2011), a fall of ground (hanging wall) of 2500 tons took place in Robinson Deep Mine during August 1908 but apparently not the slightest shock was observed at the surface. In the absence of any data regarding seismicity due to fall of ground, numerical simulations were made for a fall of a volume of 8750 m^3 from a height of 5 m in a dry and flooded void. In preliminary simulations, this size of the fall generated ground motion (velocity history) compatible to a seismic event of magnitude around M_L 2 to 3.

There is no direct evidence that fall of ground is a cause of observed seismicity in the deep gold mines. This scenario is included for the sake of completeness and also to cover the possibility that a major fall of ground may be caused by an impulsive event. The selected volume of the simulated collapse is somewhat arbitrary, representing a 5 m collapse over an area of 25 m x 70 m.

5.12.2. Conceptual considerations

The existing / expected conditions in abandoned mines relevant to fall of ground are conceptualized as following:

- With the passage of time, the rock mass in abandoned mines is undergoing stability deterioration due to stress relief, tensile opening, weathering, etc.
- In water flooded voids, deterioration is likely to be more severe due to the ingress of water in the sheared rock mass at the exposed periphery.
- In a dry mining void, the fall of ground can travel faster and undergo repetitive rebounds until all the kinetic energy is consumed.
- The separation of rock especially from the roof is likely to be a time-dependent process therefore significant seismicity at the time of rock separation (from parent rock) is less likely. However, the possibility of a sudden fall triggered due to some nearby seismic event cannot be ruled out resulting in relatively larger seismicity at the time of rock separation (from the parent rock).
- In case of a flooded void, a fall of ground is likely to induce stresses in all directions i.e., walls, floor and roof depending on the level of water in the void. The seismic waves are likely to have different characteristics than those generated in a dry void where fall of ground experiences a free fall and repetitive rebounds.
- The larger the volume of fall of ground, the larger are the ground motions.

5.12.3.3DEC Simulation aspects common to fall of ground in dry and flooded conditions

For the simulation of seismicity due to fall of ground, the model is initially run to establish initial static equilibrium under given conditions of in-situ stresses and gravity as shown in Figures 5.30 and 5.31. After the initial static equilibrium, the excavation is made and the model is run again to establish equilibrium conditions as shown in Figures 5.32 through 5.34.

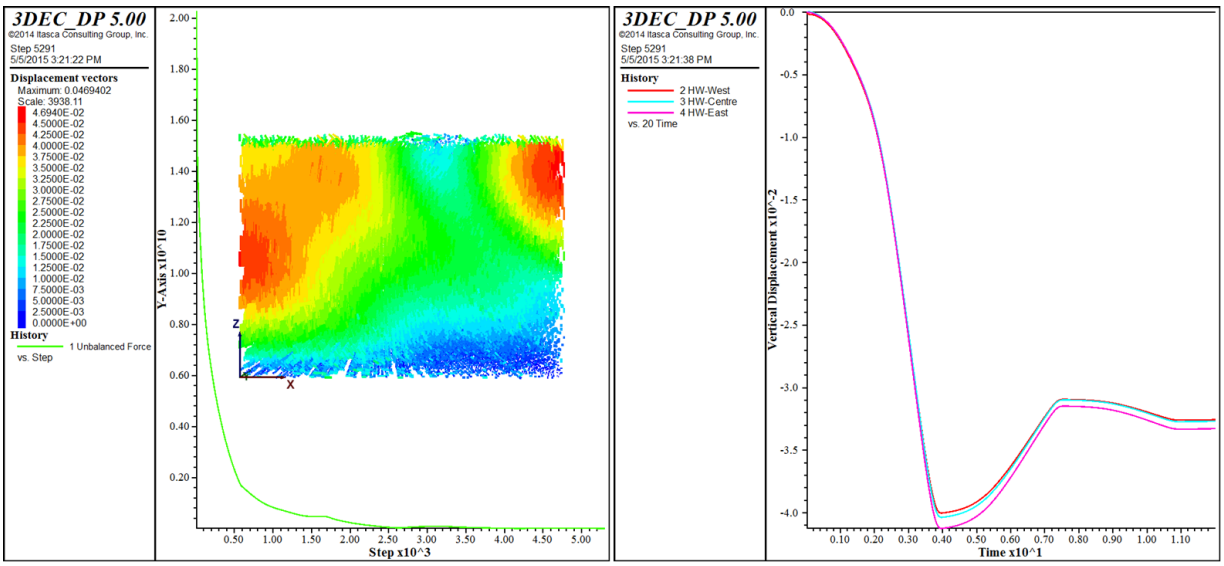


Figure 5.30 Static equilibrium; left-plot of unbalanced force, right-plot of vertical displacement histories in Hanging Wall

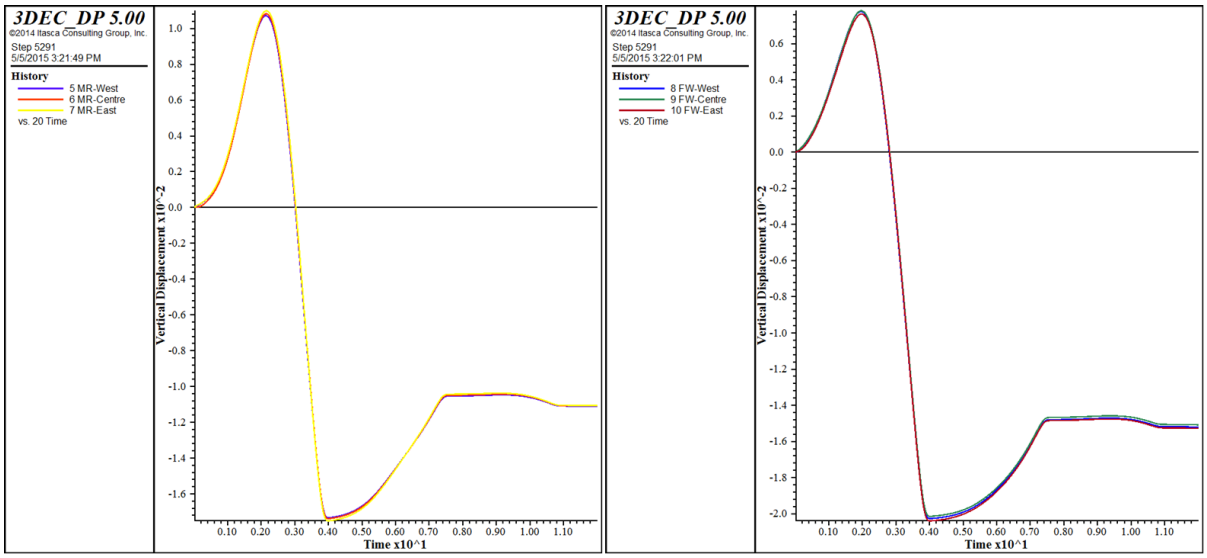


Figure 5.31 Static equilibrium; left-plot of vertical displacement histories in Main Reef, right-plot of vertical displacement histories in Foot Wall

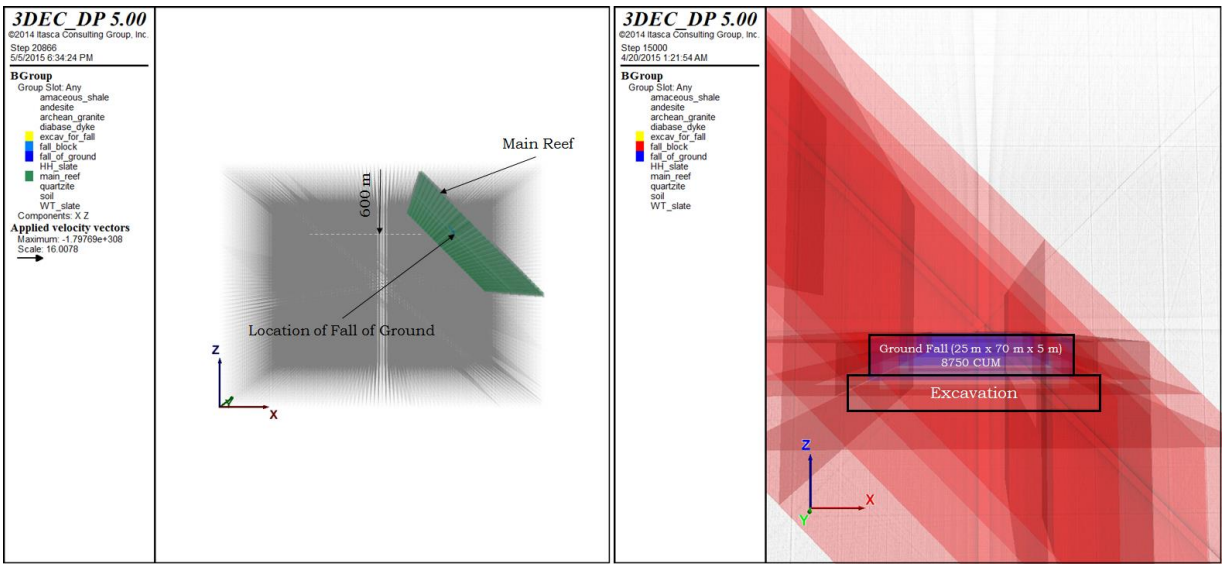


Figure 5.32 Excavation; left-location of Main Reef and Fall of Ground, Right-close-up of Excavation and Fall of Ground

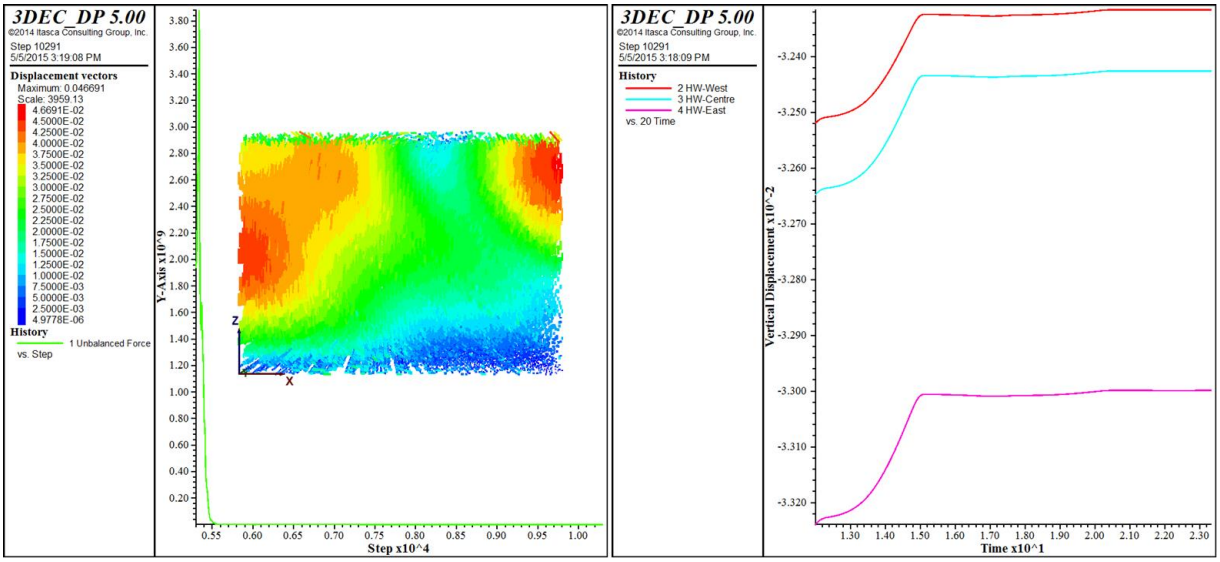


Figure 5.33 Post excavation equilibrium; left-plot of unbalanced force, right-plot of displacement histories in Hanging Wall

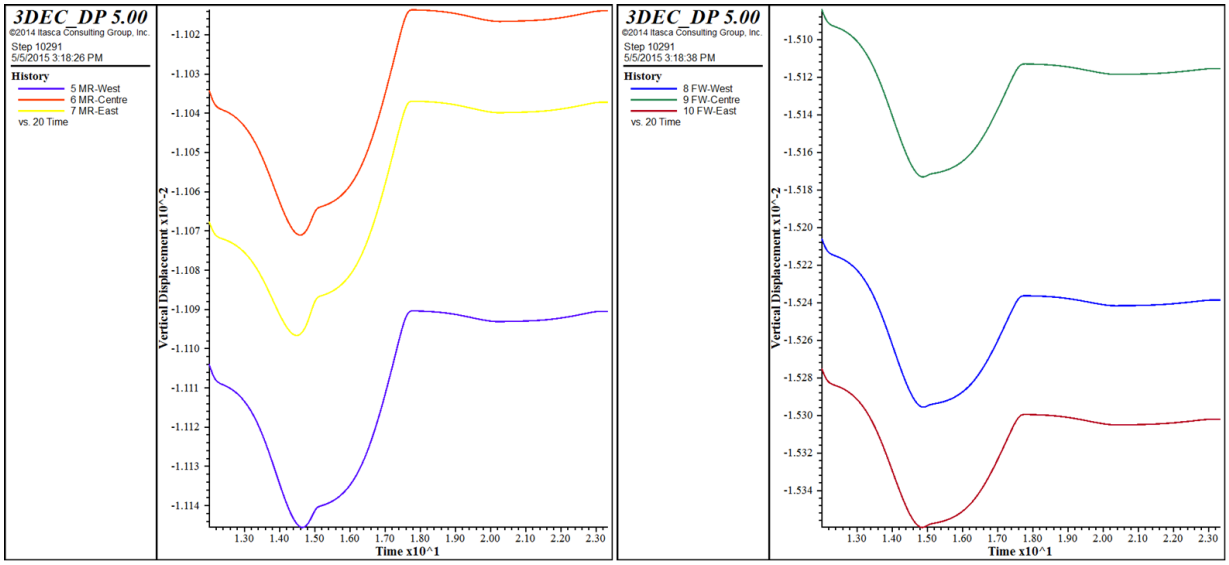


Figure 5.34 Post excavation equilibrium; left-plot of vertical displacement histories in Main Reef, right-plot of vertical displacement histories in Foot Wall

5.12.4. Simulation for fall of ground in a dry void

- A rock with the volume of 8750 m^3 is allowed to fall from a height of 5 m in a dry void. The rock has a thickness of 5 m, a width of 25 m and length of 70 m.
- To mimic the sudden fall of the rock, the excavation is made below the intended fall of ground. Location of the fall of ground is shown in Figure 5.32.
- Since a free fall of the ground (rock) requires extremely long numerical time, a velocity of 10 m/sec is applied at the top of the rock fall to accelerate the fall (the effect of gravity is automatically taken into account in 3DEC code). This velocity is removed before the impact and the ground is allowed to fall under its own kinematics.
- Ground motions due to a fall of ground in a dry void are shown in Figures 5.35 through 5.38.

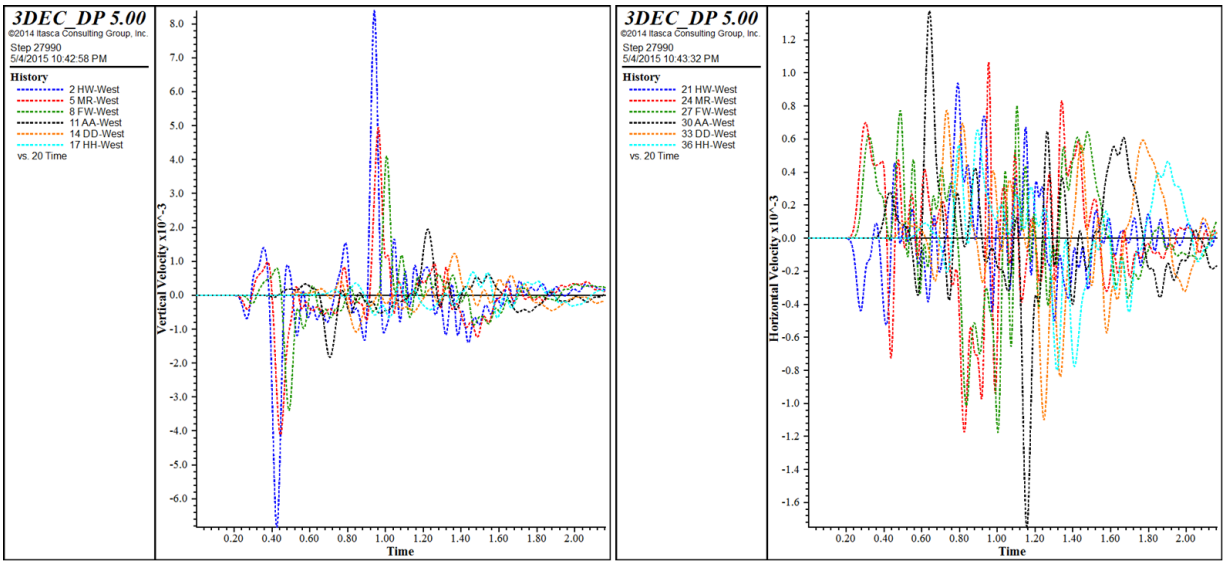


Figure 5.35 Ground motions due to fall of ground on the west edge of the model; Left-vertical velocity time histories, Right-horizontal velocity time histories

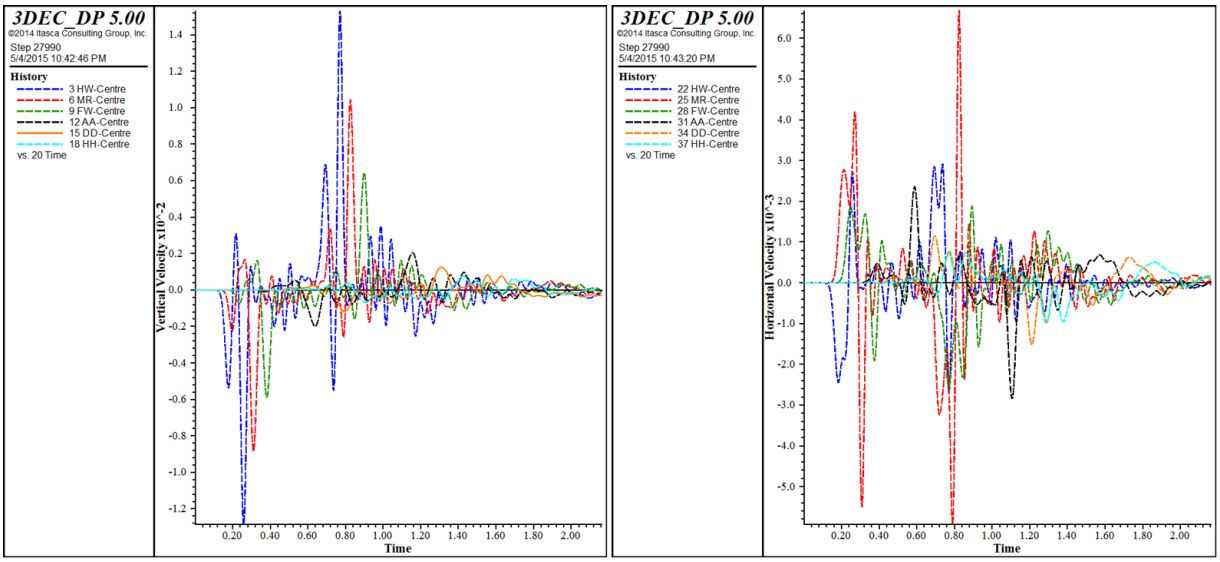


Figure 5.36 Ground motions due to fall of ground at the centre of the model; Left-vertical velocity time histories, Right-horizontal velocity time histories

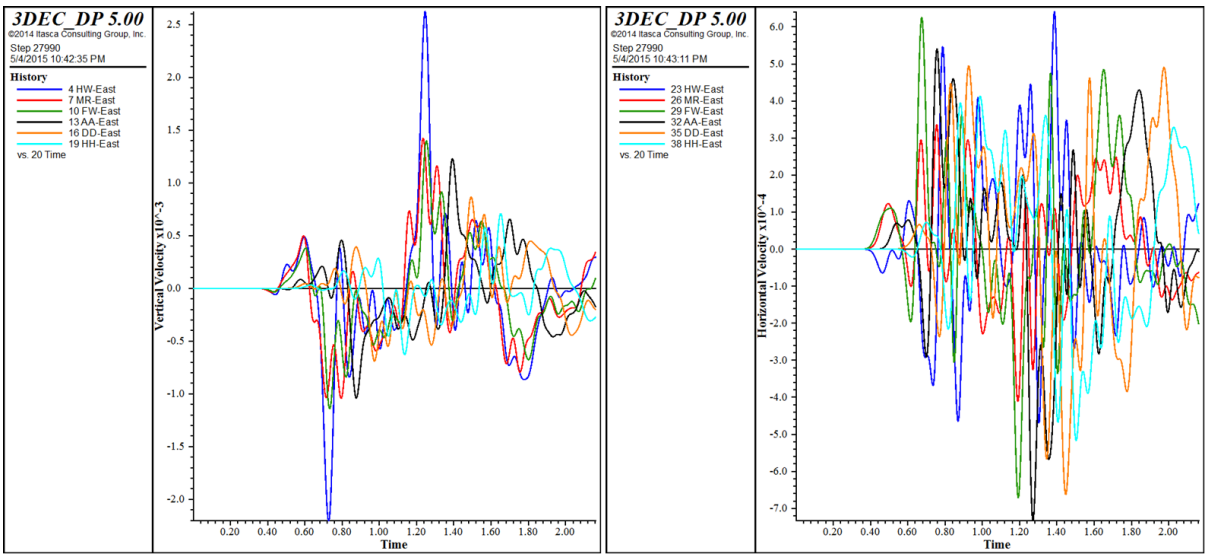


Figure 5.37 Ground motions due to fall of ground at the east of the model; Left-vertical velocity time histories, Right-horizontal velocity time histories

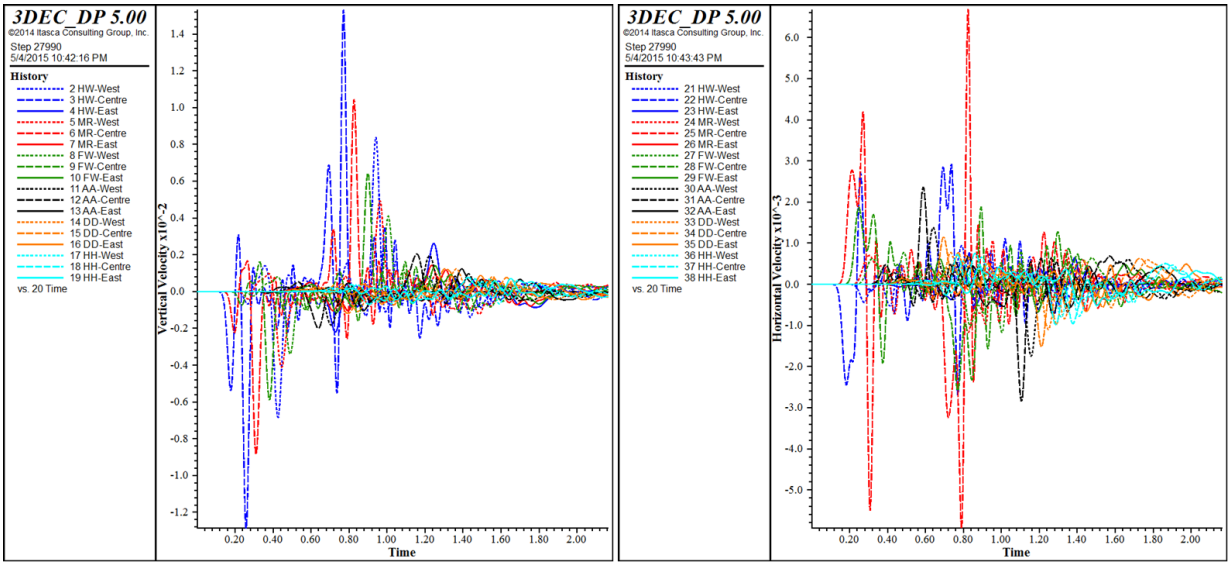


Figure 5.38 Ground motions due to fall of ground at the entire model; Left-vertical velocity time histories, Right-horizontal velocity time histories

5.12.5. Discussion on ground motions due to fall of ground in a dry void

The maximum velocity amplitudes of the ground motions generated due to impulsive slip are given in Table 5.5.

Table 5.5 Ground motions due to fall of ground in a dry void

Location	East		Centre		West	
	Vertical cm/sec	Horizontal cm/sec	Vertical cm/sec	Horizontal cm/sec	Vertical cm/sec	Horizontal cm/sec
HW	0.26	< 0.01	1.48	0.30	0.82	< 0.01
MR	0.14	"	1.0	0.68	0.50	"
FW	0.44	"	0.60	0.20	0.38	"
AA	0.10	"	0.20	0.30	0.20	"
DD	0.08	"	0.40	0.17	0.10	"
HH	0.06	"	0.30	0.05	0.08	"

HW-Hanging Wall (Quartzite), MR-Main Reef (Conglomerate), FW-Foot Wall (Amaceous Shale), AA-Amygdaloidal Andesite, DD-Diabase Dyke, HH-Hospital Hill Slates

Salient points of the results are listed below:

- In an event of a fall of ground, both vertical and horizontal velocity time history has two components; an initial component which mimics the process of separation from the parent rock (roof in this case) and the second simulates the impact of rock with the floor.
- The initial component (rock separation) is characterized by relatively smaller amplitude than the later component (impact with the floor) but shorter duration.
- Before the vibrations induced by rock detachment/stress relief diminish, vibrations due to impact are induced/recorded.
- The vertical velocity at the centre of the Main Reef are in the range cm/sec; at all other points in the model, velocity histories are in the range of mm/sec.
- Vertical velocity histories are greater than respective horizontal velocity histories. It suggests that fall of ground in a dry void generates greater vertical

velocity histories. The largest vertical velocity history of 1.48 cm/sec occurs at the centre point of the Hanging Wall.

- Ground motions at the centre of each geological unit are larger than the points at west and east of the model.
- Ground motions in the Hanging Wall are observed to have a downward (southward) trend whereas ground motions in Main Reef and Foot Wall initiate with an upward (northward) trend. It suggests that a seismic event due to fall of ground in dry void is similar to movements during Normal-Dip-Slip phenomenon.
- Vibrations after the impact are repetitive; after the first impact the rock rebounds and impacts again which makes the waveform complex.

5.12.6. Simulations for fall of ground in a flooded void

- According to Itasca, (2014), 3DEC considers fluid flow in rock mass only through fractures and flow through rock mass itself is not considered.
- In 3DEC simulations, there is no provision for incorporating flooded voids (mine excavations filled with water). However, for the purpose of simulation, the effect of the flooded void is incorporated indirectly by setting appropriate stresses along the boundaries of the excavation.
- Boundary stress; representative of the water pressure equivalent to the groundwater table at a depth of 100 m from the bedrock is set along six sides of the excavation. This corresponds to the stress of 5e6 Pa.
- Ground motions due to fall of ground in a flooded void are shown in Figures 5.39 through 5.42.

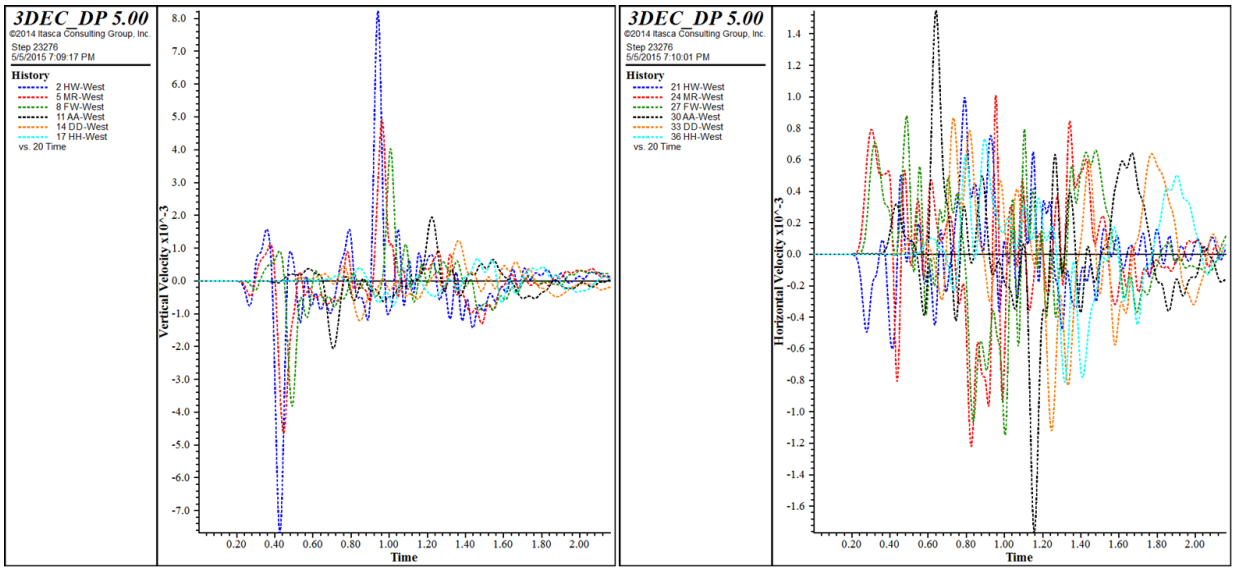


Figure 5.39 Ground motions due to fall of ground at the west edge of the model; Left-vertical velocity time histories, Right-horizontal velocity time histories

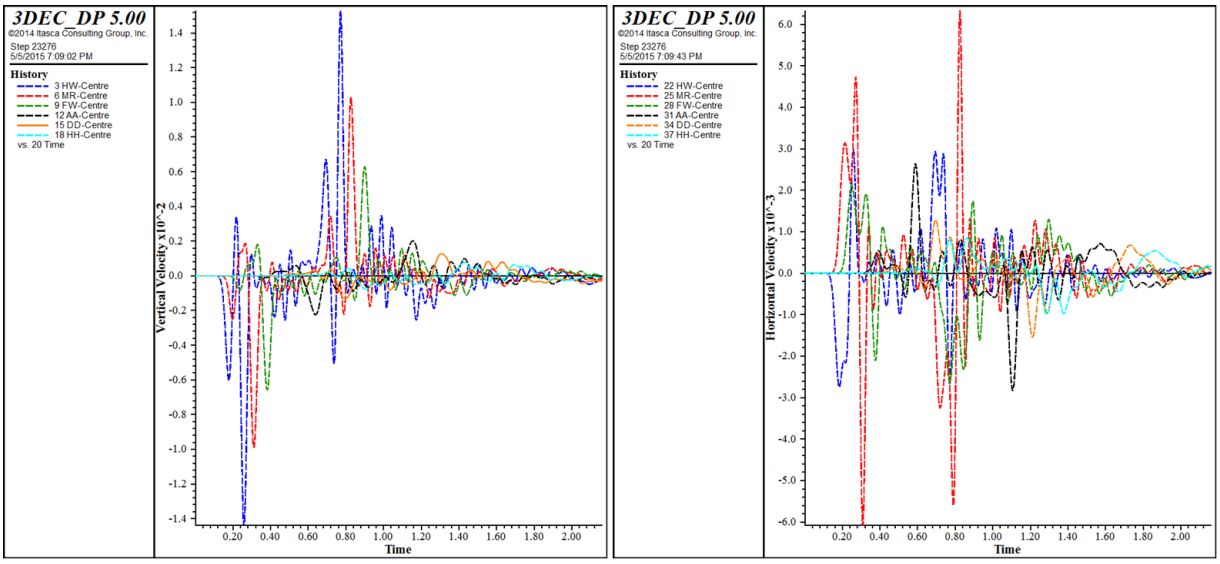


Figure 5.40 Ground motions due to fall of ground at the centre of the model; Left-vertical velocity time histories, Right-horizontal velocity time histories

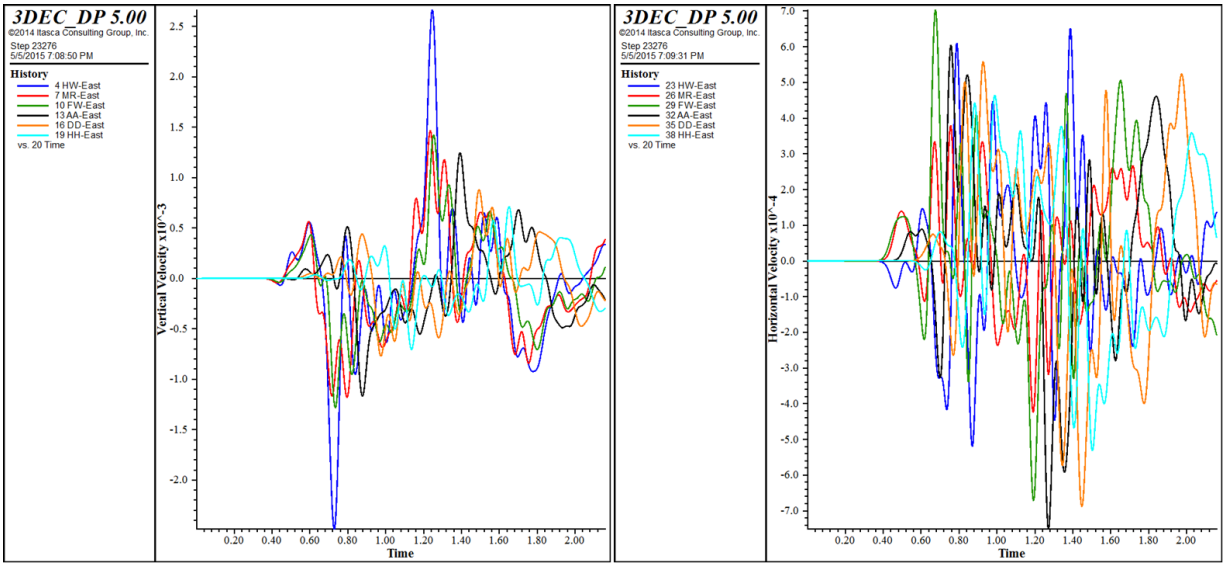


Figure 5.41 Ground motions due to fall of ground at the east of the model; Left-vertical velocity time histories, Right-horizontal velocity time histories

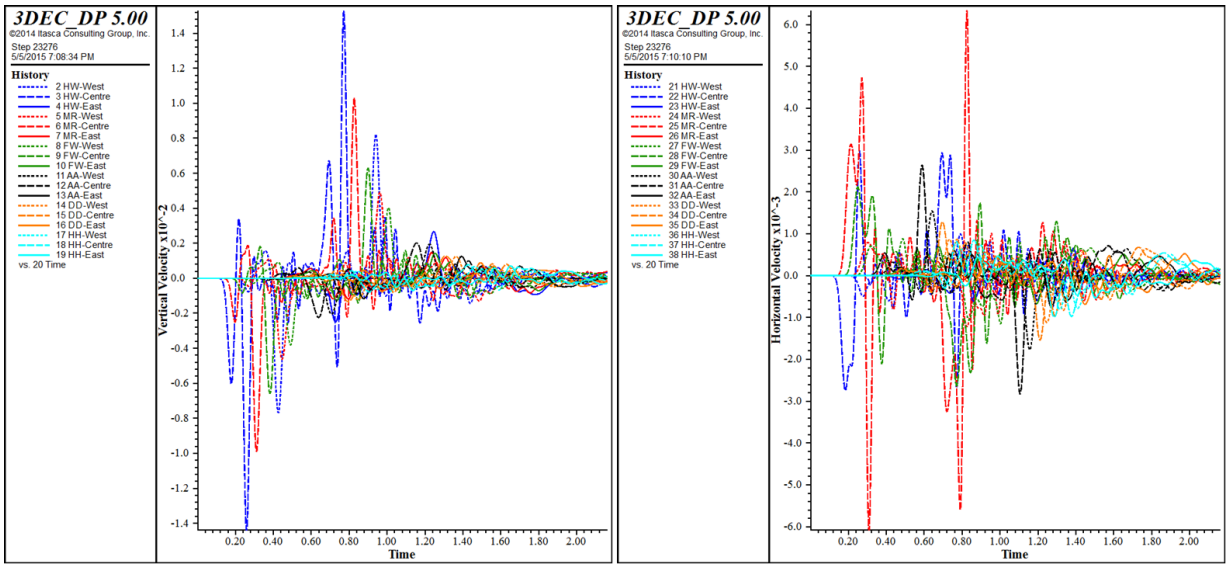


Figure 5.42 Ground motions due to fall of ground at the entire model; Left-vertical velocity time histories, Right-horizontal velocity time histories

5.12.7. Discussion on ground motions due to fall of ground in a flooded void

The maximum velocity amplitudes of the ground motions generated due to impulsive slip are given in Table 5.6.

Table 5.6 Ground motions due to fall of ground in a flooded void

Location	East		Centre		West	
	Vertical cm/sec	Horizontal cm/sec	Vertical cm/sec	Horizontal cm/sec	Vertical cm/sec	Horizontal cm/sec
HW	0.27	< 0.01	1.52	0.28	0.81	< 0.01
MR	0.14	"	1.40	0.60	0.50	"
FW	0.13	"	0.64	0.22	0.38	"
AA	0.12	"	0.20	0.28	0.20	"
DD	0.10	"	0.10	0.16	0.10	"
HH	0.08	"	0.02	0.05	0.10	"
HW-Hanging Wall (Quartzite), MR-Main Reef (Conglomerate), FW-Foot Wall (Amaceous Shale), AA-Amygdaloidal Andesite, DD-Diabase Dyke, HH-Hospital Hill Slates						

Salient points of the results are listed below:

- In an event of a fall of ground in a flooded void, ground motions are generated in both vertical and horizontal directions.
- Both vertical and horizontal velocity time histories have two components; initial component which mimics the process of separation from the parent rock (roof in this case) and the second simulates the impact of rock with the floor.
- The initial component (rock separation) is characterized by relatively smaller amplitude than the later component but shorter duration.
- Before the vibrations induced by rock detachment/stress relief diminish, vibrations due to impact are induced/recorded.
- The vertical velocity at the centre of Main Reef are in the range cm/sec; at all other points in the model, velocity histories are in the range of mm/sec.

- Vertical velocity histories in all the geological groups are generally greater than respective horizontal velocity histories. It suggests that fall of ground in a flooded void generates greater vertical velocity histories, similar to the fall of ground in a dry void.
- The largest vertical velocity history of 1.52 cm/sec occurs at the centre point of the Hanging Wall.
- Ground motions at the centre of each geological unit are larger than the points at west and east edge of the model.
- The horizontal ground motions in the Hanging Wall exhibit a downward (southward) trend whereas in Main Reef and Foot Wall, these are generated with an upward (northward) trend. It suggests that a seismic event due to fall of ground in a flooded void results in Normal-Dip-Slip phenomenon. This is similar to a fall of ground in a dry void.
- Vibrations after the impact are repetitive; after the first impact the rock rebounds and impacts again which makes the waveform complex.

5.12.8. Comments / comparison of ground motions due to fall of ground in a dry and flooded void

- The ground motions are observed in both vertical and horizontal directions in an event of fall of ground in a dry and a flooded void.
- The ground motions have two components; due to rock separation and impact with the floor in an event of fall of ground in a dry and a flooded void.
- Generally vertical ground motions are larger in magnitude than horizontal ground motions in an event of fall of ground in a dry and a flooded void.
- Ground motions in the flooded void are slightly greater than those observed in a dry void; the highest velocity in the flooded void is 1.52 cm/sec against 1.48 cm/sec in a dry void. The difference in velocities is very small and is ignored for practical purposes.
- In both cases, the waveform is similar and has the same duration.
- Considering the first cycle (after which waveform becomes complex due to reflections and refractions of the seismic waves) the frequency is approximated as 10 Hz.

- Keeping in view the number of cycles of the simulations (more time is needed for the waves to completely decay), the duration of the ground motions is approximated as 2.0 seconds.

5.13. Simulation of Seismicity Due to Collapse of Pillar (s)

In this scenario, it is assumed that the large number of small pillars collapse simultaneously. Although the mining methods did not include a system of regular pillars as commonly used in shallow platinum and coal mining, there are remnant pillars between the raise lines and also in areas adjacent to faults. The possibility that these may fail cannot be excluded and therefore this aspect is included in the study. Simulation of seismicity due to failure of pillar is covered under following headings:

- Empirical considerations for estimating the seismic magnitude.
- 3DEC numerical model considerations.
- Simulation for estimating ground motions due to collapse of mining voids in dry and water filled conditions.
- Results and discussion on ground motions estimated due to the collapse of mining voids in dry and wet conditions.

5.13.1. Empirical considerations

To approximate the simultaneous failure of large number of pillars vis-à-vis magnitude of seismicity, an effort is made to use correlations proposed by Sjoberg et al., (2011) and Hanks and Kanamori, (1979), Equation 5.6 and Equation 5.7 respectively. Equation 5.6 correlates strain energy with stresses and volume of a pillar (considering linear-elastic material) and equation 5.7 correlates earthquake magnitude with the seismic moment.

$$E_{s-tot} = \int \sigma\epsilon \, dV = \int \frac{\sigma^2}{E} dV, \qquad \text{Equation 5.6}$$

Where E_{s-tot} is the total strain energy, σ is the stress (major principal stress used), ϵ is the strain, E is the Young's modulus of rock, V is the volume.

$$M = \frac{2}{3} \, log \, M_{\circ} - 10.7, \qquad \text{Equation 5.7}$$

Where M is the seismic magnitude (Richter scale) and $M_\circ$ is the seismic moment (dyne-cm).

$$M = \frac{2}{3}\ log\ M_\circ - 10.7 = \ M = \frac{2}{3}\log E_{s-tot}\ - 10.7, \qquad \text{Equation 5.8}$$

According to Sjoberg et al., (2011), seismic magnitude due to pillar collapse (and slip) can be estimated using Equation 5.8 (in lieu of better, site-calibrated, alternatives). Since this equation assumes that all the strain energy is converted into seismic energy, therefore, the estimated magnitude belongs to the upper limit of possible earthquake magnitude. According to Equations 5.6 and 5.7, a collapse volume of 500000 m^3, generates a seismic magnitude of M_L 4.28 (higher bound value). The following parameters are used to estimate the seismic magnitude:

- Young's modulus (E) 90 GPa
- Stress (major principal) (σ) 16.20 MPa ($\sigma z = 0.027 \times z$)

  Where z = depth, ERPM Simple Stress Model, Birch and Handley (2012).

5.13.2. 3DEC considerations

The existing / expected conditions relevant to pillar collapse are described as follows:

- It is assumed that the model material is elastic and anisotropic.
- The block material boundaries/faults are considered welded with high joint stiffness and shear strength properties. During simulation, the faults do not slip but act as boundaries between different materials for the propagation of seismic waves. The combined effect of all the faults is a phenomenon of reflections and refraction of seismic waves.
- The simultaneous failure of a large number of pillars in abandoned mines is attributed to the ongoing stability deterioration due to stress relief and weathering of rock mass (of mine, roof and floor).
- The size of the area considered for the simultaneous failure of a large number of pillars is an arbitrary size such that it generates ground vibrations comparable to earthquakes observed in the Witwatersrand Basin of magnitudes M_L 3 to 5.3.

- With rising ground water in abandoned mines, deterioration is likely to be faster and more severe due to the ingress of water in the sheared rock mass at the exposed periphery of the excavations.
- Under dry conditions, the failure of a large number of pillars is likely to be more violent than a situation where the voids are filled with water.

5.13.3. 3DEC simulation aspects common to pillar (s) collapse in dry and flooded void

- The model size is 4000 m x 4000 m x 3000 m with origin (0, 0, 0) at the bottom left corner as shown in Figure 5.43.
- The model geometry, zoning (meshing), material and joint properties are similar to those used for simulation of Impulsive Slip and Fall of Ground.
- Fixed boundary conditions are used.
- To establish the initial static equilibrium of the model, the model is run in static mode with the auto damping option.
- After the initial equilibrium is established, excavations are made and the model is again brought to equilibrium.
- Since it is not possible to model excavations and pillars in detail, voids and pillars are simulated in the form of large excavations and pillars for the research purpose.
- The length of the mined out reef area along strike is 500 m and along dip it is 100 m comprising three excavations and two pillars, Figures 5.43 and 5.44.
- The size of the each excavation and pillar is 100 m x 100 m. This is a simplified assumption made to idealize a portion of abandoned mines composed of a large number of smaller excavations and pillars.
- Plots of unbalanced force and vertical displacement histories after the initial static equilibrium are shown in Figures 5.45 through 5.47.
- Plots of unbalanced force and vertical displacement histories after the excavations are shown in Figures 5.48 through 5.50.

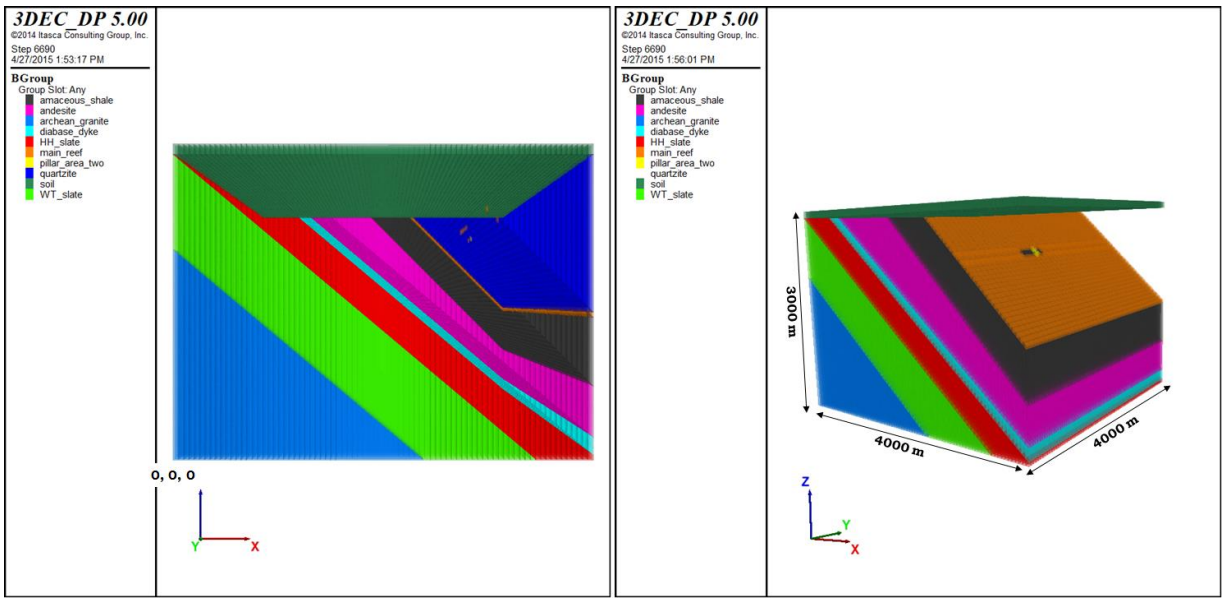


Figure 5.43 Model geometry (left) and Main Reef (right), hanging wall is removed to show location of excavations and pillars

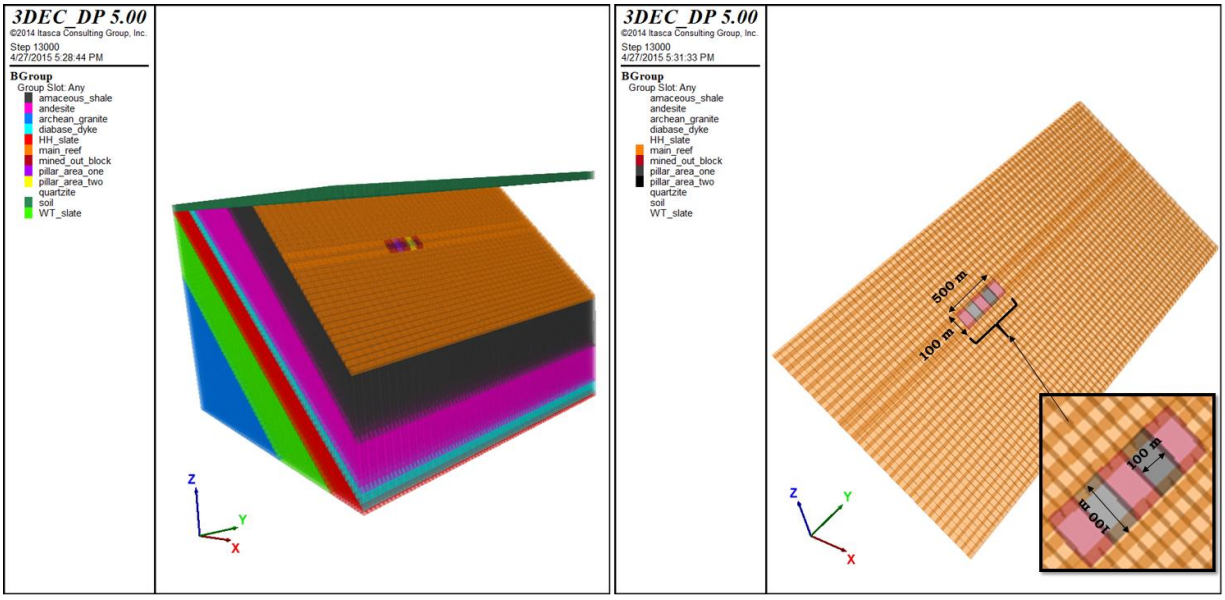


Figure 5.44 Location and layout of mining pillars (shown in grey colour) and excavations (shown in pink colours)

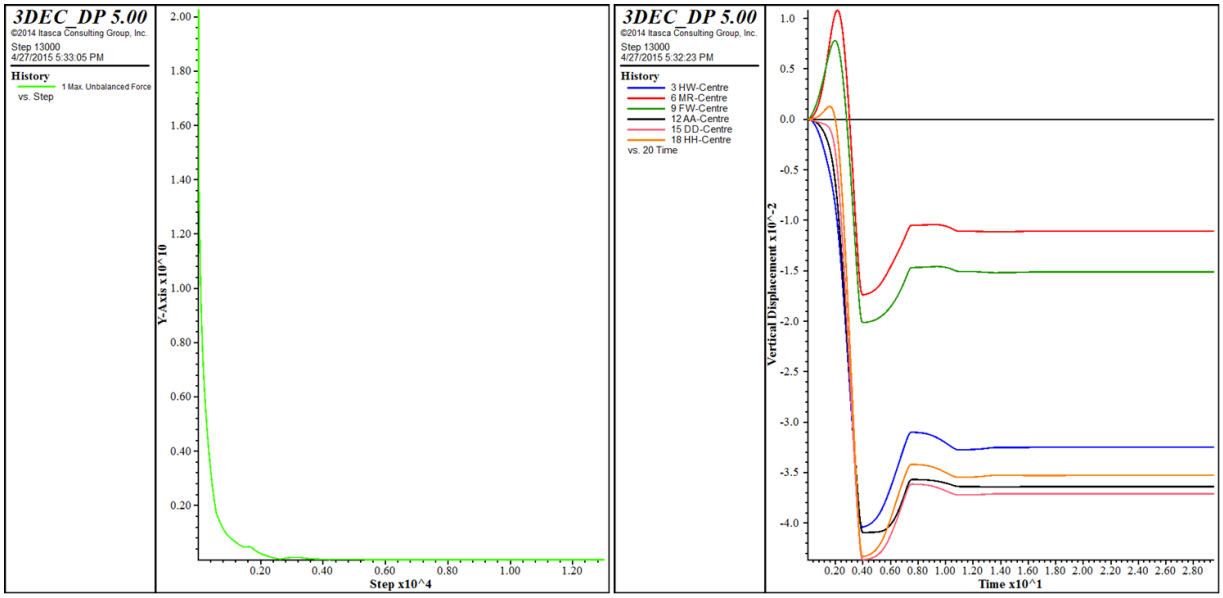


Figure 5.45 Initial static equilibrium condition of the model; plot of unbalanced force on left and vertical displacement histories at the centre points on the right

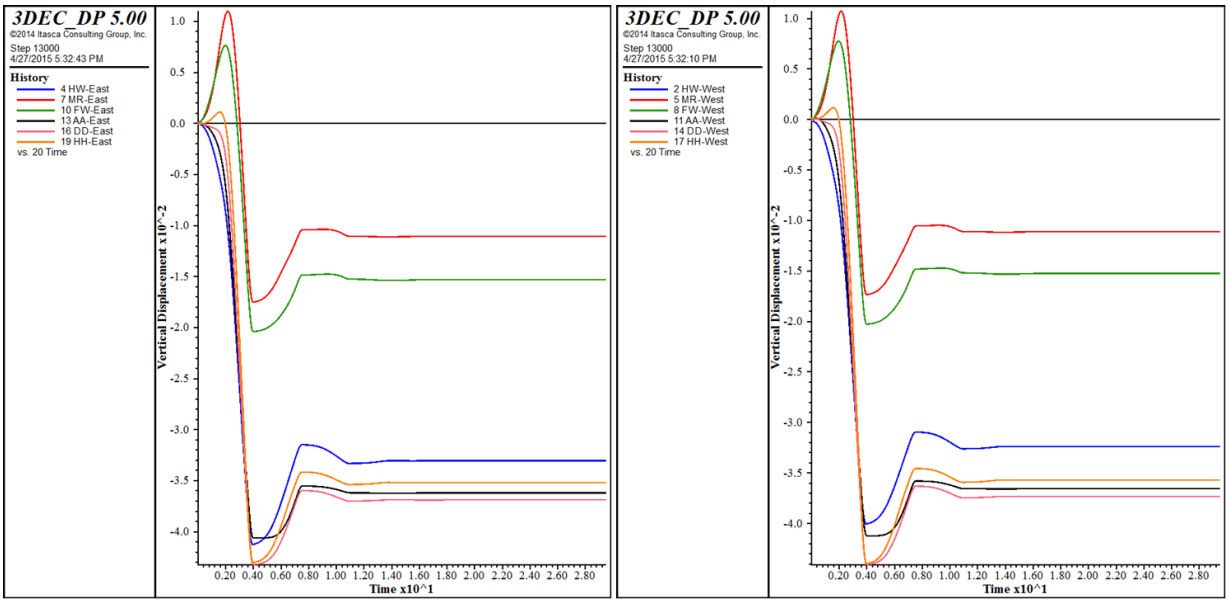


Figure 5.46 Initial static equilibrium condition of the model; left; plot of vertical displacement histories on eastern points, right; vertical displacement histories at the western points on the model

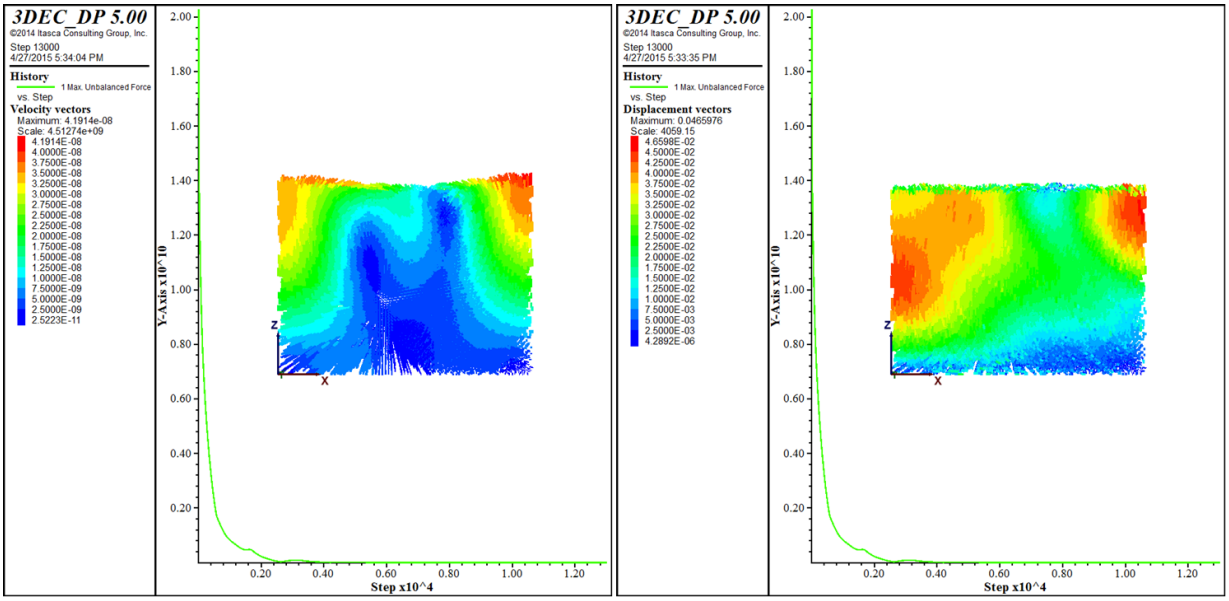


Figure 5.47 Initial static equilibrium condition of the model; left; plot of velocity vectors, right; displacement vectors

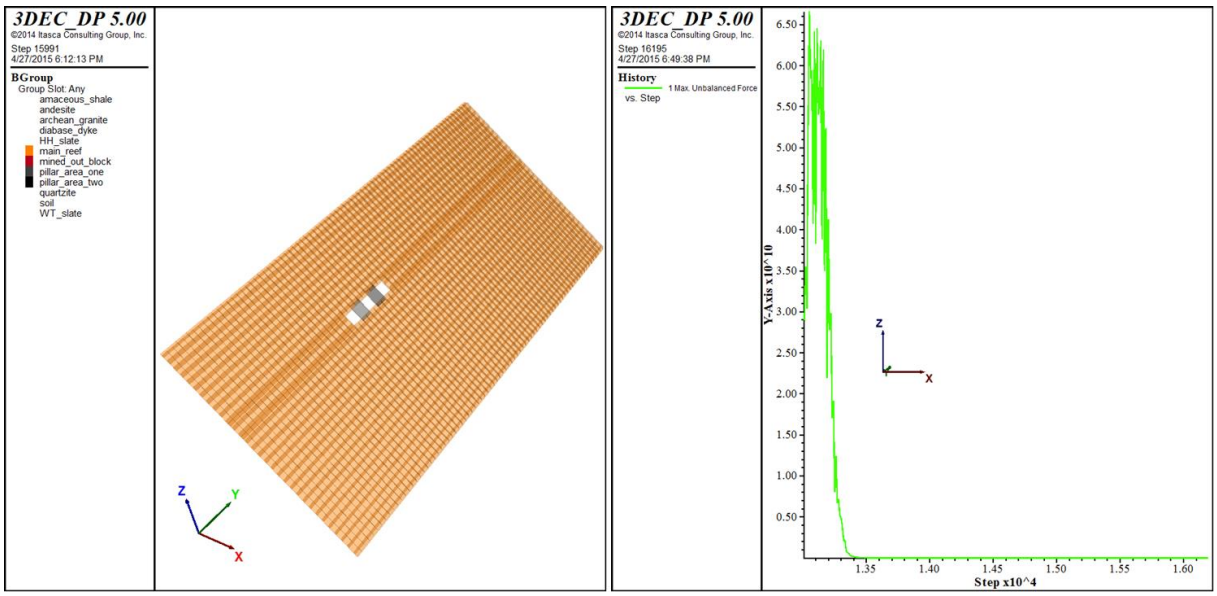


Figure 5.48 Excavations shown in white colour in the left figure, plot of unbalanced force on right

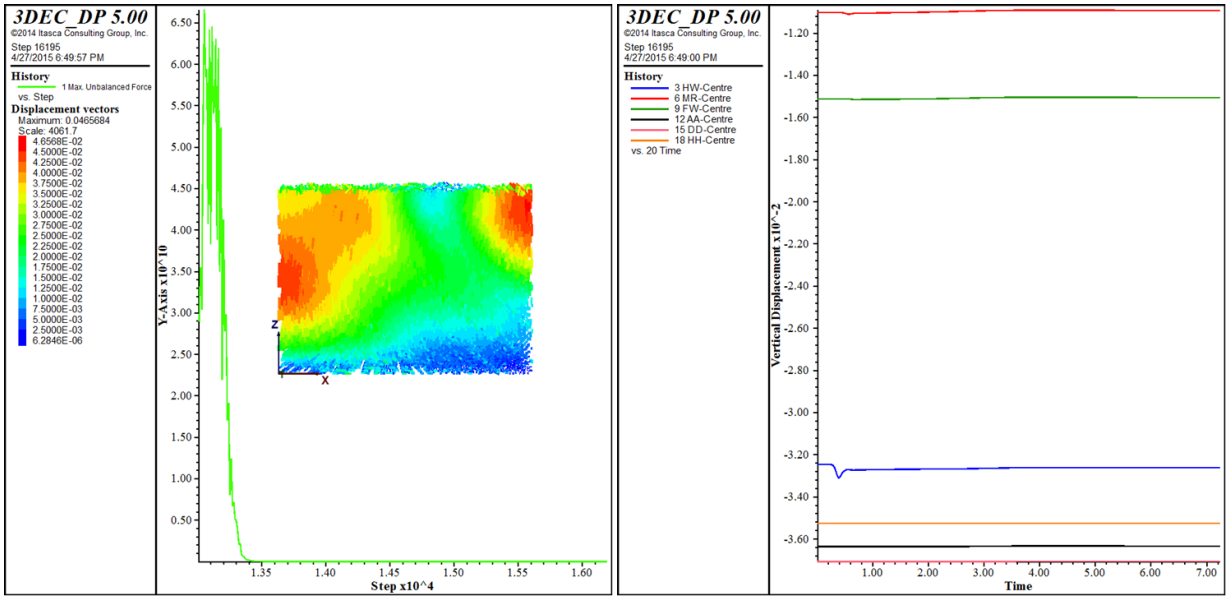


Figure 5.49 Plot of displacement vectors on left, vertical displacement histories at the centre points on the model shown on right

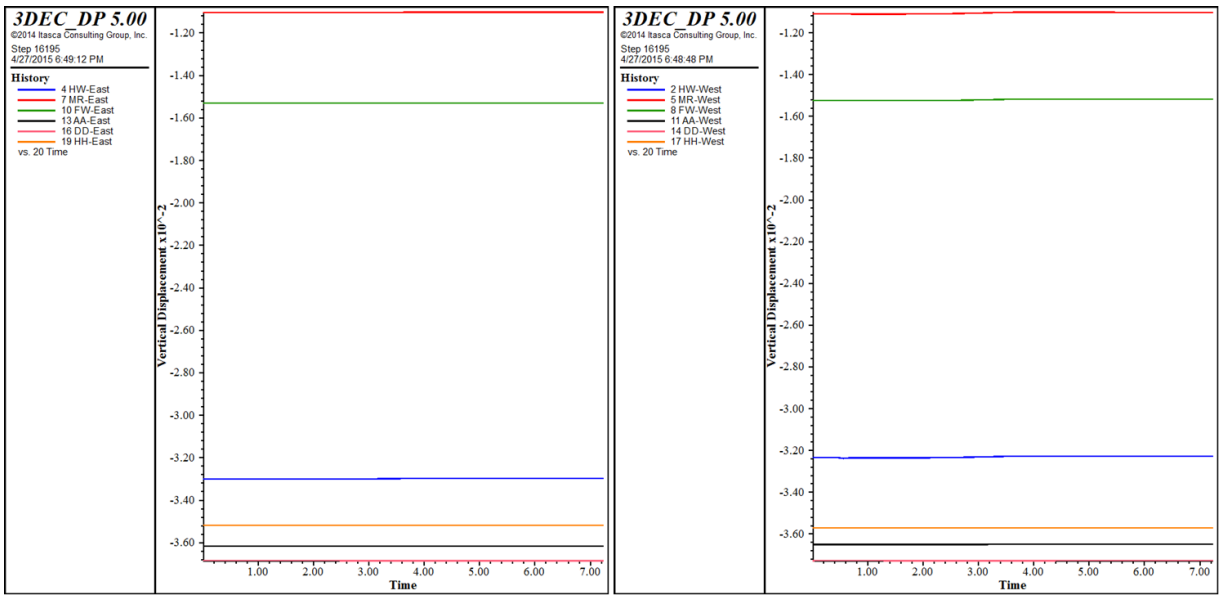


Figure 5.50 Plot of vertical displacement histories of point located on the eastern points is shown in the figure on left and western points on the right

5.13.4. Simulation of simultaneous failure of large number of pillars in dry condition

- The failure of a large number of pillars is simulated in a large area (100 m x 100 m) so as to generate ground motions which are generally caused by

earthquakes of magnitudes around M_L 4.0. According to Boore, (1980), earthquakes of M_L 3.6, 3.9, 4.0 and 4.7 at various locations in the USA, generated peak velocities of 1.0, 1.20, 2.1, and 7.7 cm/sec respectively.

- To mimic the sudden collapse of voids, the pillar area is excavated in one step and the model is run with the dynamic option.
- The simulation is made with the dynamic option.
- Stiffness proportional damping is used with the fraction of critical damping (ξ_{min}) of 2% (1% in terms of total damping) along with the input frequency (f_{min}) of 8 Hz. The model is critically damped using these parameters as shown by the plot of unbalanced force in Figure 5.51.
- Ground motions in terms of vertical and horizontal velocity time histories are given in Figures 5.51 through 5.55.
- Velocity time histories are recorded at three points (i.e., east, centre, and west) at each geological group.

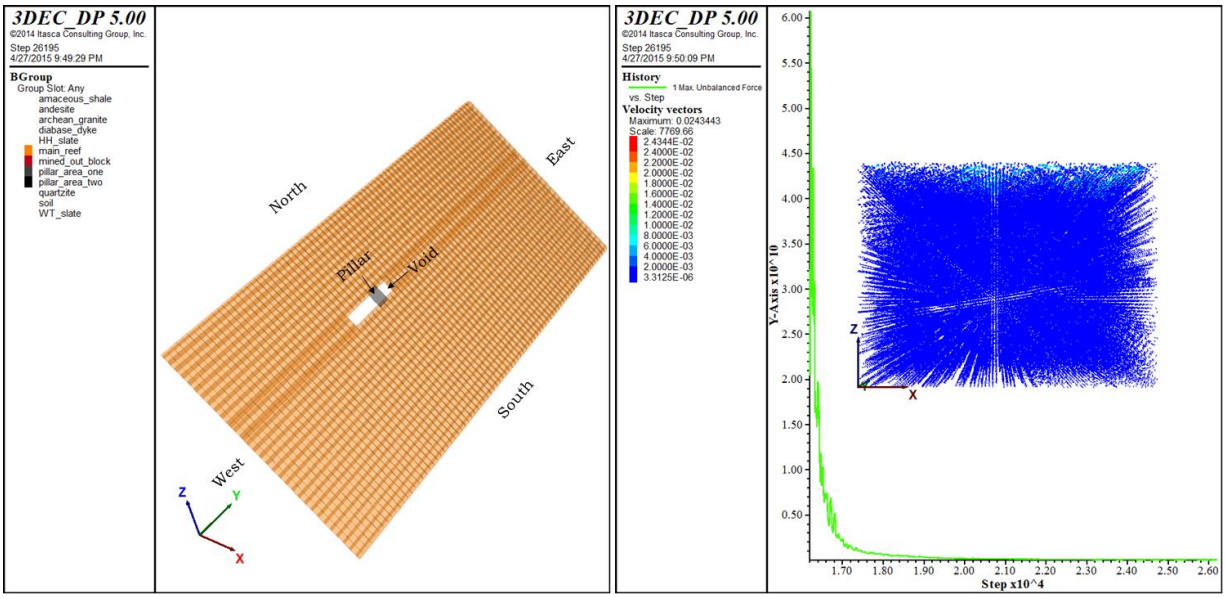


Figure 5.51 Plot on left shows excavated pillar, plot on right shows the model is critically damped

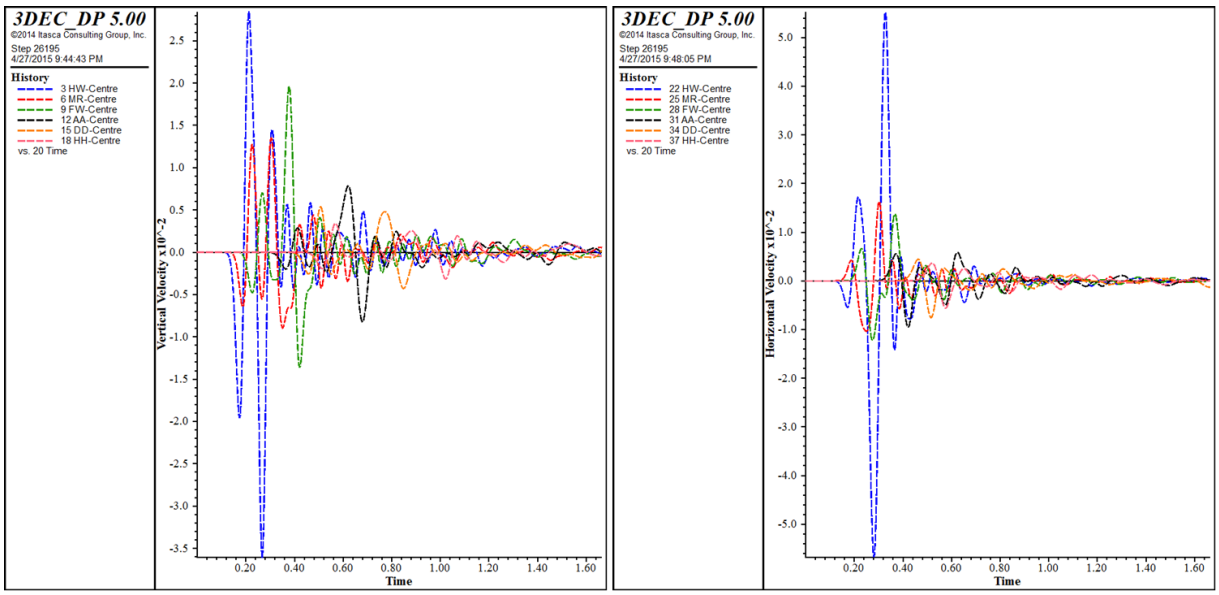


Figure 5.52 Left; vertical velocity histories, Right; horizontal velocity histories at the centre of each geological group

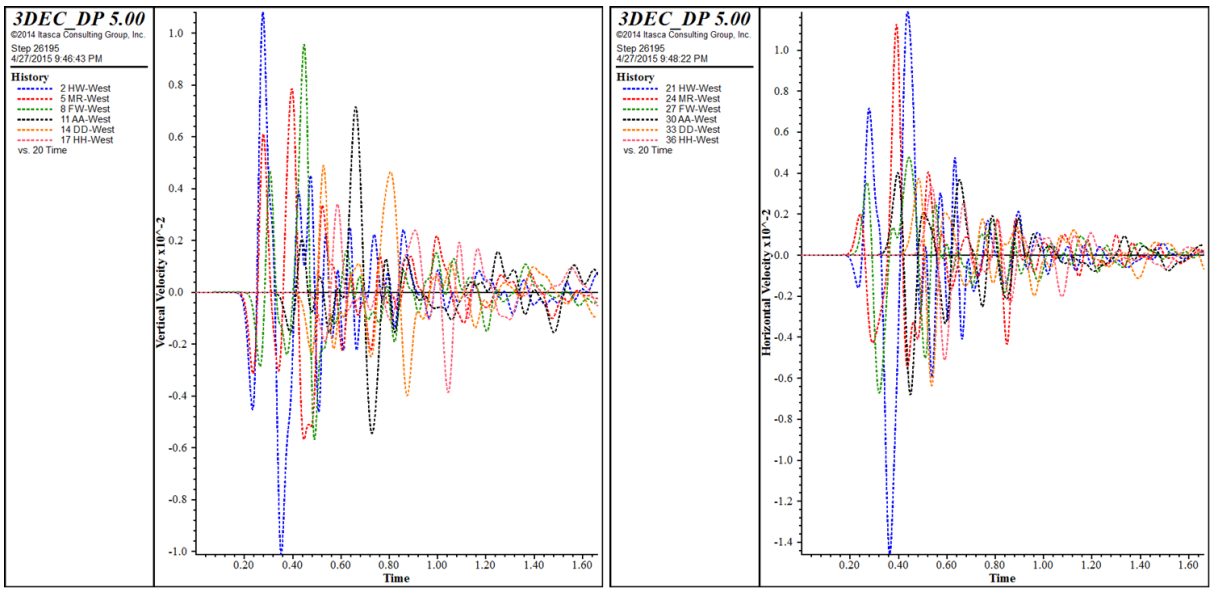


Figure 5.53 Left; vertical velocity histories, Right; horizontal velocity histories at the western edge of each geological group

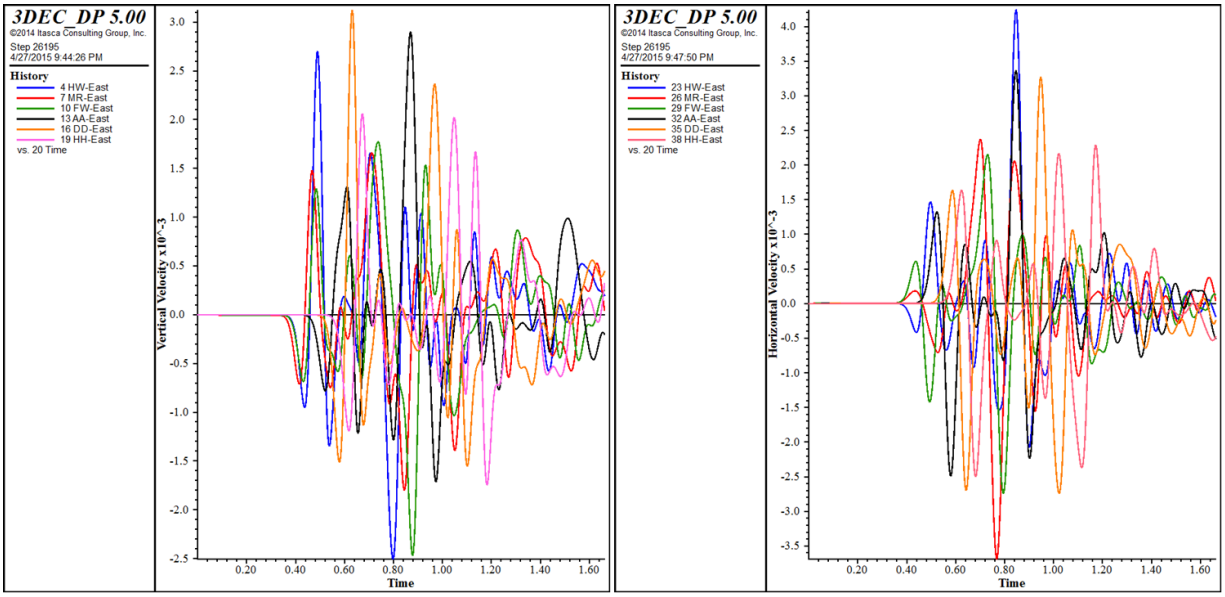


Figure 5.54 Left; vertical velocity histories, Right; horizontal velocity histories at the eastern edge of each geological group

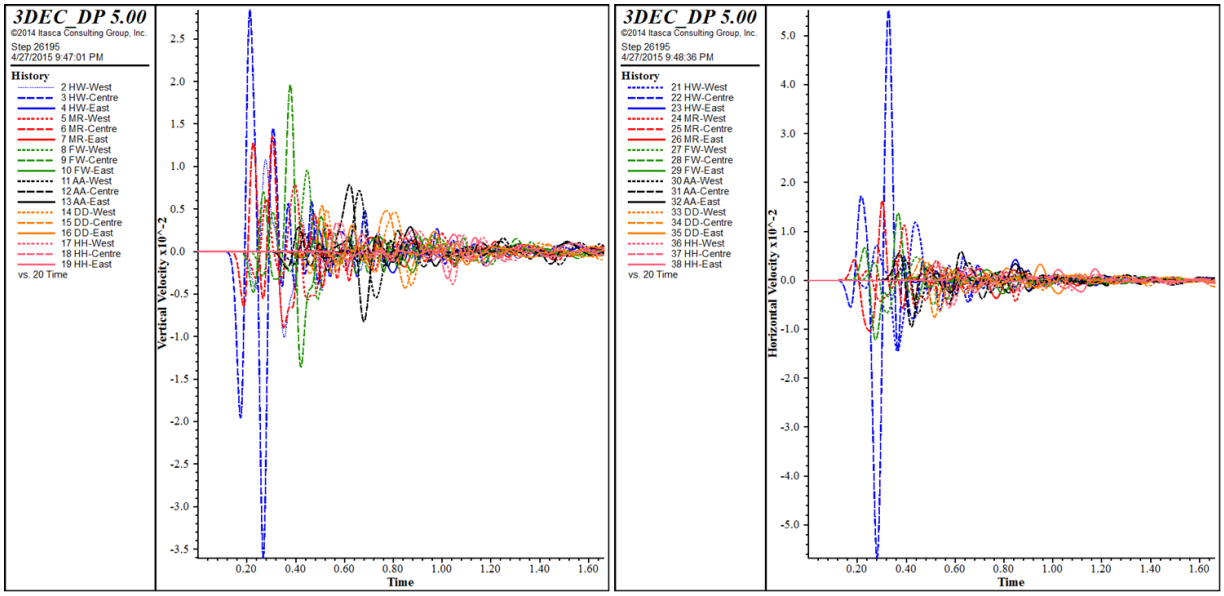


Figure 5.55 Left; all vertical velocity histories, Right; all horizontal velocity histories

5.13.5. Discussion on ground motions due to simultaneous collapse of a large number of pillars under dry conditions

A summary of ground motions due to simultaneous failure of large number of pillars under dry conditions is given in Table 5.7. For the purpose of comparison

and discussion, only the higher peak velocity (either of the positive or negative side) is tabulated.

Table 5.7 Ground motions due to collapse of mining voids under dry conditions

Location	East		Centre		West	
	Vertical mm/sec	Horizontal mm/sec	Vertical cm/sec	Horizontal cm/sec	Vertical cm/sec	Horizontal cm/sec
HW	2.70	4.0	3.6	5.3	1.10	1.41
MR	1.70	3.50	1.4	1.6	0.78	1.20
FW	2.50	2.50	**1.9**	**1.3**	**0.90**	**0.60**
AA	3.0	3.50	0.8	0.9	0.70	0.70
DD	3.10	3.30	0.5	0.6	0.44	0.60
HH	2.0	2.40	0.3	0.5	0.38	0.40
HW-Hanging Wall (Quartzite), MR-Main Reef (Conglomerate), FW-Foot Wall (Amaceous Shale), AA-Amygdaloidal Andesite, DD-Diabase Dyke, HH-Hospital Hill Slates						

- At the model scale, magnitudes of the ground motions (the term ground motions is used for describing velocity time histories) are a maximum at the centre followed by the west side and minimum on the east side.
- Amongst all the geological groups, the ground motions are most pronounced in HW followed by MR and FW.
- Within each geological group, ground motions are mostly larger at the centre than west and east sides.
- Within each geological group, ground motions are larger on the west side than the east side. This is due to the existence of a pillar and a void (Figure 5.51) in the path of the seismic waves travelling to the east side.
- A comparison between vertical and horizontal ground motions (Table 5.9) within each geological group reveals that horizontal ground motions are larger than the vertical except at the centre and west points of FW.
- Both vertical and horizontal ground motions in the HW start with the negative zone. This shows that the HW, in case of a seismic event at the Main Reef,

moves down relative to the rest of the model; this is analogous to the normal dip-slip phenomenon.

- In MR, FW the vertical ground motions start with the negative zone whereas horizontal ground motions start with positive zone. That means the ground motions are along the dip direction of the mine.
- The aspects described above suggest following:
  - For the seismic event to take place with a magnitude around 3 to 4 with ground motions around 5 cm/sec, a large number of pillars have to fail (or collapse of large number of voids).
  - The ground motions are highest in an area directly above the seismic source and reduce in magnitude in areas away from the source.
  - The existence of mining voids and pillars in the travelling path of seismic waves lowers the magnitude of ground motions. Therefore, the ground motions are relatively more pronounced in the areas in the north-south direction compared to the east-west direction.
  - At any given point in time during the seismic event, predominance of the type of ground motion (vertical or horizontal velocity) and mode of vibration (vertical or horizontal displacement) is different at different points in the model area.

5.13.6. Simulation for failure of large number of pillars in the flooded voids

- According to Itasca (2014), 3DEC considers fluid flow in the rock mass only through fractures and flow through rock mass itself is not considered.
- Regarding the representation of the effect of flooding along joints, the same restrictions apply as discussed in Paragraph 5.12.6.
- Ground motions due to the collapse of mining voids vary from few cm/sec to mm/sec and are given in Figures 5.56 through 5.60.

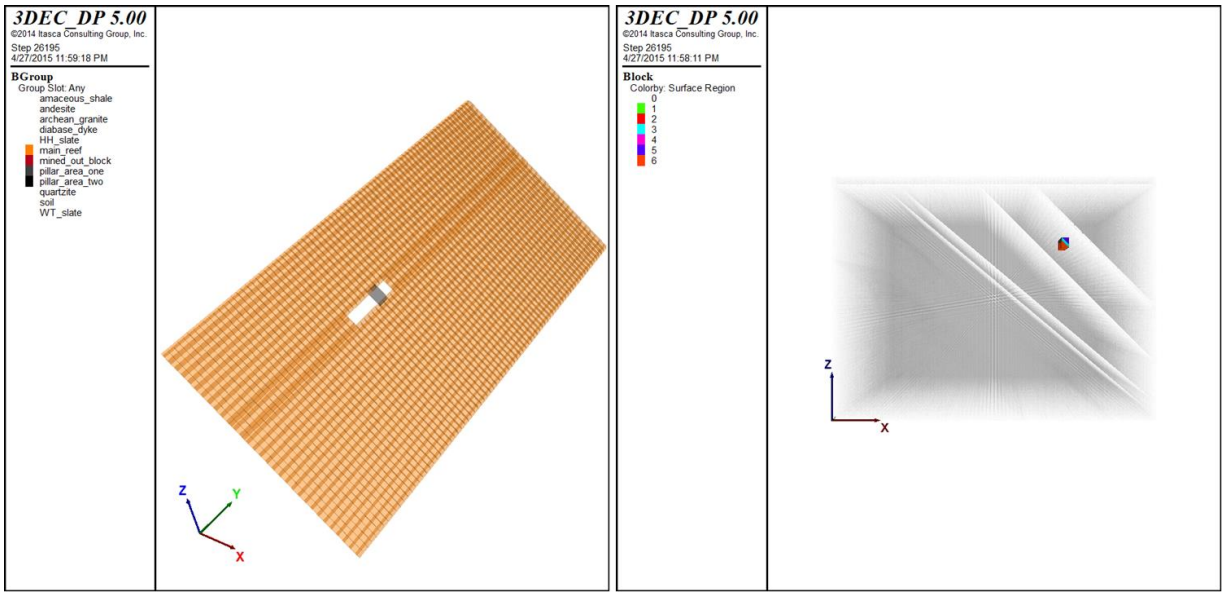


Figure 5.56 Left; one pillar excavated, Right; creation of six regions for setting boundary stress to represent effect of water filled voids

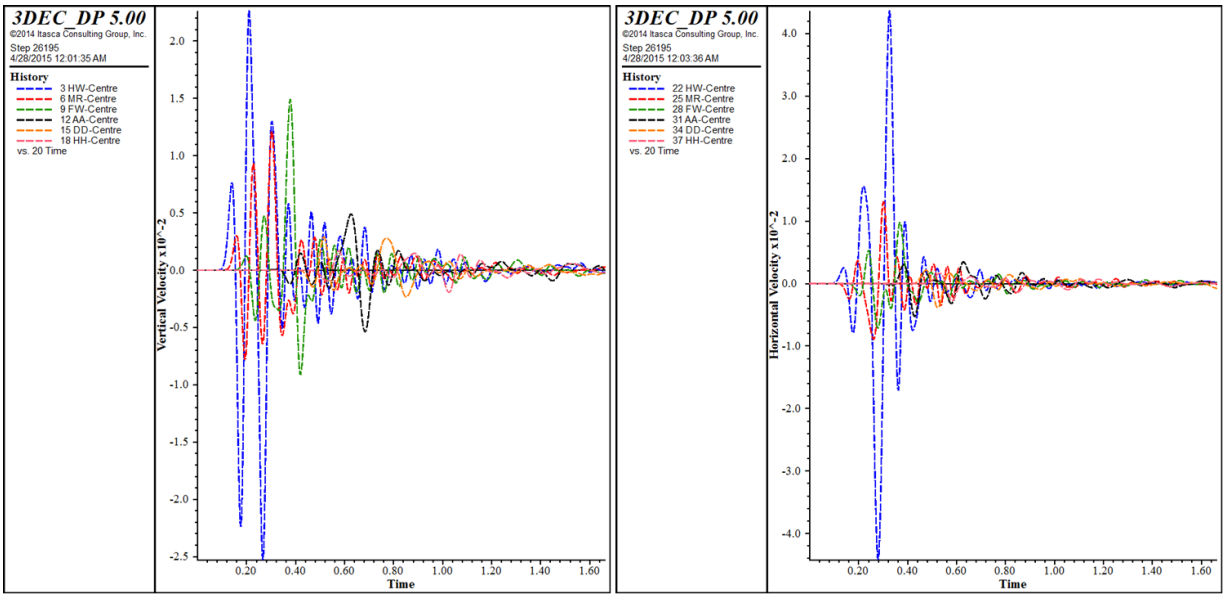


Figure 5.57 Left; vertical velocity histories, Right; horizontal velocity histories at the centre of each geological group

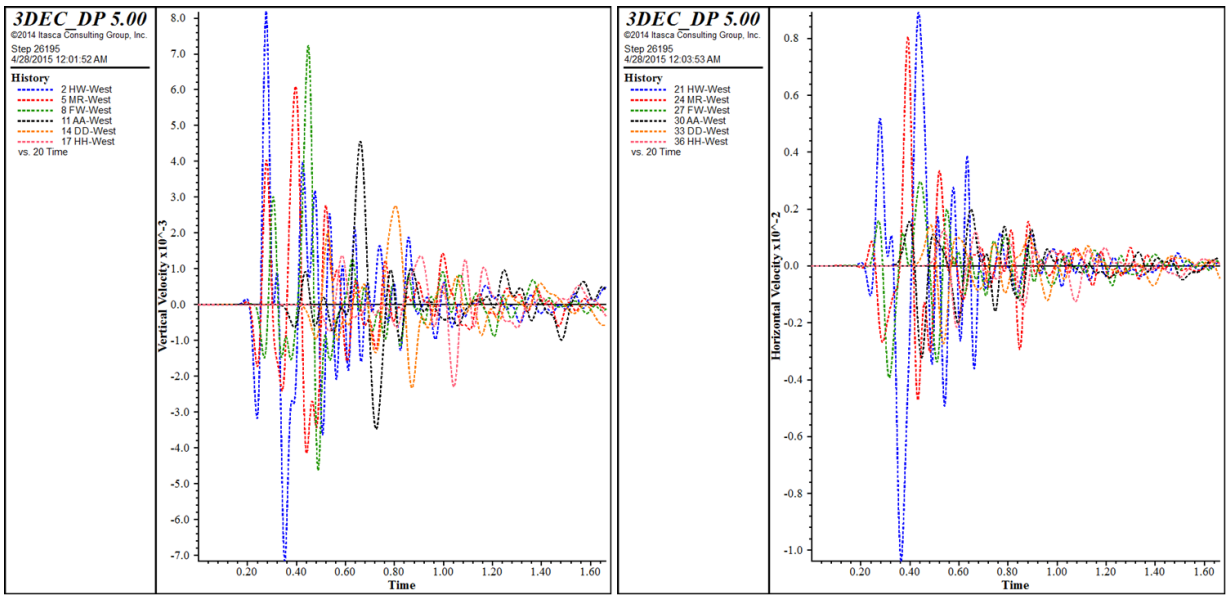


Figure 5.58 Left; vertical velocity histories, Right; horizontal velocity histories at the western edge of each geological group

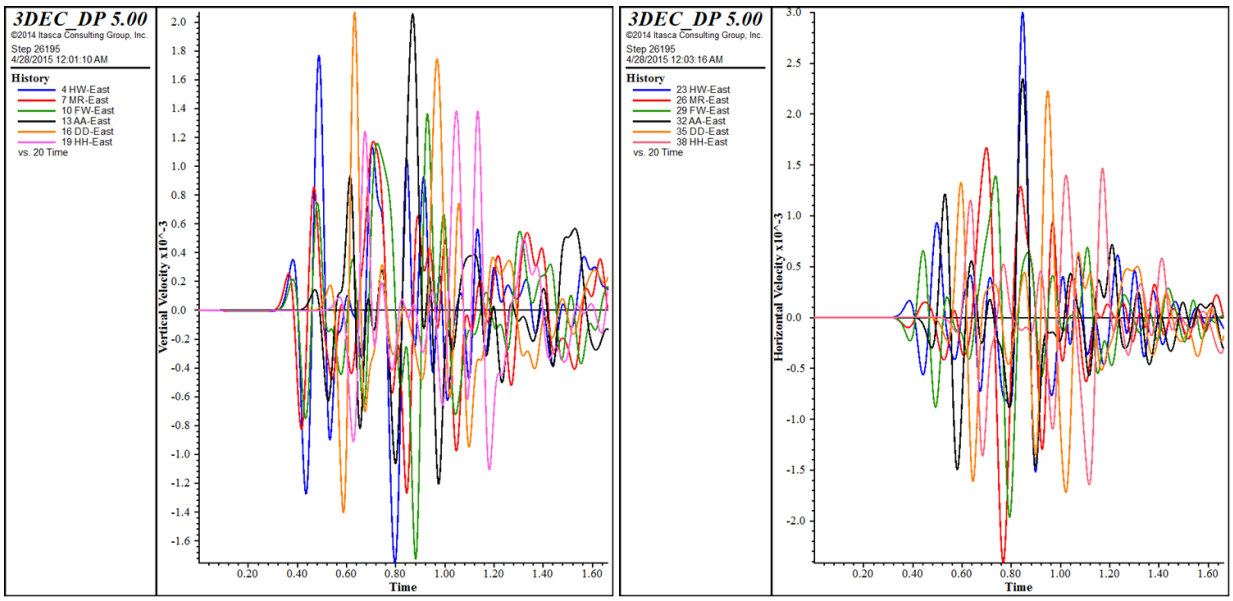


Figure 5.59 Left; vertical velocity histories, Right; horizontal velocity histories at the eastern edge of each geological group

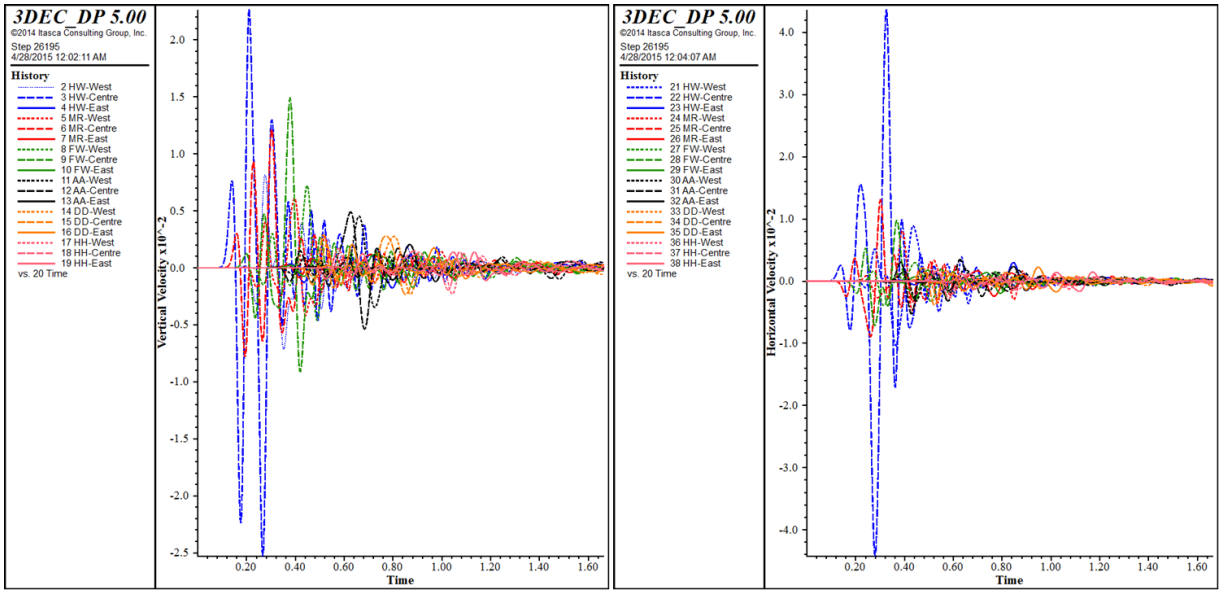


Figure 5.60 Left; all vertical velocity histories, Right; all horizontal velocity histories

5.13.7. Discussion on ground motions due to the simultaneous failure of large number of pillars under flooded conditions

A summary of ground motions due to the simultaneous failure of a large number of pillars under water filled void conditions is given in Table 4.8. For the purposes of comparison and discussion, only the higher peak velocity (either of the positive or negative side) is tabulated. The ground motion velocity time histories range from few cm/sec on the centre and west to mm/sec on the east side of the model.

Table 5.8 Ground motions due to collapse of mining voids under water filled void conditions

Location	East		Centre		West	
	Vertical mm/sec	Horizontal mm/sec	Vertical cm/sec	Horizontal cm/sec	Vertical mm/sec	Horizontal cm/sec
HW	1.78	3.0	2.55	4.20	8.0	1.0
MR	1.20	2.40	1.20	1.40	6.0	0.80
FW	1.68	1.90	1.50	1.0	7.40	0.40
AA	2.0	2.0	0.50	0.60	4.50	0.20
DD	2.15	2.20	0.30	0.40	3.0	0.18
HH	1.20	1.50	0.20	0.30	1.40	0.10

- At the model scale, magnitudes of the ground motions are a maximum at the centre followed by the west side and are a minimum on the east side.
- Amongst all the geological groups, ground motions are most pronounced in the HW followed by the MR and FW, except on the east of the FW (highlighted in Table 5.10).
- Within each geological group, ground motions are larger at the center than the points on the west and east sides.
- Within each geological group, ground motions are larger on the west side than the east side. This is due to the existence of a pillar and a void (Figure 5.51) in the path of seismic waves travelling to the east side.
- A comparison between vertical and horizontal ground motions (Table 5.10) within each geological group reveals that the horizontal ground motions are larger than the vertical ground motions.
- In flooded voids, the seismicity is different than in dry conditions in the following ways:
    - The magnitudes of both vertical and horizontal ground motions are lower in all geological groups and at all respective points at the centre, east and west sides. This suggests that voids completely filled with water act as some sort of support to the roof at the time of pillar failure. Thus the phenomenon of a pillar failure is likely to be less violent in abandoned mines filled with water.
    - Both vertical and horizontal ground motions in the HW start with a positive zone unlike dry conditions. This shows that the HW, in case of a seismic event under water filled conditions at the Main Reef, moves up relative to the rest of the model. This is analogous to a reverse dip-slip phenomenon.
- The aspects described above suggest following:
    - Although water in the excavations is likely to adversely affect the stability conditions and increase the possibility of the seismic event taking place, the magnitude of ground motions is likely to be smaller than in dry conditions.

- Similar to dry conditions, for seismic events of magnitude around 3 to 4 to take place with ground motions around 4 cm/sec, a large number of pillars have to fail (or collapse of a large number of voids).
- The ground motions are highest in the area directly above the seismic source and reduce in magnitude in areas away from the source.
- The existence of mining voids and pillars in the travelling path of seismic waves lowers the magnitude of ground motions. Therefore, the ground motions are relatively more pronounced in the areas in the north-south direction compared to east-west direction.
- At any given point in time during the seismic event, predominance of the type of ground motion (vertical or horizontal velocity) and mode of vibration (vertical or horizontal displacement) is different at different areas in the model area.

5.14. Summary of Findings of 3DEC Simulations for Ground Motions Common to All Scenarios

5.14.1. Applicability of 3DEC for estimating mining induced ground motions

- The 3DEC code developed by Itasca is capable of simulating mining induced seismicity due to the foreseeable causal factors such as Slip along a Fault/Discontinuity, Fall of Ground and, Pillar(s) Collapse.
- 3DEC allows modelling of complex geometry, geological structures and flooded conditions.
- 3DEC allows simulation of high-frequency waves typical of mining induced seismicity. Seismic waves with a frequency as high as 8 Hz are modelled with the mesh size of 50 m edge length. With a finer mesh, it is possible to simulate even higher frequencies but that would require much longer run time.
- 3DEC allows recording of ground motion histories at any point in the model which allows visualization of the ground behaviour at any point in the study area at a particular time during the mining induced seismic event.

5.14.2. Characteristics of the Estimated Ground Motions (Velocity Time Histories) Mining Induced Seismicity

- A summary of mining induced ground motions due to impulsive slip, fall of ground and pillar collapse are shown in Figure 5.61.
- Mining induced seismicity is characterized by high frequency and very short duration. A frequency of 8 Hz was observed which manifested in a complex waveform.
- In all three cases of source mechanism, the waveform with dynamic loading resembles a peak in the velocity history followed by a sudden drop in velocity at all history points, Figure 5.61.
- In all three cases, attenuation is very fast, the durations of seismic events are approximately equal and measure around 2 seconds.
- The frequency of seismic waves diminishes very rapidly, however, the low frequency component takes much longer to diminish.
- The modelled mining induced seismicity is comparable to explosive/impulsive loading.
- The amplitude of seismic waves is largest directly above the area of slip, fall of ground or mine collapse within the HW, MR and FW. In other areas, the variation in the ground motions is much less.
- Geometry and geological structures affect the nature and magnitude of ground vibrations.
- The size of the area of slip, rock fall, mine collapse (and number of collapsing mines) has a direct effect on the nature and magnitude of the ground vibrations.
- The results are used as a benchmark for the mining induced seismic characteristics of frequency, amplitude and duration.
- Waveforms estimated from numerical simulations can also be compared to the waveforms recorded from seismographs installed in the Central Rand to classify the type of source.
- Both Impulsive Slip and Fall of Ground source mechanisms, manifest with two components; the first component appears at the start of slip and first impact of a fall.

- The normal dip-slip phenomenon is also observed in this scenario.

5.14.3. Effects of flooding on mining induced seismicity

- Numerical modelling of the effects of flooding in abandoned mines highlighted that it affects geomechanics of the surrounding rocks, intensity of ground motions and transmission of seismic waves.
- The effects of flooding on the ground motions were studied and it was observed that flooding affects in the following ways:
  - Flooded voids induce vertical ground motions as well.
  - Ground motions (both vertical and horizontal) induced at the time of rock separation/detachment is negligible compared to those induced at the time of impact.
  - There are no repetitive impacts in the flooded voids.
- The frequency and duration of ground motions are larger in flooded voids than the dry voids.
- There are minor variations in the ground motions in dry and flooded conditions. It suggests that flooding has little effect on the intensity of seismic waves, however flooding does pose the potential to trigger a particular source.
- The peak velocity of the largest ground motion estimated under flooded conditions was 6.3 mm/sec (Figure 5.61). This was higher than the peak velocity of 5mm/sec (Figure 2.17) of existing seismic events of M_L 4, which was used for dynamic structural analysis. The dynamic structural analysis therefore simulated performance under existing and flooded conditions of abandoned mines.

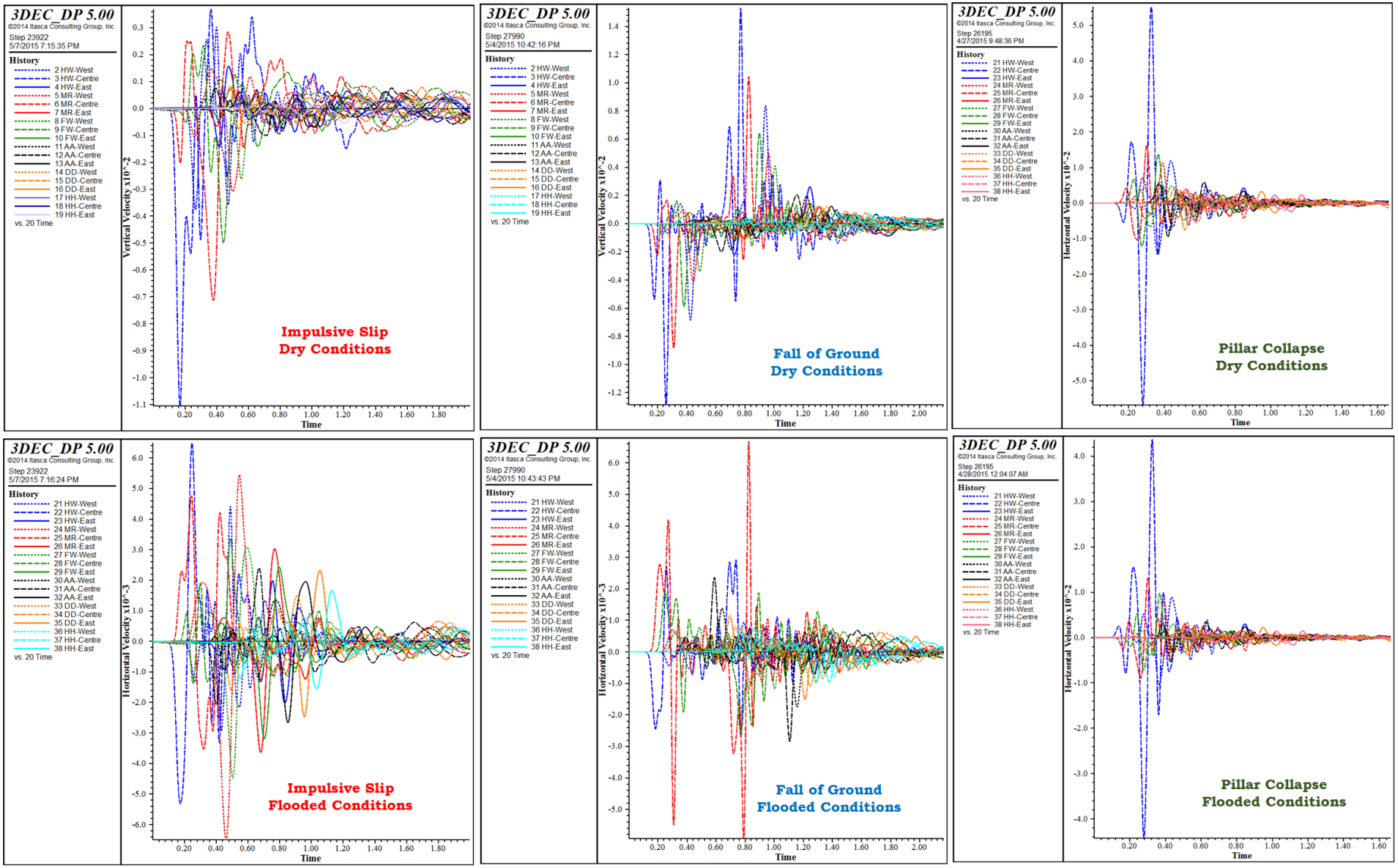


Figure 5.61 Plots of horizontal velocity histories under dry and flooded conditions in all the three scenarios; left-Impulsive Slip, centre-Fall of Ground, right-Pillar Collapse

5.15. Ground Motion Recommendations for Evaluation of effects on Surface Structures

With a view to evaluate the effects on surface structures, the ground motion – horizontal velocity time history at the centre point of the Main Reef is used for dynamic structural analysis. This ground motion corresponds with a magnitude M_L 3 to 4 (MMI of III to IV), Figure 2.17, USGS Shake Map. The recommended seismic parameters are given in Table 5.9.

Table 5.9 Seismic parameters for dynamic structural analysis

Parameter	Value
Duration of ground motion (t)	2.0 seconds
Frequency of ground motion (F)	8 to 10 Hz
Period of the ground motion (1/F)	0.1 to 1 sec
Peak Velocity (amplitude)	6.3 mm/sec

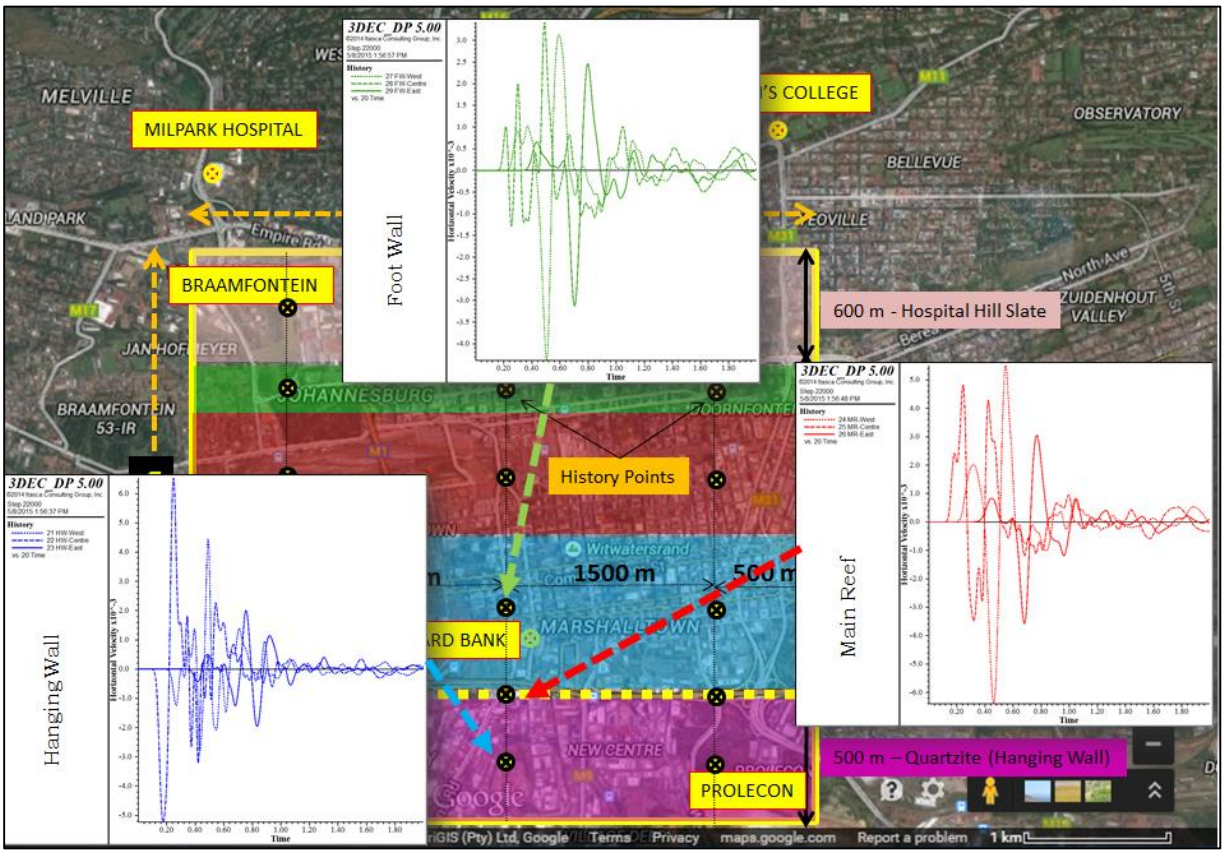


Figure 5.62 Ground motion recommendations for seismic structure analysis

5.16. Conclusion

The chapter discussed the necessity for evaluation of mining induced seismicity, geomechanical considerations, seismic considerations and numerical considerations. Numerical simulations were made for the three possible seismic scenarios; Impulsive Slip, Fall of Ground and Pillar Collapse. Results were tabulated and discussed. The outcome of this chapter is the ground motions in terms of the velocity time histories.

The next chapter evaluates effects of seismic ground motions evaluated in this chapter on selected typical surface structures. The structures considered include a masonry building, concrete framed buildings and a tailings dam. Evaluation of the stability of a jointed rock and soil slope is included in the next chapter. Finally, a risk assessment of the structures is also included.

6. EFFECTS OF MINING INDUCED SEISMICITY ON SURFACE STRUCTURES

6.1. Introduction

During recent mining induced seismicity, low rise buildings suffered most from the damage located in close vicinity of the earthquake sources, Durrheim et al. (2006). This chapter evaluates the effects of ground motions estimated using 3DEC (Chapter 5) on surface structures, shown in Figure 6.1, in the CBD area.

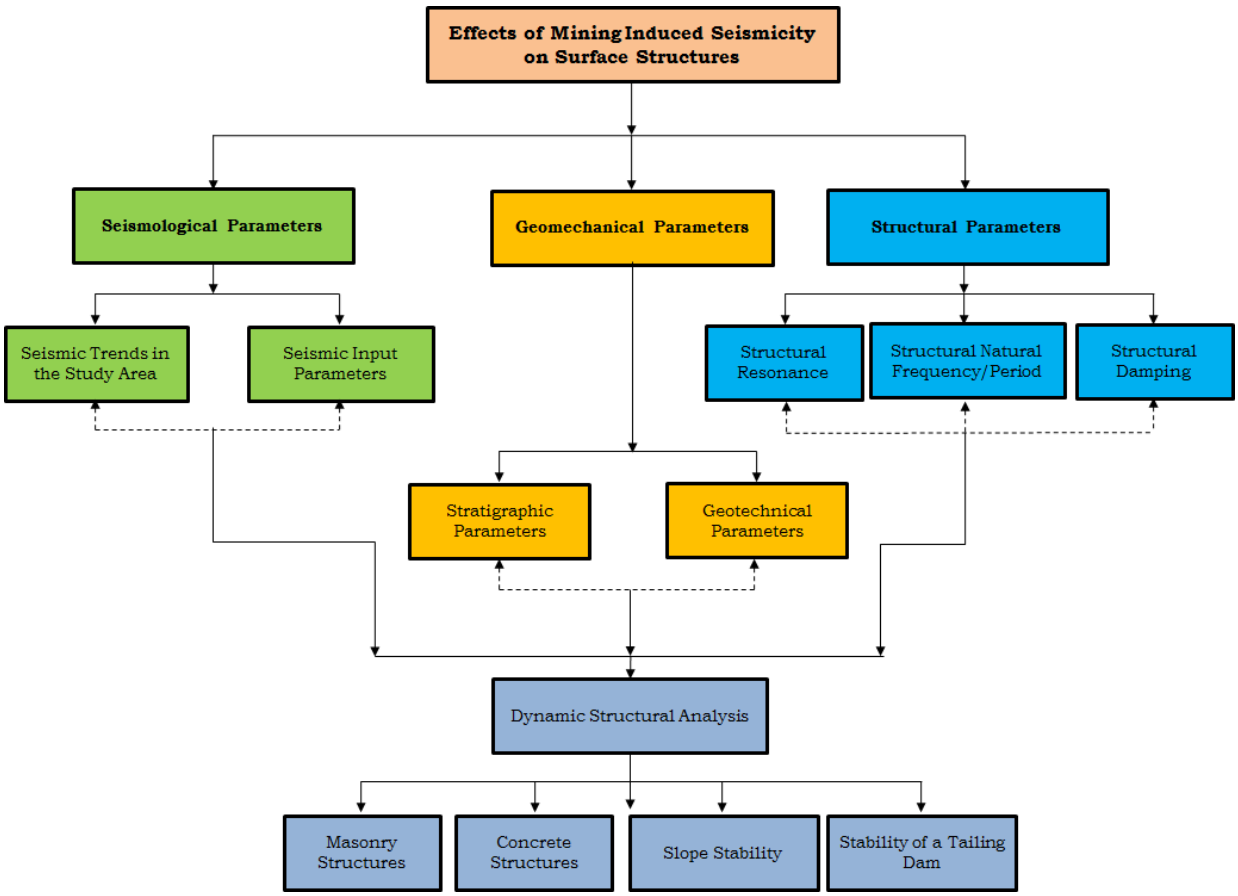


Figure 6.1 Considerations for evaluation of the effects of the mining induced seismicity on surface structures in CBD Area

6.2. Seismological Parameters

Unlike tectonic seismicity, mining induced seismic events are characterized by high frequencies, rapid attenuation and shorter duration. The high frequencies attenuate very rapidly and therefore their destructive power is minimized. The seismological parameters are briefly discussed under the headings of “seismic sources” and “input parameters”.

6.2.1. Seismic sources

The seismic sources affect the generation of seismic waveforms/ground motions. Ground motions generated due to Impulsive Slip and Fall of Ground are characterized by two distinctive peaks as shown in Figure 6.2. The first peak corresponds with the initiation of slip/first impact whereas the second peak depicts the later behaviour (slip and impact) of the sources. Ground motions due to pillar collapse are characterized by only one peak as shown in Figure 6.2.

6.2.2. Seismic input parameters

Ground motions estimated at centre points in the Hanging Wall, Main Reef and Foot Wall revealed a variation in the intensity of velocity time histories as shown in Figure 6.2. In view of the greater possibility of occurrence, ground motions are selected from Impulsive Slip for evaluating the effects on surface structures. In view of their more destructive effects, horizontal ground motions evaluated from "Impulsive Slip" at the centre of the Hanging Wall under flooded conditions are used for dynamic structural analysis, as shown in Figure 6.3.

The selected ground motion corresponds to Richter Magnitude of M_L 3 to 4 and Mercalli Intensity scale of IV, as shown in Figure 2.17, USGS Shake Map of Orkney Earthquake in 2014. Events of such magnitudes are felt by people and also result in the rocking of free standing objects. The seismic parameters are given in Table 6.1.

Table 6.1 Seismic parameters for dynamic structural analysis

Parameter	Value
Maximum amplitude of velocity	6.3 mm/sec
Frequency	7 to 12 Hz
Time Period	0.08 to 0.1 sec
Duration of input velocity histories	2 sec

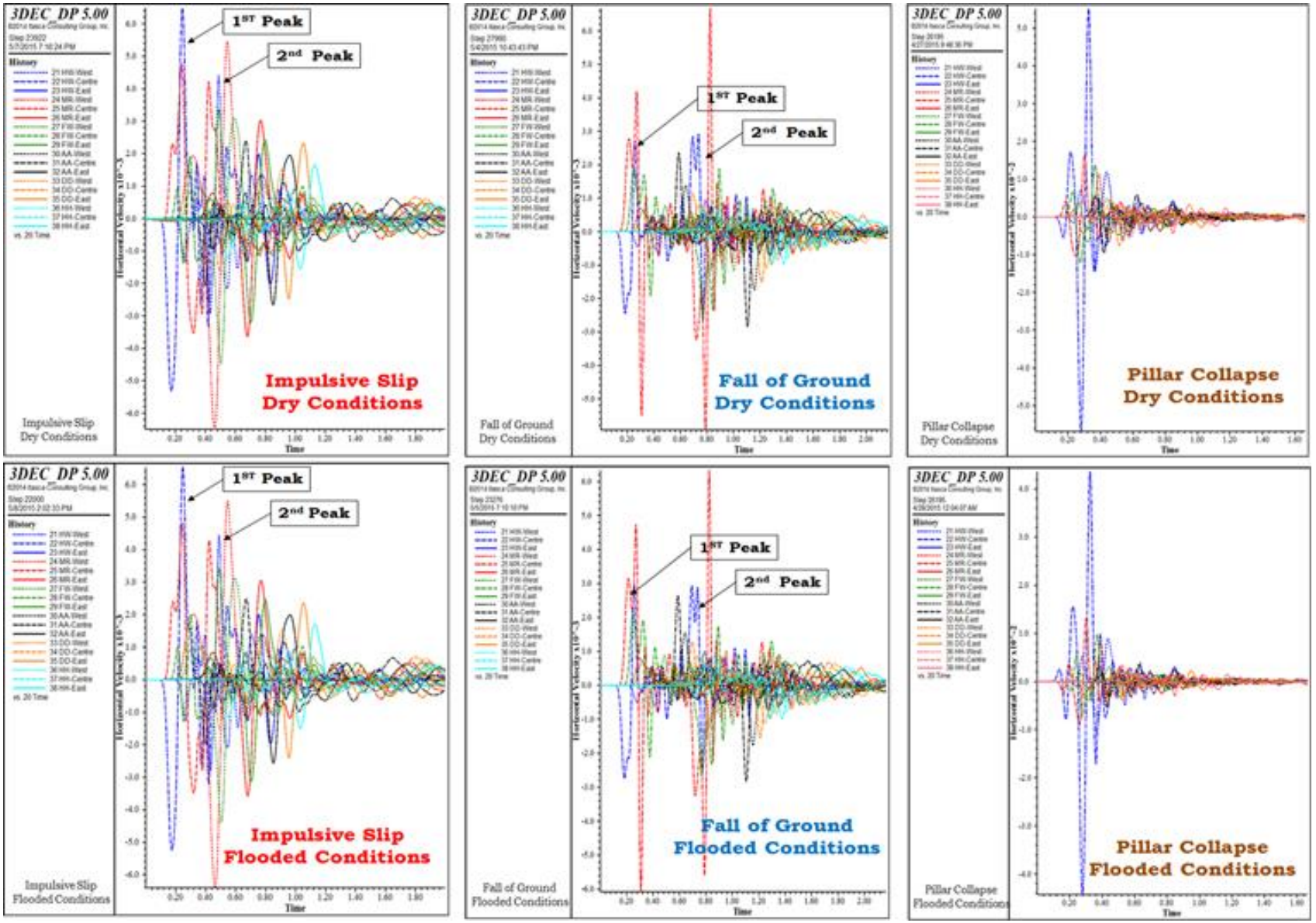


Figure 6.2 Ground motions in terms of horizontal velocity time histories in dry and flooded condition

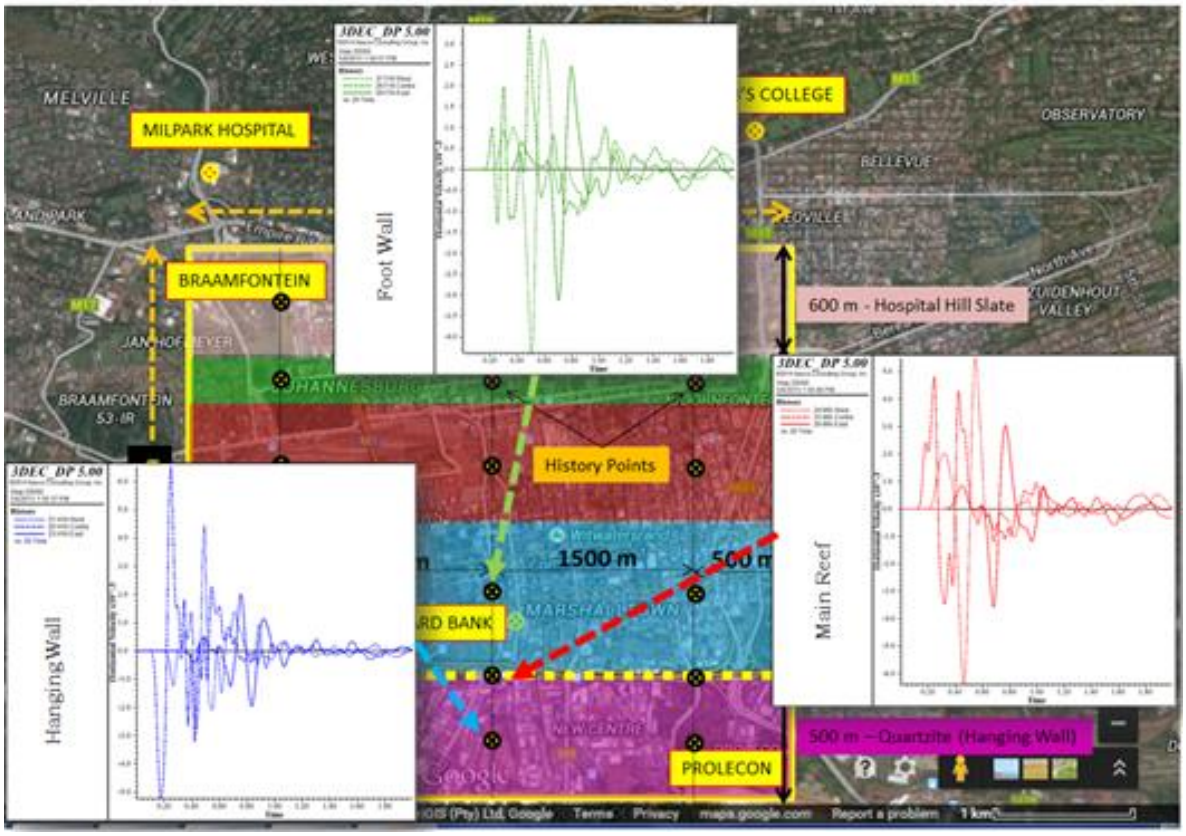


Figure 6.3 Ground motions estimated at Hanging Wall, Main Reef and Foot Wall

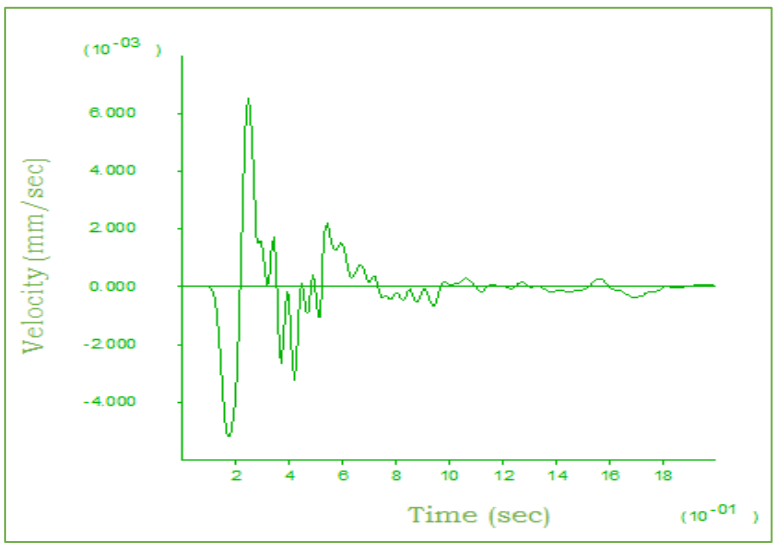


Figure 6.4 Ground motion (horizontal velocity time history) selected for dynamic structural analysis

6.3. Geomechanical Parameters

The evaluation of seismic effects on surface structures necessitates acquisition of geomechanical data comprising site specific mechanical and dynamic properties of the rocks and soils underlying the candidate structure. The seismic

input parameters are very important for evaluation of ground behaviour whereas mechanical parameters are important from the remedial viewpoints. The research site CBD Area is located close to the abandoned mines.

Static and dynamic mechanical properties of the foundation rock/soil affects the amplification/de-amplification of seismic waves during the course of propagation from the source to the site. Generally, soil layers which are moist and soft enhance the amplification (magnitude and duration). Seismic wave amplification is relatively more pronounced at longer periods and vice versa, Arnold (2013). The post Loma Prieta 1989 earthquake studies have shown an amplification of 3 to 6 times in areas where foundation soils comprised soft clays. Surface structures built close to the abandoned mines or constructed over soft pockets of fills and high water contents are likely to suffer larger damage unless the structures were built according to the site specific seismic design.

According to Krinitzsky et al. (1993), the strength and compressibility of rocks and clay soils are less affected during seismic loading/shaking (cyclic stresses and strains), however saturated cohesionless soils (sands) undergo loss in shear strength due to the development of positive pore pressures resulting in liquefaction and/or settlement. Therefore site specific geomechanical parameters (geology, stratigraphy, ground water conditions, index properties and dynamic properties) are very important to perform reliable seismic structural analysis. Since geomechanical parameters are different for each structural analysis, these are described separately for each structural analysis.

6.4. Structural Parameters

Structural parameters for the dynamic analysis include structural geometry (height, width, and length), type of material (masonry, concrete, steel, etc.) and type of foundation. Structural parameters of structures are listed separately for each type of structural analysis.

6.5. Dynamic Structural Analysis

In view of the diversity of structures and structural response to a single seismic event. The following structures are considered for dynamic analysis using advanced numerical codes:

- Dynamic analysis of a two storey masonry building founded on rock using 3DEC.
- Dynamic analysis of a two storey concrete building founded on rock using 3DEC.
- Dynamic analysis of a four storey concrete building founded on rock using 3DEC.
- Dynamic analysis of eight storey concrete building founded on rock using 3DEC.
- Dynamic analysis of a jointed rock slope with building load at the crest using 3DEC.
- Dynamic analysis of a tailings dam slope founded on soil for liquefaction potential using FLAC.
- Dynamic analysis of a soil slope for evaluation of stability using FLAC.
- Dynamic analysis for evaluation of slip potential of a rock block with confined joint using 3DEC.

For masonry and concrete structures, the dynamic analysis is performed with a view to estimate the drift (horizontal displacement) of surface structures. In civil engineering terminology, design drift is the maximum horizontal displacement a building can sustain without affecting its structural integrity and function. Dynamic analyses of two, four and eight storey concrete buildings are carried out to compare the horizontal displacement caused by dynamic loading of the selected mining induced ground motion. The rock and soil slope is analysed to evaluate the magnitude of shear displacement for assessing the stability under the selected ground motion. A tailings dam slope is analysed for evaluation of the soil deformation (displacement) to assess liquefaction potential. A rock block with a confined joint is analysed to evaluate the slip potential due to the selected ground motion. The following assumptions /considerations are made for the dynamic structural analysis:

- Depth of seismic source i.e., impulsive slip takes place at a depth of 600 m.
- The foundation materials (rock/soil) are considered elastic. For rock and soil, the dynamic properties are considered such that no plastic deformations are allowed.

- Joint properties (required by 3DEC code as input parameters) are considered such that no shear displacement is allowed along the joints.
- For dynamic analysis using 3DEC, dynamic loading is applied at the bedrock as shown in Figure 6.5.
- 3DEC dynamic analysis requires critical damping and frequency to be specified. A critical damping value of 2% and frequency of 8 Hz are used for all the analyses. For liquefaction analysis using FLAC, hysteric damping is also considered.
- Structural damping is not considered for dynamic rock (soil) structural analyses.

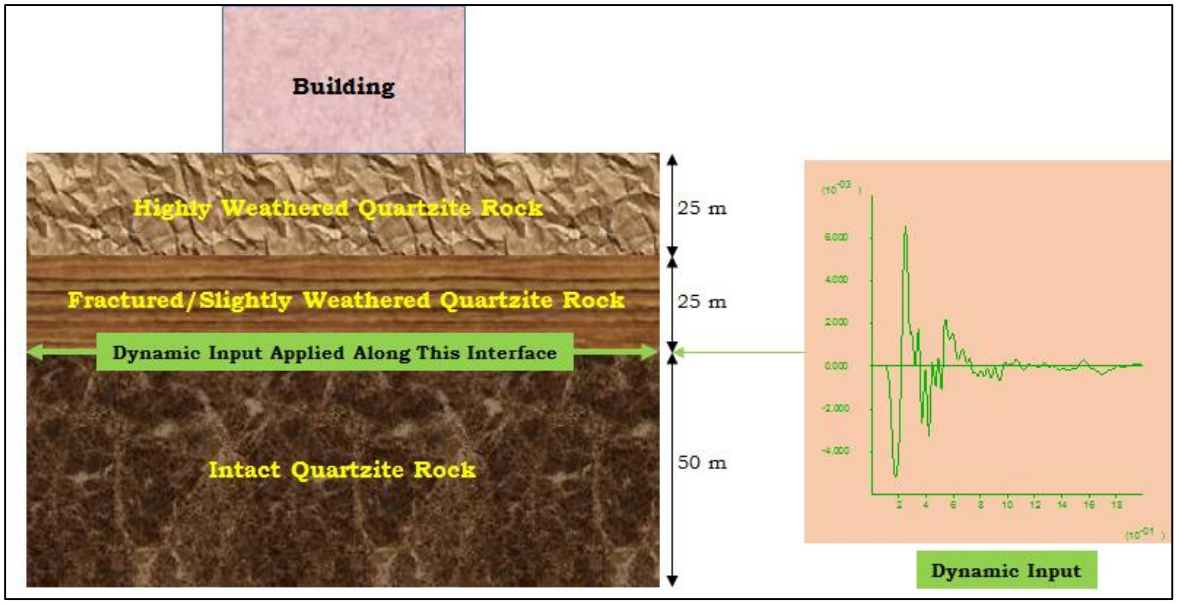


Figure 6.5 Dynamic application at the bedrock

- Structural response is estimated in terms of absolute displacement (displacement-vectors) and horizontal drift (x-displacement contours).
- Plots of displacement vectors (absolute/total magnitude) are aimed at visualizing the behaviour of the entire model at any given point in time i.e., every 0.5 sec interval.
- Plots of x-displacement contours (the horizontal displacement/drift) are aimed at visualizing the horizontal drift of the building at any given point in time i.e., every 0.5 sec interval.

- Positive displacements are considered in the eastward (right side of the model) and negative displacements are considered westward (left side of the model).
- In view of the large computational time involved in the analysis, structural response is monitored for a duration of 2 sec i.e., duration of the seismic ground motion considered for the structural analysis, at every 0.5 sec interval.

6.6. Dynamic Analysis of a Two Storey Masonry Building

From structural distress analysis viewpoints, high frequency components of seismic waves are not considered as these do not possess energy contents sufficient to cause structural damage. However, some researchers have argued that the damaging effects of high frequency seismic waves are important in stiff masonry structures. According to Patrick et al. (2007), high frequency waves affect stiff masonry structures in two ways:

- High frequency waves induce vertical inter-stone/brick vibrations manifesting in irreversible stone-to-stone displacements. After a certain duration, these irreversible relative displacements can trigger gravitational forces strong enough to cause collapse of masonry structures.
- Densification of soft/loose granular core of unreinforced masonry walls causes it to undergo an enhanced outward thrust. Seismic events with longer duration can cause collapse of masonry structures.

6.6.1. Model size, geometry and properties

The masonry building consists of two stories, as shown in Figure 6.6 and 6.7. Since it is not possible to include all construction details such as infill mortar, actual size of the bricks, etc., the building is built with rectangular blocks staggered in both horizontal and vertical extents. The dynamic material and joint properties considered for the blocks and joints are given in Tables 6.2 and 6.3 respectively. All concrete elements (foundation, door frames and window frames) have similar material properties.

Table 6.2 Material properties of two storey masonry building

Material	Density (kN/m^3)	Bulk Modulus (GPa)	Shear Modulus (GPa)
Brick blocks	2000	28	21
Concrete elements	2240	42	31
Highly weathered quartzite	2800	30	20
Weathered quartzite	3000	34	26

Table 6.3 Joint properties in two storey masonry building

Property	Weathered/ highly weathered rock	Highly weathered rock/foundation	Brick/brick brick/concrete
Joint Normal Stiffness (N/m)	5e10	5e10	5e10
Joint Shear Stiffness (N/m)	5e10	5e10	5e10
Joint Friction (degrees)	40	38	33
Joint Cohesion (Pa)	10e10	5e4	5e4
Joint Tensile Strength (Pa)	1e10	1e4	1e4

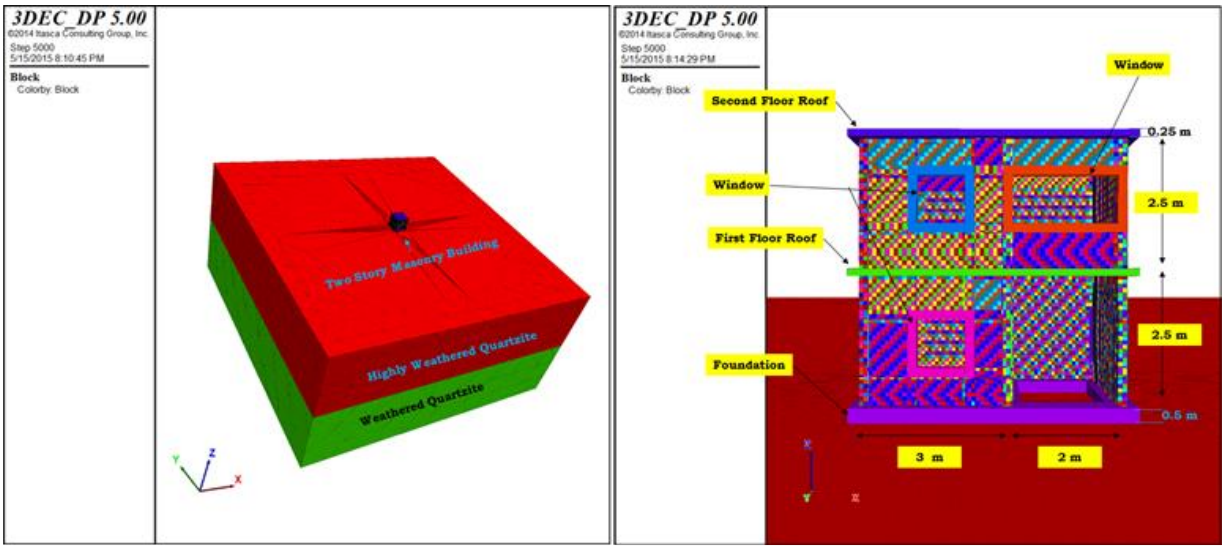


Figure 6.6 Model Geometry; left-foundation ground (quartzite rock), right-geometry and layout of two storey masonry building

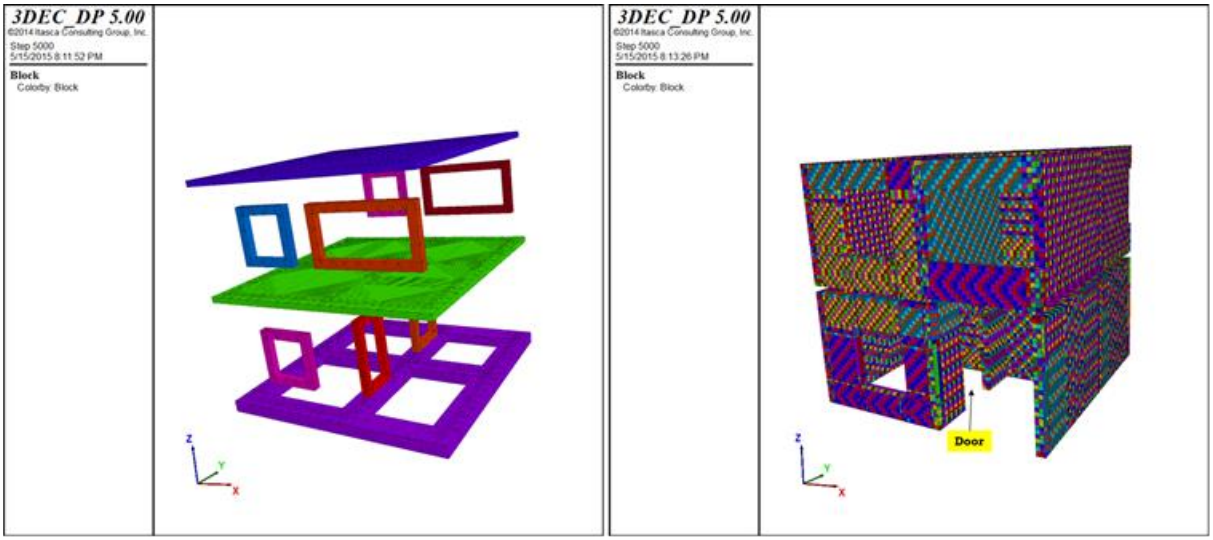


Figure 6.7 Model Geometry; left-concrete elements (foundation, windows, doors, roofs), right-geometry of brick walls of 1st and 2nd stories

6.6.2. Initial static equilibrium

Prior to running dynamic simulations, the model is run to establish static equilibrium under gravity. Plots of unbalanced fore and vertical displacement histories shown in Figure 6.8 indicate that the initial equilibrium is established.

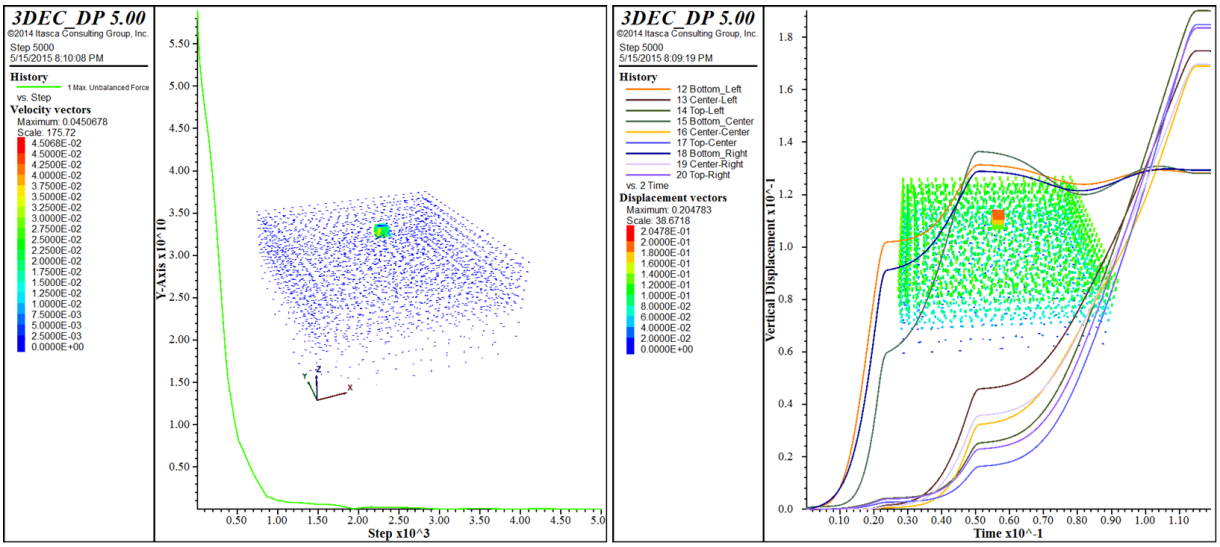


Figure 6.8 Initial equilibrium; left-plot of vertical velocity, right-plots vertical displacements

6.6.3. Dynamic simulations

The model is analyzed in four different simulations, recording displacements at a 0.5 sec interval. Plots of displacement vectors (absolute displacement

magnitude) and horizontal displacement contours at intervals of 0.5, 1.0, 1.5 and 2.0 sec are recorded and are shown in Figures 6.9 through 6.12. In each figure, the displacement vector plot on the left indicates the overall picture of the entire model whereas the plot of x-displacement on the right side of each figure indicates a closer view of the masonry building. Results of the simulations are described separately for each interval.

Plots of displacement at the end of dynamic loading for 0.5 sec are shown in Figure 6.9. The following observations are made:

- A total displacement of 11.85 mm is observed at the foundation level whereas the displacements in the building vary from 3 to 4 mm, Figure 6.9 (left).
- The displacement in the foundation (rock) is very small. The magnitude of x-displacement in the building varies from 0 to 3 mm.
- In some parts of the walls, x-displacement of 2 mm is observed. The front wall for 1st storey experiences the maximum horizontal displacement of 2 to 3 mm.
- Such phenomenon in masonry buildings manifests in shear cracks (diagonal/x-shape) in the walls especially around doors and windows.

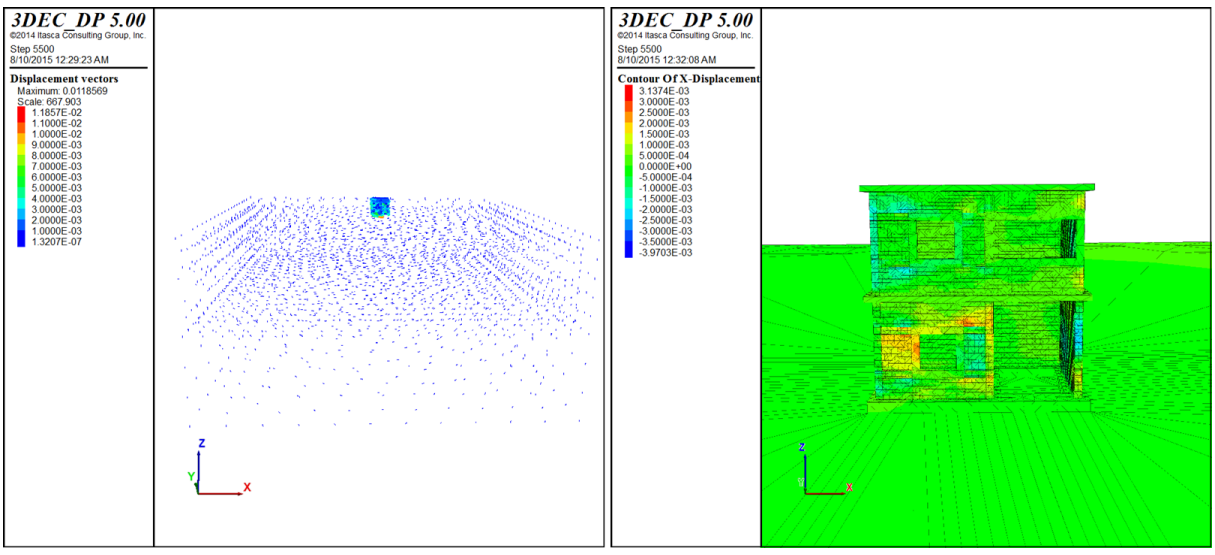


Figure 6.9 Horizontal displacement at T =0.5 sec

Plots of displacement at the end of dynamic loading for 1.0 sec are shown in Figure 6.10. The following observations are made:

- A total displacement of 25 mm is observed in the walls for 1st storey whereas the displacements in the rest of the building varies from 15 to 22 mm, Figure 6.10 (left).
- The displacements in the foundation (rock) are 2 to 5 mm and very small compared to the building.
- The 1st storey experiences more displacement. One of the wall in the 1st storey (having door within) undergoes a displacement of as high as 22.50 mm.
- The 2nd storey undergoes a horizontal displacement of as high as 7.5 mm.
- In both the 1st and 2nd storey, a horizontal displacement of 17.25 mm is also observed in the reverse (left side) direction.
- Such a phenomenon in masonry buildings manifests in shear cracks (diagonal/x-shape) in the walls especially around doors and windows (since the response of the building is highly dependent on the type of material, construction and quality, no specific correlation between shear displacement and cracking is specified for this research).

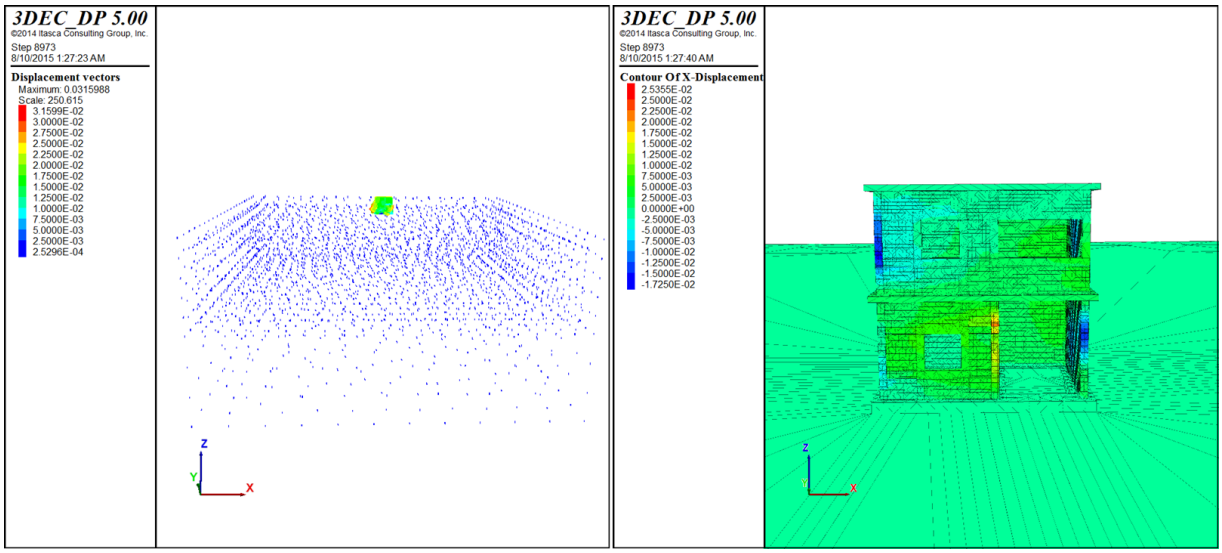


Figure 6.10 Horizontal displacement at T =1.0 sec

Plots of displacement at the end of dynamic loading for 1.50 sec are shown in Figure 6.11. The following observations are made:

- A total displacement of 53.65 mm is observed in the outer walls (left) and roof whereas the displacements in the rest of the building vary from 25 to 40 mm, Figure 6.11 (left).
- The foundation undergoes displacements varying from 5 to 10 mm.
- The displacements in the foundation (rock) are 0.17 to 5 mm and very small compared to the building.
- The 1st storey and some parts of the 2nd storey experience more displacement of up to 7.5 mm compared to rest of the building.
- One of the walls in the 1st storey (having a door within) undergoes a displacement of as high as 12.50 mm.
- The upper parts of the 2nd storey undergo horizontal displacement of as much as 2.5 mm in the reverse direction.
- Outer walls in both 1st and 2nd storey, experience horizontal displacement of 12.50 to 22.50 mm in the reverse direction.

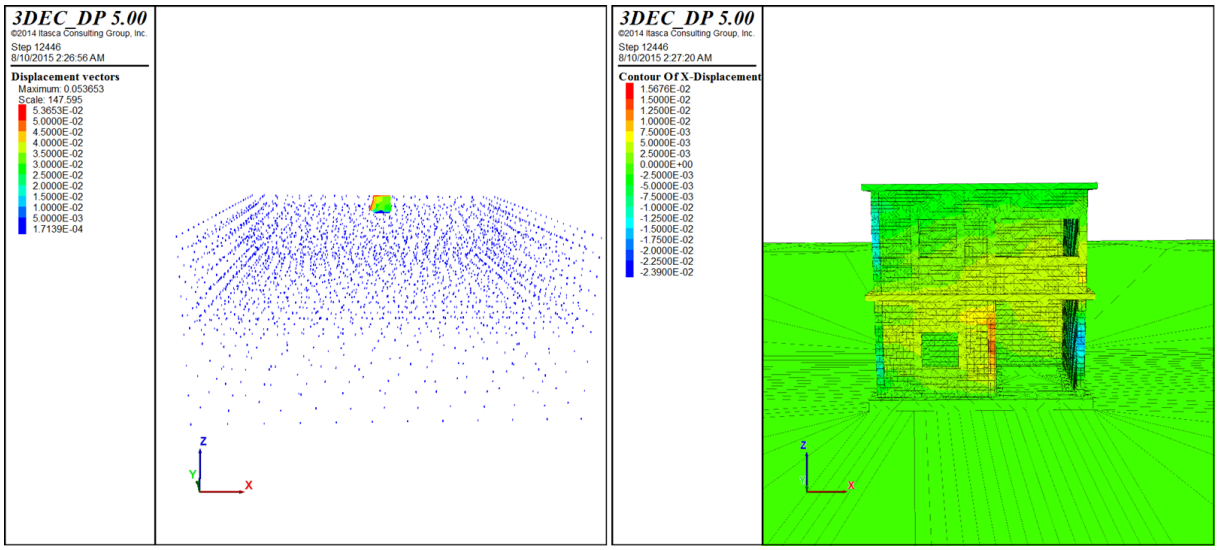


Figure 6.11 Horizontal displacement at T =1.5 sec

Plots of displacement at the end of dynamic loading for 2.0 sec are shown in Figure 6.12. The following observations are made:

- A total displacement of 53.00 mm is observed in the 2nd storey whereas the displacement in the 1st storey is around 35 mm, Figure 6.12 (left).

- The foundation undergoes displacements varying from 1.5 to 10 mm.
- The displacements in the foundation (rock) are 1.5 to 5 mm and small compared to the building.
- The 2nd storey experience more displacement than the 1st storey (Figure 6.12 (left)).
- From Figure 6.12 (right), it is observed that the upper of the 1st storey and lower part of the 2nd storey experienced more x-displacement (around 5 mm) than the rest of the building.
- Also, the x-displacements in the walls of 1st storey vary from 10 mm (positive) to 19.76 mm (negative).
- An outer wall of the 2nd storey undergoes a horizontal displacement of 5 mm in the reverse direction.

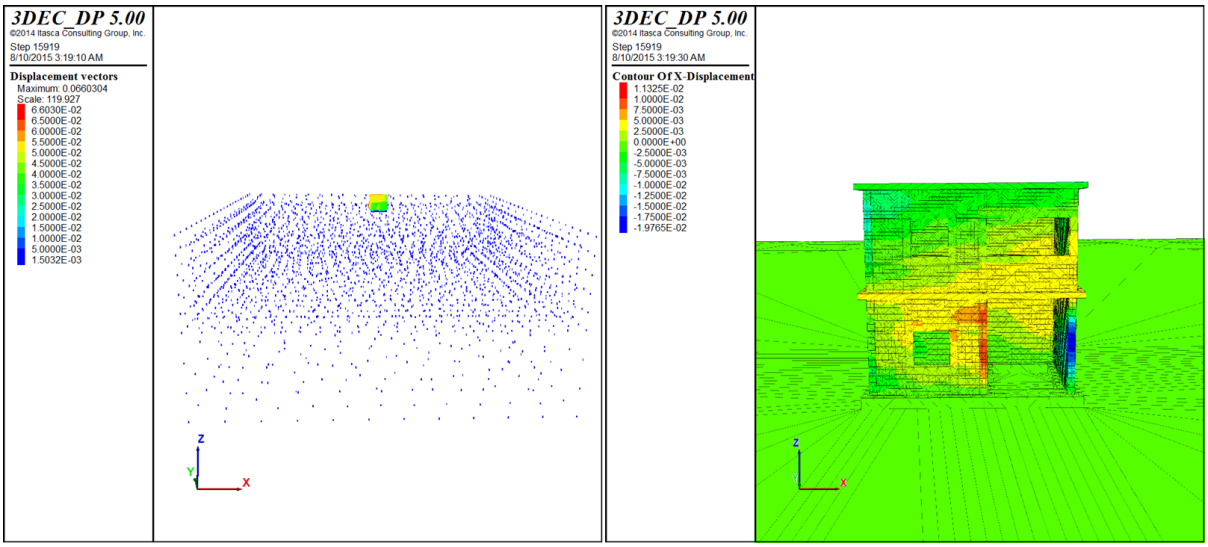


Figure 6.12 Horizontal displacement at T =2.0 sec

6.6.4. Comments on the response of the two storey masonry building

From the response of the masonry building to the selected ground motion, it is noted that the drift patterns are different for different points in the building (both in terms of direction and magnitude). The maximum x-displacement/horizontal drift (irrespective of the direction) at the end of the dynamic loading is given in Table 6.1.

From the displacement record shown in Table 6.4, it is observed that the response of the building is quite different at different points in time during the course of dynamic loading. This agrees with the typical behaviour of non-

monolithic structures such as masonry buildings during earthquake shaking. According to Itasca, (2014), during seismic loading, a significant portion of the deformation in masonry structures is accounted for by the relative motion between the masonry blocks. Since the model is considered to be elastic and it was not possible to numerically model the bricks in real sense, the displacements are considered to be conservative (towards higher side).

Table 6.4 Displacement record of two storey masonry building

Duration (sec)	Maximum Displacement (Total) (mm)			X-displacement (mm) (Horizontal Drift)	
	1st Storey	2nd Storey	Foundation	1st Storey	2nd Storey
0.5	4	4	12	3.13	2
1.0	25	25	5	15	17.5
1.5	53	53	10	20	15
2.0	75	53	10	19.76	12.5

6.7. Dynamic Analysis of a Two Storey Concrete Building

A 3D seismic analysis using 3DEC of a two storey concrete building was performed to evaluate its stability by monitoring the horizontal displacement during the dynamic simulation. The seismic/dynamic loading [evaluated for Hanging Wall (Quartzite Rock) in Chapter 5 and shown in Figures 6.3, 6.4 and 6.5 is used for the dynamic simulation. The building is considered to be located in the Hanging Wall area comprising highly weathered quartzite rock (50 m thick) underlain by fractured/slightly weathered rock (50 m thick) which overlies the intact quartzite bedrock. The analysis is performed in two stages; Stage-1 to bring the model to initial equilibrium under gravity and in Stage-2 the simulations are made at intervals of 0.50 sec each for a total duration of 2.0 sec.

6.7.1. Model size, geometry and properties

The model size and geometry are shown in Figure 6.13. The details of the foundation material are indicated in Figure 6.13 (left) and dimensions of the two storey concrete building are shown in Figure 6.13 (right). The assumed dynamic material properties (elastic) required for 3DEC analysis are given in Table 6.5. The joint properties required for 3DEC analysis are given in Table 6.6.

Table 6.5 Material properties of two storey concrete building

Property	Density (kN/m^3)	Bulk Modulus (MPa)	Shear Modulus (MPa)
Weathered quartzite rock	2800	34	26
Highly weathered quartzite rock	2500	30	20
Foundation	2240	42	31
Columns	2400	45	35
Roofs	2400	45	35

Table 6.6 Joint properties in two storey concrete building

Property	Weathered/highly weathered rock/foundation	Foundation/ column/roof
Joint Normal Stiffness (N/m)	10e10	2e11
Joint Shear Stiffness (N/m)	10e10	2e11
Joint Friction (degrees)	40	40
Joint Cohesion (Pa)	20e6	20e10
Joint Tensile Strength (Pa)	20e6	20e10

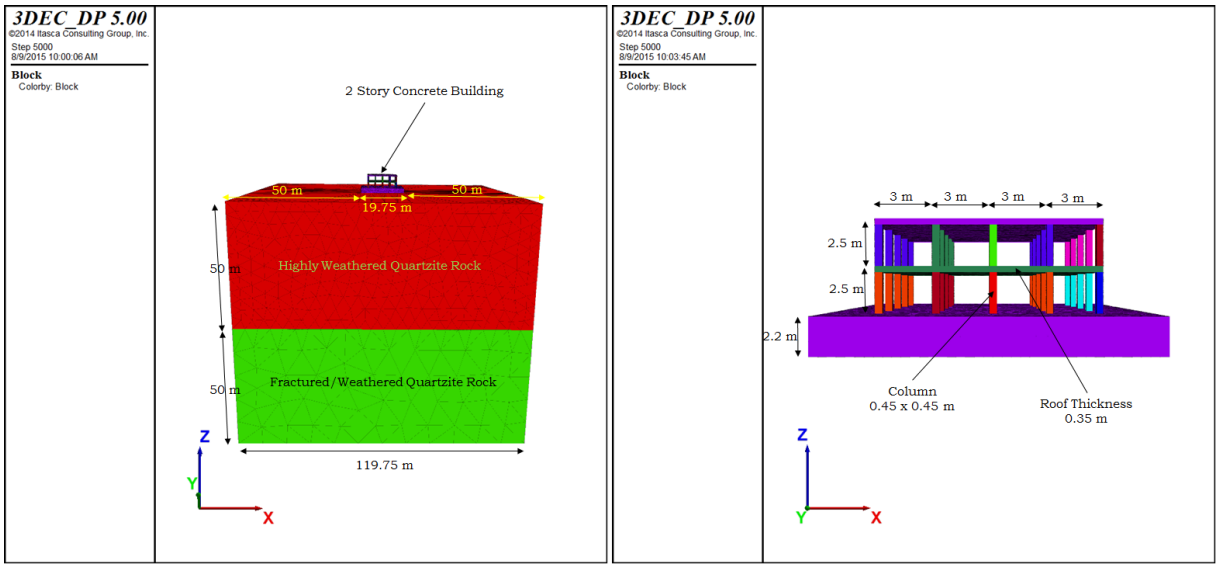


Figure 6.13 Model size and geometry of two storey concrete building

6.7.2. Initial static equilibrium

Prior to running dynamic simulations, the model is run to establish static equilibrium conditions under gravity. The plot of unbalanced force in Figure 6.14 (left) shows that the model reached equilibrium in 5000 steps. The plots of vertical velocity histories in Figure 6.14 (right) and vertical displacement histories in Figure 6.15 (left) also indicate that initial equilibrium is established. Contours of x-displacement in Figure 6.15 (right) indicate very small displacements.

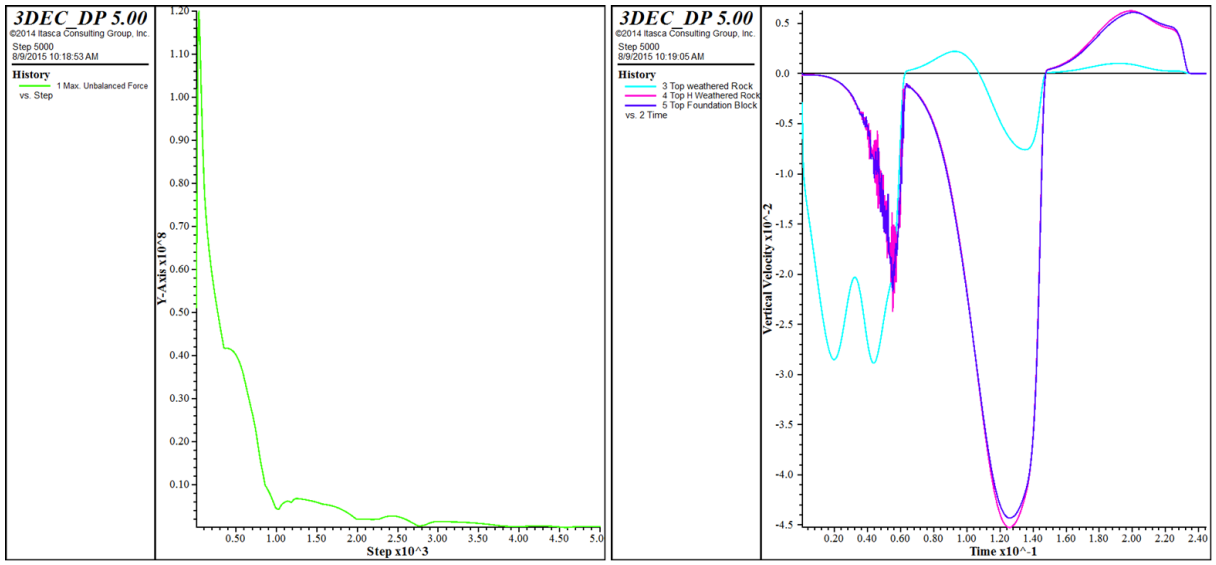


Figure 6.14 Plot of unbalanced force (left) and vertical velocity histories (right)

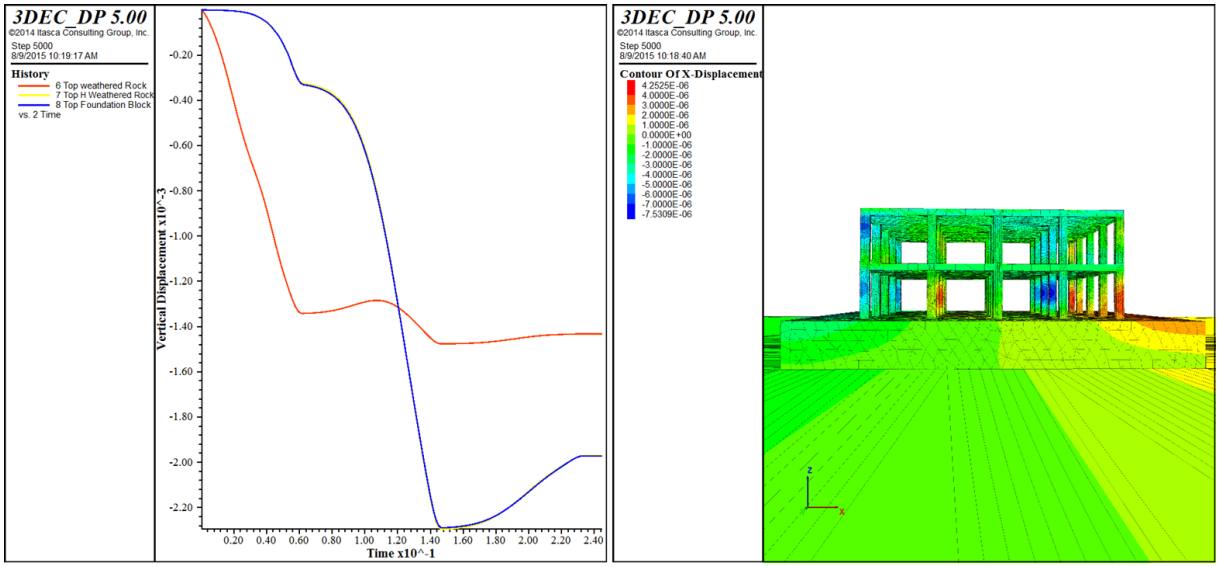


Figure 6.15 Plot of vertical displacement histories (left) and contour of horizontal displacement (right)

6.7.3. Dynamic simulations

The model is again analyzed in four different simulations and recording displacements at a 0.5 sec interval. Plots of displacement vectors (absolute displacement magnitude) and horizontal displacement contours at intervals of 0.5, 1.0, 1.5 and 2.0 sec are recorded and shown in Figures 6.16 through 6.19. In each figure, the displacement vector plot on left indicates the overall picture of the entire model whereas the plot of x-displacement on right side of each figure indicates a closer view of the concrete building. Results of the simulations are described separately for each interval.

Plots of displacement at the end of dynamic loading for 0.5 sec are shown in Figure 6.16. The following observations are made:

- A total displacement of 1.59 mm is observed in the lower part of the weathered quartzite.
- Displacements in the rest of the model i.e., highly weathered rock, foundation and building are less than 1 mm, Figure 6.16 (left).
- X-displacements in the building are negligible, Figure 6.16 (right).

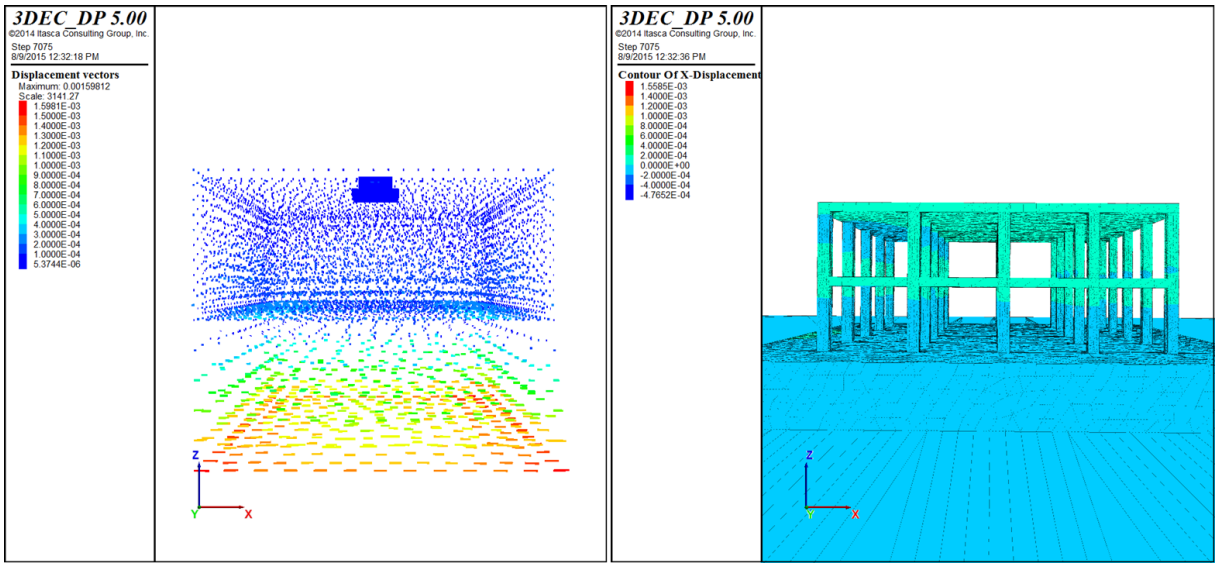


Figure 6.16 Horizontal displacement at T =0.5 sec

Plots of displacement at the end of dynamic loading for 1.0 sec are shown in Figure 6.17. The following observations are made:

- A total displacement of 0.9 mm is observed in the lower part of the weathered quartzite, displacements of 0.3 mm are noted in the highly weathered rock, Figure 6.17 (left).
- Displacements in the foundation and building are negligible.
- X-displacements in the building are negligible i.e., 0.1 mm, Figure 6.17 (right).

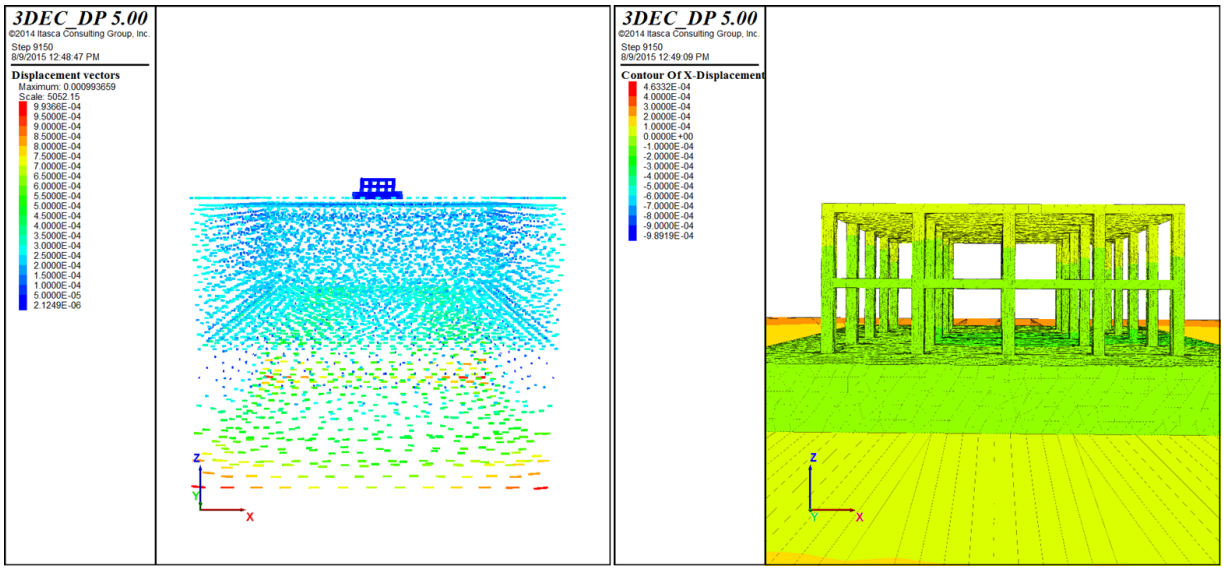


Figure 6.17 Horizontal displacement at T =1.0 sec

Plots of displacement at the end of the dynamic loading for 1.50 sec are shown in Figure 6.18. The following observations are made:

- A total displacement of 1.25 mm is observed in the lower part of the weathered quartzite, displacements of 0.8 mm are noted in the highly weathered rock, Figure 6.18 (left).
- Displacement in the foundation is 0.6 mm whereas displacement in the building is negligible, Figure 6.18 (right).
- X-displacements in the walls of the 1st storey are 0.4 mm whereas displacement in the 2nd storey are negligible, Figure 6.18 (right).

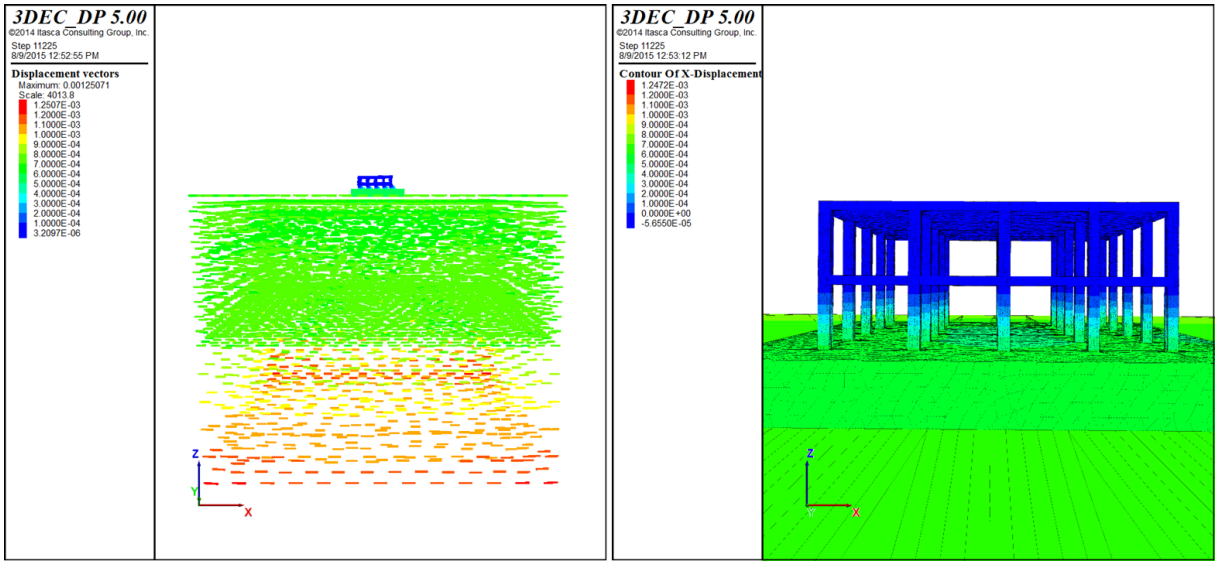


Figure 6.18 Horizontal displacement at T =1.50 sec

Plots of displacement at the end of dynamic loading for 2.0 sec are shown in Figure 6.19. The following observations are made:

- A total displacement of 1.57 mm is observed in the weathered quartzite layer. The highly weathered rock layer experiences a displacement of 1.40 mm, Figure 6.18 (left).
- Displacements in the foundation, 1st storey and 2nd storey are 1.30 mm, 1.0 mm and 0.20 mm respectively, Figure 6.18 (right).
- X-displacements in the walls of 1st storey varies from 1 to 1.30 mm. Maximum x-displacement in the 2nd storey is 0.9 mm, Figure 6.18 (right).

6.8. Comments on the dynamic response of two storey concrete building

The response of a two storey concrete building to the selected ground motion reveals varying drift patterns at different points in the building (both in terms of direction and magnitude). The maximum x-displacement/horizontal drift (irrespective of the direction) at the end of the dynamic loading is given in Table 6.7. Maximum x-displacement (drift) of 1.30 mm is observed in the two storey building.

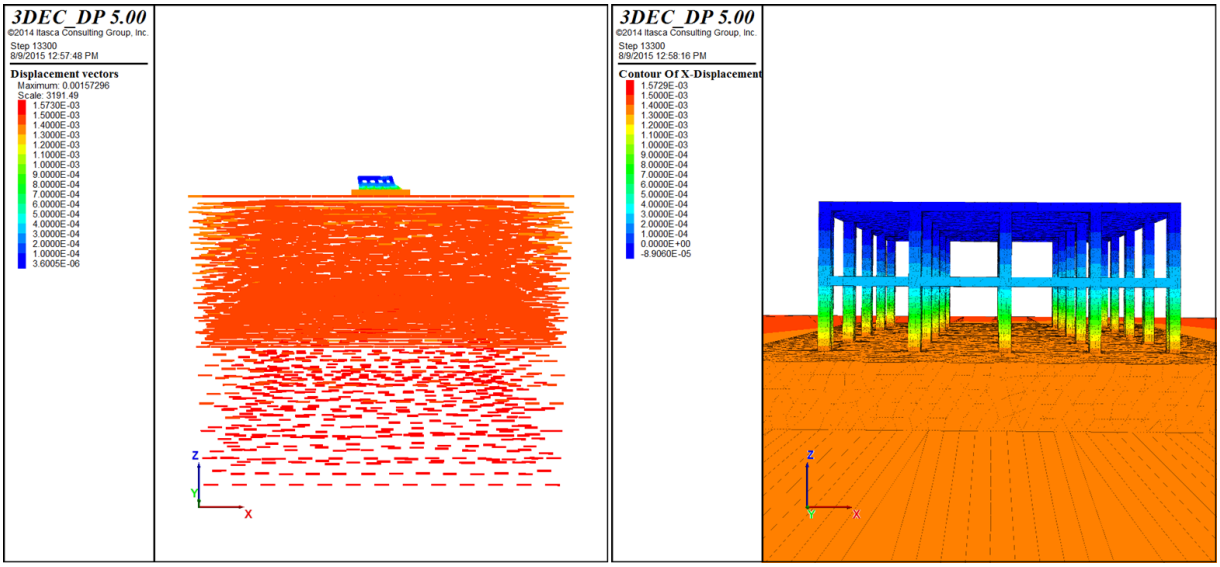


Figure 6.19 Horizontal displacement at T =2.0 sec

Table 6.7 Displacement record of two storey concrete building

Duration (sec)	Maximum Displacement (Total) (mm)			X-displacement (mm) (Horizontal Drift)	
	1st Storey	2nd Storey	Foundation	1st Storey	2nd Storey
0.5	0.10	0.10	0.10	0	0.20
1.0	0.05	0.05	0.30	0.20	0.10
1.5	0.80	0.10	0.80	0.40	0.10
2.0	0.90	0.10	1.30	1.30	0

6.9. Dynamic Analysis of a Four Storey Concrete Building

A 3D dynamic analysis of a four storey concrete building using 3DEC is performed to evaluate its stability by monitoring the horizontal displacement during the dynamic simulation. The dynamic loading [evaluated for Hanging Wall (Quartzite Rock) in Chapter 5 and shown in Figure 6.4/6.5] is used for the dynamic simulation. The analysis is performed in two stages; Stage-1 to bring the model under initial equilibrium under gravity and in Stage-2, the simulations are made at intervals of 0.50 sec each for a total duration of 2.0 sec.

6.9.1. Model size, geometry and properties

The model size and geometry are shown in Figure 6.20. The details of the foundation material are indicated in Figure 6.20 (left) and dimensions of the four storey concrete building are shown in Figure 6.20 (right). The assumed material properties (elastic) and joint properties are same to those considered for the two storey concrete building.

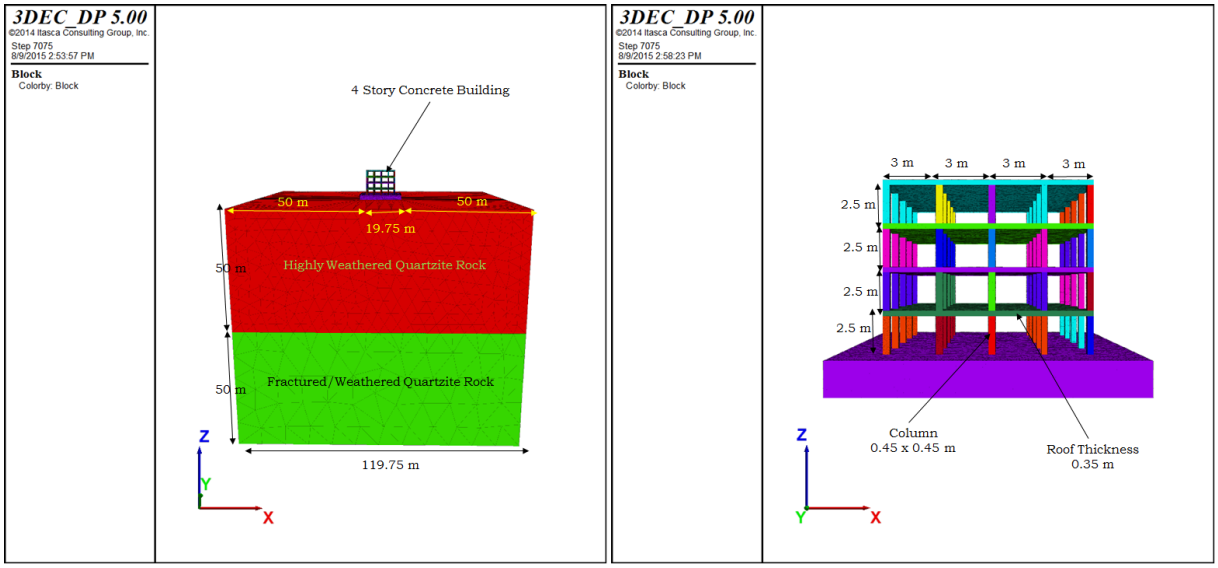


Figure 6.20 Model size and geometry of four storey concrete building

6.9.2. Initial static equilibrium

Prior to running dynamic simulations, the model is run to establish static equilibrium conditions under gravity. The plot of unbalanced force in Figure 6.21 (left) shows that the model reached equilibrium in 5000 steps. The plots of vertical velocity histories in Figure 6.21 (right) and vertical displacement histories in Figure 6.22 (left) also indicate that initial equilibrium is established. Contours of x-displacement in Figure 6.22 (right) indicate very small displacements.

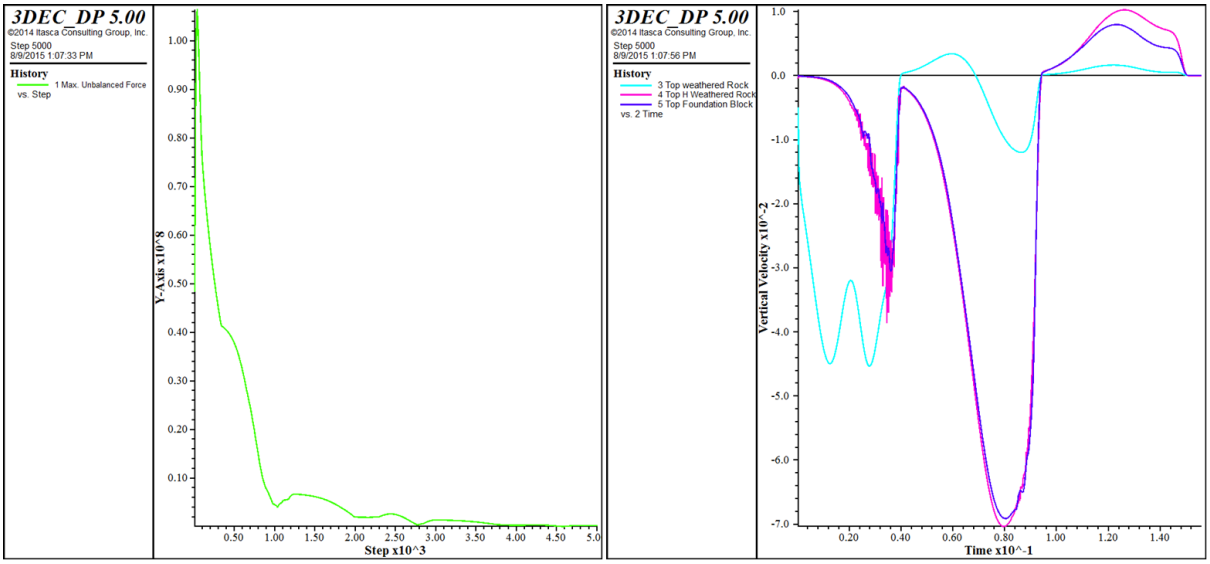


Figure 6.21 Plot of unbalanced force (left) and vertical velocity histories (right)

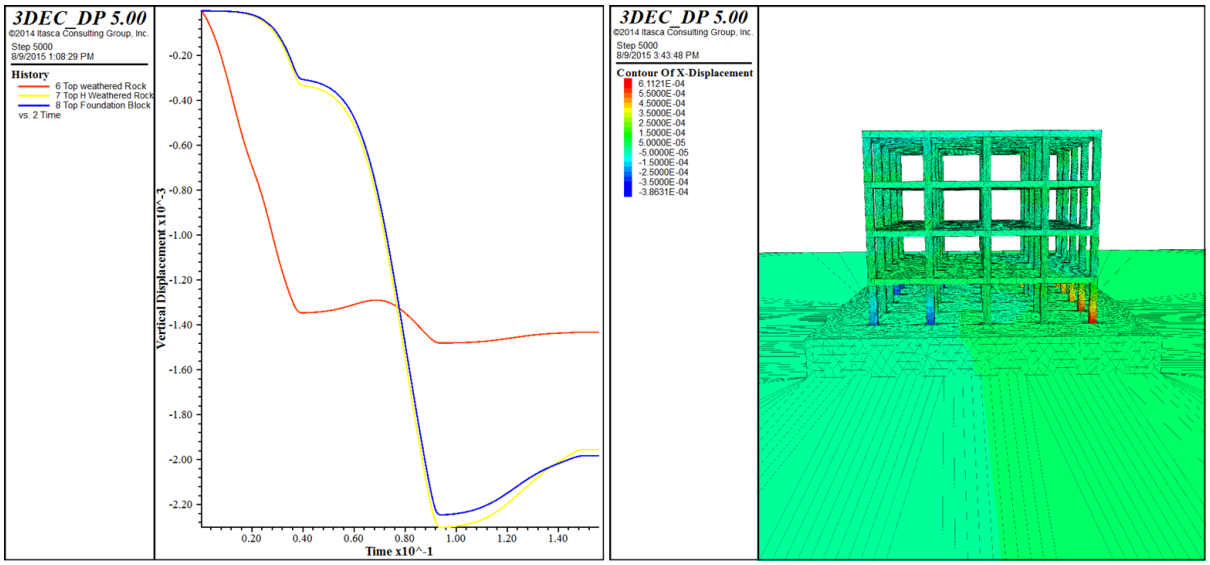


Figure 6.22 Plot of vertical displacement histories (left) and contour of horizontal displacement (right)

6.9.3. Dynamic simulations

The model is analyzed in four different simulations and recording displacements at 0.5 sec intervals. Plots of displacement vectors (absolute displacement magnitude) and horizontal displacement contours at intervals of 0.5, 1.0, 1.5 and 2.0 sec are recorded and shown in Figures 6.23 through 6.26. In each figure, the displacement vector plots on the left indicate the overall picture of the entire model whereas the plots of x-displacement on right side of each figure

indicate the closer view of the concrete building. Results of the simulations are described separately for each interval.

Plots of displacement at the end of dynamic loading for 0.5 sec are shown in Figure 6.23. The following observations are made:

- Displacement vectors in the weathered quartzite vary from 0.4 to 0.8 mm, Figure 6.23 (left).
- Displacements in the highly weathered rock and foundation vary from 0.1 to 0.2 mm, Figure 6.23 (left).
- Displacements in the side walls of the building vary from 0.4 to 0.7 mm whereas displacements in the inner parts of the building vary from 0.1 to 0.4 mm, Figure 6.23 (left).
- X-displacement in the building varies from 0.39 mm in the front parts of the building to 0.88 mm in the rear side of the building, Figure 6.23 (right).

Plots of displacement at the end of dynamic loading for 1.0 sec are shown in Figure 6.24. Following observations are made:

- Displacement vectors in the weathered and highly weathered quartzite layers vary from 0.1 to 0.3 mm, Figure 6.24 (left).
- Displacements in the side walls of the building vary from 0.4 to 1.0 mm whereas x-displacements in the inner parts of the building vary from 0.1 to 0.2 mm, Figure 6.24 (left).
- Maximum x-displacement of 0.15 mm is observed in the 2nd storey of the building whereas x-displacement of 0.1 mm is noticed in the rest of the building, Figure 6.24 (right).
- X-displacement of 0.10 mm is observed in the foundation, Figure 6.24 (right).

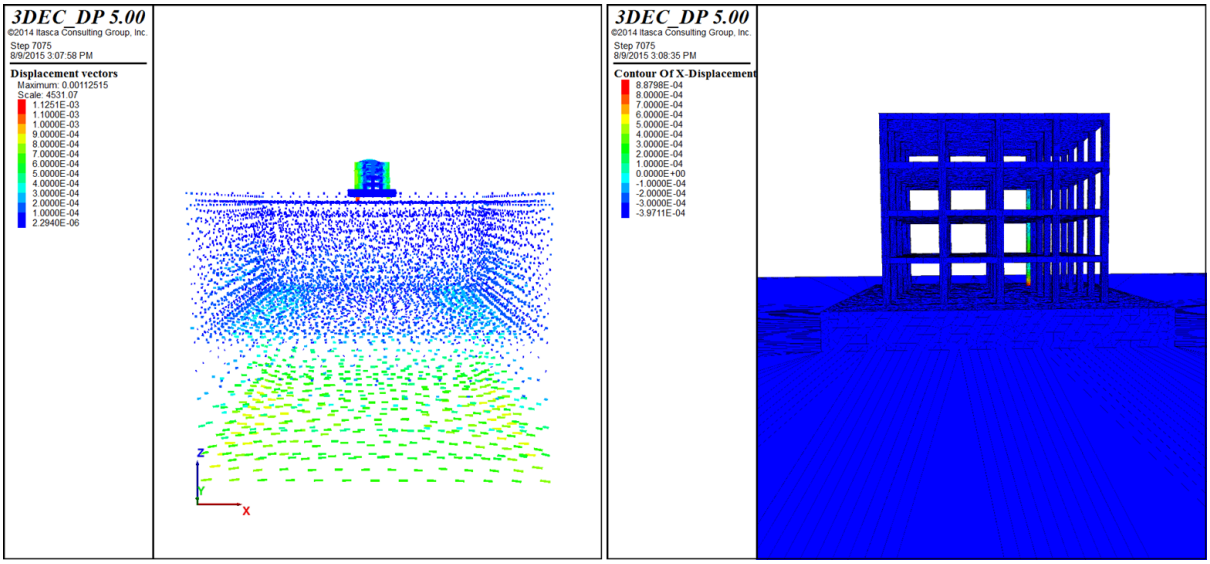


Figure 6.23 Horizontal displacement at T=0.5 sec

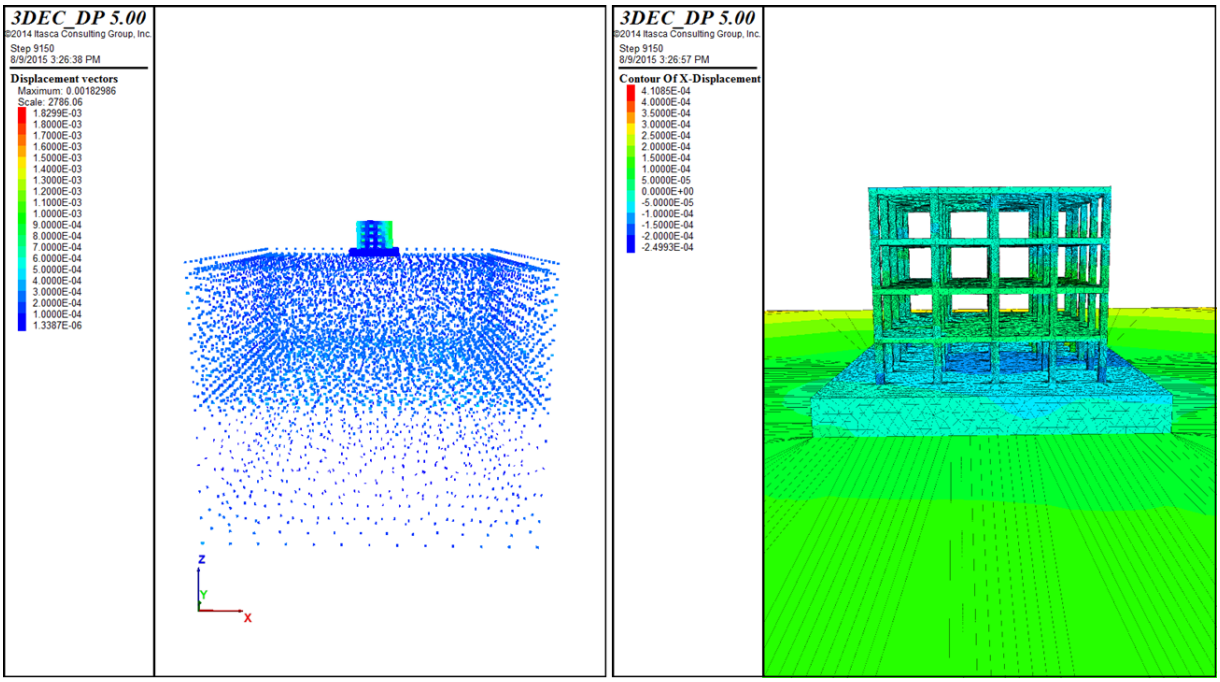


Figure 6.24 Horizontal displacement at T=1.0 sec

Plots of displacement at the end of dynamic loading for 1.50 sec are shown in Figure 6.25. The following observations are made:

- Displacement vectors in the weathered and highly weathered quartzite layers vary from 0.7 to 1.10 mm, Figure 6.25 (left).
- Displacements in the side walls of the building vary from 0.40 to 0.60 mm whereas x-displacements in the inner parts of the building vary from 0.10 to 0.20 mm, Figure 6.25 (left).

- Maximum x-displacement of 0.30 mm is observed in the 1st storey of the building whereas x-displacements are negligible in the rest of the building, Figure 6.25 (right).
- X-displacement of 0.60 mm is observed in the foundation, Figure 6.25 (right).

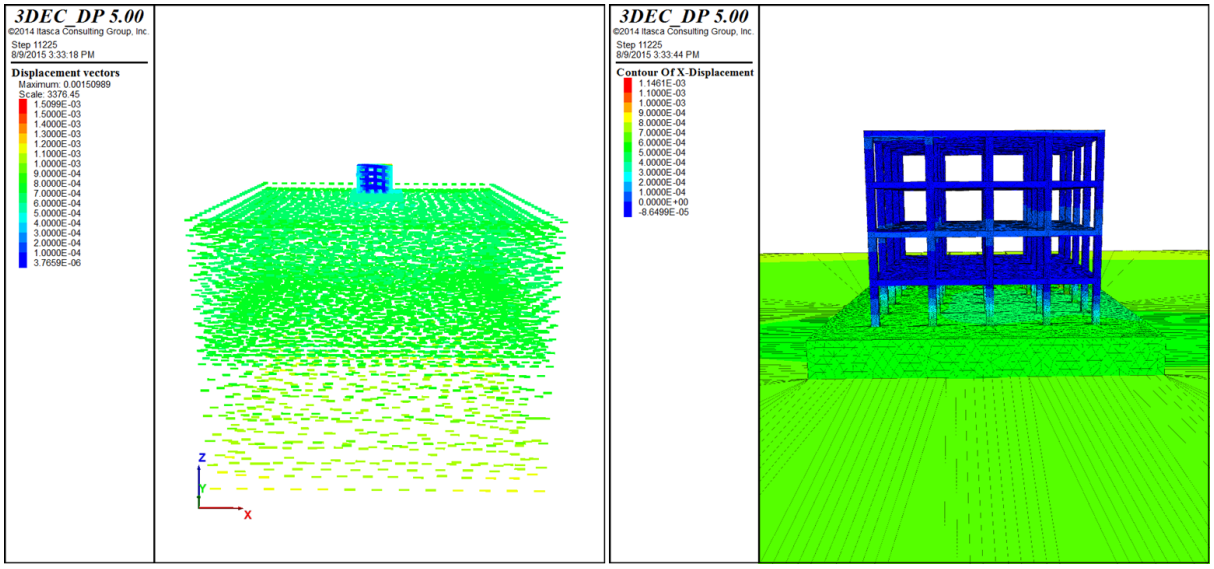


Figure 6.25 Horizontal displacement at T=1.5 sec

Plots of displacement at the end of dynamic loading for 1.50 sec are shown in Figure 6.26. The following observations are made:

- Displacement vectors in the weathered and highly weathered quartzite layers vary from 1.30 to 1.58 mm, Figure 6.26 (left).
- Displacements in the side walls of the building vary from 0.50 to 1.0 mm whereas x-displacements in the inner parts of the building vary from 0.10 to 0.20 mm, Figure 6.26 (left).
- Maximum x-displacement of 1.20 mm is observed in the 1st storey of the building whereas x-displacements are negligible in the rest of the building, Figure 6.26 (right).
- X-displacement of 1.30 mm is observed in the foundation, Figure 6.26 (right).

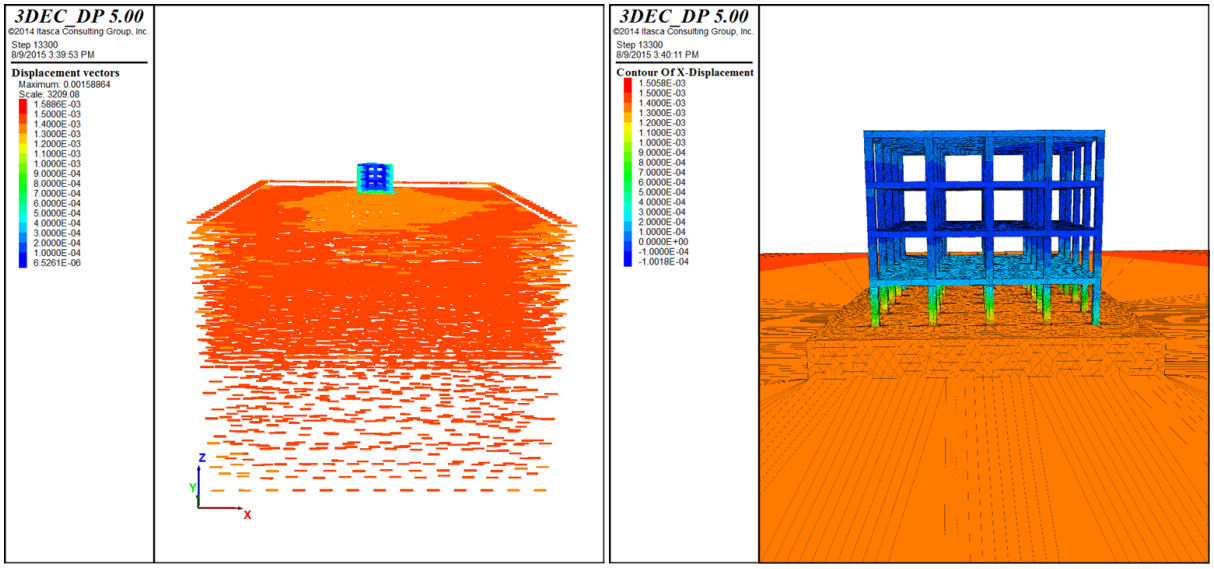


Figure 6.26 Horizontal displacement at T=2.0 sec

6.9.4. Comments on the dynamic response of four storey concrete building

The response of the two storey building to the selected ground motion reveals varying drift patterns at different points in the building (both in terms of direction and magnitude). The maximum x-displacement/horizontal drift (irrespective of the direction i.e. left or right) at the end of the dynamic loading is given in Table 6.8. Maximum x-displacement (drift) of 1.10 mm is observed in the four storey building.

Table 6.8 Displacement record of four storey concrete building

Duration (Sec)	Maximum Displacement (Total) (mm)				X-displacement (mm) (Horizontal Drift)			
	1st	2nd	3rd	4th	1st	2nd	3rd	4th
0.50	0.7	0.7	0.7	0.7	0.3	0.4	0.3	0.3
1.0	0.8	0.8	0.8	0.8	0	0.1	0.1	0
1.50	0.5	0.5	0.5	0.5	0.3	0	0	0
2.0	0.9	0.9	0.9	0.9	1.10	0.2	0	0

6.10. 3D Seismic Analysis of an Eight Storey Concrete Building

A 3D dynamic analysis of an eight storey concrete building using 3DEC is performed to evaluate its stability by monitoring the horizontal displacement (drift) during the dynamic simulation. The dynamic loading [evaluated for Hanging Wall (Quartzite Rock) in Chapter 5 and shown in Figure 6.3, 6.4 and 6.5] is used for the dynamic simulation. The analysis is performed in two stages;

Stage-1 to bring the model to initial equilibrium under gravity and in Stage-2, the simulations are made for at intervals of 0.50 sec each for a total duration of 2.0 sec.

6.10.1. Model size, geometry and properties

The model size and geometry are shown in Figure 6.27. The details of the foundation material are indicated in Figure 6.27 (left) and dimensions of the four storey concrete building are shown in Figure 6.27 (right). The assumed material properties (elastic) and joint properties are same to those considered for two and four storey concrete buildings.

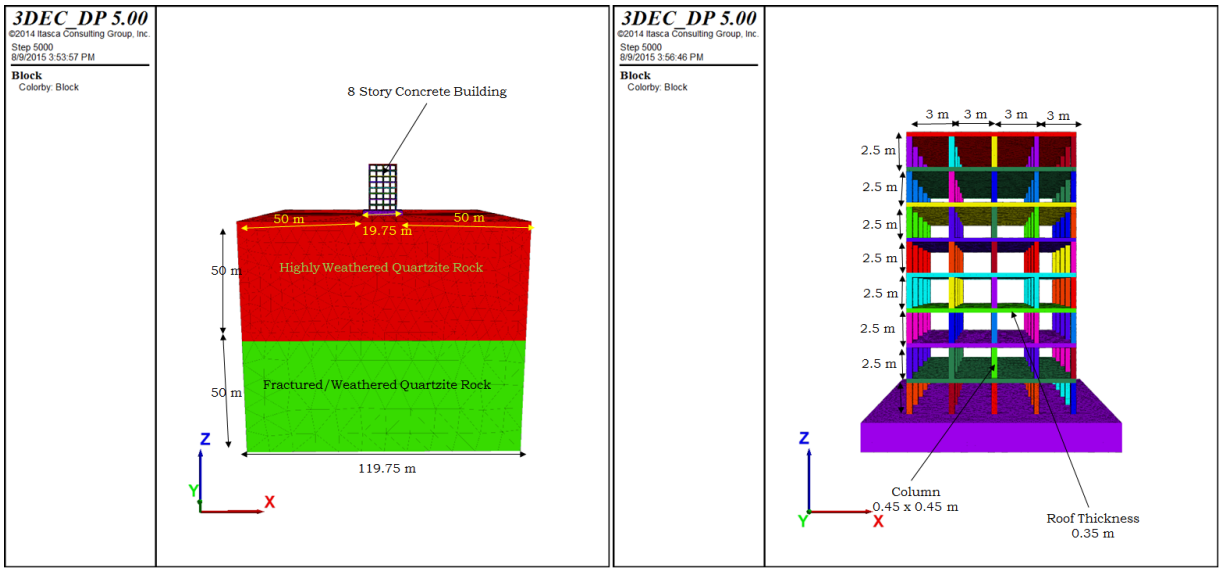


Figure 6.27 Model size and geometry of eight storey concrete building

6.10.2. Initial static equilibrium

Prior to running dynamic simulations, the model is run to establish static equilibrium conditions under gravity. The plot of unbalanced force in Figure 6.28 (left) shows that the model reached equilibrium in 5000 steps. The plots of vertical velocity histories in Figure 6.28 (right) and vertical displacement histories in Figure 6.29 (left) also indicate the initial equilibrium is established. Contours of x-displacement in Figure 6.29 (right) indicate very small displacements.

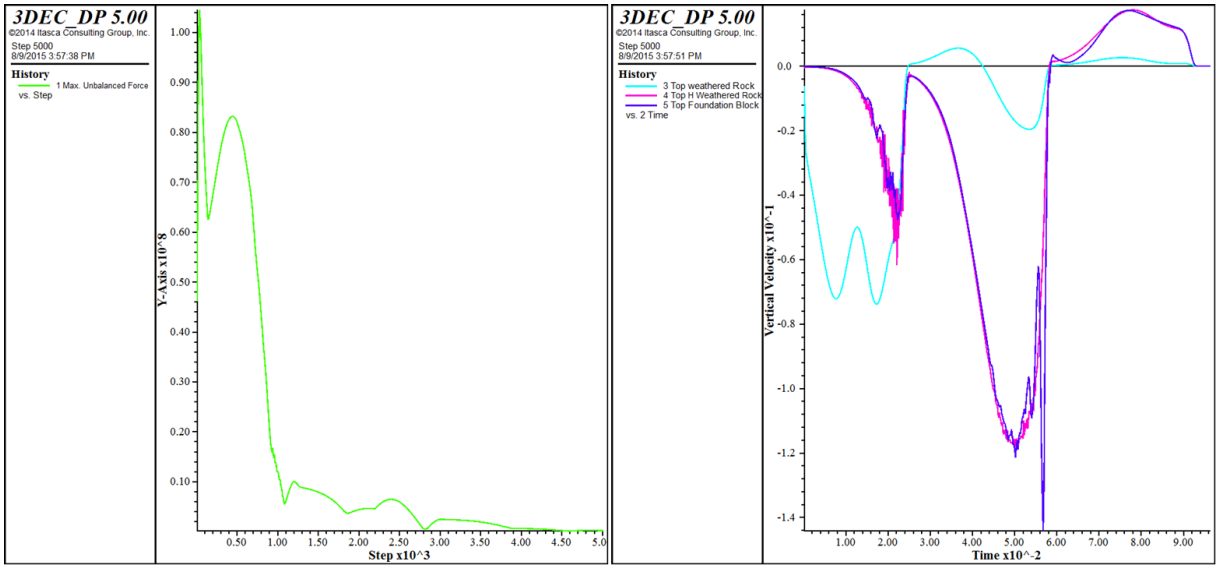


Figure 6.28 Plot of unbalanced force (left) and vertical velocity histories (right)

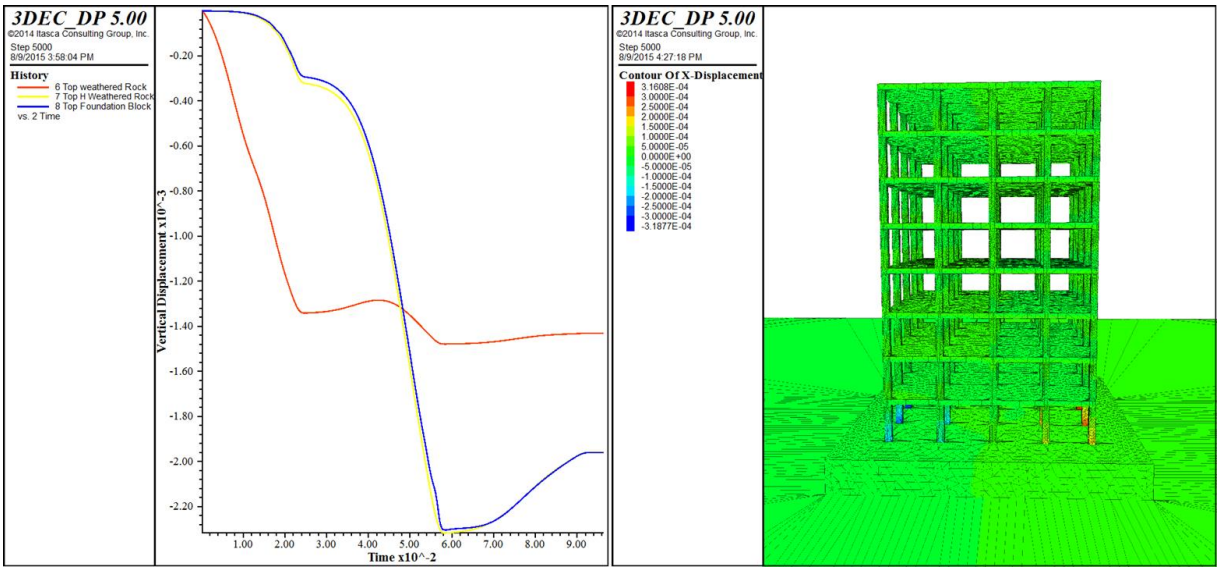


Figure 6.29 Plot of vertical displacement histories (left) and contour of horizontal displacement (right)

The model is analyzed in four different simulations and recording displacements at 0.5 sec intervals. Plots of displacement vectors (absolute displacement magnitude) and horizontal displacement contours at intervals of 0.5, 1.0, 1.5 and 2.0 sec are recorded and shown in Figures 6.30 through 6.33. In each figure, the displacement vector plots on the left indicate the overall picture of the entire model whereas the plots of x-displacement on right side of each figure indicate a closer view of the concrete building. Results of the simulations are described separately for each interval.

Plots of displacement at the end of dynamic loading for 0.5 sec are shown in Figure 6.30. The following observations are made:

- Displacement vectors in the weathered quartzite vary from 1.90 to 1.0 mm, Figure 6.30 (left).
- Displacements in the highly weathered rock and foundation vary from 0.10 to 0.20 mm, Figure 6.30 (left).
- Displacements in the building vary from 0.20 to 0.70 mm, Figure 6.30 (left).
- X-displacement in the left part of the building measures 0.2 mm (eastward) whereas in right part of the building, the same magnitude of x-displacement (0.20 mm) is observed in the opposite (westward) direction, Figure 6.30 (right).

Plots of displacement at the end of dynamic loading for 1.0 sec are shown in Figure 6.31. The following observations are made:

- Displacement vectors in the weathered quartzite vary from 0.30 to 0.70 mm, Figure 6.31 (left).
- Displacements in the highly weathered rock and foundation vary from 0.10 to 0.30 mm, Figure 6.31 (left).
- Displacements in the building vary from 1.0 to 1.20 mm, Figure 6.31 (left).
- X-displacements in the building vary from 0.10 to 0.30 mm, Figure 6.31 (right).

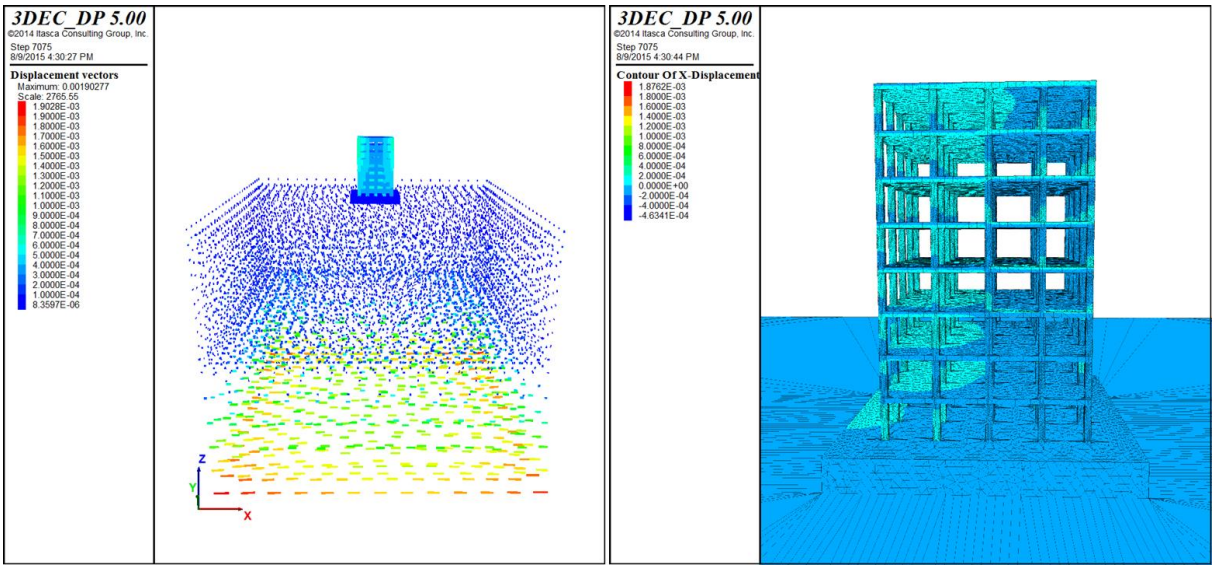


Figure 6.30 Horizontal displacement at T=0.5 sec

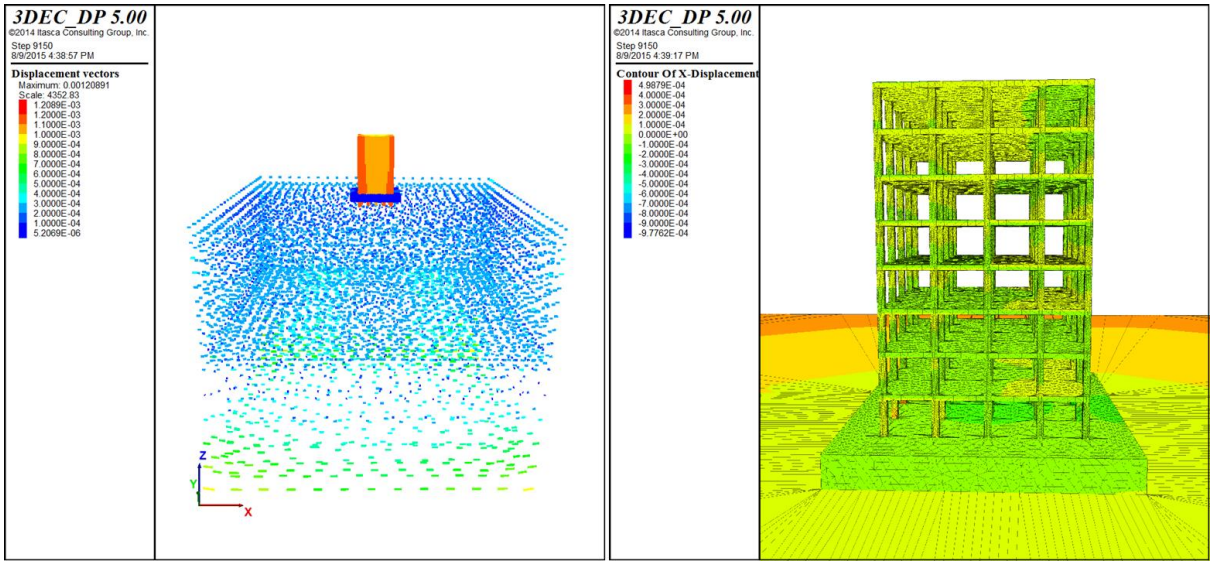


Figure 6.31 Horizontal displacement at T=1.0 sec

Plots of displacement at the end of dynamic loading for 1.50 sec are shown in Figure 6.32. The following observations are made:

- Displacement vectors in the weathered and highly weathered quartzite layers vary from 0.60 to 0.80 mm, Figure 6.32 (left).
- Displacements in the building vary from 1.8 to 2.08 mm, Figure 6.32 (left).
- X-displacements in the building measures around 0.10 mm, Figure 6.32 (right).

Plots of displacement at the end of dynamic loading for 2.0 sec are shown in Figure 6.33. Following observations are made:

- Displacement vectors in the weathered and highly weathered quartzite layers vary from 1.20 to 1.80 mm, Figure 6.33 (left).
- Displacements in the building vary from 2.0 to 2.67 mm, Figure 6.33 (left).
- X-displacements in the building vary from 0.2 mm to 0.90 mm, Figure 6.33 (right).

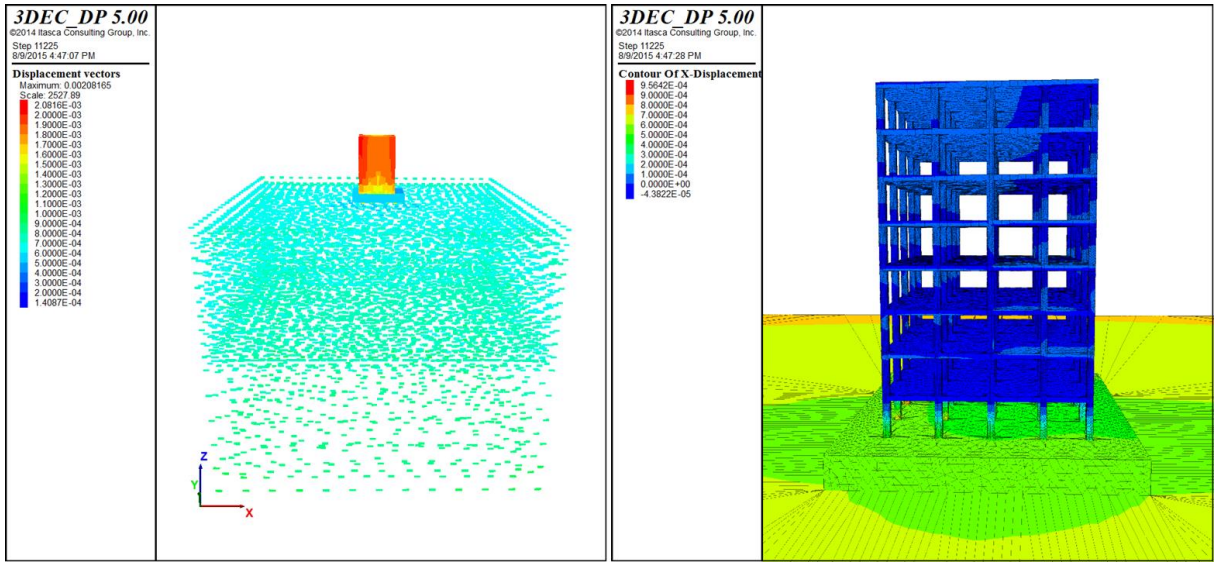


Figure 6.32 Horizontal displacement at T=1.5 sec

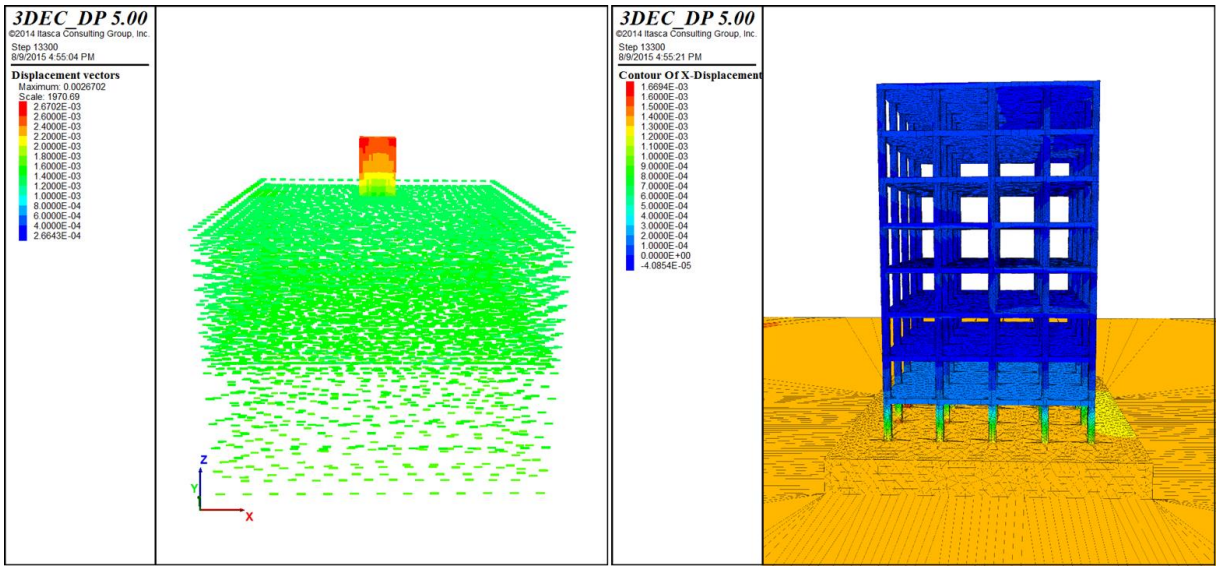


Figure 6.33 Horizontal displacement at T =2.0 sec

6.10.3. Comments on dynamic response of eight storey concrete building

The response of the eight storey building to the selected ground motion reveals varying drift patterns at different points in the building (both in terms of direction and magnitude). The maximum x-displacement/horizontal drift (irrespective of the direction) at the end of the dynamic loading is given in Table 6.9. Maximum x-displacement (drift) of 0.90 mm is observed in the eight storey building.

Table 6.9 Displacement record of eight storey concrete building

Storey Time	Maximum Displacement (Total) (mm)				X-displacement (mm) (Horizontal Drift)			
	0.5 sec	1.0 sec	1.5 sec	2.0 sec	0.5 sec	1.0 sec	1.5 sec	2.0 sec
1	0.60	1.20	1.60	2.67	0.20	0.10	0.40	0.90
2	0.60	1.20	1.60	2.20	0.20	0.10	0	0.20
3	0.60	1.20	2.0	2.20	0.20	0.10	0	0
4	0.60	1.20	2.0	2.20	0.20	0.10	0	0
5	0.60	1.20	2.0	2.67	0.20	0.10	0	0
6	0.60	1.20	2.0	2.67	0.20	0.10	0.10	0
7	0.60	1.20	2.0	2.67	0.20	0.10	0.10	0
8	0.60	1.20	2.0	2.67	0.20	0.10	0.10	0

6.11. Dynamic Analysis of a Jointed Rock Slope with Building Load at the Crest Using 3DEC

6.11.1. Model size, geometry and properties

A 3D seismic analysis using 3DEC of a jointed quartzite rock slope is performed to evaluate its stability against dynamic loading of mining induced ground motion. The slope comprises three layers; massive quartzite bedrock, overlain by weathered quartzite and highly weathered/fractured quartzite at the top layer. The upper layer of the slope is characterized by non-persistent joints. A building load is considered in the form of a building block at the crest. The slope geometry and properties considered for the analysis are given in Figure 6.34 and Table 6.10. Parameters of the joint sets are given in Figure 6.35. The analysis is performed to evaluate stability conditions under dynamic loading of mining induced ground motion.

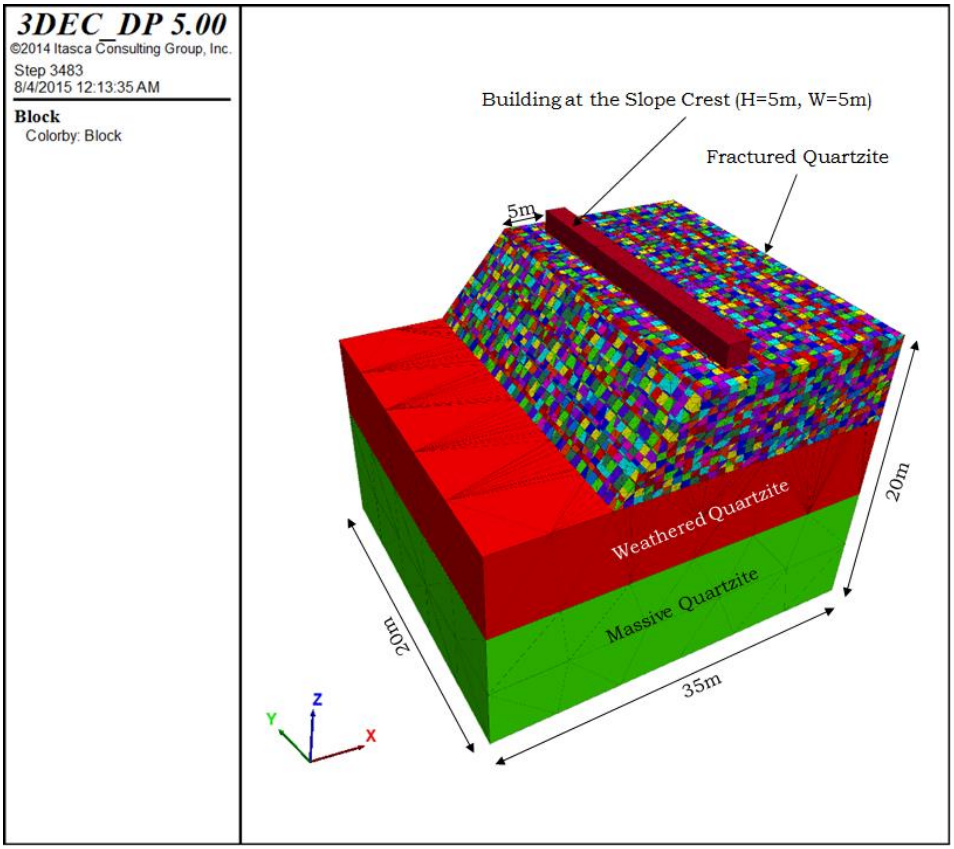


Figure 6.34 Quartzite slope geometry

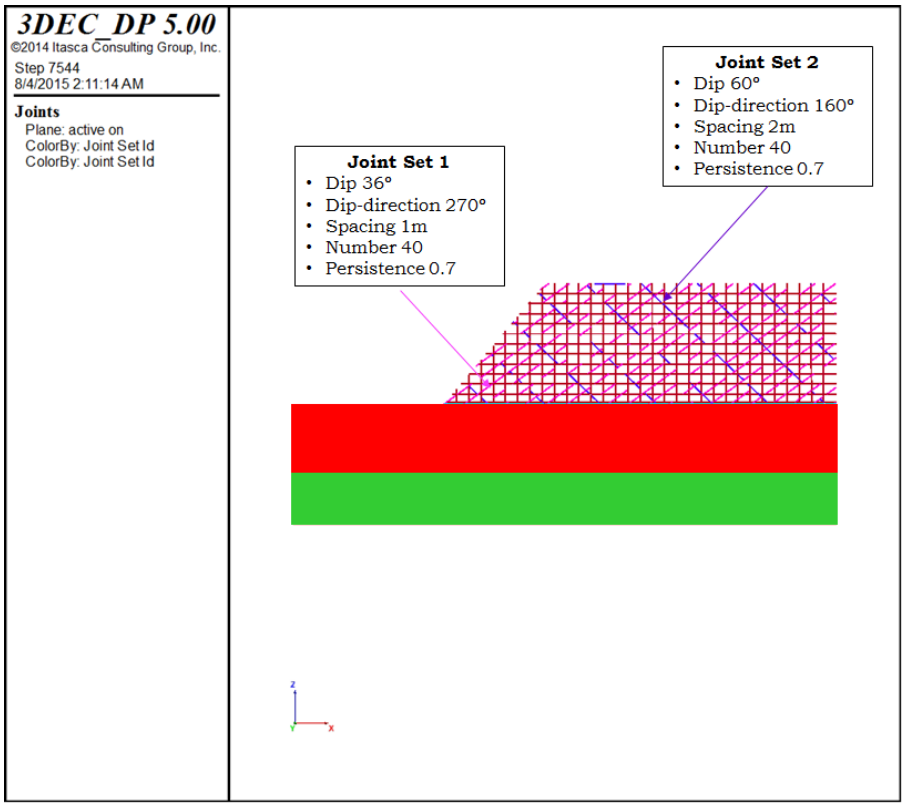


Figure 6.35 Joint sets in the slope

Table 6.10 Material properties of the quartzite slope

Property	Massive Quartzite	Weathered Quartzite	Highly fractured/weathered Quartzite	Building Block
Dry density (kg/m^3)	2800	2500	2200	2000
Cohesion (Pa)	1e6	0.55e6	0.5e6	10e6
Angle of internal friction (Degrees)	40	35	30	40
Bulk modulus (GPa)	40	30	20	40
Shear modulus (GPa)	30	18	12	30

6.11.2. Initial static equilibrium

This stage is performed to bring the model to initial static equilibrium under the given conditions of geometry, material properties and gravity. Plot of unbalanced force and vertical displacement history (shown in yellow cross) are shown in Figure 6.36 and 6.37 respectively. These plots show that the model is in equilibrium for the dynamic analysis.

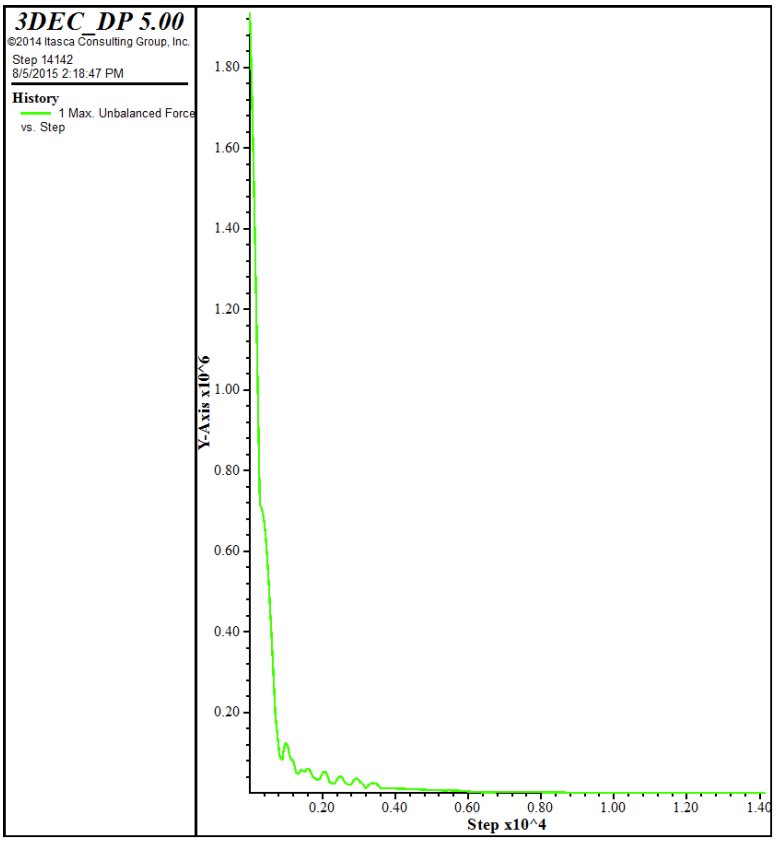


Figure 6.36 Plot of unbalanced force

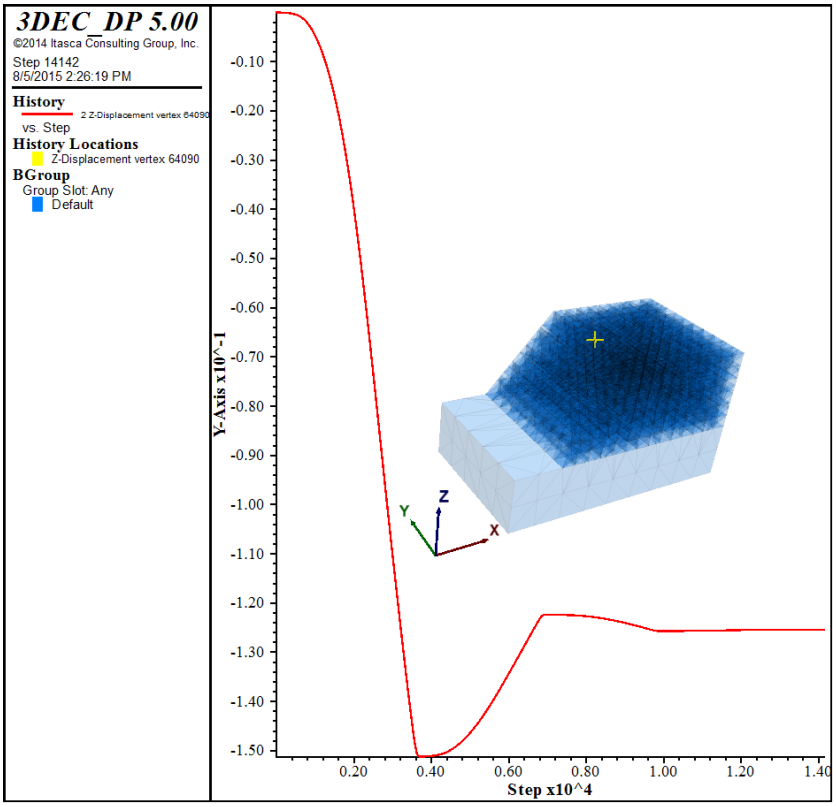


Figure 6.37 Plot of vertical displacement history of a point (shown in yellow cross) at the crest

6.11.3. Dynamic simulations

The slope is analyzed by applying the ground motions in 0.5 second interval to a total of 2 seconds.

Slope movement after 0.5 second

Contours of displacement, velocity and joint shear displacement are shown in Figures 6.38 through 6.40 for the initial 0.5 sec. A maximum displacement of 2.75 mm is observed in the building block and 4 mm at a few points in the slope crest whereas along joint sets, the maximum displacement reaches 4 mm, Figure 6.40. A maximum velocity of 2.5 cm/sec is observed in the valley side of the slope crest whereas a velocity of 5 mm/sec to 1.5 cm/sec is observed in the rest of the slope. It is evident that a peak velocity of 6 mm/sec applied at the base of the slope amplified to 2.5 cm/sec at the slope crest after a duration of 0.5 sec. A maximum joint shear displacement of 1 mm is observed at a few points in the slope face only whereas rest of the slope does not undergo any shear displacement along the joints, Figure 6.40.

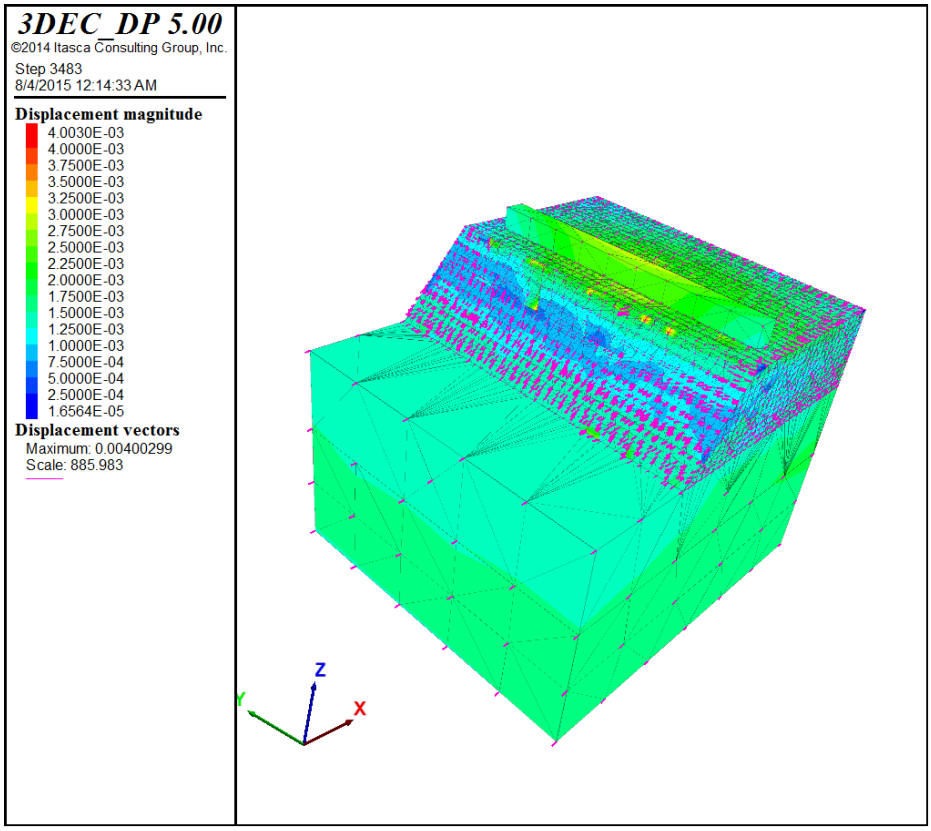


Figure 6.38 Displacement contours and vectors at 0.5 sec duration

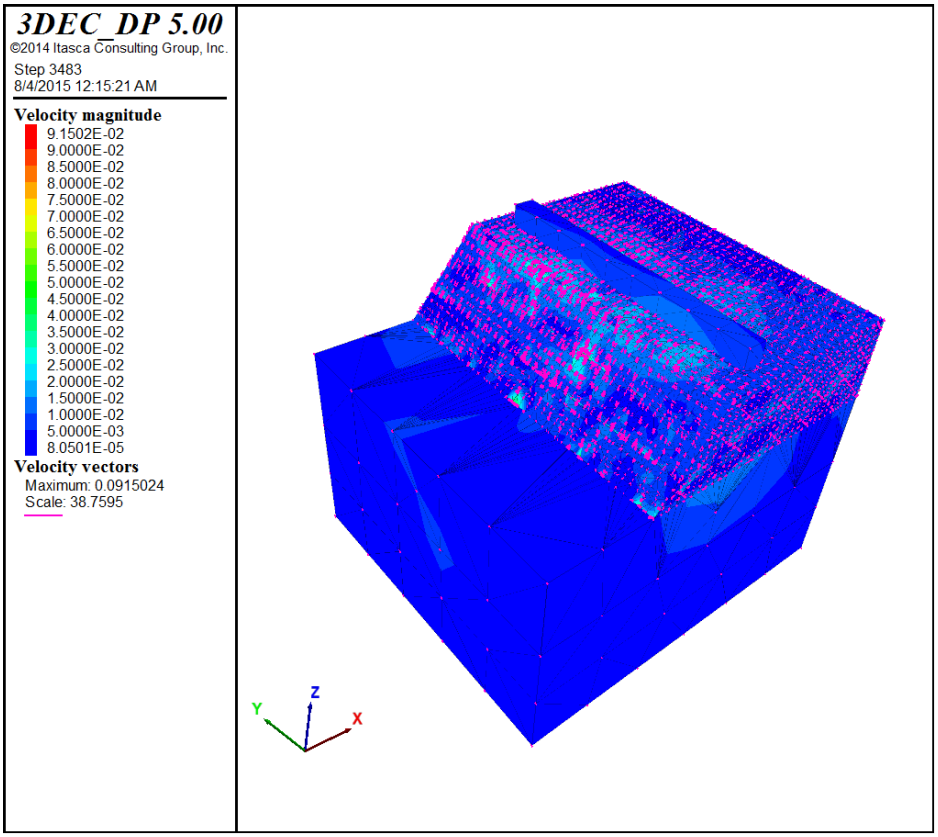


Figure 6.39 Velocity contours and vectors at 0.5 sec duration

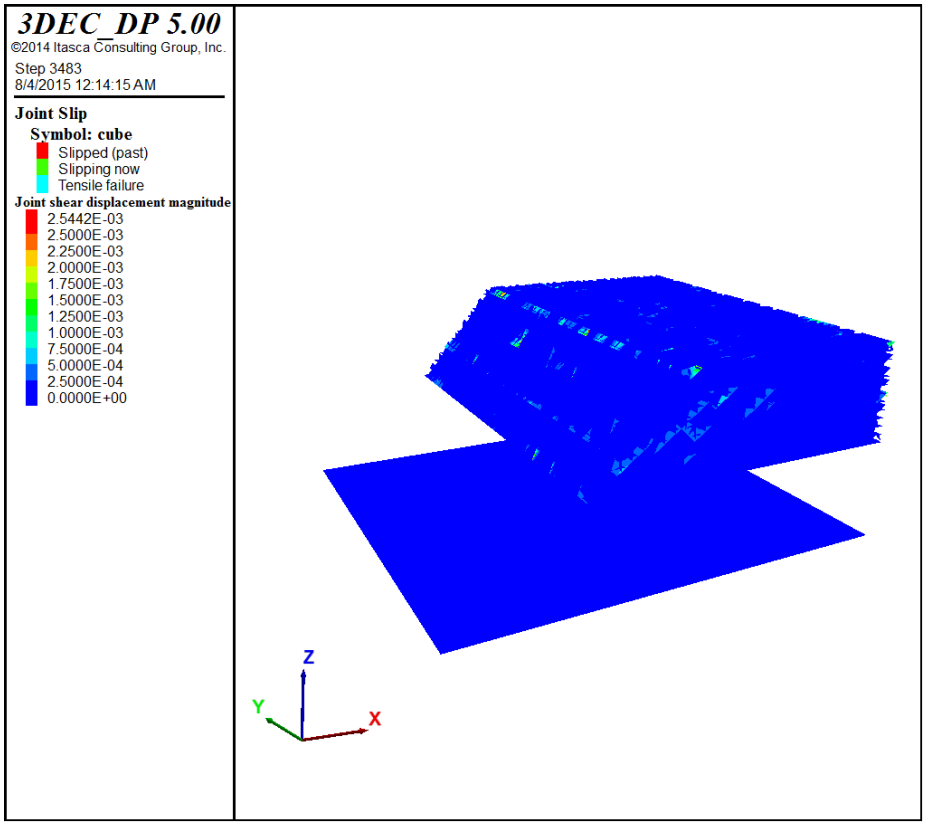


Figure 6.40 Joint shear slip magnitude at 0.5 sec duration

Slope movement after 1.0 second

The analysis is carried out for a duration of 0.5 sec after the initial 0.5 sec. (total time 0.5+0.5=1.0 sec). Contours of displacement, velocity and joint shear displacement are shown in Figures 6.41 through 6.43. A maximum displacement of 6 mm is observed in the building block and slope whereas along joint sets, the maximum displacement reaches 9.15 mm, Figure 6.41. A maximum velocity of 2.0 cm/sec is observed in the valley side of the slope crest and building block whereas a velocity of 5 mm/sec is observed in the rest of the slope.

It is observed that a peak velocity of 6 mm/sec applied at the base of the slope amplified to 2.0 cm/sec at the slope crest after a duration of 1.0 sec. A maximum joint shear displacement of 2 mm is observed at very few points in the slope face only whereas rest of the slope does not undergo any shear displacement along the joints, Figure 6.43.

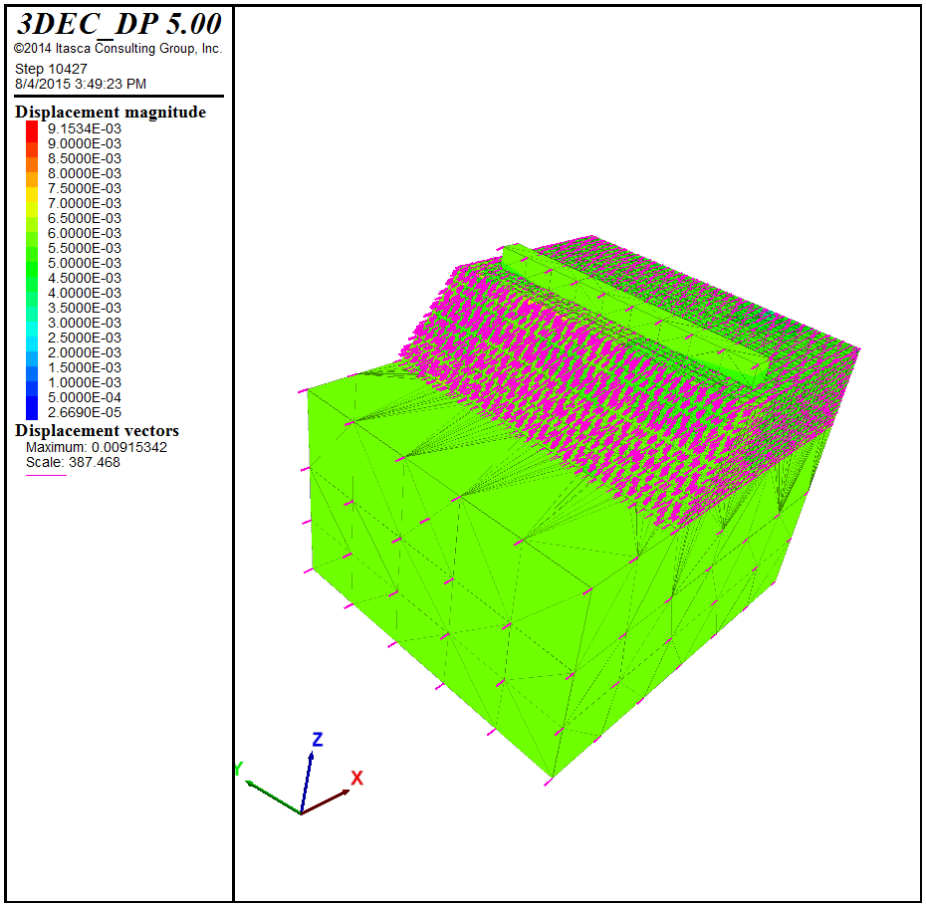


Figure 6.41 Displacement contours and vectors at 1.0 sec duration

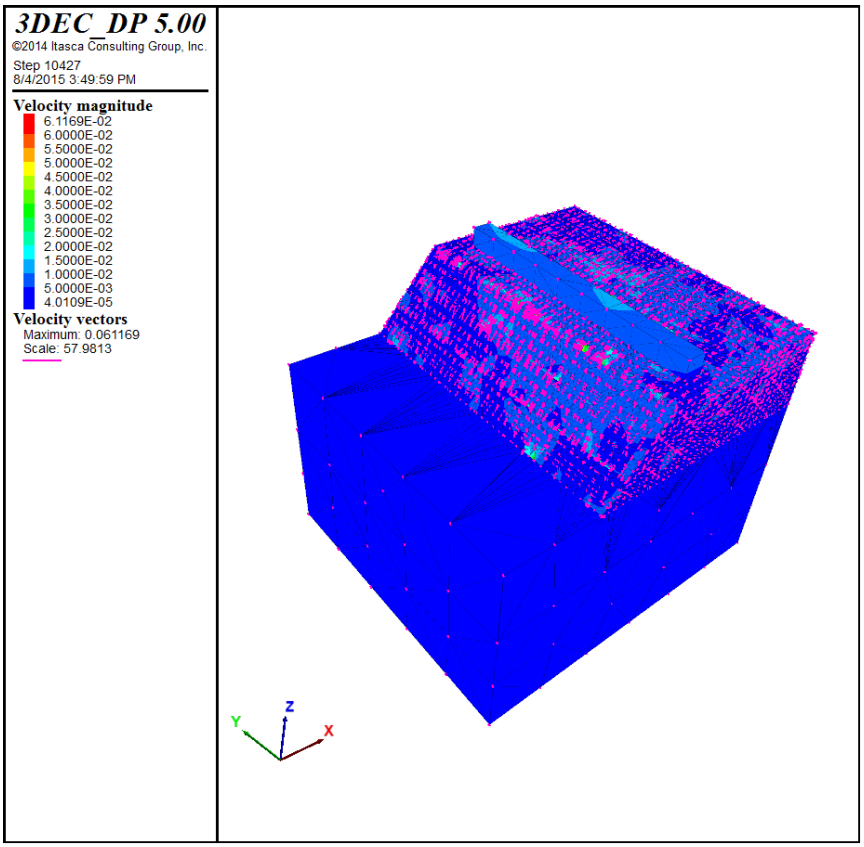


Figure 6.42 Velocity contours and vectors at 1.0 sec duration

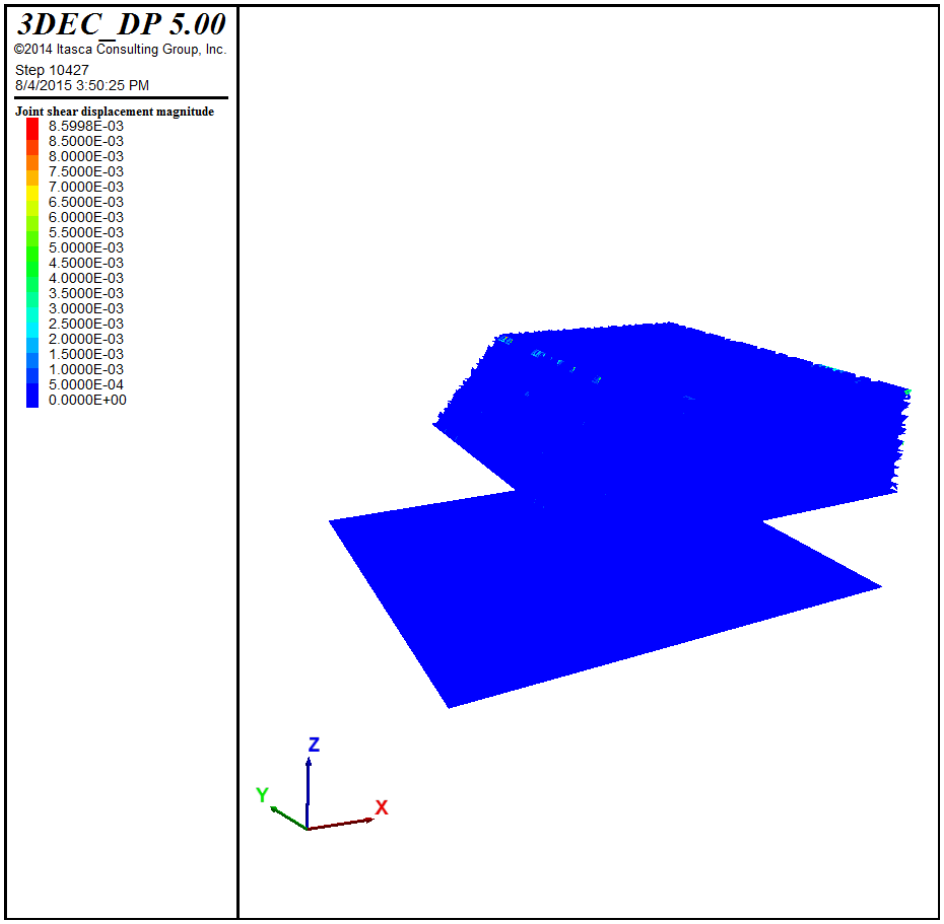


Figure 6.43 Joint shear slip magnitude at 1.0 sec duration

Slope movement after 1.5 second

The analysis is carried out for a further duration of 0.5 sec (total time 0.5+0.5+0.5=1.50 sec). Contours of displacement, velocity and joint shear displacement are shown in Figures 6.44 through 6.46. A maximum displacement of 1.2 cm is observed in the building block and slope whereas along joint sets, the maximum displacement reaches 1.30 cm, Figure 6.44. A maximum velocity of 1.25 cm/sec is observed in the valley side of the slope crest and building block whereas a velocity of 5 mm/sec is observed in the rest of the slope.

It is observed that a peak velocity of 6 mm/sec applied at the base of the slope amplified to 1.25 cm/sec at the slope crest after a duration of 1.50 sec. A maximum joint shear displacement of 2.50 mm is observed at very few points in the slope face only whereas rest of the slope does not undergo any shear displacement along the joints, Figure 6.46.

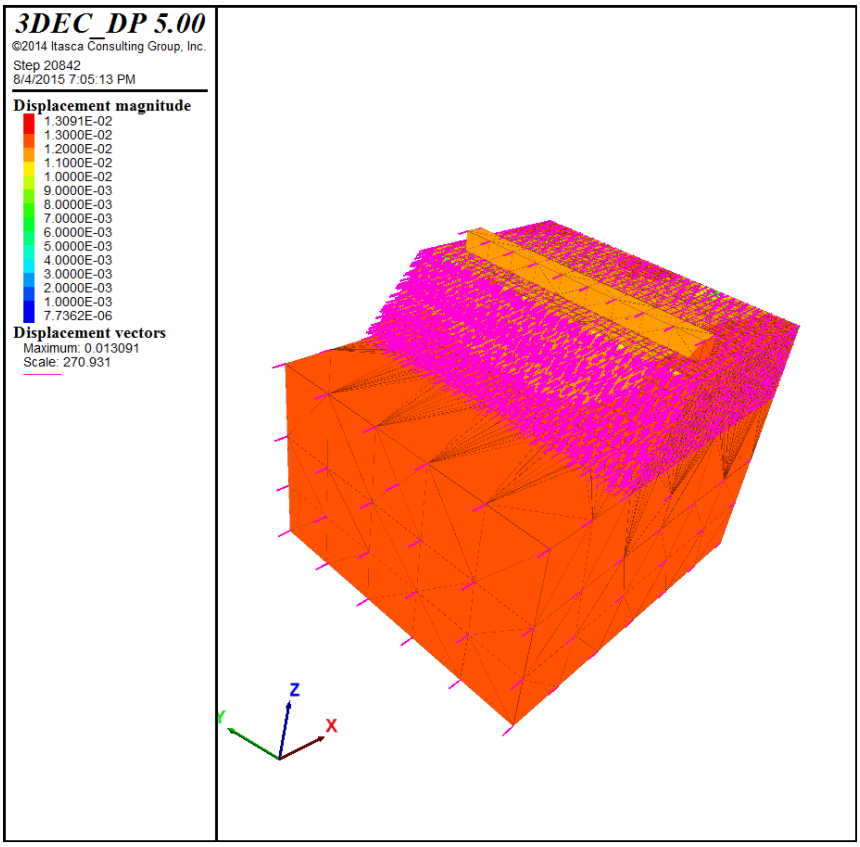


Figure 6.44 Displacement contours and vectors at 1.5 sec duration

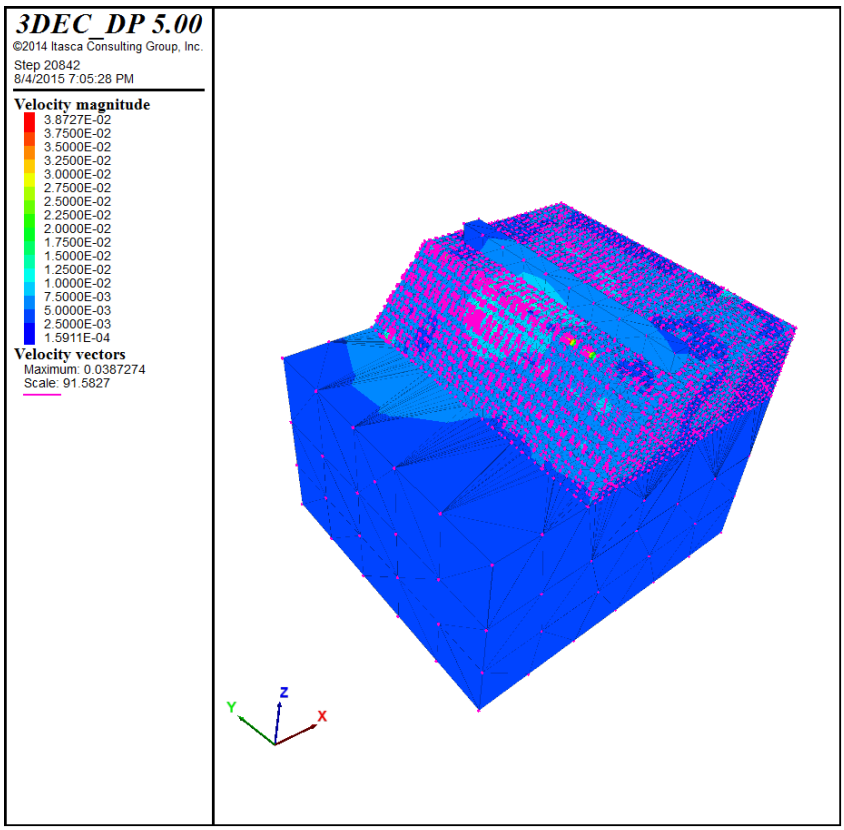


Figure 6.45 Displacement contours and vectors at 1.5 sec duration

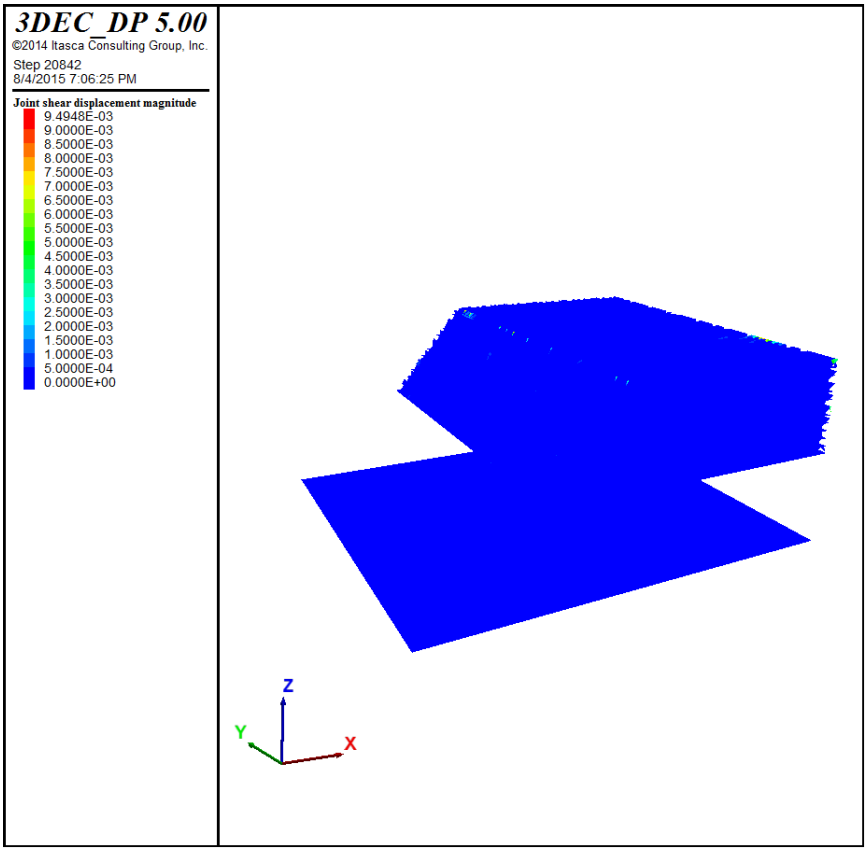


Figure 6.46 Joint shear slip magnitude at 1.5 sec duration

Slope movement after 2.0 second

The analysis is carried out for a further duration of 0.5 sec (total time 0.5+0.5+0.5+0.5=2.0 sec). Contours of displacement, velocity and joint shear displacement are shown in Figures 6.47 through 6.49. A maximum displacement of 2 cm is observed in the building block and slope whereas along joint sets, the maximum displacement reaches 2.27 cm, Figure 6.46. A maximum velocity of 1.0 to 1.25 cm/sec is observed at a few points in the valley side of the slope crest whereas a velocity of 2.5 mm/sec is observed in the rest of the slope.

It is observed that a peak velocity of 6 mm/sec applied at the base of the slope amplified to 1.25 cm/sec at the slope crest after a duration of 2.0 sec. A maximum joint shear displacement of 1.0 mm is observed in the slope, Figure 6.49.

The magnitudes of displacement, velocity and joint shear displacement in the slope, at the end of the dynamic analysis for a period of 2 sec reach values of 20 mm, 10 mm/sec and 1 mm respectively, Table 6.11. The highly weathered and

fractured slope behaves like a granular (soil like) material. According to Koo et al. (2013), a slope experiencing a displacement in excess of 70 mm due to a dynamic loading is usually considered at a significant risk of failure. ASCE/SCEC (2002) recommends a maximum threshold of 50 mm displacement for typical slopes to avoid a risk of failure. Since displacements observed in the slope due to mining induced ground motion are very small, it is deduced that the stability of a slope with characteristics similar to those considered for analysis is not at a risk.

Table 6.11 Comparison of the displacement, velocity and joint shear displacement

Parameter	0.5 sec	1.0 sec	1.5 sec	2.0 sec
Displacement (mm)	2.75	6	12	20
Velocity (mm/sec)	25	20	12.50	10
Joint shear displacement (mm)	1	2	2.5	1

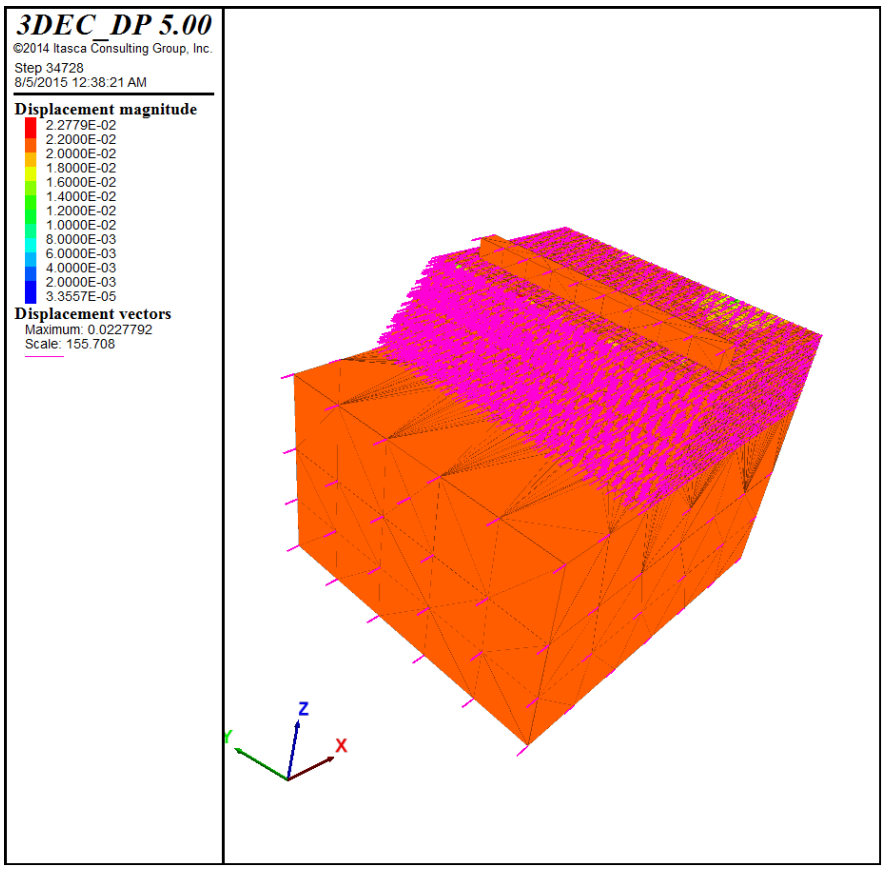


Figure 6.47 Displacement contours and vectors at 2.0 sec duration

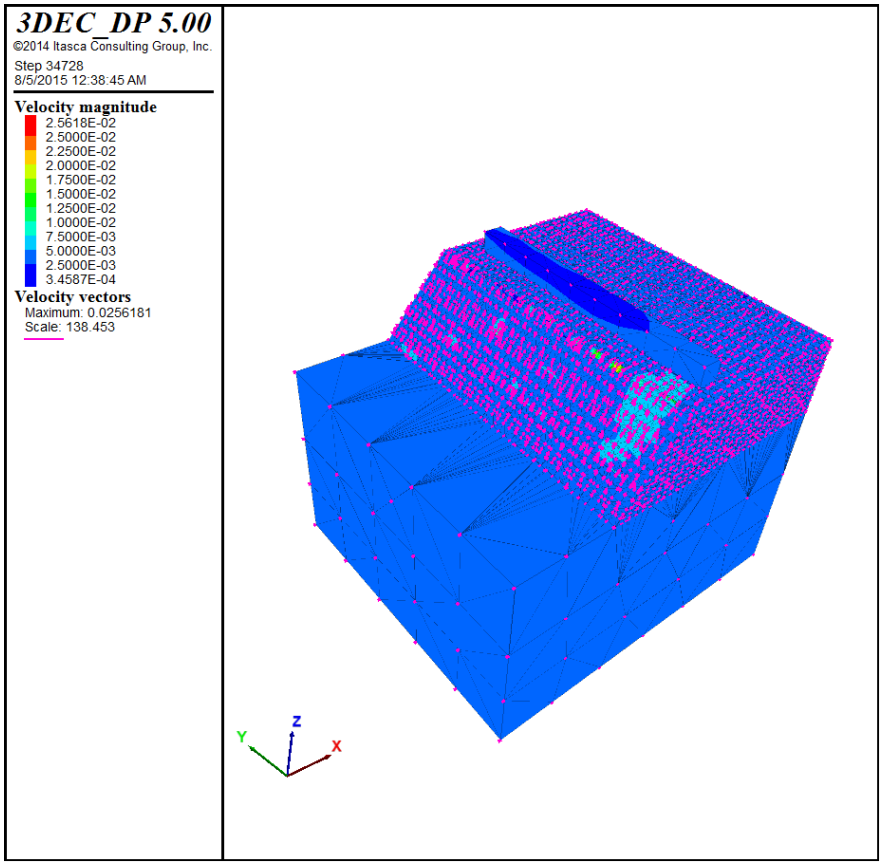


Figure 6.48 Velocity contours and vectors at 2.0 sec duration

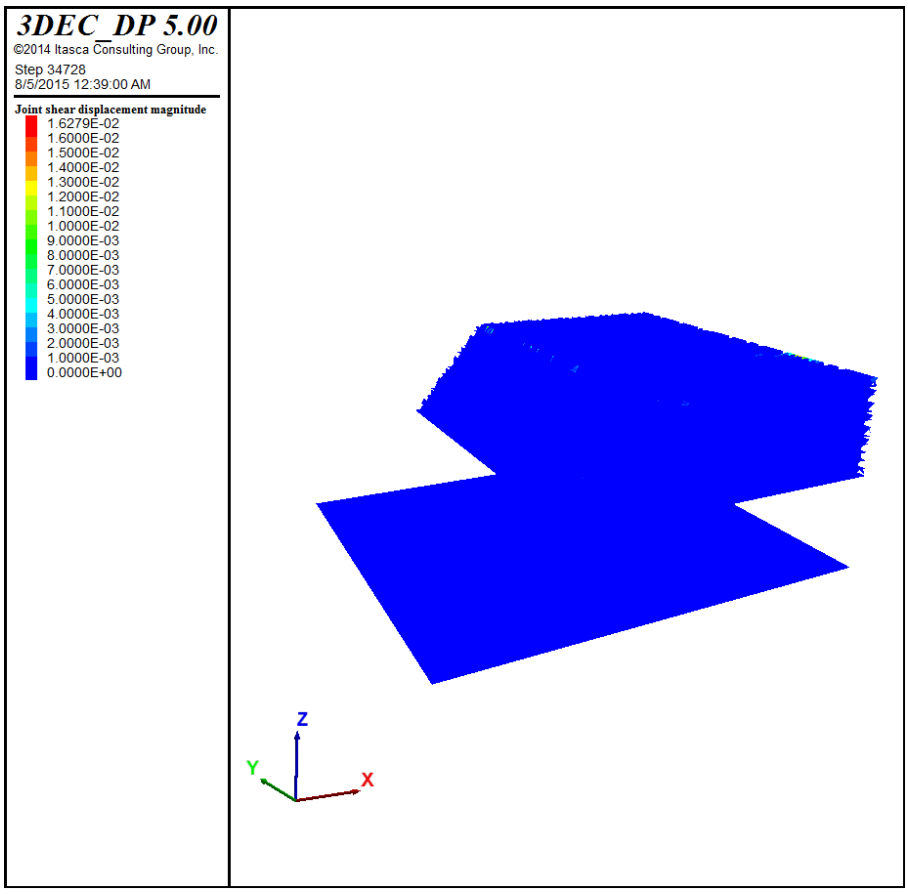


Figure 6.49 Joint shear slip magnitude at 2.0 sec duration

6.12. Dynamic Analysis for Evaluation of Liquefaction Potential in a Tailings Dam Slope Using FLAC

With a view to evaluate liquefaction potential of a slope of a tailings dam, guidelines are taken from Itasca (2014) regarding geometry and characteristics of the liquefiable soil layers.

6.12.1. Model size, geometry and properties

A seismic risk to the stability of a slope comprising liquefiable soils of a tailing dam is assessed due to the mining induced ground motions evaluated in Chapter 5. 2D seismic analysis is performed to evaluate deformation of liquefiable soils using the dynamic option and liquefaction modelling facility in FLAC.

The problem geometry comprises three soil layers as shown in Figure 6.50. The slope has an angle of 30^0. The properties considered for the three soil layers are shown in Table 6.12. A porosity of 0.3 and permeability of $10e^{-7}$ m/sec is assumed for the upper three layers. In view of the properties considered, the upper two layers are characterized as liquefiable, Itasca (2014).

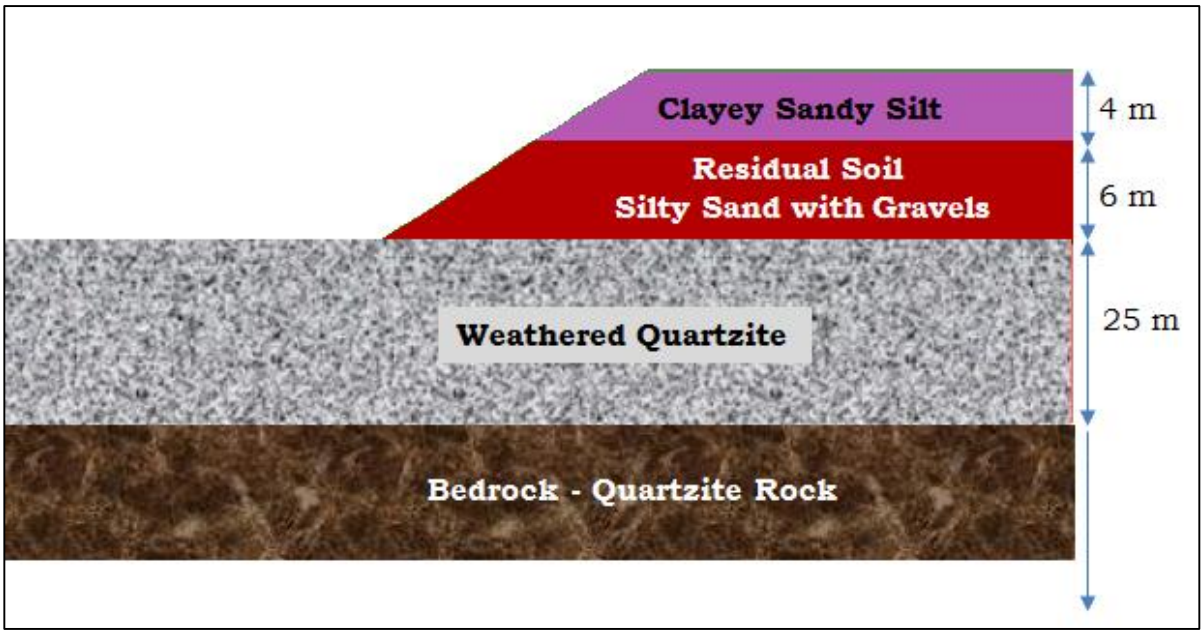


Figure 6.50 Geological profile of the tailings dam slope

Table 6.12 Tailings dam slope properties

Property	Upper Layer	Middle Layer	Lower Layer
Dry density (kg/m^3)	1700	1800	2200
Cohesion (Pa)	2000	2000	4000
Angle of internal friction (Degrees)	30	35	40
Dilation angle (degrees)	0	0	0
Young's modulus (MPa)	163	163	650
Poisson's ratio	0.3	0.3	0.3
Bulk modulus (MPa)	136	136	510
Shear modulus (MPa)	63.0	63.0	235.0
Permeability (cm/sec)	1e-10	1e-10	1e-10
Shear wave velocity (m/sec)	175	200	375

The FLAC model geometry is shown in Figure 6.51. Only three layers (full thickness of upper two layers and part of 3rd layer) are modelled to minimize the model run time. The liquefaction analysis comprised four stages.

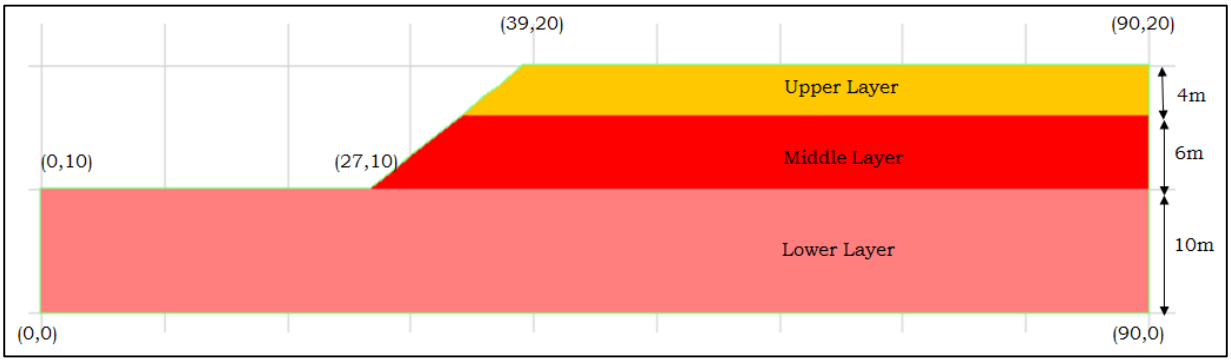


Figure 6.51 Geometry of the model

6.12.2. Initial static equilibrium

This stage is performed to bring the model to initial static equilibrium under the given conditions of geometry, material properties and gravity. This stage is performed in three steps.

- Firstly, the model is brought to static mechanical-equilibrium considering elastic conditions (to prevent any large deformation or plastic failure).
- In the 2nd step, the water level is raised and equilibrium of the submerged slope is established. In this step, the pore-pressure gradient (corresponding to elevation of 20 m (y = 20m)) is applied on the sides of the model to achieve steady state flow conditions and the model is run including the weight of the water and with the groundwater flow option activated for mechanical equilibrium under submerged conditions.
- Figure 6.52 shows that the model reached equilibrium in 2000 steps. A plot of pore-pressure contours is shown in Figure 6.53 and that of vertical stress contours in Figure 6.54. The gradual gradient of the contours indicate that the model has reached equilibrium under submerged conditions.

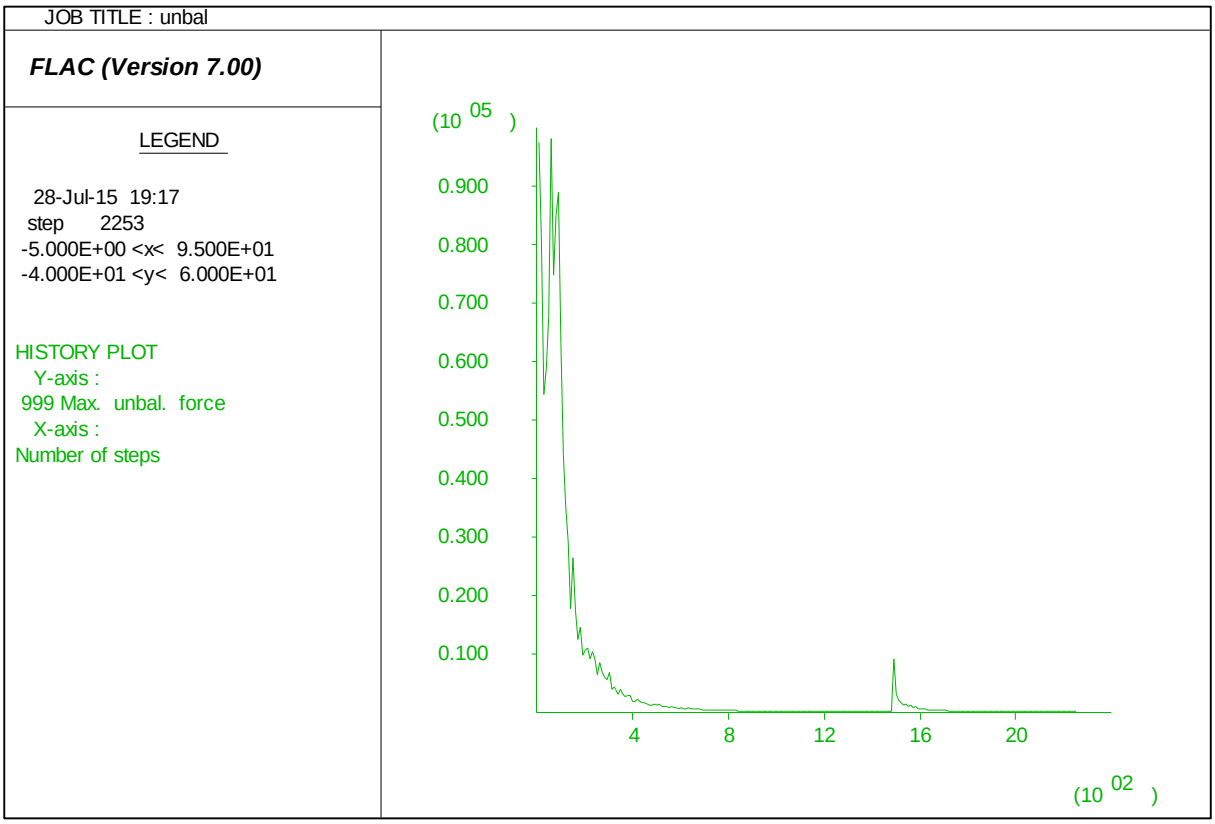


Figure 6.52 Plot of unbalanced force showing the model reached equilibrium

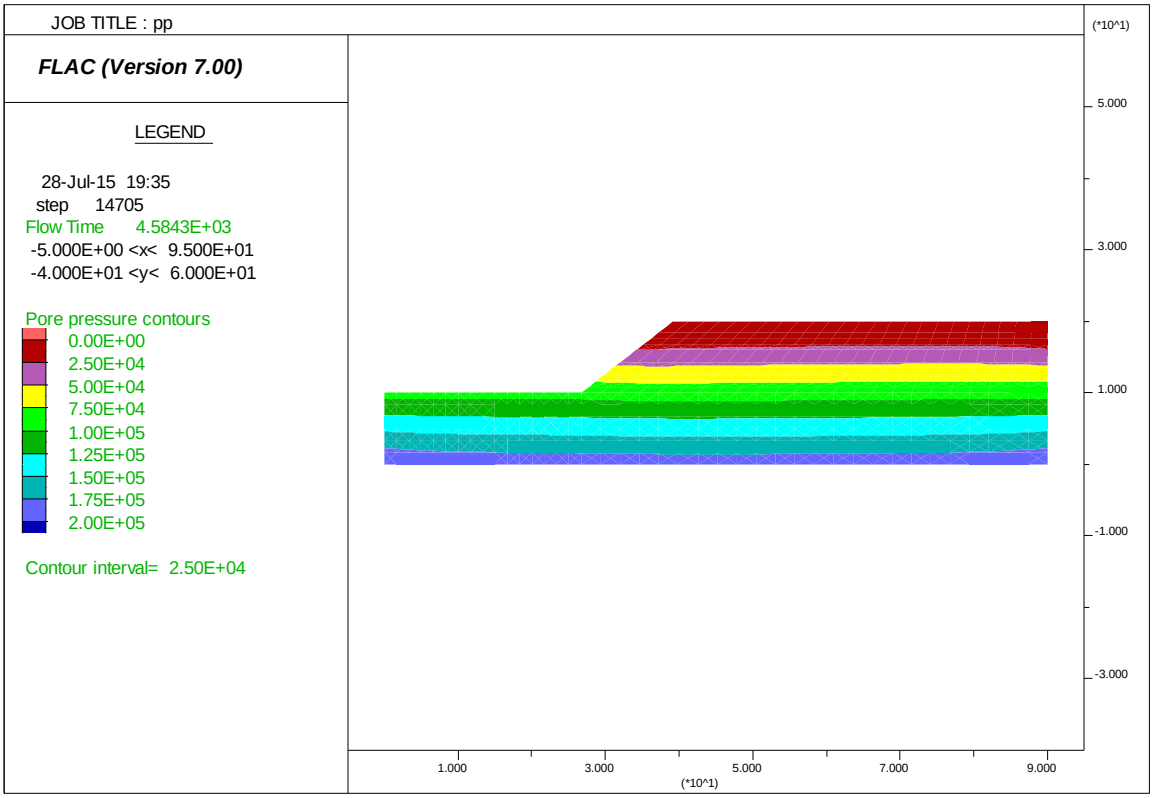


Figure 6.53 Plot of pore-pressure contours showing equilibrium (steady state condition)

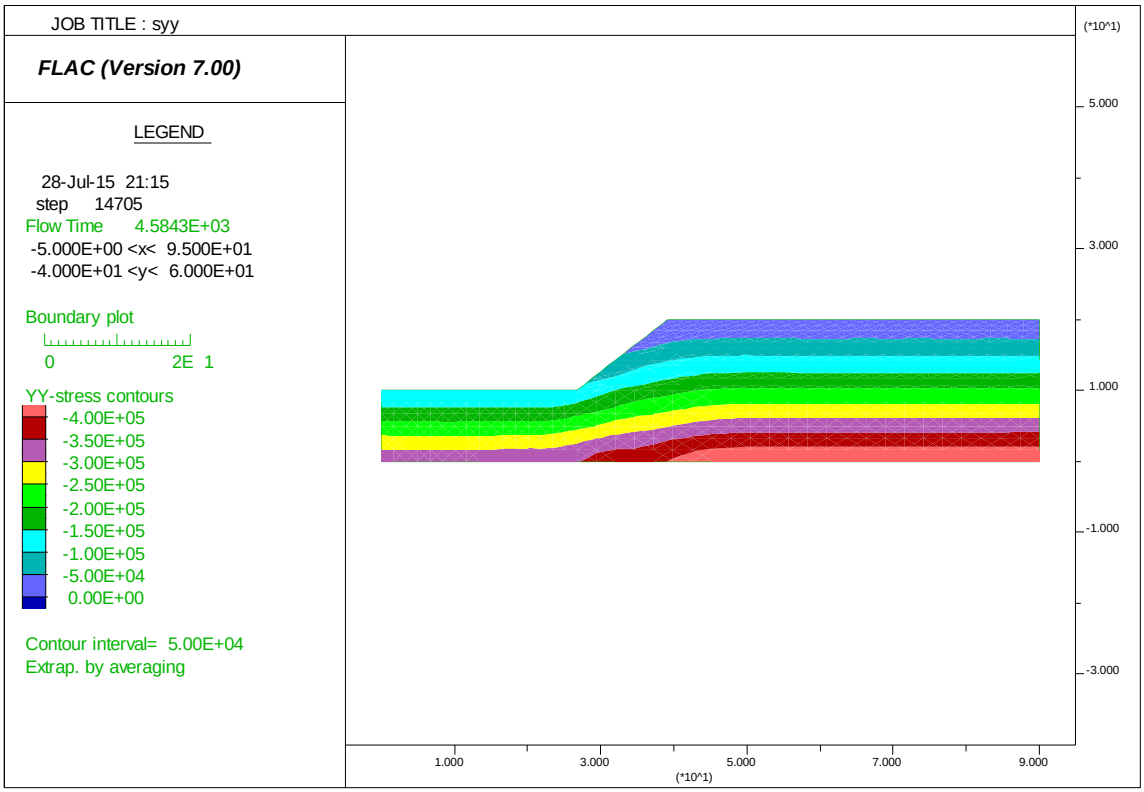


Figure 6.54 Plot of contours of vertical stress showing equilibrium (gradual distribution)

6.12.3. Elastic un-damped simulation

Preliminary elastic un-damped model runs are carried out to evaluate the effects of model boundary conditions and to estimate the maximum level of cyclic shear strains and extent of plastic failure. Two types of preliminary runs are made; un-damped elastic material analysis to estimate shear strains and velocity levels in the entire model and un-damped Mohr-Coulomb material runs to estimate the approximate extent of plastic failure. These runs are made with the dynamic option activated and applying the mining induced ground motion, Figure 6.55. Free-field boundaries are applied on the sides of the model and quiet-boundaries are applied at the base of the model.

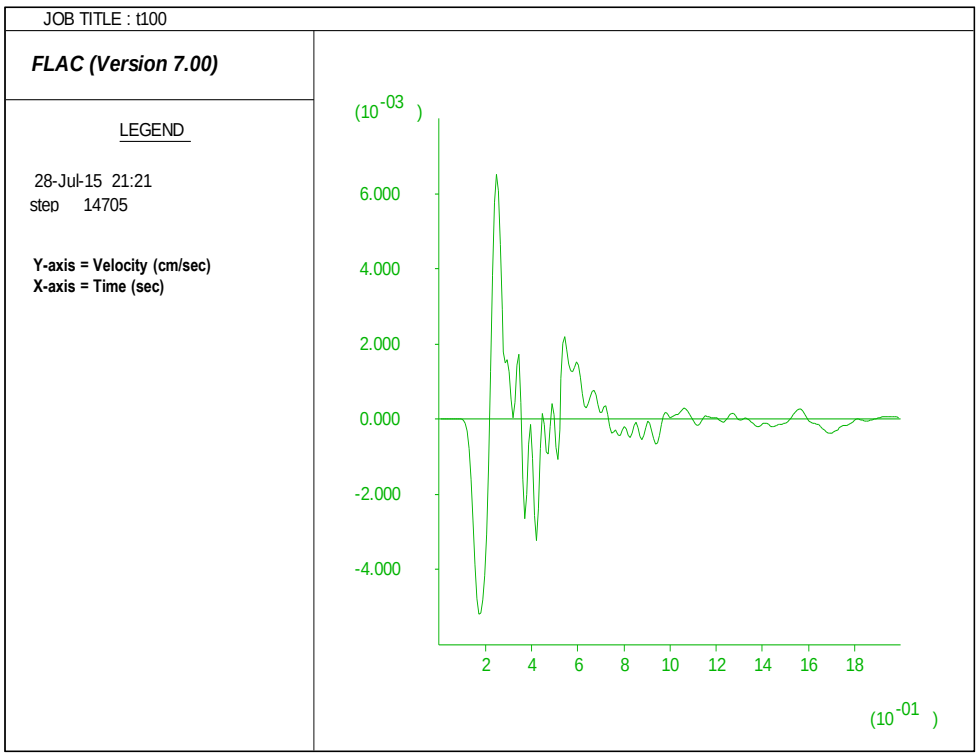


Figure 6.55 Input ground motion (velocity time history)

In view of the quiet boundaries applied at the base, the input ground motion has to be applied in the form of shear stress wave history, Itasca (2014). According to Itasca (2014), the velocity history is converted to stress history using Equation 6.1.

$$\sigma_s = factor\ x\ (\rho\ C_s)\ v_s, \qquad \text{Equation 6.1}$$

Where σ_s = applied shear stress, ρ = mass density of the material at the boundary, C_s = speed of s-wave propagation through the medium at the boundary, v_s = input shear particle velocity (Figure 6.55).

A *factor* of 2 is normally used to account for the input energy dividing into upward and downward propagating waves, Itasca (2014). Maximum shear strain contours as a result of un-damped and elastic material simulations are shown in Figure 6.56. It is evident that the maximum elastic strains are very small in magnitude in the entire model. For low levels of strains, hysteric damping is appropriate for use for soils with the dynamic characteristics, Itasca (2014).

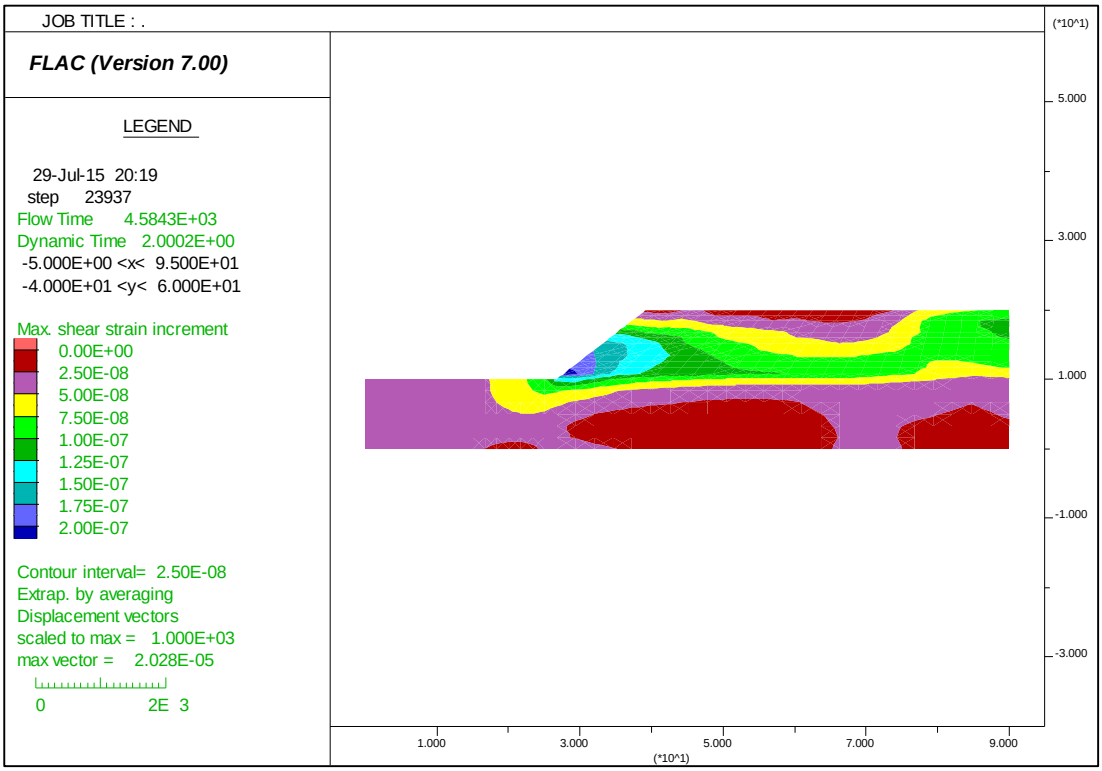


Figure 6.56 Maximum shear strain contours during un-damped and elastic material

6.12.4. Damped Mohr-Coulomb simulation assuming no liquefaction

In this stage, simulation is made using the Mohr-Coulomb model and hysteric damping to represent dynamic characteristics of the upper two layers of the tailings dam slope. The FLAC default hysteric damping parameters described in Figure 3.9 and Figure 3.10 are used in the simulation. In this stage, simulation is made considering the Mohr-Coulomb constitutive model assuming no

liquefaction occurs in the upper two soil layers. The maximum shear strain contours shown in Figure 6.57 are not very different from those observed in the un-damped simulation. The magnitude of strain levels is very low and reveals that the possibility of liquefaction is very low.

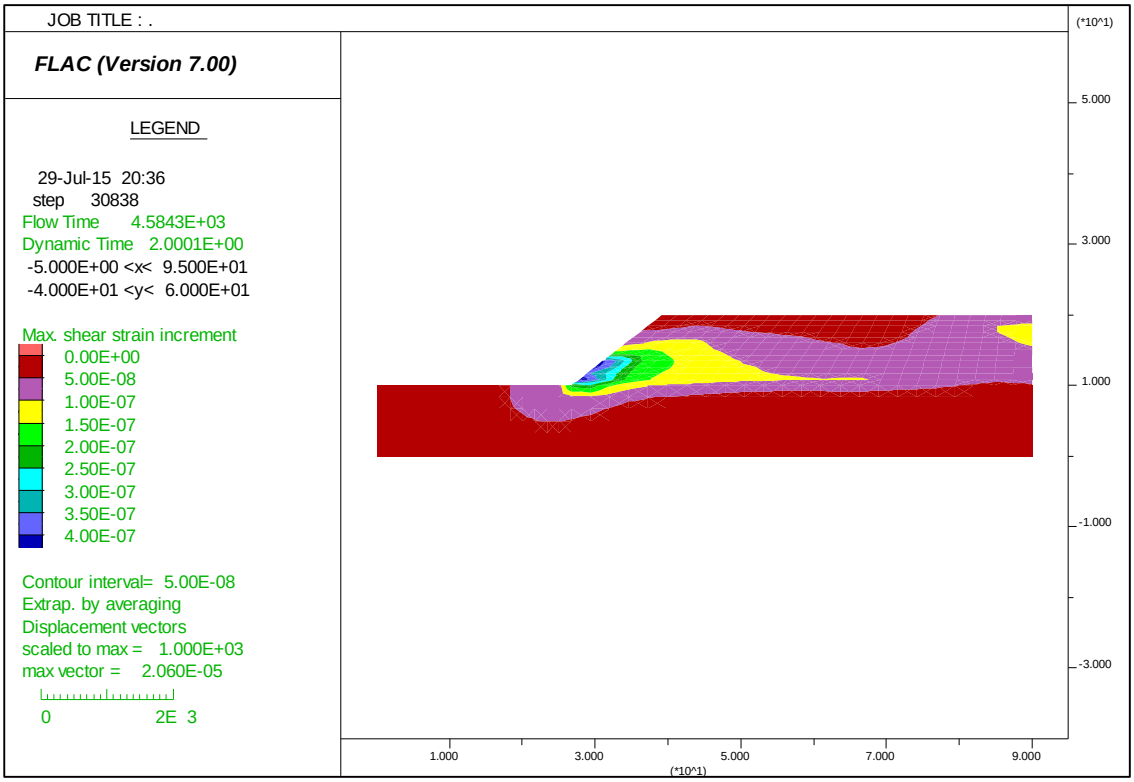


Figure 6.57 Maximum shear strain contours; damped Mohr Coulomb simulation

6.12.5. Finn-Byrne simulation

In this stage, simulation is made with the Finn-Byrne constitutive model assuming liquefaction can occur in the model. The constitutive models for the upper two layers is changed from Mohr-Coulomb to the Finn-Byrne Model. Dynamic boundary conditions and loading are applied in the same manner as described in the previous section. A normalized SPT (standard penetration test) value of 10 is prescribed for the upper two soil layers to represent potential for liquefaction, Itasca (2014). Maximum shear strain contours shown in Figure 6.58 observed in the Finn-Byrne simulation are very small and do not show any plastic failure or liquefaction. Also, smooth pore pressure contours are shown in Figure 6.59. Since plastic strain is not observed, further details on liquefaction phenomenon are not discussed.

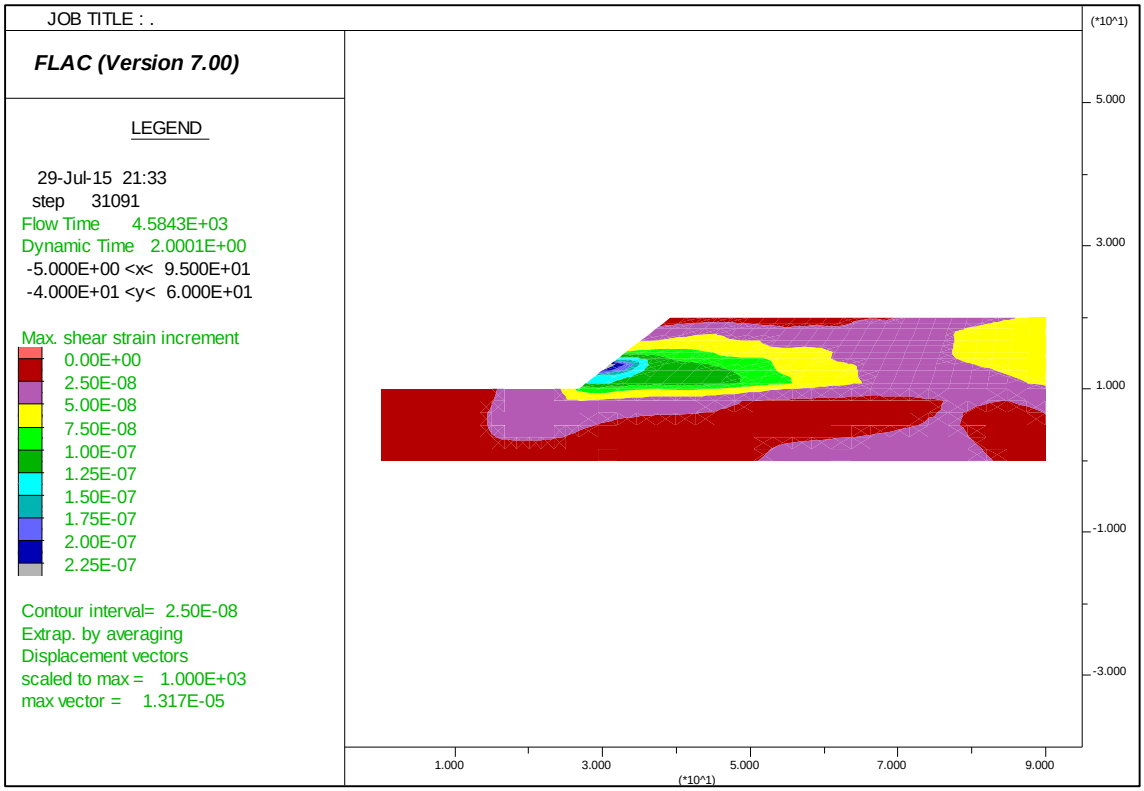


Figure 6.58 Maximum shear strain contours; damped Finn-Byrne model

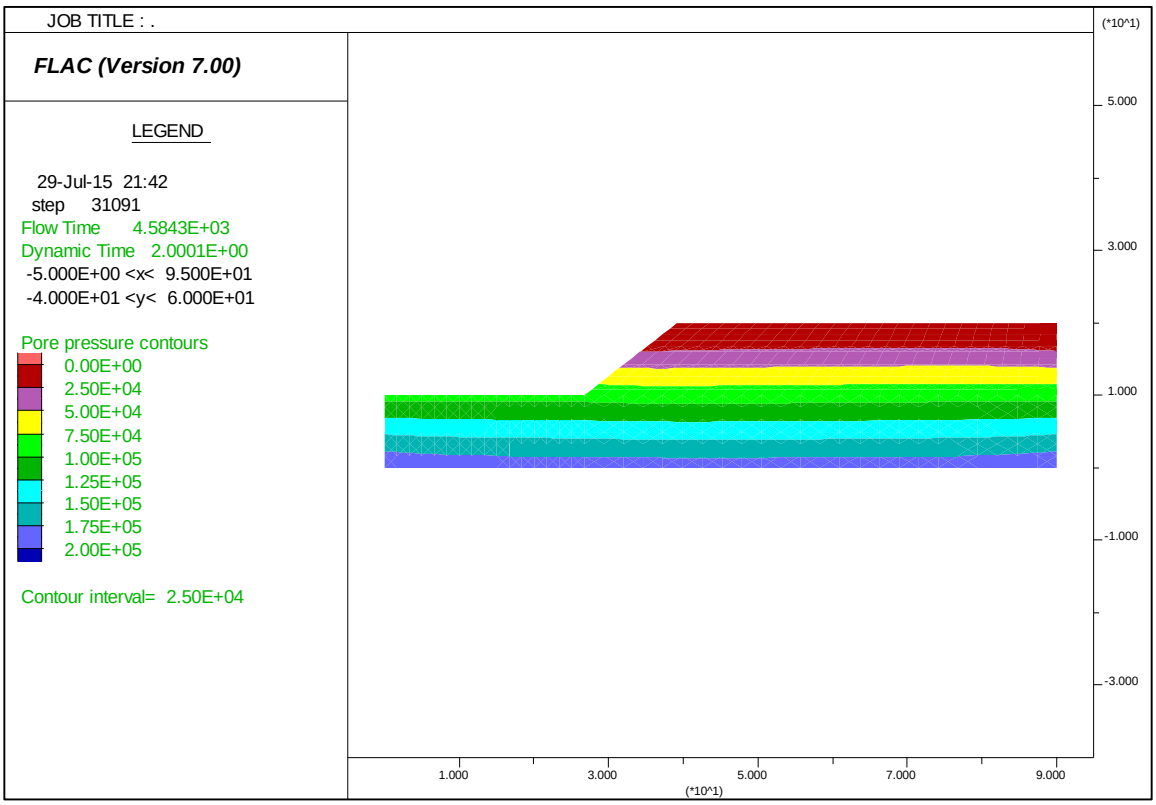


Figure 6.59 Pore-pressure contours; gradual gradients show no signs of plastic deformation/liquefaction

6.13. Dynamic Analysis to Evaluate Stability a Soil Slope using FLAC

6.13.1. Model size, geometry and properties

A 2D seismic analysis using FLAC of a soil slope is performed to evaluate its stability against dynamic loading of mining induced ground motion. The slope comprises frictional material (sandy silt) of two layers. The slope geometry and properties considered for the analysis are given in Figure 6.60 and Table 6.13. The analysis is performed to evaluate the factor of safety under static conditions and under dynamic loading of mining induced ground motion.

2D seismic simulation is performed in four stages; initial equilibrium, evaluation of factor of safety under static conditions, setting-up of dynamic loading and boundary conditions and finally evaluation of factor of safety under mining induced ground motion.

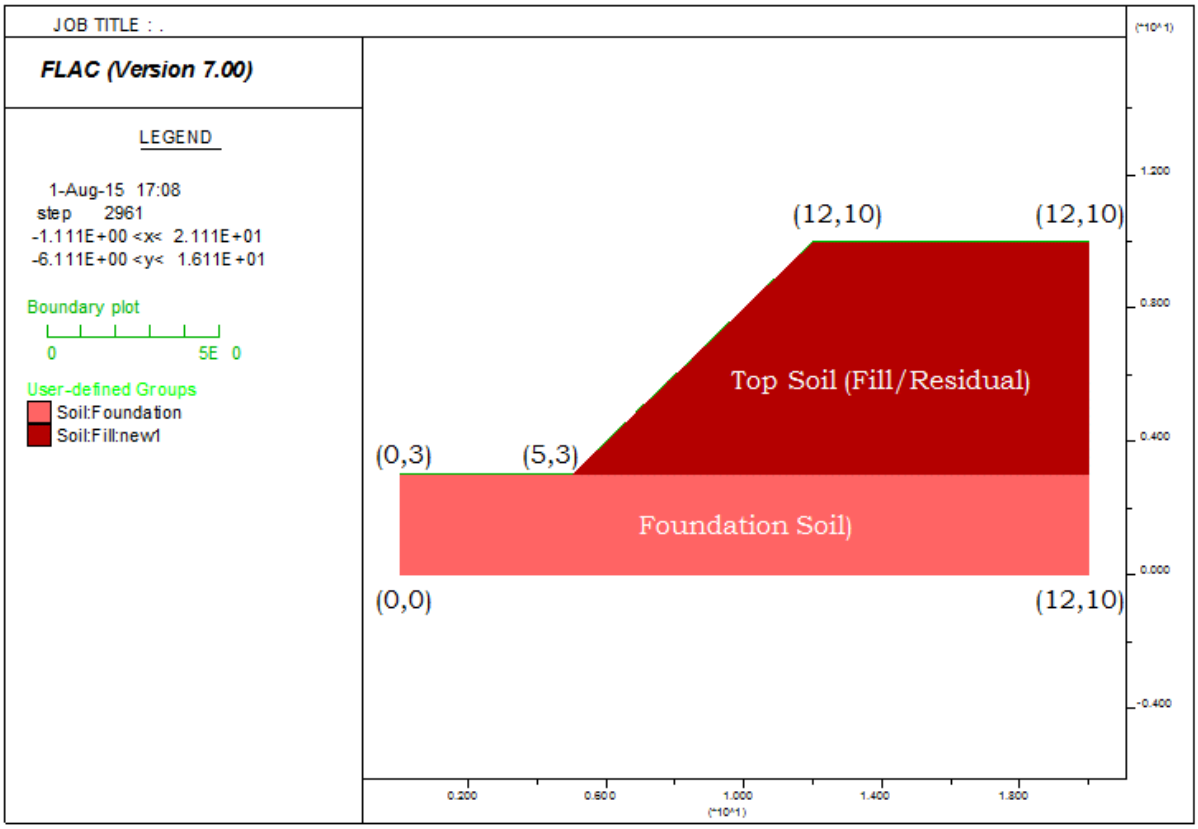


Figure 6.60 Slope geometry

Table 6.13 Material properties of the soil slope

Property	**Top Soil** Sandy Silt	**Foundation** Clayey Sandy Silt
Density (kN/m^3)	1600	1600
Bulk Modulus (MPa)	1.7e8	1.7e8
Shear Modulus (MPa)	1e8	1e8
Angle of Internal Friction (Degrees)	35	40
Cohesion (Pa)	10000	20000

6.13.2. Initial static equilibrium

In this stage, the geometry is set up, material properties assigned, side boundaries fixed along the x-direction, base fixed in both x and y extents and the model is run to establish initial equilibrium under gravity, Figure 6.61 and Figure 6.62. The elastic model is considered for the foundation soil and the Mohr Coulomb model for the top soil.

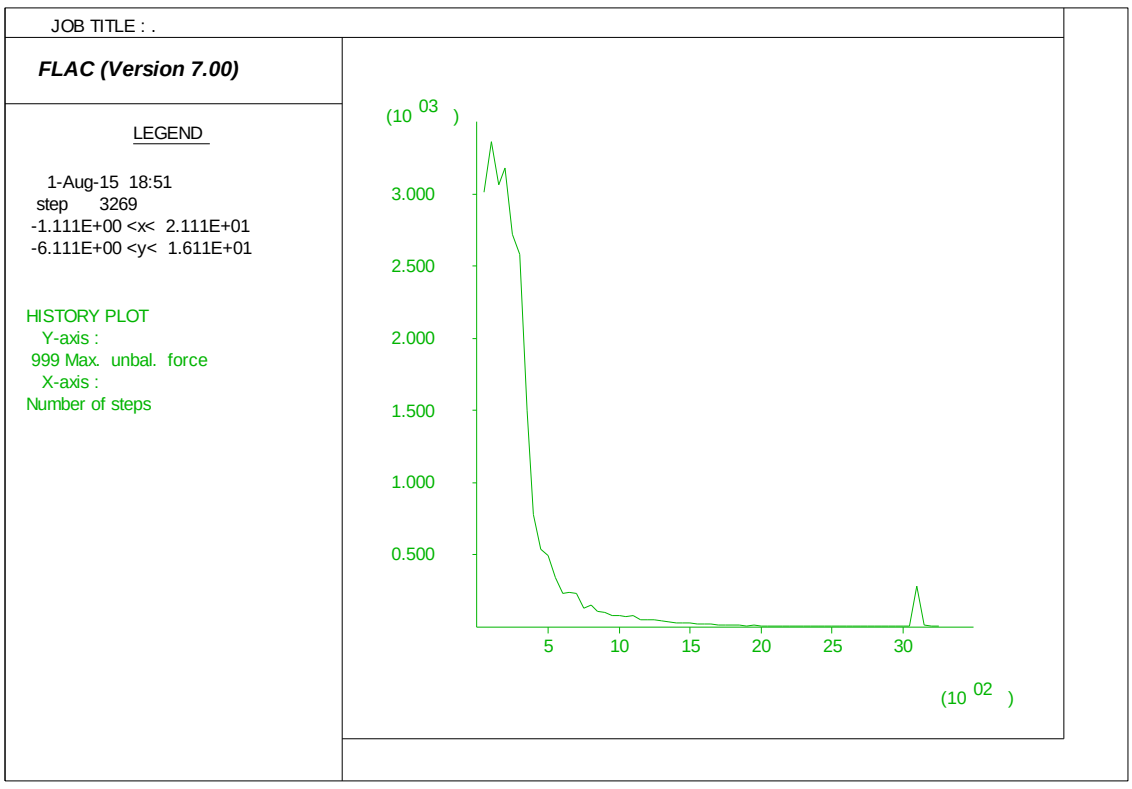


Figure 6.61 Plot of unbalanced force; initial static equilibrium

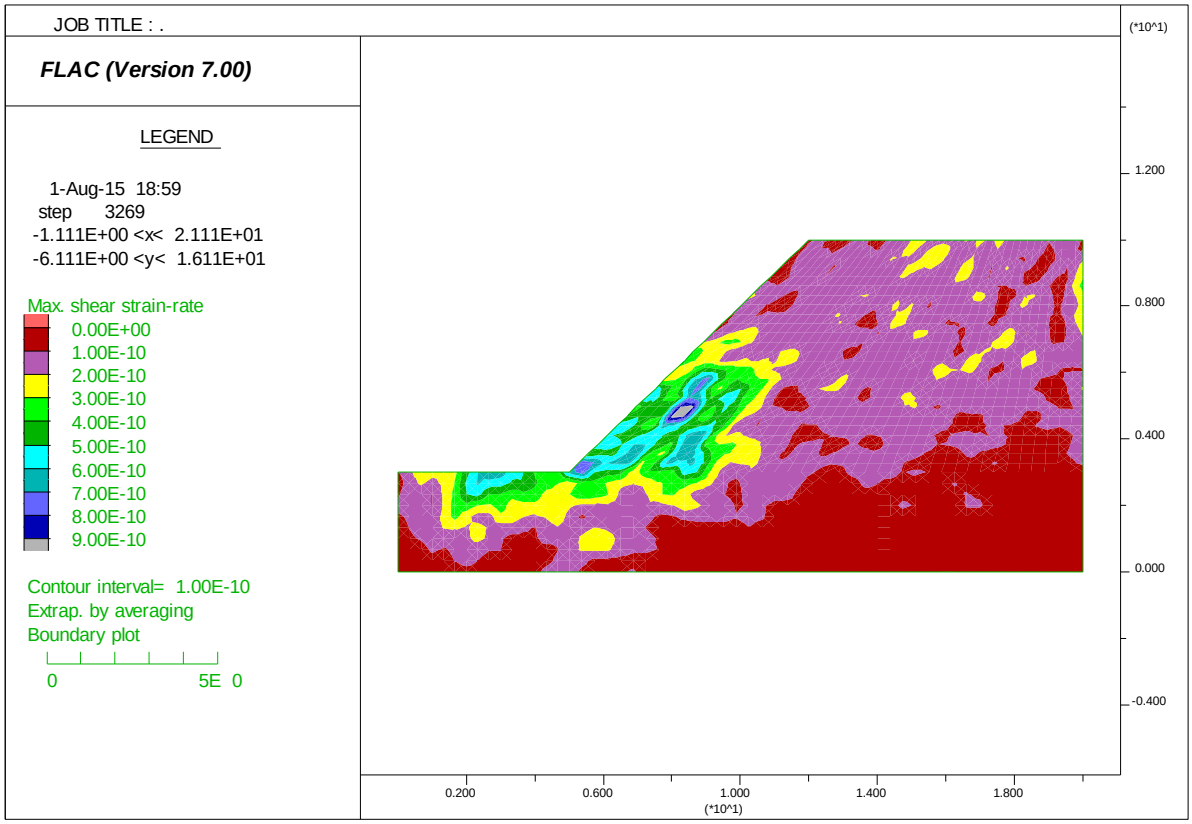


Figure 6.62 Plot of shear strain contours showing elastic strain range

6.13.3. Factor of safety under static conditions

The slope is analyzed for factor of safety under static conditions. The plot of unbalanced force shown in Figure 6.63 and of horizontal displacement shown in Figure 6.64 indicate that the model is still in equilibrium after the simulation for factor of safety. The plot of shear strain contours in Figure 6.65 show that the magnitude of strains is very low and in the elastic range. A factor of safety of 1.62 and plot of plasticity state (inelastic deformation) is shown in Figure 6.66. The plot of shear strains and plasticity state reveal the possible failure mechanism of the slope.

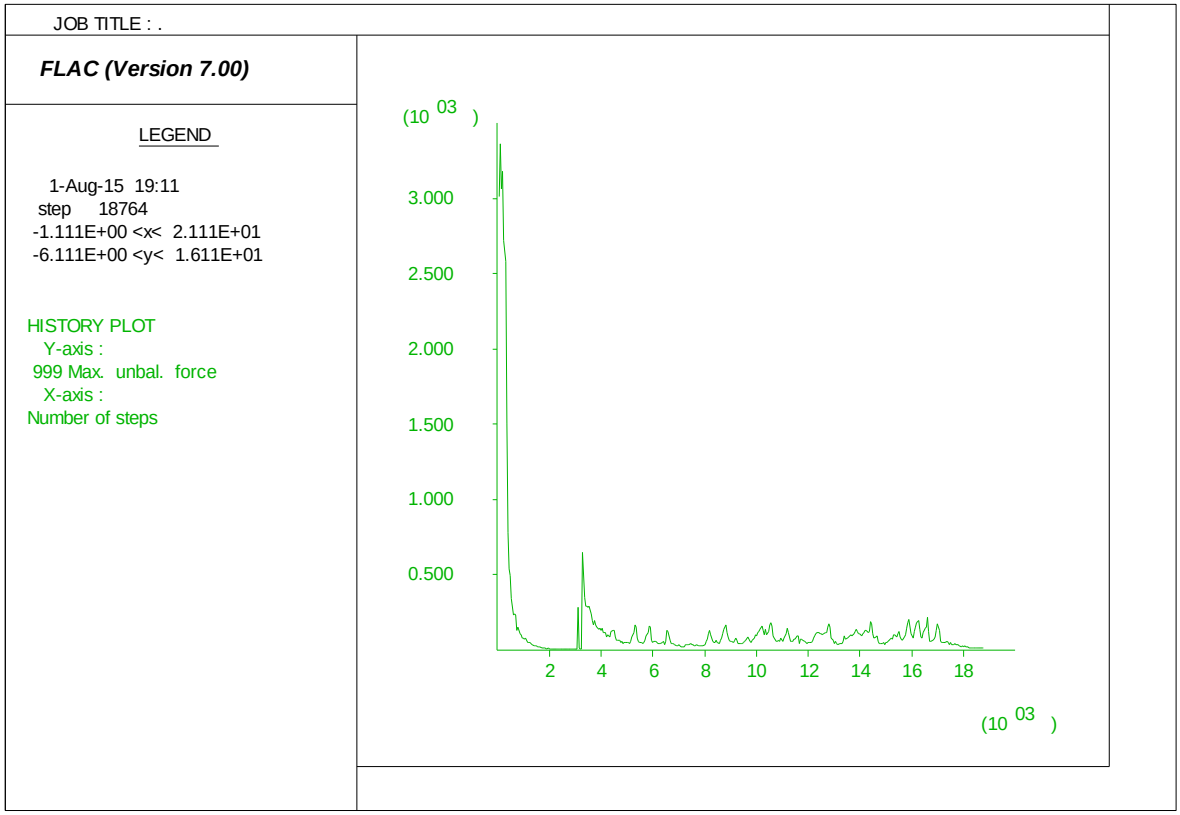


Figure 6.63 Plot of unbalanced force

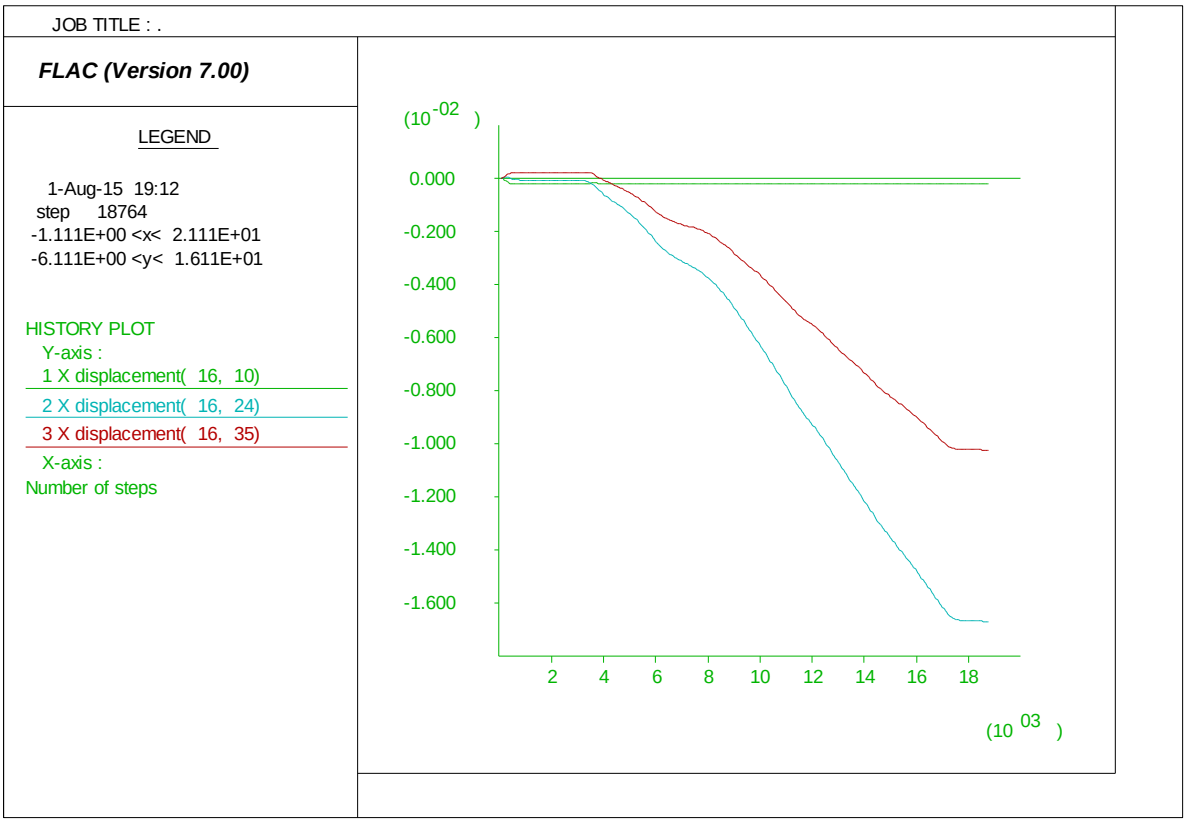


Figure 6.64 Plot of x-displacement histories

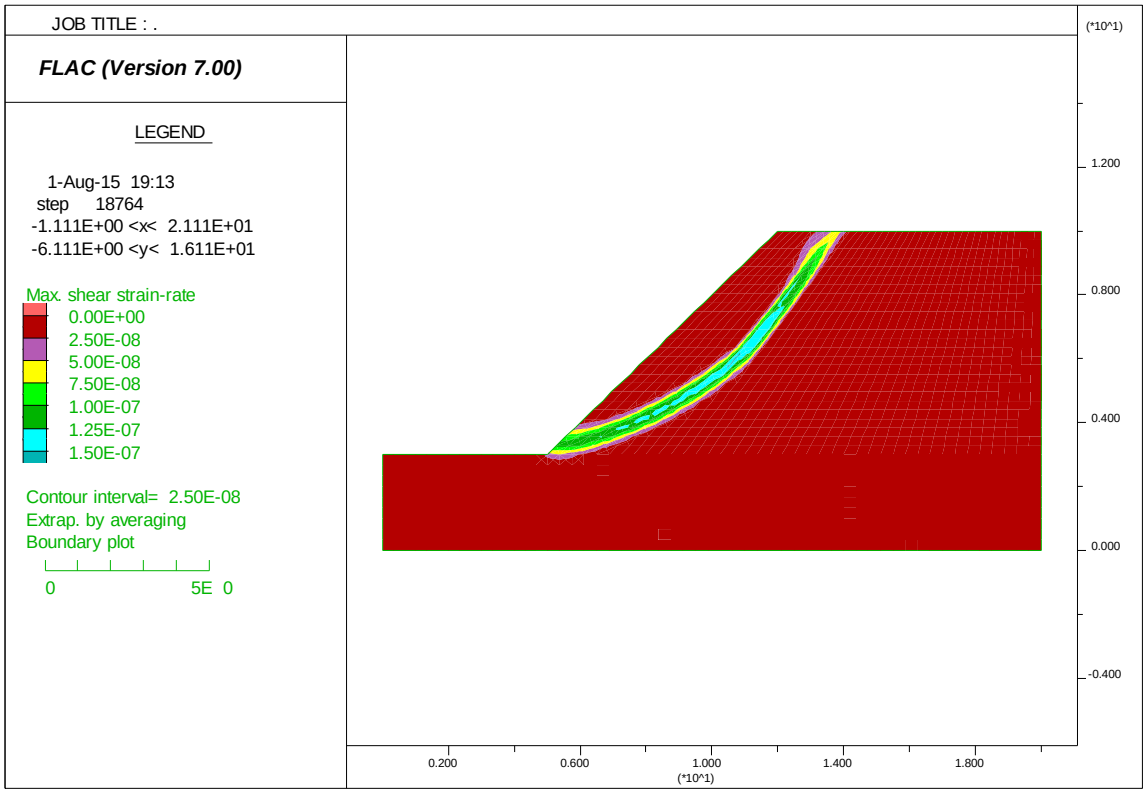


Figure 6.65 Plot of shear strain contours

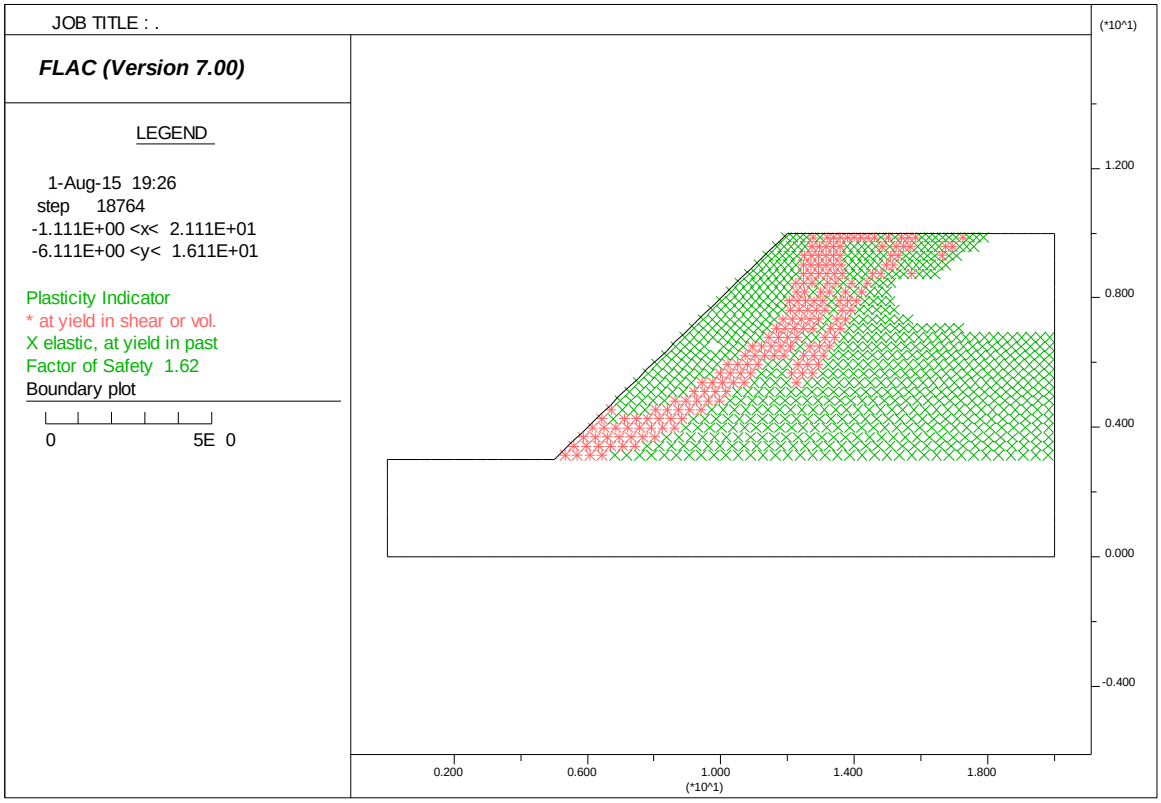


Figure 6.66 Plot of plasticity indicator and factor of safety

6.13.4. Dynamic loading and boundary conditions

For the dynamic analysis of the slope, boundary conditions are re-defined. Free-field boundaries are applied on the sides to absorb the wave reflection, Itasca (2014). The sides of the model which were fixed during the static analysis, are freed before the dynamic loading is applied. The dynamic loading is applied in the form of velocity time history along the base of the model. Also, the base of the model is prevented from moving by applying zero velocity at the base.

At the end of the dynamic loading for a period of 2 sec, the plot of x-displacement (Figure 6.67) and y-displacement (Figure 6.68) indicate a maximum x-displacement of 12.50 mm and maximum y-displacement of 10 mm along the slope crest. According to Koo et al. (2013), a slope experiencing a displacement in excess of 70 mm due to a dynamic loading is usually considered at a significant risk of failure. ASCE/SCEC (2002) recommends a maximum threshold of 50 mm displacement for typical slopes to avoid a risk of failure.

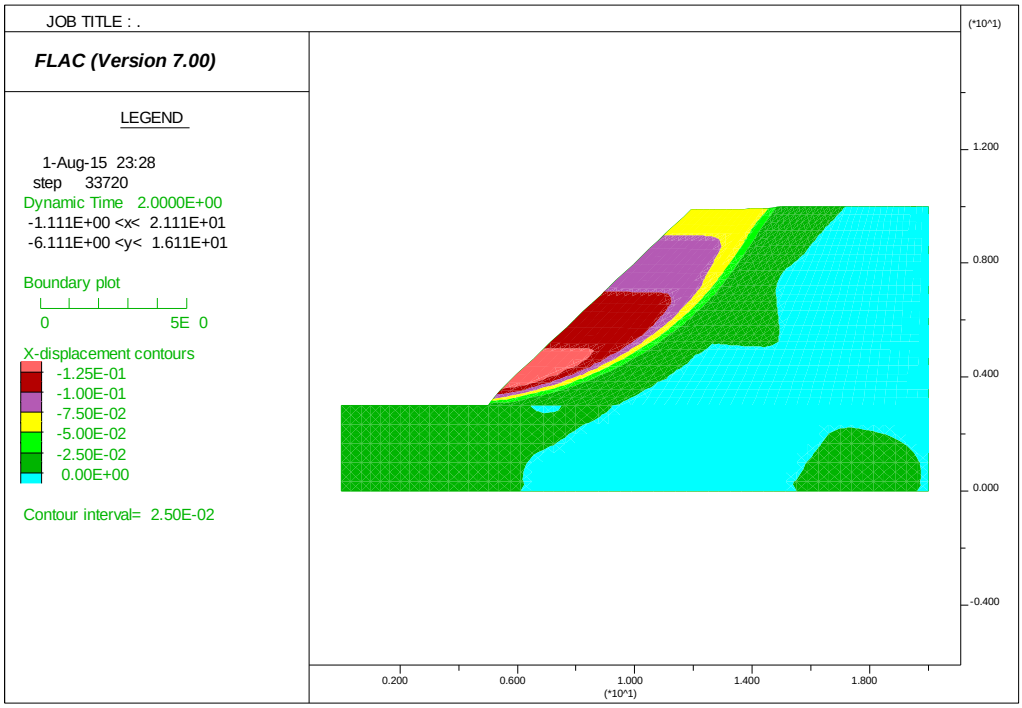


Figure 6.67 Plot of x-displacement contours

Since displacements observed in the slope due to mining induced ground motion are very small, it is deduced that the stability of a soil slope with characteristics similar to those considered for analysis is not at a risk. The plot of plasticity

indicators shown in Figure 6.69, agrees well with the possible failure mechanism revealed in the static analysis.

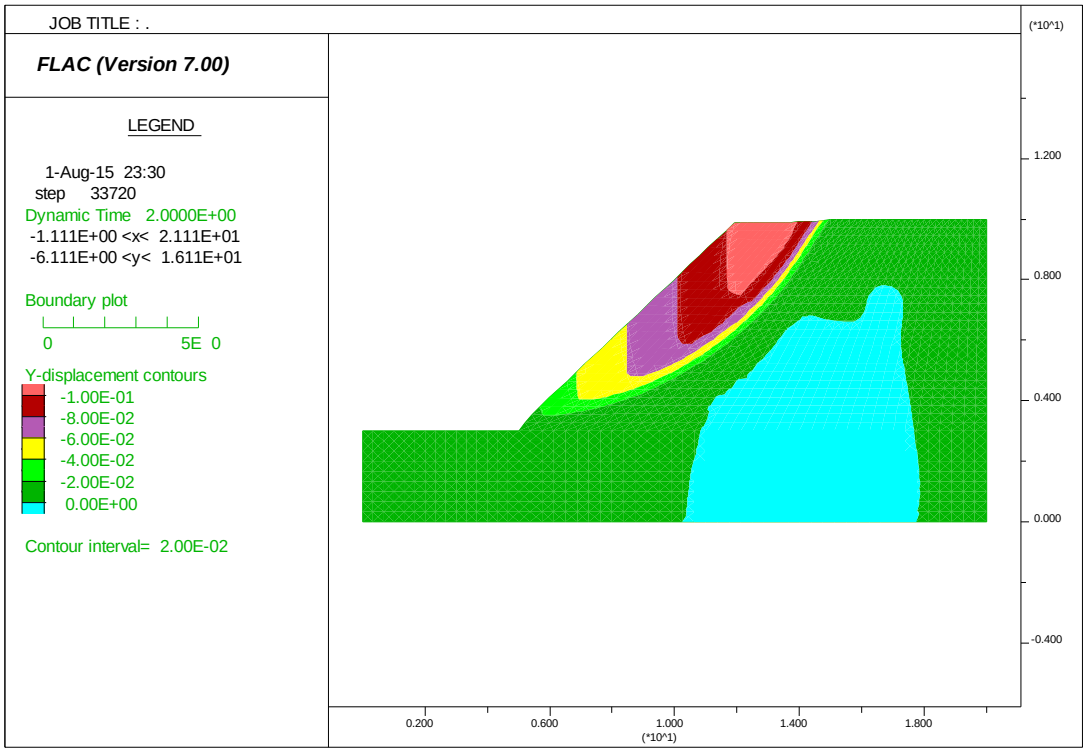


Figure 6.68 Plot of y-displacement contours

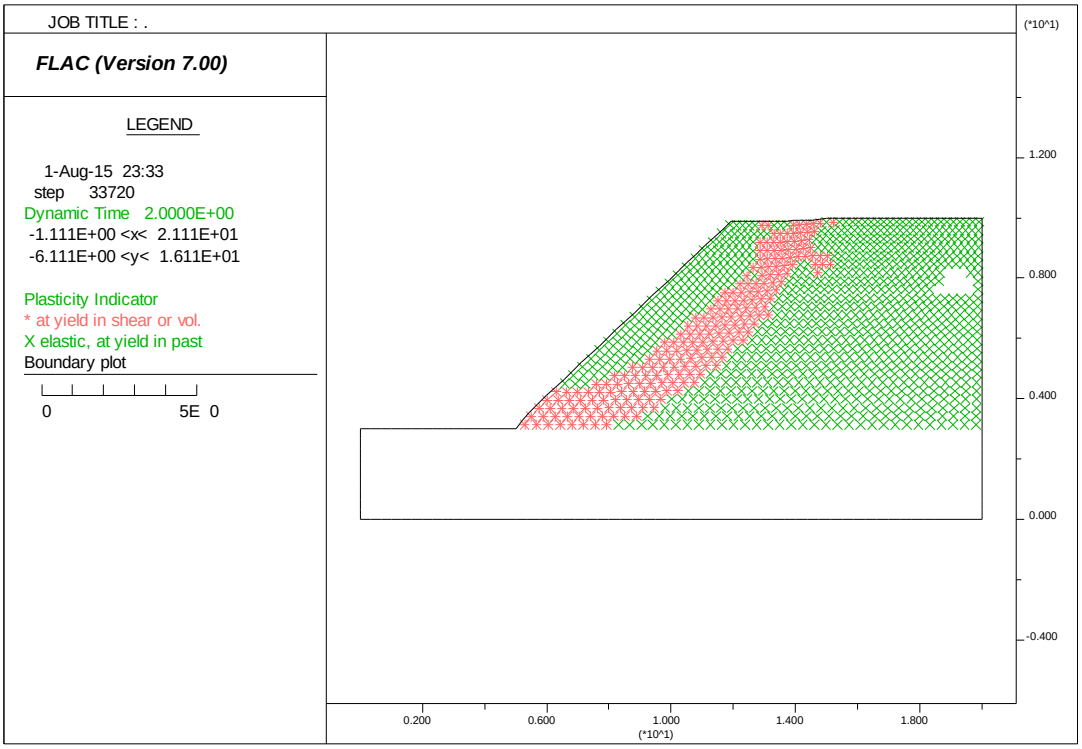


Figure 6.69 Plot of plasticity indicators

6.14. Dynamic Analysis to Evaluate Stability of a Rock Block with a Confined Joint

6.14.1. Model size, geometry and properties

Potential risk to the rock block with slipping joints (and/or faults) is evaluated under the estimated ground motion from mining induced seismicity. A 3D rock block with enclosed and inclined joint which extends along the entire length of the block (along y-axis) is considered for the dynamic analysis. The geometry of the block and joints is shown in Figures 6.70 and 6.71 respectively.

The rock block is considered linearly elastic, homogenous and isotropic. Three joints are considered in the block; a confined joint dipping at 60º and the other dipping at 20º, as shown in Figure 6.71 and two other joints dipping at 60º. The confined joint extends through the entire block along the y-axis. Stability of the rock block is evaluated under dynamic loading evaluated due to mining induced seismic event. The analysis is performed in two stages; static and dynamic. The rock and joint (all) properties are given in Table 6.14.

Table 6.14 Material and joint properties of rock block with a confined joint

Property	Value
Density (kN/m^3)	3000
Bulk modulus (GPa)	34e9
Shear modulus (Pa)	26e9
Joint normal stiffness (N/m)	2e11
Joint shear stiffness (N/m)	2e11
Joint friction (degrees)	40º
Joint Cohesion (Pa)	10e6
Insitu stresses, σ_{xx}, σ_{yy}, σ_{zz} (GPa)	-60e6, -60e6, -81e6

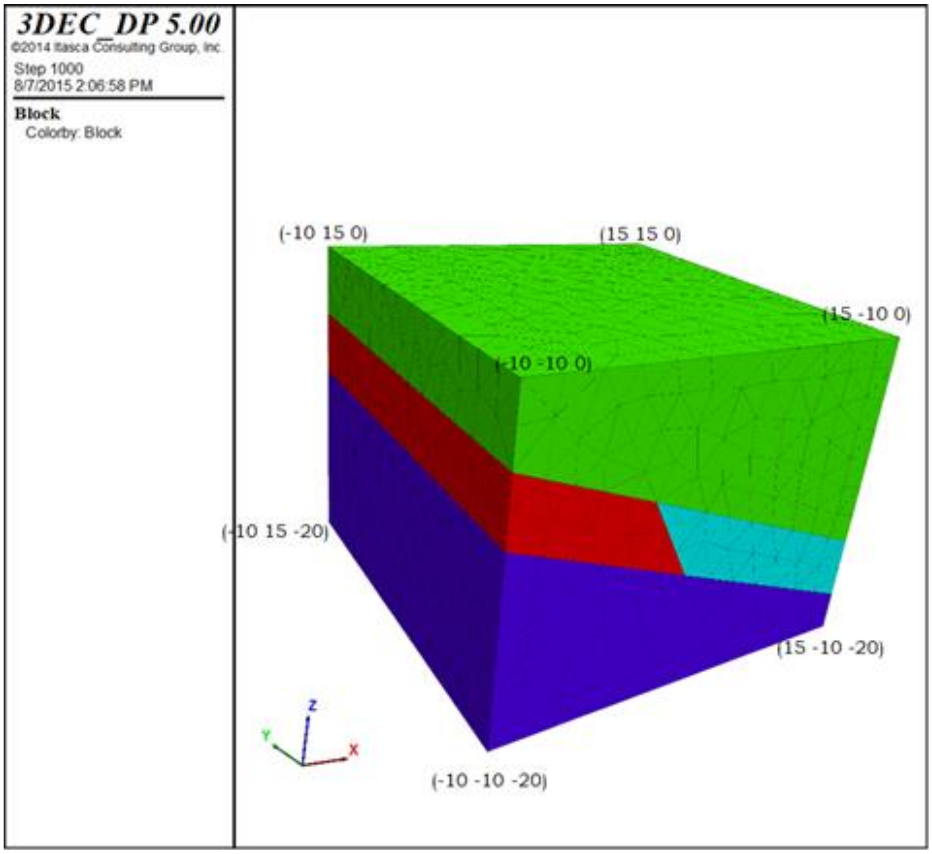


Figure 6.70 Geometry of the rock block

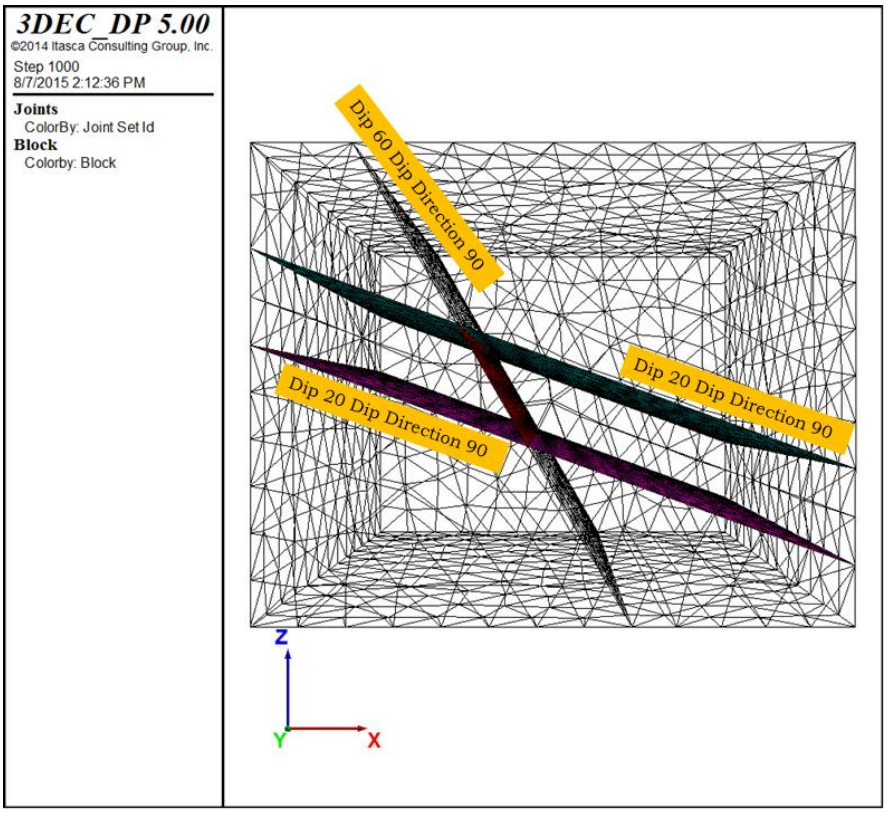


Figure 6.71 Location and orientation of the joints

6.14.2. Initial static equilibrium

A static analysis is performed for 1000 steps to bring the model to equilibrium under insitu stresses. At the end of the static analysis, the plot of joint shear displacement is shown in Figure 6.72. No appreciable joint shear displacement is observed along any of the joints.

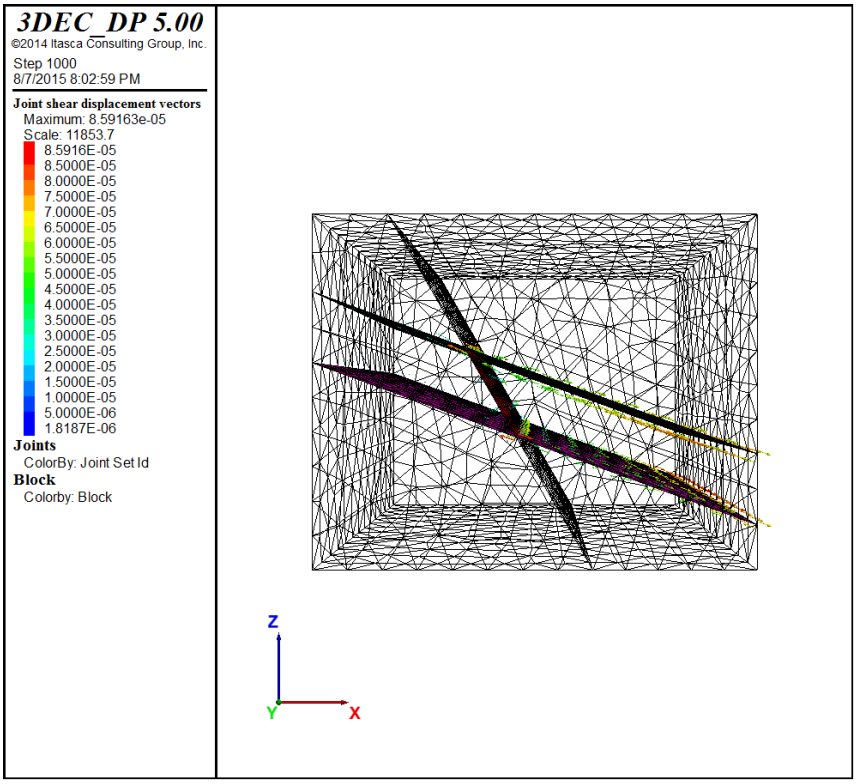


Figure 6.72 Joint shear displacement at the end of static simulation

6.14.3. Dynamic simulations

The dynamic simulation was made for 1000 steps. Stresses from the static analysis are removed from the model boundaries and dynamic boundaries are applied prior to dynamic simulation. At the end of the dynamic simulation, joint shear displacement of 9 mm is observed as shown in Figure 6.73. The seismic simulation shows that the considered dynamic loading when applied to a rock block with properties and joints as considered results in small shear displacement.

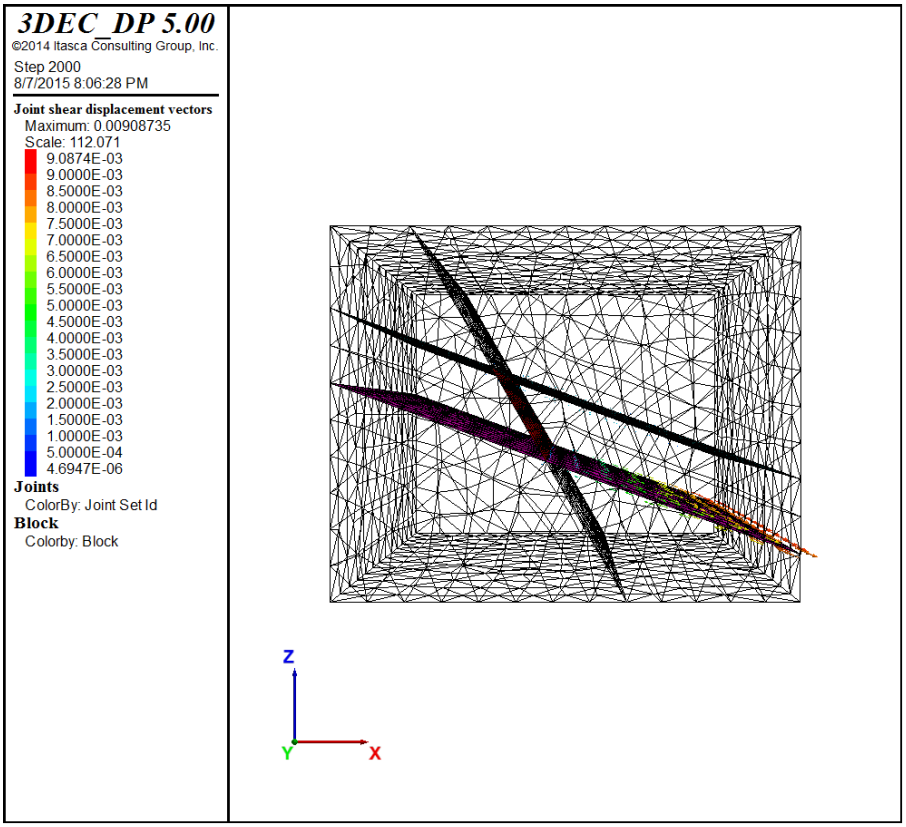


Figure 6.73 Joint shear displacement at the end of the dynamic simulation

6.15. Conclusion

This chapter analyzed the stability of certain surface structures due to dynamic loading by the selected mining induced ground motion (evaluated in Chapter 5). The conclusions of these analyses are given in Table 6.15.

Table 6.15 Drift (horizontal displacement of structures)

Type of Structure	Drift (horizontal displacement)
2 storey masonry building	53 mm
2 storey concrete building	0.90 mm
4 storey concrete building	0.90 mm
8 storey concrete building	2.67 mm

- The horizontal displacement vectors (absolute magnitude) of the two storey masonry, two, four and eight storey concrete buildings are 53 mm, 0.90 mm, 0.90 mm and 2.67 mm respectively.

- The x-displacements of the two storey masonry, two, four and eight storey concrete buildings are 19.76 mm, 1.30 mm, 1.10 mm and 0.90 mm respectively.
- The displacements of the buildings evaluated during the dynamic analysis, are plotted on the *Spectral Acceleration-Spectral Displacement* chart proposed by Searer et al. (2004) to assess their respective risk (shown with red ellipse in Figure 6.74). This region is well below the critical curves (black and brown) proposed by various Universal Building Codes (UBC). It is therefore not likely that the considered ground motion will pose risk to the buildings, unless otherwise evaluated in terms of more site specific geomechanical data.

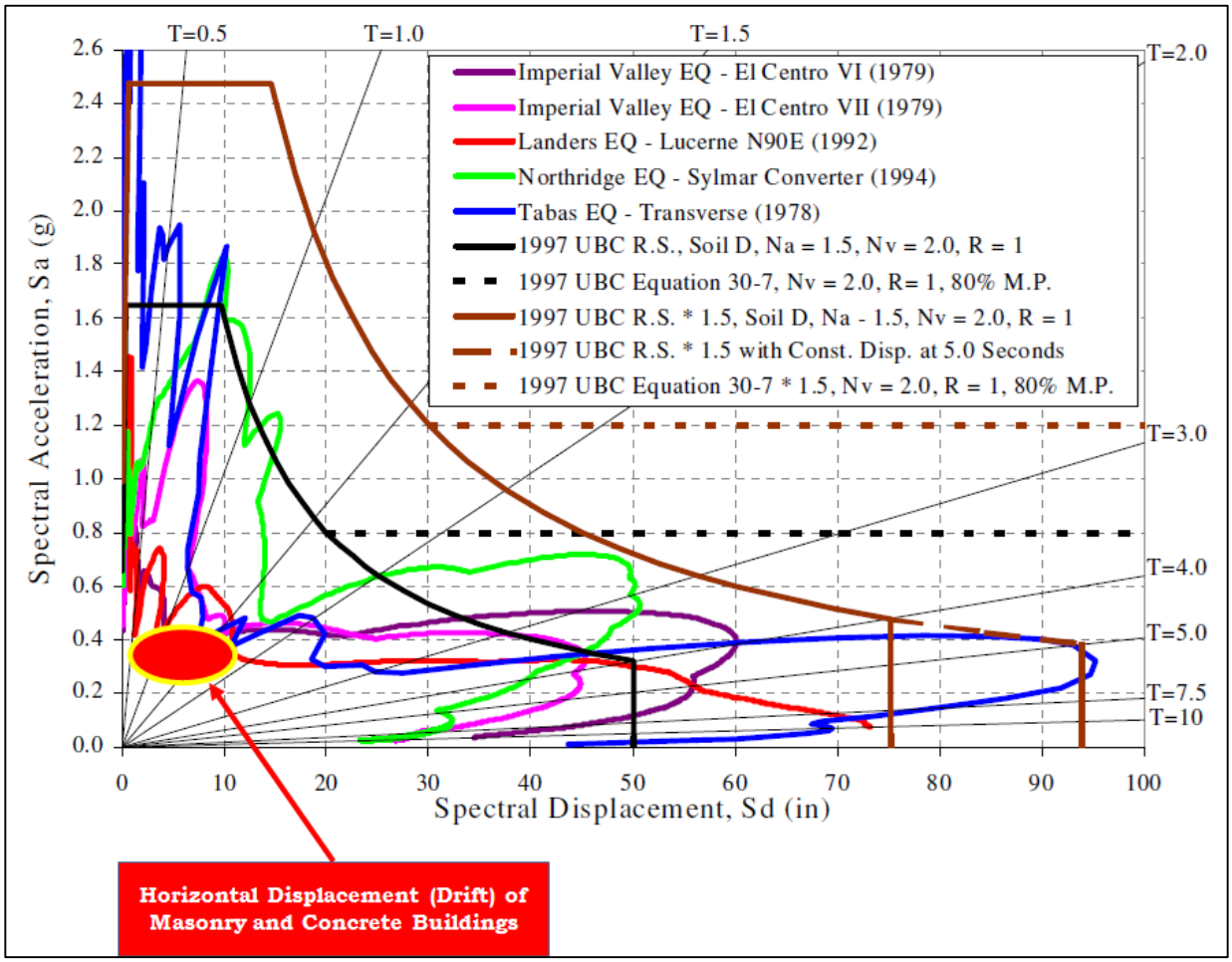


Figure 6.74 Horizontal displacements compared to "*Spectral Acceleration-Spectral Displacement*, Searer et al. (2004)"

- The selected ground motion induces minor deformations in the soil slope and jointed rock slope and is not likely to pose any significant risk to their stability.
- The selected ground motion induces minor displacements in the tailings dam slope and is not likely to pose risk of liquefaction.
- The dynamic analysis of a rock block with confined joint produces a shear displacement of 9 mm which poses a danger with respect to the stability of slipping joints
- The findings of these analyses pertain to the geomechanical parameters and ground motion considered for this research. For all other sets of parameters, fresh dynamic analyses are required.

The next chapter; Conclusions and Recommendations, covers the findings, conclusions and recommendations of the research. The recommendations also include a way forward to refine the evaluation of mining induced seismicity and its effects on the surface structures.

7. CONCLUSIONS AND RECOMMENDATIONS

7.1. General

This research was carried out to evaluate mining-induced seismicity and its effects on selected surface structures in the CBD area, Central Rand. The research commenced with a review of the existing geomechanical conditions. The 3DEC numerical code was used for numerical simulation for three source mechanisms namely Impulsive Slip, Fall of Ground, and Pillar Collapse. The research showed that it was possible to numerically simulate the seismic scenarios under dry and flooded mining voids. The capability of 3DEC to artificially generate seismic events of varying magnitudes was found to be useful to enhance understanding of mining-related seismicity. Using 3DEC, the estimation of ground motions in terms of time histories was an added capability which allowed a more realistic evaluation of the performance of surface structures.

7.2. Key Findings of the Research

Key findings of this thesis were summarized as follows:

- 3DEC was an appropriate tool to study mining-induced ground motions. It could accommodate the geomechanical parameters (including flooding of voids) and helped to estimate the ground motions.
- 3DEC allowed the study of three-dimensional seismic wave transmission through a complex medium comprising intact rock, discontinuities and mining voids (partially/fully voided).
- Ground motions generated due to impulsive slip and fall of ground were characterized by two peaks, whereas those generated due to pillar collapse were characterized by a single peak. This finding emphasized the importance of using ground motion in terms of time histories for the seismic structural analysis.
- 3DEC and FLAC were suitable codes for the study of foundation soil/rock-structure-interaction using ground motions in terms of time histories.
- It was possible to numerically study the source mechanism, generate seismic events of the desired magnitude and intensity in order to evaluate its effects on the candidate structure.

- Using 3DEC, it was also possible to study the slip potential of a discontinuity (fault, joint, etc.) and its seismic potential due to a perceived natural or mining-induced earthquake.
- The general effect of flooding in abandoned mines manifested in lowering the peaks of ground motions in all the source mechanisms in a complex pattern (Figure 5.61). For example, in case of impulsive slip along a wet joint, the peak reduced by around 35% (reduced from 10.10 mm/sec to 6.50 mm/sec) in the hanging walls, whereas it was different for the Main Reef and foot wall.
- The magnitude of decrease in the peaks was non-uniform, different in all the three cases and also different at various points in each geological group, Figure 5.61.
- The flooding phenomenon also changed the nature of the waveforms in all three cases of source mechanism, Figure 5.61.
- The fact that flooding resulted in lowering of the ground motion peaks, did not mean the influence of flooding was not detrimental. Instabilities caused by flooding in the form of weathering of rock mass/pillars, decay of wooden supports and lubrication of discontinuities should be considered. This rheological (adverse) process of the flooding was not part of the study.
- The ground motions estimated in the study were conservative in view of the elastic constitutive material model and planar nature of discontinuities considered in the model.
- Bearing in mind the conservative nature of the study, ground motions estimated in the flooded conditions were used for the seismic structural analysis, Figure 5.61.
- Seismic parameters of the seismic event of the magnitude M_L 2.5 to 4.0 caused by impulsive slip (since the likelihood of a large volume of fall of ground or collapse of large number of pillars is less likely) estimated in the hanging wall, Main Reef and foot wall were given as:
  - Ground motion (velocity time history) 2 to 6 mm/sec
  - Duration of the event 0.5 to 2.0 sec
  - Frequency 8 to 12 Hz
  - These parameters were relevant to the geomechanical properties considered for the study.

- The effect of the ground motion used for the dynamic structural analysis on different structures and slopes (analysed with respective properties) was given as follows (as explained in para 6.15 and Figure 6.74):
  - Stability of two-storey masonry building was affected to some extent.
  - Stability of the two-storey concrete building was not affected.
  - Stability of a four-storey concrete building was not affected.
  - Stability of an eight storey concrete building was not affected.
  - Liquefaction of a tailing dam slope was not likely.
  - Stability of a jointed rock slope with building load at its crest was not affected.
  - Stability of a soil slope was not affected.
  - Slip potential on a confined slipping crack/fault (low shear strength properties) was low.

7.3. Research Contribution: Framework for the Evaluation of Mining Induced Seismicity

- Bearing in mind the findings of the research (Chapter 4; Evaluation of mining-induced seismicity and Chapter 5; Effects of mining-induced seismicity on surface structures), mining engineers could evaluate the potential of seismicity caused by any of the source mechanisms studied. The seismic potential could be evaluated in terms of time histories at any point and at any depth in the area of research. Also, the methodology adopted using 3DEC allowed for the monitoring of ground motion (velocity, displacement) distribution during various time intervals of seismic duration.
- Practicing civil engineers can also use the estimated ground motions to evaluate effects on the surface structures and analyse the response of a structure during the foreseen mining- induced seismic event. The research allowed civil engineers to estimate the frequency and period of a structure-foundation system and to compare it with the structural guidelines on the frequency and period of similar structures. This information could then be used (though approximately) to design future structures so that the resonance effect would be avoided.
- The research could facilitate the re-mining activity in the Central Rand vis-à-vis safety considerations. Keeping in mind the research, simulations could

be made for various source mechanisms, site-specific ground motions evaluated both in terms of intensity and distribution (variation) over the candidate area to limit the distance between the re-mining areas and structures. However, such a site-specific evaluation would necessitate site-specific detailed geological information, hydrological profile, geotechnical parameters and performance standards of the candidate structure.

- The research could prove useful for carrying out a seismic micro-zonation for the development of building standards. The research provided a framework for the evaluation of site-specific mining-induced seismicity at an area of interest, illustrated in Figure 7.1.
- While only general (as opposed to actual site specific) input parameters were used, the study indicated that for seismic events in the range M_L 3 to 4, the Johannesburg CBD is not at risk of major catastrophe. Large events and the effects of repetitive events were not included in the study.

7.4. Research Limitations

- The research limitations related to the geomechanical and computational aspects. As far as the geomechanical aspect was concerned, the Office of Council for Geoscience, Pretoria was approached for provision of site-specific data (geotechnical properties of the site and discontinuities, hydrological profile, etc.). However the office was unable to provide the requisite data due to client confidentiality issues. Therefore, the geomechanical data used in evaluations was the estimated data.
- Whereas the approach adopted in the research could be used for similar purposes, the findings are relevant only to the data used. For any practical purpose, evaluations have to be made for site conditions under consideration.
- As far as computational limitations were concerned, it is worth mentioning that the accuracy of the numerical simulations was greatly dependent on the discretization (mesh size). The finer discretization required higher computational powers (type and number of processors, processing speed, memory, graphics, etc.).



Figure 7.1 Framework for evaluation of mining induced seismicity

- Keeping in mind the available computational system (Samsung Series 5 Ultra with COREi7 and 8GB RAM), the research was limited to 4000 m x 4000 m x 3000 m discretization with mesh size of 50 m. However, with more powerful computers, that is, greater number of processors and RAM more than 16 GB, a larger size of the area could be modelled and studied. However this does not detract from the value of the process that has been illustrated.

7.5. Recommendations for the Future Research Work

- The research had been conducted within the data and computational limitations described earlier. Further research with actual site-specific geomechanical data and finer discretization is recommended.
- Although the focus for this work was on the Johannesburg area, where it had been shown that post mining seismic events are of similar magnitude to those experienced during the active mining phase, the larger events that resulted in substantial damage should also be simulated.
- It is also recommended that the School of Mining Engineering should liaise with the Council for Geoscience to record data on ground motions for the Central Rand.
- In years to come, integration of the numerical evaluations and seismic data from the seismological network of Council for Geoscience has a potential to refine/enhance understanding of the mining seismicity especially against the backdrop of possible re-mining scenario in the Central Rand.
- To optimize the efforts to enhance the safety of the built up areas around mining districts, all stakeholders are recommended to engage in an integrated approach, such as:
    - All mines should prepare detailed GIS based 3D geomechanical maps of the respective areas along with mining layouts and seismological history.
    - The Johannesburg City Council and other affected councils should prepare GIS based damage pattern maps (type and distribution) from the data gathered on the structural damage during past seismicity.
    - The School of Mining Engineering, University of the Witwatersrand, equipped with the capacity in the most advanced and unparalleled numerical modelling techniques in the world, is an ideal platform to

integrate further research in mining-induced seismicity and its effects on surface structures.

- The outcome of the research should be shared with the South African Building Standard Division with a view to formulate seismic standards for new constructions, risk assessment and remediation of old constructions in the affected areas.

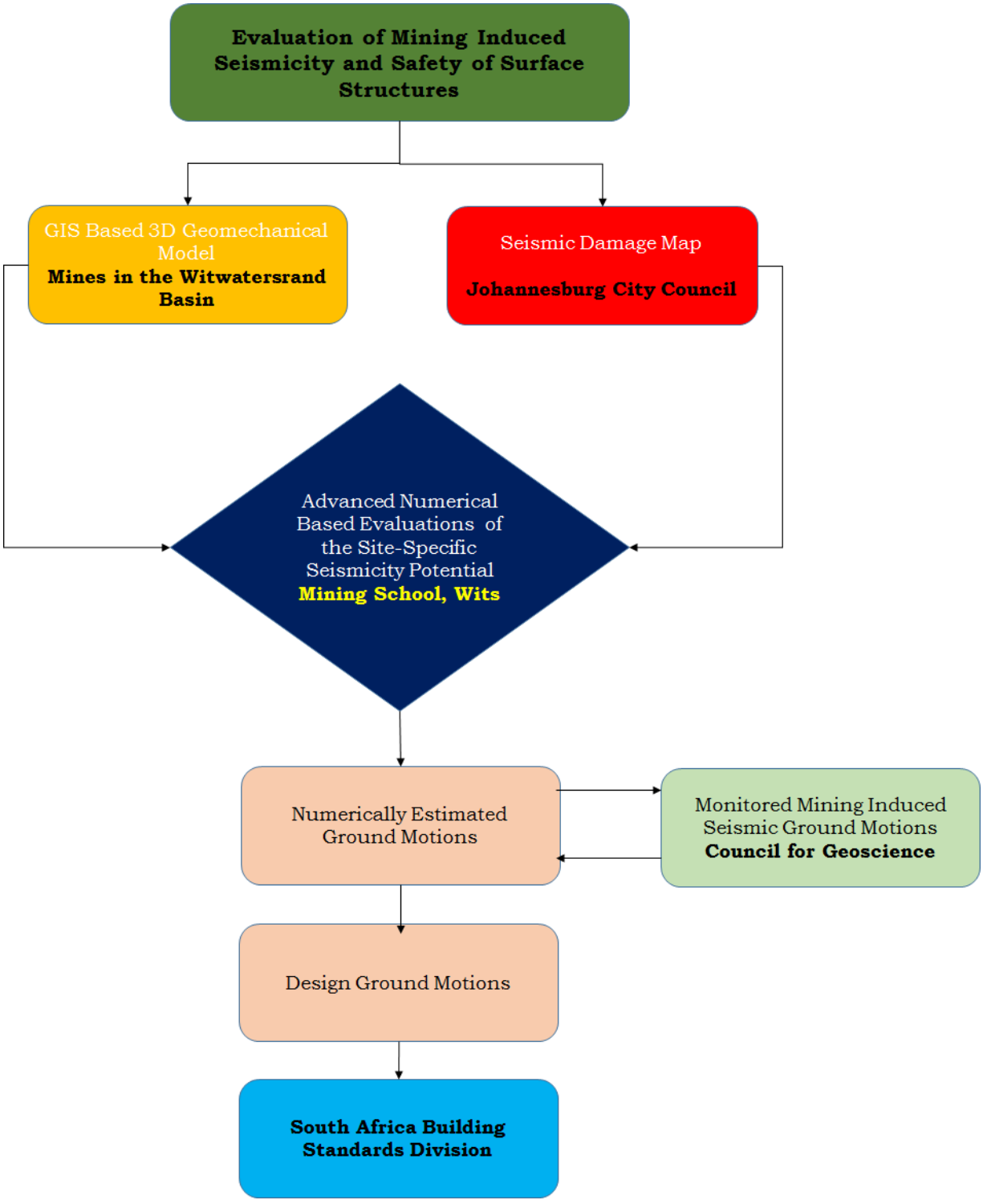


Figure 7.2 Proposed framework for evaluation of mining induced seismicity

References

Aki, K. and Richards, P.G. (1980) *Quantitative Seismology, Theory and Methods*. Volume 1, W.H. Freeman & Co. San Francisco.

Alabi, A., Akinyemi, O. A. and Adewale, A. (2013) *Seismicity Pattern in South Africa from 1986 to 2009*. Earth Science Research, Vol 2. No. 2:2013: Canadian Center of Science and Education.

ASCE/SCEC (2002). *Recommendation Procedure for Implementation of DMG Special Publication 117 Guidelines for Analysing and Mitigating Landslide Hazards in California.* Australian Centre for Geomechanics. March 2005. Perth, Australian Centre for Geomechanics.

Bailey, A. C., Law, J. D. M., Cadle, A. B. and Phillips, G. N. (1990) *The Zandfontein Quartzite Formation, a Marine Deposit in the Central Rand Group, Witwatersrand Supergroup.* South African Journal of Geology. Volume 93. p. 135-146.

Bathe, K. J. and Wilson, E. L. (1976) *Numerical Methods in Finite Element Analysis.* Englewood Cliffs, New Jersey. Prentice-Hall Inc.

Christopher, A. (2013) *Earthquake Effects on Buildings*. Risk Management Series: Designing for Earthquakes – A Manual for Architects, US Department of Homeland Security, Federal Emergency Management Agency, FEMA (454). p. 4-1 – 4-27.

Bennitt, T. J., Marshall, M. E., McLaughlin, K. L. ; Barker, B. W. ; Murphy, J. R. (1995) *Seismic Characteristics and Mechanism of Rockbursts.* Sponsored by AFSOR. Virginia. p. 542-551.

Bejaichund, M. and Hattingh, E. (2009) *Collection of Isoseismal Maps for South Africa*. Council for Geoscience publication on Natural Hazards, vol. 50, pp. 403-408.

Beukes, N. J. and Nelson, J. P. (1995) *Sea-level Fluctuation and Basin Subsidence Controls on the Setting of Auriferous Paleoplacers in the Archean*

Witwatersrand Supergroup: a Genetic and Sequence Stratigraphic Approach. Extended Abstract, South African Geocongress. p. 860-863.

Biggs, J.M. (1964) Introduction to Structural Dynamics. New York: McGraw-Hill, 1964.

Birch, D. and Handley, M. (2012) *Investigating Rock Mass Stability after Mine Flooding in Central Rand Basin; Strategic Water-Management Project.* Unpublished.

Board, M.P. (1994) *Numerical examination of mining-induced seismicity*. A Thesis Submitted in Partial Fulfilment of the Requirements of University of Minnesota for the Degree of Doctor of Philosophy. University of Minnesota, USA.

Bobet, A. (2010) *Numerical Methods in Geomechanics*. The Arabian Journal for Science and Engineering, Volume 35 (1B). p. 27-48.

Boore D. M. (1980) *On the Attenuation of Peak Velocity*. 7th World Conference on Earthquake Engineering Istanbul, Turkey, 1980. Volume 2. p. 577-584.

Brandt, M. B. C., Bejaichund, M., Kgaswane, E. M., Hatting, E., and Robin, D. L. (2005) *Seismic History of Southern Africa*. Seismographical Series No. 37. Pretoria: Council for Geoscience.

Brummer, R. K. and Rorke, A. J. (1990) *Case Studies on Large Rockbursts in South African Gold Mines.* Fairhurst, C. (ed). Rockbursts and Seismicity in Mines. Balkema, Rotterdam. p. 323-329.

Byerlee, J. (1978) *Friction of Rocks*. US Geological Survey, California, USA. Volume 16 (1978). p. 616-626.

City of Johannesburg, (2014). *Task Team for Acid Mine Drainage*. [Online] April 2011. Available from http://www.joburg.org.za/index.task-team-for-acid-mine-drainage. [Accessed: 29 July 2014]

Cook, N. G. W., Hoek, E., Pretorius, J. P. G., Ortlepp, W. D. and Salamon, M. D. G. (1966) *Rock mechanics applied to the study of rockbursts*. Journal of South African Institute of Mining and Metallurgy, 1966, 66 (10): 435–528.

Council for Geoscience (CGS), (2013). *Location of Seismic Events in Central Goldfields*. [Online] June 2013. Available from: http://www.geosciences.or.za /290-information /geoclips/june-2013-edition/1914-location-of-seismic-events-in-the-central-rand-goldfields. [Accessed: 11/2014]

Council for Geoscience (CGS). (2014) *Johannesburg Locality Map with detailed Geology and Borehole Location.* Council for Geoscience (CGS), Pretoria.

Dankert, B. T. and Hein, K. A. A. (2010) *Evaluating the Structural Character and Tectonic History of the Witwatersrand Basin.* Elsevier Journal of Precambrian Research, vol. 177 (2010), pp. 1-22.

De Beers, D. H. (1965) *A Detailed Geological and Soil Map of The Johannesburg City Area*. A Thesis Submitted in partial fullfilment of the Requirements of the Witwatersrand University for the Degree of Doctor of Philosphy. Johannesburg, University of the Witwatersrand.

Dor, O., Reches, Z. and Van Aswegen, G. (2001) *Fault Zones Associated with Matjhabeng Earthquakes 1999.* Eland shaft, Welkom. Proceedings of the 5th International Symposium in Rockbursts and Seismicity in Mines. South African Institute of Mining and Metallurgy, Johannesburg. pp 109-112.

Durrheim, R.J., Anderson, L.R., Cichowicz, A., Ebrahim-Trollope, R., Hubert, G., Kijko, A., McGarr, A., Ortlepp, W.D., and van der Merwe, N. (2006) *Investigation into the risks to miners, mines, and the public associated with large seismic events in gold mining districts* (volume 2). Department of Mineral Resources, Republic of South Africa, March 2006.

Eitzenberger, A. (2012) *Wave Propagation in Rock and Influence of Discontinuities.* A Thesis Submitted in Partial Fulfilment of the Requirements of Lulea University for the Degree of Doctor of Philosophy. Lulea University, Sweden.

Fernandez L.M. and J.A. Guzman, (1977) *the Seismic Event of the 8th December 1976 at Welkom, Orange Free State.* Pretoria: Council for Geoscience, report.

Fernandez, L. M. and Van der Heever, P. K. (1984) *Ground movement and damage accompanying a large seismic event in the Klerksdorp District*, Proceeding of the 1st International Symposium on Rockbursts and Seismicity in Mines (RaSiM1)South African Institute of Mining and Metallurgy, Johannesburg (1984), pp. 193-198.

Fernandez, L. M., Graham, G. and Du Plessis, A. (1992) *the Carletonville Erath Tremor of March 1992*. Pretoria: Council for Geoscience Report.

Gardner, G. H. F, Wyllie, M. R. J. and Droschak, D. M. (1964) *Effects of Pressure and Fluid Saturation on the Attenuation of Elastic Waves in Sands.* Journal of Petroleum Tech. vol. 16, pp. 189-198

Gibowicz, S.J. and Kijko, A. (1994) *an Introduction to Mining Seismology.* In: Durrheim et al. (2006) Investigation into the risks to miners, mines, and the public associated with large seismic events in gold mining districts (volume 2). Department of Mineral Resources, Republic of South Africa, March 2006.

Gibson, G. and Sandiford, M. (2013) *Seismicity and Induced Earthquakes:* A background paper to the office of the NSW Chief Scientist and Engineer providing information and a discussion about induced seismicity, micro seismic monitoring and natural seismic impacts. University of Melbourne, 2013.

Gold Fields (2013) *Mineral Resources and Mineral Reserves Overview, Geological Setting and Mineralization*. [Online] December 2011. Available from: http://www.goldfields.co.za/reports/ar_dec_2011/minerals/ops_sa_kloof_ geo. php

Goldbach, O. D. (2009) *Seismic Risks Posed by Mine Flooding*. The Southern African Institute of Mining and Metallurgy, Hard Rock Safety Conference 2009. P. 149-174.

Handley, J.R.F. (2014) *Historic Overview of the Witwatersrand Goldfields: A Review of the Discovery, Geology, Geophysics, Development, Mining, Production, and Future of the Witwatersrand Goldfields as Seen Through Geological and Financial Association Spanning 50 Years.*

Hanks, T. C. and Kanamori, H. (1979) *a Moment Amplitude Scale. Journal of Geophysics* Research. 84. p. 2348-2350.

Hasegawa, H. S., Wetmiller, R. J. and Gendzwill, D. J. (1989) *Induced Seismicity in Mines in Canada – an Overview.* Pure and Applied Geophysics. Vol. 129, Nos. 3/4, p. 423-453.

Hill, F. G. (1981) *The Stability of the Strata Overlying the Mined-out Areas of Central Witwatersrand*. Journal of the South Africa Institute of Mining and Metallurgy, June 1981, pp 145-191.

Hoek, E. and Diederichs, M. S. (2005) *Estimation of Rock Mass Modulus.* International Journal of Rock Mechanics and Mining Sciences, vol. 43, pp. 203-215.

ITASCA. (2014). Three *Dimensional Distinct Element Code Online Manual (Optional –Dynamic Analysis)*. Minneapolis: Itasca Consulting International Inc., USA.

Julia, J., Nyblade, A. A., Durrheim, R., Linzer, L., Gok, R., Dirks, P. and Walter, W. (2009) *Source Mechanisms of Mine Related Seismicity, Savuka Mine, South Africa.* Bulletin of the Seismological Society of America, Vol. 99, No. 5, p. 2801-2814.

Kazerani, T. and Zhao, J. (2010) *Micromechanical Parameters in Bonded Particle Method for Modelling of Brittle Material Failure*. International Journal for Numerical and Analytical Methods in Geomechanics Volume 34. p. 1877-1895.

Kijko, A. and Cichowicz, A. (2006) Origin, Intensity and Damage Potential of Tectonic and Mining Seismic Events. Seismological Unit, Council for Geoscience. Appendix 4.2, pp. 1-29.

Koo, R. C. H, Pappin, J. W., Rule, D.C., Wallace, M. I. and Yim, I. P. H. (2013) *Dynamic Analyses of Slopes in Hong Kong*. [Online] 2013. http\\:www.aees.org.au/wp-content/uploads/2013/11/42-PAPPIN-jack.pdf. [Accessed: 01/08/2015]

Krinitzsky, L. E., Gould, P. J. and Edinger, H. P. (1993) *Fundamentals of Earthquake Resistant Construction*. Toronto. John Wiley & Sons, Inc.

Kuhlmeyer, R. L. and Lysmer, J. (1973) *Finite Element Method Accuracy for Wave Propagation Problems*. Journal of Soil Mechanics and Foundations Division. ASCE 99(SM5). p. 421-427.

Lama, D. R. and Vutukuri, S. V. (1978) *Hand Book on Mechanical Properties of Rocks* (volume II), 1978. Australia. Trans Tech Publications.

Leehman (1957) *Observations on extent of fracture zone around excavations in Central Rand mines*; Association of Mine Managers, S.A. , 1958-1959; fig 250, p. 359.

Linzer, L. M., Bejaichund, M., Cichowicz, A., Goldbach, O. D., Kijko, A., Milev, A., Saunders, I., Spottiswoode, S. M. and Webbet, S. J. (2006) *A Summary of Recent Research in Seismology in South Africa*. Council for Scientific and Industrial Research (CSIR), Auckland Park, South Africa.

Lysmer, J. and Kuhlmeyer, R. L. (1969) *Finite Dynamic Model for Infinite Media.* Journal of Soil Mechanics and Foundations Division. ASCE 95:E4. p. 859-877.

McCarthy, T. S. (2011) *The Impact of Acid Mine Drainage in South Africa*. South African Journal of Science. Volume 105 (5/6). p. 712-719.

McDonald, A. J. (1982) *Anthropogenic Seismicity in Johannesburg*. A thesis submitted in partial fulfilment of the Requirements of University of the Witwatersrand for the Degree of Masters in Science, University of the Witwatersrand.

McGarr, A, (1971) *Tectonic Stresses in Mine Seismicity: Are They Significant?* [Wong, G. I. (1993)]. In: Rockbursts and Seismicity in Mines. Young, (ed.). Balkema, Rotterdam, 1993. p.276.

McGarr, A. J., Bicknell, E., Sembera and Green, R.W.E. (1989), Analysis of Exceptional Large Tremors in Two Gold Mining Districts of South Africa, Journal of Pure Applied Geophysics, 129, pp 295-307.

McGarr, A. (2002) *Control of Strong Ground Motion of Mining-Induced Earthquakes by the Strength of Seismogenic Rock Mass.* Journal of the South African Institute of Mining and Metallurgy, Vol. 102 (No. 4). p. 225.

McGarr, A., Simpson, D. and Seeber, L. (2002) *Case Histories of Induced and Triggered Seismicity*. In: International Handbook of Earthquake and Engineering Seismology, Volume 81A. National Science Foundation, Committee of Education. pp 647-661.

Milev, A. M., and Spottiswoode, S. M. (2005) *Strong Ground Motion and Site Response in Deep South African Mines.* The Journal of South African Institute of Mining and Metallurgy, Volume. 105. P. 515-524.

Mphephu, N. F. (2001) *Environmental issues related to the underground workings of the Central Rand gold fields, Johannesburg, South Africa*. MSc dissertation. Faculty of Science, University of the Witwatersrand, Johannesburg, South Africa. 102 p.

Myer, L.R. Pyrak-Nolte, L.J., Cook, N.G.W. (1990) *Effects of Single Fractures on Seismic Wave Propagation across Rock Joints.* pp. 467-473. Balkema, Rotterdam.

Norman, N. and Whitfield, G. (2006) *Geological Journeys*. p. 38-49, 60-61. Struik Publishers, Cape Town.

Ortlepp W D. (2005) *RaSiM Comes of Age - a Review of the Contribution to the Understanding and Control of Mine Rockbursts:* Selected Contribution to 6th International Symposium on Rockbursts and Seismicity in Mines (RaSiM6), 2005.

Patrick, M., Ochendorf, J., Germaine, J. and Eduardo, K. (2007) *The Impact of High-Frequency/Low-Energy Seismic Waves on Unreinforced Masonry. Earthquake Spectra*: February 2007, Vol. 23. No. 1. p. 77-94.

Perino, A. (2013) *Wave Propagation through Discontinuous Media in Rock Engineering.* A Thesis Submitted in Partial Fulfilment of the Requirements of Torino University for the Degree of Doctor of Philosophy. Torino University, Italy.

Porter Geoconsultancy. (2007) *Witwatersrand Deposit Description*. [Online] 2007. Available from: http://www.portergeo.com.au/database/mineinfo.asp. [Accessed: 22nd December 2014]

Potvin, Y. and Wesseloo, J. (2010) *Towards an Understanding of Dynamic Demand on Ground Support*. The Journal of the South African Institute of Mining and Metallurgy. Volume 113 (12). p. 913-922.

Pyrak-Notle, L. J., Myer, L. R. and Cook, N. G. W. (1990b) *Effects of Multiple Parallel Joints on Apparent Wave Attenuation in Rocks.* Journal of Geophysical Research. 95 (B7). p.11345 - 11358.

Randgold (2010) *An Independent Mineral Asset Valuation Report on the Weltevreden and Jeanette Gold Projects*, Free State Province, South Africa.

Riemer, K. L. and Durrheim, R. J. (2012) *Mining Seismicity in the Witwatersrand Basin: Monitoring, Mechanisms and Mitigation Strategies in Perspective.* Journal of Rock Mechanics and Geotechnical Engineering, South Africa. Vol. 3/3. pp. 250-259.

Rosner, T. (1999) *The Environmental Impact of Seepage from Gold Mine Tailings Dams Near Johannesburg, South Africa.* A Thesis Submitted in Partial Fulfilment of Pretoria University for the Degree of Doctor of Philosophy. University of Pretoria, Republic of South Africa.

Ryder, J. A. and Jager, A. J. (eds). (2002) *Rock Mechanics for Tabular Hard Rock Mines.* The Safety in Mines Research Advisory Committee (SIMRAC).

SABS Standards Division (2009) *Basis of Structural Design and Actions for Buildings and Industrial Structures. Part 4: Seismic Actions and General Requirements for Building.* SABS Standards Division: Pretoria

Saeibimughaddam, A. (2010) *Liquefaction of Early Age Cemented Past Backfill.* Thesis Submitted in partial fulfilment of the Requirements of Toronto University for the Degree of Doctor of Philosophy. Toronto University.

SANS 10160-4. (2009) *Draft South African Standards (DSS): Public Enquiry Stage.* [Online] October 2009. Available from: http://www.saice.org.za /downloads/other/SANS10160-4_dss.pdf. [Accessed: 23/01/2015]

Satratta, J. (1987) *Manual of Seismic Design.* Prentice-Hall, Englewood Cliffs, NJ

Saunders, I., Brandt, M. B. C. and Kgaswane, E. (2007) *Preliminary Appraisal of the Effect of a Magnitude M_L = 5.3 Event of 9 March 2005*, Klerksdorp, South Africa. Report No. 2005-2006. Pretoria: Council for Geoscience.

Scott, R. (1995) *Flooding of the Central and East Rand gold mines: an investigation into controls over the inflow rate, water quality and the predicted impacts of the flooded mines*. Report to the Water Research Commission by the Institute for Groundwater Studies, University of the Orange Free State, WRC Report no. 486/1/95, WRC, Pretoria, South Africa.

Searer, G. R. and Freeman, S. A. (2004) *Design Drift Requirements for Long Period Structures.* In 13th World Conference on Earthquake Engineering, 1st to 6th August 2004. Vancouver: paper no. 3292.

Shi, G. H. and Goodman, R. E. (1988) *Discontinous Deformation Analysis – A New Method For Computing, Strain and Sliding of Block systems*. [Online] June 1988. Available from: http://www.onepetro.org/conference-paper/ARMA-88-0381. [Accessed: 15 August 2015]

Singh A. K. (2012) *Studies on Mining Induced Vertical Stress ahead of Depillaring Face in Indian Geo-Mining Conditions*. A Thesis Submitted in partial fullfilment

of the Requirements of Bengal Engineering and Science University for the Degree of Doctor of Philosphy. Shibpur, Bengal Engineering and Science University.

Sjoberg, J., Dahner, C., Malmgren, L. and Perman, F. (2011) *Forensic Analysis of Rock Burst Event at Kiirunavaara Mine - Results and Implications for Future.* [Online] 2011. Available from: http://www.itasca.se/pdf/02-05.pdf. [Accessed: 20/01/2015]

Spottiswoode, S. M. and McGarr, A. (1975) *Some Parameters of Tremors in a Deep Level Gold Mine.* Itasca FLAC/DEM Symposium 2011, Melbourne, Australia.

Spottiswoode, S. M. (1971) *Perspectives on seismic and rockburst research in the South Africa Gold Mining Industry.* In: Young, P. (ed). Rockbursts and Seismicity in Mines. Balkema, Rotterdam, 1993.

Stacy, T. R., Kirsten, H. A. D. and Wiid, B. L. (1983) *5th International Congress of the International Society for Rock Mechanics*, Melbourne, Australia, April 1983.

Superior Mining Group (2013) Typical Cross section of Witwatersrand Goldfield Geology. [Online] November 2014. Available from: http: //superiormining.com/properties/south_africa/mangalisa/geology. [Accessed: 2013]

The Council for Science and Industrial Research (CSIR). *(2014) Earthquakes – Mining or Nature?* [Online] August 2014. Available from: http://www.csir.co.za/news/2014/08/earthquake. [Accessed: 20th December 2014]

Toksoz, M. N., Johnston, D. H. and Timur, A. (1979) *Attenuation of Seismic waves in Dry and Saturated Rocks: Laboratory Measurements*. The International Society of Applied Geophysics, Volume 44 (4). p. 681-690.

Trollope, E. R., Smith, G. and Durrheim, R. J. (2014) *Failure Mechanism, Source Parameters and the Quantification of the Size of Mining-Induced Seismic Events*

in the Witwatersrand Basin, South Africa. South African Rock Engineering Symposium, at Cradle of Humankind, South Africa.

USGS (2014) USGS *Shake Map of Earthquake on 5 August 2014 near* Orkney, North West, South Africa.

van der Merwe (2013). Personal communication, Prof Nielen van der Merwe.

Vervaeck, A. (2014) *Deadly Earthquake in South Africa in Orkney and Klerksdorp.* [Online] August 2014. Available from: http://www.earthquake-report.com/2014/08/05/strong-earthquake-south-africa-on-august-5-2014/. [Accessed: August 2015]

Viljoen, M. (2009) *The Life, Death and Revival of the Central Goldfield.* World Gold Conference. The Southern African Institute of Mining and Metallurgy, 2009. p. 131-138.

Winde, F. (2011) *Desktop Assessment of the Risk for Basement Structures of Buildings of Standard Bank and ABSA in Central Johannesburg to be Affected by Rising Mine Water Levels in the Central Basin.* Springer International Publishing, Switzerland, pp. 201-210.

Wong, I. G. (1993) *Tectonic Stresses in Mine Seismicity: Are They Significant?* In: Young, P. (ed). Rockbursts and Seismicity in Mines. Balkema, Rotterdam, 1993. p. 273-278.

Wood, O. and Neumann, F. (1931) *Modified Mercalli Intensity Scale of 1931.* Bulletin of the Seismological Society of America, 21, 277-283. [Online] 26 April 2013. Available from: http://www.earthquakescanada.nrcan.gc.ca /info /gen/scales-schelles/ mercalli-eng.php. [Accessed: 9 August 2015]

Wright C., Kijko, A.J., Linzer, L.M. and Smithet, M. (2003) *Recent Research in Earth Structure, earthquakes, Mine Seismology and Seismic Hazard Evaluation in South Africa.* South African Journal of Science, vol. 99, pp. 389-394.

Xie, Y. S. and Zhao, Y. S. (2009) *Numerical Simulation of the Top Coal Caving Process using Discrete Element Method.* [Online] 2012. Available from:

http//www.arunkumarsingh_mining_2012_completephdthesis(1).pdf. [Accessed: 15 August 2015]

Zembaty, Z. (2003) *Rockburst Induced Ground Motions - A Comparative Study.* The journal of Soil Dynamics and Earthquake Engineering, 24 (2004). p. 11-23.

Zhao, J., Zhao, X. B., Hefny, A. M. and Cai, J. G. (2006) *Normal Transmission of S-wave across Parallel Fractures with Coulomb Slip Behaviour.* The Journal of Engineering Geomechanics. Volume 132 (6). p. 641-650.